Understanding and Modelling Manual Wheelchair Propulsion and Strength Characteristics in People with C5-C7 Tetraplegia

By
Laura Hollingsworth

A thesis submitted for the degree of
Doctor of Philosophy

Bioengineering,
The University of Canterbury.

January 2010

Abstract

Spinal Cord Injuries (SCIs) are debilitating injuries where damage to the spinal cord causes a loss of mobility and feeling in muscles innervated below the injury point. Tetraplegia refers to an SCI in the cervical region of the spinal cord that impacts on the functionality of all four limbs. 'Complete' tetraplegia results in complete paralysis of the legs, partial or complete paralysis of the arms and trunk, and in the most severe cases, the neck. The independence of people living with tetraplegia is heavily dependent on assistive and mobility devices.

Understanding the strength characteristics of people with tetraplegia is crucially important for the suitable and effective design of mobility and rehabilitative devices such as wheelchairs. A study using a stationary dynamometer and video capture measured kinetic and kinematic characteristics of wheelchair propulsion for 15 subjects with C5-C7 tetraplegia. This study differentiated between subjects with different injuries, at two different test resistances, and was more comprehensive than other reported studies on MWC propulsion.

Some of the subjects in the study with C5-C6 injuries had no elbow extension capability, while others had undergone a deltoids-to-triceps tendon transfer procedure called TROIDS, which restores some elbow extension capability. No differences were found in any of the push phase metrics between those who had undergone the TROIDs procedure, and those who had not, suggesting that TROIDs provides no significant benefit for mobility. As expected, subjects with C7 tetraplegia recorded velocity and power outputs significantly higher than those for subjects with C5-C6 tetraplegia.

To better understand the strength characteristics over the full range of motion in the sagittal plane, and thus potentially modify the design of mobility devices to better suit these characteristics, a novel method for gathering strength data in multiple directions and positions was developed. This method had advantages over other commonly used methods. In particular, it was inclusive of complex muscle and joint interactions that would otherwise be very difficult to build into a model.

Sagittal horizontal push strength was measured using this method for 8 able bodied and 4 tetraplegic subjects. There were clear trends in the data from the able-bodied subjects, and a fourth order polynomial (R-squared = 0.8) was fitted to the data for modelling purposes. Data for the tetraplegic subjects varied significantly from the

able-bodied data, but inter-individual variation was such that no model would provide a satisfactory fit to the data indicating a very high degree of patient-specific behaviour. One multi-directional data set, consisting 1584 measurements in the sagittal plane, was gathered for an able-bodied subject. The main trends in this measured data were successfully captured by a model consisting of twelve fourth-order polynomials.

Building on these measurements, and employing a human model in the constraint modelling environment, SWORDS, this thesis develops a conceptual design tool for comparing the effectiveness of different hand force paths. Initial simulations using hypothetical hand paths indicated that the proposed method for predicting the direction of the applied force needs to be verified, and likely refined, for hand paths that differ significantly from the traditional wheelchair push-rim path. This proposed procedure has the potential to be a powerful tool for optimising and modifying the design of wheelchairs or human powered devices to utilise previously untapped abilities for any given population.

Acknowledgments

The work presented in this thesis was carried out in the Department of Mechanical Engineering at the University of Canterbury and at Burwood Hospital Spinal Unit, Christchurch, New Zealand. Financial support for this study was provided in part by Independent Research Limited (IRL) and by the University of Canterbury, for which I am most grateful.

I would like to thank Professor Geoff Chase, Dr Shayne Gooch and Dr Tim Woodfield at the University of Canterbury and Professor Tony Medland from the University of Bath for their input, supervision and guidance over the course of my PhD studies, and help with editing this thesis. Margot Beck from the mechanical engineering department helped me on many occasions by sorting out enrolment, financial and administrative issues, I can't thank her enough for the stress she saved me. I would also like to thank Jennifer Dunn of Burwood hospital, Alistair Rothwell from the Christchurch school of medicine, and the researchers I worked with at IRL, particularly Lan Lengoc and Andrew Lintott, for their valuable support, time and input for this study.

On a personal note, many people shared in and supported me through the the ups and downs of my PhD years. My university office-mates, Jac, Lisa, Lindsey, and Thanh, over the years became some of my best friends. I will miss our daily laughs, the girly chats, which are otherwise a rarity in Engineering, and of course the baking! My other friends in the engineering department, particularly Joe, Geoff and Ben, for their friendship and the many coffee dates. My flatmates, Tom, Volker, Kieran, Ivor and Tamlin, have became like family to me,

During my postgraduate years I filled almost every spare slot of my time with tramping trips and road cycling, these pursuits kept me sane, balancing out the many hours spent in front of the computer, and through them I met some wonderful people. I'd particularly like to thank all the people of the Canterbury University Tramping Club who shared my many weekend trips into hills, including some 'epics' . It has been a blast and I take away many amazing and humorous memories. I'd also like to acknowledge all my cycling friends who taught me a lot, inflicted much pain racing up the port hill roads, and some of whom became like second parents to me.

I have been blessed with a wonderful family, whose love and support mean so much to me. I will be forever grateful to my parents and my three beautiful sisters for their patience and encouragement, not only during my university years, but also during my formative primary and secondary years. I am deeply indebted to my inspirational nana and granddad for their love, support and generosity over the years. I would also particularly like to thank my great aunt and uncle Bern and Ron - my family in Christchurch, who opened their home to me from the day I arrived Christchurch as a first-year undergraduate student - thank you so much for your support and hospitality. To all my family and friends; I love you all.

Lastly I'd like to thank the patients from Burwood Hospital and the able-bodied individuals who participated in this study. Without your time, patience and cooperation, this study would not have been possible, cheers.

Contents

Chapter 1

Introduction and Motivation

Tetraplegia is a condition where an injury to the cervical region of the spinal cord causes impaired functionality in all four limbs. Complete tetraplegia is where the entire cross section of the spinal cord is damaged resulting in complete paralysis of the legs, partial or complete paralysis of the trunk and arms, and in the most severe cases, paralysis of the neck. The extent of upper body paralysis is determined by the location of the spinal cord injury. Over 90% of all spinal cord injuries have traumatic causes (NSCISC, 2005), meaning most victims are healthy, active, and most often young people, who suddenly find themselves living with this debilitating condition. People living with a spinal cord injury (SCI) are reliant on assistive and mobility devices for their independence.

Understanding the strength characteristics of a person with tetraplegia is crucially important for suitable and effective design of rehabilitative, assistive or orthotic devices. A design tool capable of modelling interaction between a human subject and such a device would increase the efficiency of the design process, allowing more design modifications and evaluations to occur virtually before being necessary to build a prototype and conduct human trials. Increasing the amount of 'virtual' design refinement possible generally reduces the number of human trials required in a typically iterative design process, and thereby reduces the length and cost of the design process. Such a tool could also help optimise and modify designs to utilise previously untapped abilities in a given population, but to achieve this the strength and movement characteristics of people with different spinal cord injuries must first be understood.

There is considerable variation in functional an strength abilities among people with tetraplegia. The most significant factor for determining the capabilities of a person with tetraplegia is the level and extent of the spinal cord injury. Physiological differences

between males and females and age related factors also cause differences in strength characteristics. Since functional ability is largely dependent on the part and amount of the spinal cord injured, at a given injury level in the spine, there is significantly more variation in abilities amongst people with an incomplete injury, where only part of the spinal cord is damaged, than amongst those with a complete injury, where the entire spinal cord is damaged at the point of injury.

For nomenclature purposes, the spine is divided into four sections according to the vertebrae location: the cervical (C) region in the neck, the thoracic (T) region in the back, the lumbar (L) region in the lower back, and the sacral (S) region in the tailbone. Vertebrae within each region are numbered from top to bottom. Peripheral nerves branch out from the spinal column at each vertebra. Spinal injuries are classified by the level in the spine at which the spinal cord is injured. The spinal cord finishes at the L2 vertebrae, below this point nerves branch off and are contained within the spinal column; this is called the cauda equina. Injuries below L2 damage the cauda equina rather than the spinal cord. Generally, a person's body functionality is affected below the point of injury.

Injuries to the C5 and C6 vertebrae together account for approximately half of all cases of tetraplegia (NSCISC, 2005). Additionally, approximately 80% of all spinal cord injury victims are males. In America young men aged between 16 and 30 are the demographic with the highest incidence of spinal cord injuries, accounting for over half of all spinal cord injuries each year (NSCISC, 2005).

People with a complete spinal cord injury at or above the C6 vertebrae typically lose function of their triceps resulting in loss of elbow extension function. Upper limb deltoid to triceps tendon transfer surgery (TROIDS) is an option for those with C5-C6 injuries, in this procedure the still functional posterior third of the deltoid is reattached to the elbow to substitute for the inactive triceps. This procedure anecdotally improves subjects' functional capabilities including their ability to propel a manual wheelchair. Earlier studies have quantified the improvement in shoulder extension strength (Woodfield, 1996) but not specifically examined or quantified the effect of this procedure on wheelchair propulsion characteristics. Subjects with a complete C7 injury retain use of their triceps.

1.1 Research Objectives

This PhD study ultimately aims to develop or propose a method for evaluating the effectiveness of different hand force paths that could be used for driving any human powered device, but in particular manual wheelchairs. To achieve this, several secondary objectives must first be satisfied.

A first study seeks to first better understand manual wheelchair (MWC) propulsion characteristics and capabilities for subjects with C5-C7 tetraplegia, to identify any significant differences between injury groups and determine if the three injury levels can be grouped to be modelled, or if they must be modelled and subsequently designed for independently. It was hypothesised that there would be characteristic differences in hand path shapes between subjects with and without elbow extension. If this were so, these characteristic paths could be later analysed.

A model of strength capabilities is required for input into the proposed design tool. A second study second study aims to identify the best method for constructing such a model, and either through published values or strength tests, develop an appropriate model. Ideally this model would be for tetraplegic subjects, but depending on the availability of existing data and the extent of any data measurement required, data for able-bodied subjects would be adequate for the initial development of the tool.

Finally, this thesis aims to use the strength model from the first model together with insight from the first MWC propulsion study to develop a method for comparing the effectiveness of different force hand paths.

1.2 Overall Methodology and Thesis Organisation

This thesis primarily comprises two main studies; a first study into the wheelchair propulsion characteristics in people with C5-C7 tetraplegia, a second study that investigates and models strength capabilities in the sagittal plane. Insight from the first study and the model from the second study are used to propose a method for comparing the effectiveness of different hand paths. This methodology is shown schematically in Figure 1.1.

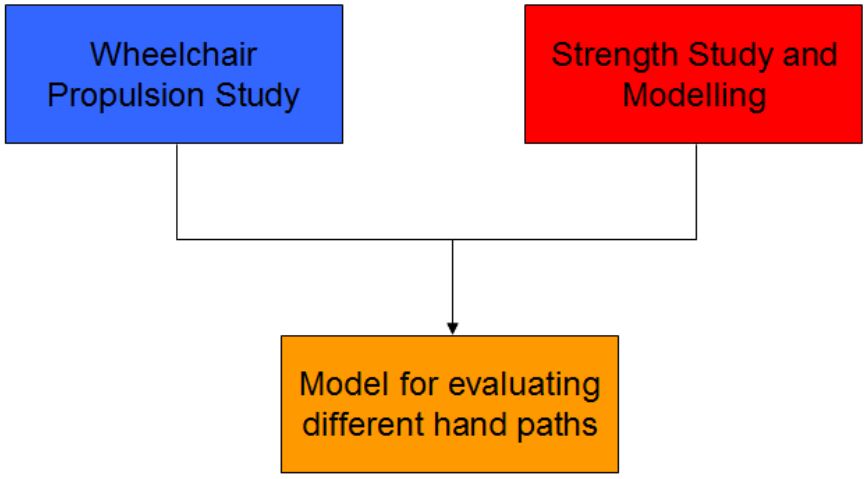

Figure 1.1: Overall methodology

This thesis is organised according to these two studies. Chapters 2 to 4 present the first study into manual wheelchair propulsion. The background and methodology for this first study are outlined in chapter 2, and the results are presented and discussed in chapter 3. Chapter 4 presents a method for predicting the magnitude and direction of the force applied to the wheelchair wheel by a subject during wheelchair propulsion, as studies have shown this to be different to the tangential force, and applied forces were estimated for the experimental data from chapter 3.

Chapter 5 introduces constraint modelling software SWORDS, developed at the University of Bath, and the SWORDS human manikin model, developed in collaboration between the University of Bath and the Technical University of Delft. This model and software was used to predict the posture of a person when their hands are at given point space. Chapter 5 develops the capability of the SWORDS manikin to allow forces to be applied and reaction forces calculated within the constraint modelling environment.

The second study, which investigates and models strength capabilities, is presented in Chapters 6 to 8. Chapter 6 reviews published strength studies and their methods of measuring and modelling strength data. Chapter 7 evaluates these methods and models and develops a protocol for collecting strength data. Chapter 8 presents experimental strength data gathered in this study, and where appropriate, develops models for this data.

Using the strength model from the second study, the force direction prediction method and insight from the first study, and the SWORDs based manikin model, Chapter 9 consolidates all this work and proposes a conceptual design tool for comparing the effectiveness of different hand force paths.

Finally, the conclusions and contributions of this thesis are summarised in Chapter 10 along with suggestions for further research in this field.

Chapter 2

Wheelchair Propulsion Study - Methodology

Subjects with C5-7 tetraplegia have significantly reduced upper body and arm functionality compared to persons with paraplegia, and therefore it is likely that they will also exhibit different manual wheelchair (MWC) propulsion techniques and kinetics.

This chapter introduces the manual wheelchair propulsion study, which forms the first study in this thesis. Previous studies of manual wheelchair propulsion are reviewed in section 2.1, then section 2.2 presents the experimental methodology used in this study for observing and measuring kinematic and temporal dynamics of MWC propulsion in persons with C5-7 tetraplegia. The remainder of this chapter outlines the data processing and methods used to collect had path data from video frames, and for calculating velocity, acceleration and power from encoder data. Experimental trials were conducted according to the methodology outlined in this chapter, the results from these trials are presented in Chapter 3.

2.1 Introduction

2.1.1 Prior Art

Over the last fifteen years numerous researchers have investigated the different aspects of wheelchair propulsion. Studies have covered propulsion velocities, upper body and limb kinematics, push-rim force application characteristics, and joint biomechanics. For accuracy and practical reasons, most of this data has being collected in an artificial laboratory environment using ergometers and dynamometers, rather than a real propulsion environment, such as outdoors on the pavement. These methods facilitate

accurately measuring chair kinematics, such as velocity, power, and work, where the load can be controlled thus allowing direct comparisons between users.

When using wheelchair ergometers and dynamometers, the wheelchair is tied down. Consequently inertial forces acting on the chair from movement of the arms and torso that normally cause chair accelerations and decelerations, are immeasurable (Vanlandewijck et al., 2001). In subjects with SCIs, movement capability of the torso diminishes with higher SCI lesions, and so the error from ignoring these inertial effects also decreases. Ergometers are also unable to consider the effect of shifting of the subject's centre of gravity, that normally influences balance and rolling resistance (Vanlandewijck et al., 2001).

Many studies using Ergometers and dynamometers (e.g. Dallmeijer and Kappe, 1994; Finley et al., 2004; Kulig et al., 2001; Newsam et al., 1999, 1996; Robertson et al., 1996; Shimada et al., 1998) did not test test subjects in their own wheelchairs. Instead they employ a 'test' wheelchair that is set up in the test rig and sometimes fitted with instrumented wheels. In most of these studies foot height and backrest height were the only adjustable wheelchair parameters. Thus these studies neglect the effect of wheelchair prescription on propulsion characteristics. Wheelchair prescription differs between subjects with tetraplegia and paraplegia and inter-individually within these groups. Seat tilt, seat position, back height and wheel camber are the most commonly varied both for functional reasons and personal preference (Batavia et al., 2001; Brubaker, 1986; Di Marco et al., 2003; Kotajarvi et al., 2004; Richter, 2001). Consequently, testing people in chairs they are not accustomed to and that differ from their prescribed chairs is likely to result in different propulsion characteristics from those they normally display in their own chairs. The subject's performance in these tests is then likely to be poorer than for in their own chair, or the trends between users obtained in these studies may differ, negating some conclusions.

Most of these studies (e.g. Finley et al. 2004; Kulig et al. 2001; Newsam et al. 1999, 1996; Robertson et al. 1996; Shimada et al. 1998) also used instrumented push rims such as the SMARTwheel^{TM} to measure applied applied propulsive forces. Most studies observed wheelchair propulsion while the subject was in their own chair replaced the wheels on the chair and used these instrumented rims (e.g. Boninger et al., 2002; Koontz et al., 2002; Richter et al., 2007).

A preliminary study by Yao (2007) that observed push technique in 17 subjects with L1-C6 SCIs showed that propulsion using push rims exclusively was the least common

propulsion style, with only F subjects (T9-C6) using this technique. Over half of the subjects grasped both the tyre and the push rim. It was hypothesised that this behaviour was due to the fact that the tyre offered more friction and a larger contact surface. The remaining subjects in Yao (2007) wedged their hands between the tyres and the push rims. This third method was the most common method for subjects with C5-C6 injuries and may be due to the reduced grip capabilities in this population. Therefore, these studies with different wheels also prevented the test subjects from using their own chairs as they normally would, potentially impacting on the results and conclusions of these studies.

2.1.2 Testing Procedures

A wide range of testing procedures have been used by researchers studying MWC propulsion. Some studies require subjects to propel the chair at specified speeds (e.g. Boninger et al., 2002; Finley et al., 2004; Koontz et al., 2002; Robertson et al., 1996; Shimada et al., 1998). These studies typically used a speedometer in the participant's view. While others allowed subjects to propel their chairs at a self-selected speed (e.g. Dallmeijer and Kappe, 1994; Kulig et al., 2001; Newsam et al., 1996, 1999; Richter et al., 2007). Resistance in these tests ranged from a single fixed resistance for all subjects (Shimada et al., 1998), to resistance selected to simulate a smooth flat surface (Kulig et al., 2001; Newsam et al., 1999; van Drongelen et al., 2005), a rough surface (Koontz et al., 2005) or specific inclines (de Groot et al., 2005; Newsam et al., 1996; Raison et al.; Sabick et al., 2004). These studies have typically covered a limited range of what is encountered in everyday propulsion.

2.1.3 Terminology

The wheelchair propulsion cycle is typically divided into two phases, the push phase and the recovery phase. The push phase is the period where the hand is in contact and applying force to the wheel. It is a closed-chain event where the path of the hand is defined by the rim of the wheel or the tyre where it is grasped and thus influenced by the wheel shape, design and location. The recovery phase is the phase between releasing the wheel and where the hand is returned to the start of the push phase before grabbing the wheel again.

To describe timing characteristics of wheelchair propulsion, the terminology used extensively in other propulsion studies was also adopted for this study. Push time (PT) and recovery time (RT) are the periods of the push phase and recovery phase of the

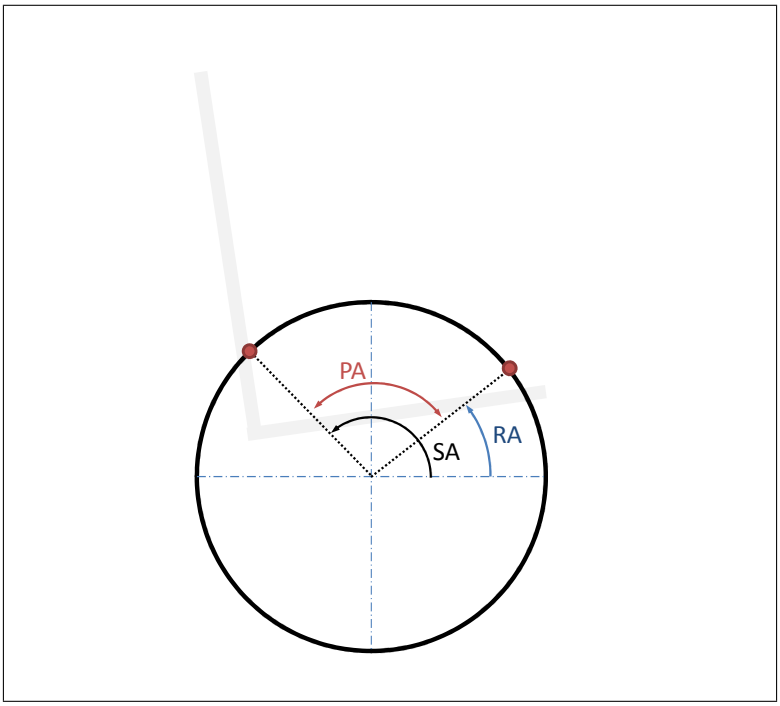

Figure 2.1: Wheelchair propulsion parameters

cycle respectively. Cycle time (CT) is the total cycle time between the commencement of two consecutive push phases. Vanlandewijck et al. (2001) divides the propulsion cycle into three cycles; acceleration during the push-phase, a second acceleration phase due to inertial forces acting on the system, and a deceleration phase during the second part of the recovery phase. As inertial effects from movement of the arms and torso are undetectable using an ergometer or dynamometer, separation of Vanlandewijck et al.'s second and third phases would not be possible. Therefore, the classical method of dividing the propulsion cycle into two phases was adopted for this study.

The push phase of the propulsion cycle is further described geometrically using the angles shown in Figure 2.1. The start angle (SA) indicates the position on the wheel rim where the push phase commences, the release angle (RA) the point where the rim is released and the recovery phase commences. The push angle (PA) is the angle the wheel turns through during the push phase and is equivalent to SA - RA.

2.1.4 The Effect of SCIs on MWC Propulsion

Due to their reduced upper-body capabilities, persons with tetraplegia have been shown to be significantly slower in MWC propulsion than those with paraplegia (Kulig et al., 2001). Similarly, Newsam et al. (1996) found candidates with C6 lesions were capable of lower MWC propulsion speeds than those with C7 lesions, who were in turn were

slower than paraplegic candidates. Differences in cadence have also been measured between subjects with different level SCIs. Newsam (1996) found the more able a candidate, the higher a cadence they were able to attain.

Differences in cadence between injury levels were more pronounced at higher velocities, for example at a candidates 'normal' speed, Newsam found C7 candidates had a cadence comparable to paraplegics, and higher than that of the C6 candidates. At a subject's 'fast' pace however, paraplegics were able to maintain a higher cadence than the C6 and C7 subjects. Newsam also found the higher the SCI, the less difference between the subject's 'normal' and 'fast' propulsion velocities. Interestingly, where the propulsion velocity was specified, rather than self-selected by the candidates, subjects with tetraplegia demonstrated decreased contact time with the rim and a corresponding increase in stroke frequency than those with paraplegia (Finley et al., 2004). This indicated that at normal propulsion velocities, subjects with higher SCIs are working closer to their maximal capacities.

Increases in resistive load have been shown to decrease achievable propulsion speed by more in subjects with higher SCIs than those with lower lesions. Newsam et al. (1996) found candidates with C6 lesions were unable to overcome any resistance exceeding that equivalent to an 8% grade. Subjects with lower SCIs were able to overcome this resistance. Thus limiting the range of terrain subjects with C6 and higher lesions are able to propel their chairs over.

De Groot et al (2005, 2007) identified a positive correlation between a subject's power output and their maximum velocity and studies have consistently shown subjects with tetraplegia to have a significantly lower power output in MWC propulsion when compared to persons with paraplegia. For example, Dallmeijer (1998) found the average maximum power output was 63 W for paraplegic candidates (n=12), but only 19 W for those with C5-C7 tetraplegia (n=17). Mean power and absolute power values for C5-C7 subjects were approximately one third of those of the paraplegic subjects, at both moderate and high intensities. deGroot (2005) also found power output to be higher in subjects with paraplegia than for those with tetraplegia. Hence there is a clear hierarchy between subjects with paraplegia and tetraplegia.

In contrast to these points, most studies fail to distinguish between different level SCIs amongst tetraplegics. Dallmeijier (1996) differentiated between tetraplegics with high lesions (C4-C6) and low lesions (C6-C8) . Those with high lesions applied forces less

than half those of the low lesion group (approximately 1.0 N/kg and 2.2 N/kg respectively), and less power (0.16 W/kg and 0.33 W/kg respectively). However, Dallmeijier did observe considerable inter-individual differences that may have overshadowed these conclusions.

In summary, research has shown that in general, a higher SCI corresponds to a decrease in maximum achievable cadence, but an increase in cadence for a given speed. Concurrently, maximum resistive load decreases, as does power output and maximum propulsion velocity. Thus people with higher SCIs are far less able to achieve the same mobility with a manual wheelchair. However, most studies failed to investigate differences in MWC propulsion characteristics for differing level cervical injuries, despite considerable differences in upper body functionality between these injuries.

2.2 Experimental Methodology

As part of his study on wheelchair propulsion in subjects with different level SCIs, Yao (2007) gathered data for the wheelchair propulsion characteristics of subjects with all level SCIs, including 7 individuals with cervical SCIs. This present study continued the data gathering phase of Yao's study for subjects with C5-7 injuries, using the experimental procedure and rig were that developed by Yao (2007) and outlined in this section. Yao's conclusions were mainly based on qualitative observations of the kinematic data; and power and velocity outputs were not calculated for all subjects. The specific methods used for processing the trial data in Yao's study are outlined in section 2.3.

2.2.1 Subjects

The trial involved fifteen subjects with C5-C7 tetraplegia, who were all experienced wheelchair users. Of these, 7 had C7 injuries, 7 had C6 injuries and one a C5 injury. Of the C5-C6 candidates 5 had undergone the TROIDs procedure. All of the C5-C6 candidates had complete injuries, three of the C7 candidates had incomplete injuries.

2.2.2 Test Rig and Equipment

The test rig used was that designed by Yao (2007) and built at the University of Canterbury. The rig is shown in Figure 2.2, it consisted of a steel frame with a plywood deck to which anchors were attached for positioning the wheelchairs' front castor wheels. Two independent steel rollers were positioned on the rig to sit under the axis of the

wheelchair's main wheels, flywheels could be added or removed as required from the rollers' shafts to vary the rotational inertia of the system. Belts attached to the rig and were used to secure the front castor wheels to the anchors on the rig. A ramp was also fitted for access onto the rig. A rotary encoder was coupled to each of the rollers, and the signal (1000 counts per second) from the encoder processed through a PC using Labview. An LED time counter also connected to the PC was positioned so it was visible in the video recordings to enable matching of the visual data with the encoder data.

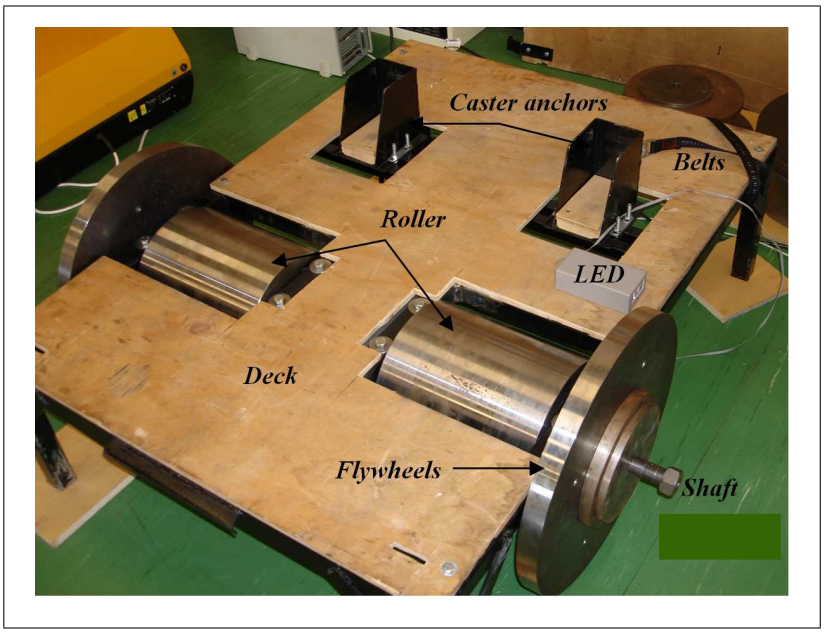

Figure 2.2: Wheelchair test rig

2.2.3 Procedure

All trials were carried out at Burwood Hospital Spinal Unit, Christchurch. Subjects were fully informed of the procedure and gave their informed consent to participate. Each subject was tested in their own chair and they were assisted up a ramp onto the rig where their chair was secured using the belts on the rig. The chair was positioned so the axle of the main wheels was directly over the rollers.

Motion Tracking

Subjects had markers placed on bony landmarks on their wrists, elbows, shoulders, necks and heads for tracking purposes, as shown in Figure 2.3. The markers were

white (non-reflective) square markers with a black dot in the centre. The motion was recorded using a video camera that produced avi files with resolution 320 x 240 pixels at 25 frames per second.

Figure 2.3: Markers

Flywheel Selection

The rotational inertia required in the system to simulate travel on a flat surface was calculated by equating the expressions for linear (KE_{linear}, Equation 2.1) and rotational kinetic energy ($KE_{rotational}$, Equation 2.2). The inertia I was calculated for each roller, where the mass, m, was the half combined weight of the subject and the chair, as the two rollers were independent. Steel flywheels were available in seven sizes; the rotational inertia of each of these flywheels was calculated and recorded. The combination of flywheels for each trial was chosen to ensure the combined inertia of the flywheels, roller and shaft was the closest match possible to the required inertia calculated from Equation (2.3).

$$KE_{linear} = \frac{1}{2}mv^2 \tag{2.1}$$

$$KE_{rotational} = \frac{1}{2}I\omega^2 \tag{2.2}$$

Where: v is the tangential velocity of the wheelchair rim and therefore the roller, and ω is the angular velocity of the roller.

By equating Equations 2.1 and 2.2, and by substitution and simplification, the expression for the total inertia required from the system may be expressed:

$$I = mr^2 \tag{2.3}$$

Where r is the radius of the roller, and $v = \omega r$.

Normal Resistance Test

These tests used the combination of flywheels calculated according to Equation (2.3) to closely model flat smooth-surface conditions. Two tests were performed at this resistance. For the first test, subjects were asked to propel their wheelchairs from rest at a self-selected 'normal, comfortable' effort. For the second test, they were asked to propel their chair from rest to maximum velocity and sustain this velocity for at least 10 seconds once reached. This test was repeated with subjects asked to propel their wheelchairs from rest to a self-selected comfortable speed that they then maintained for at least 10 seconds. The purpose of this test was to simulate everyday wheelchair propulsion at the subject's 'normal' speed.

Coast Down Test

To measure the effect of the system's resistive forces, a 'coast down' test was performed for each subject at normal resistance. For this test the subject accelerated from rest with two pushes, then ceased propulsion and the deceleration of the rollers was recorded.

Double Resistance Test

After the 'normal' resistance tests, a combination of flywheels with an inertia double the value calculated in Equation (2.3) was placed on the system to increase the resistance. Subjects were asked to propel their wheelchairs from rest at maximum effort to maximum velocity, and then to sustain this velocity for at least 10 seconds once reached. The purpose of this test was to investigate the upper capabilities of subjects with different spinal injuries, doubling the inertia of the flywheel system had a similar effect to increasing the incline of the travel surface.

2.3 Kinematic Data Processing

2.3.1 Tracking Algorithm

In Yao's study (2007), although video data was collected, movement patterns were determined by inspection or by measuring the marker's position on only a few video frames. Quantitative data representing the average hand and elbow paths is far more desirable for modelling purposes. To obtain this data, an algorithm was written to automate tracking joint markers from the video frames.

Using MATLAB, frame-by-frame jpeg images were first extracted from the avi file. The initial position of the marker being tracked was selected using the MATLAB function ginput where the operator clicks on the position of the marker in the image. Normalised cross-correlation was then performed between consecutive frames with a small 8-12 pixel square frame centered on the marker position in the first image cross-correlated to a 20-30 pixel square frame centered on the same point, but in the next image. The normalised cross-correlation calculated the movement of the smaller frame in one image to its position within a larger frame in the next image. The size of the larger frame was of the smallest size to encompass the movement of the marker between frames both during the push phase and the recovery phase. The size of the frame was proportional to the maximal speed of the marker being tracked; a larger frame was necessary for tracking the position of the wrist dot, a smaller frame for the elbow, then smaller again for the shoulder. The size of the frame in the first image was chosen to be slightly larger than the approximate marker size.

The success of this method differed between different joint markers and subjects. The algorithm was most successful in cases where the marker was clear for the entire cycle and where movement between frames was small. Even in these cases, tracking was not 100% successful, a slight error in one frame compounded in successive frames until the tracker was following an alternative point or was stationary on a point in the background.

To adjust for such errors, a periodic checking system was developed. As the algorithm ran, a point was plotted in each frame to show the tracking of the marker. Every 10 frames a dialogue box would appear to check on the success of the tracking. The user could then either confirm the success and the tracking algorithm, which would then continue tracking the next 10 frames, or they could opt to return 5 or 10 frames. After going back the selected number of frames, the marker's position was manually selected

using the ginput function for five frames, then the tracking algorithm resumed from the newly selected position.

Marker x-y coordinates in pixels were stored in a matrix for retrieval and plotting after the code was run. In this form, the pixel value is meaningless as the location of the wheelchair in the frame and distance from the camera varied between subjects, and there was no reference in the videos from which the images could be dimensioned. Therefore, all images were dimensioned using the wheel diameter and the location of the axle of the wheel to provide fixed references.

2.3.2 Fitting Representative Curves to the Wrist Stroke Path

For examining the hand path data, each trial was split into two phases: the acceleration phase and the steady-state phase. Most subjects took three pushes to get close to their final speed and start following a consistent hand path. Coordinates for the wrist markers in each frame for the first four push cycles were plotted and smoothed using a cubic smoothing spine to illustrate the changes to the hand path over these accelerating strokes. To determine the typical hand-stroke path for each subject, a single representative curve was fitted to the steady-state data. This single curve normally comprised hand paths from 6-10 push cycles. The first two-three cycles in most trials were excluded from this representative curve when they were distinctly different from the rest of the data, either in their shape, period or both.

The tracked hand path data looped pack over itself with an inconsistent period. Thus, to fit the curve to the data, the data was split into two sets. The first where the hand was moving forward, and the second where it was moving backward. This split was done using a basic algorithm that identified the peaks and troughs in the x values (Figure 2.4) and used these values to split the data. The data where the gradient was positive (hand moving forward) was grouped and sorted in ascending order by the x-coordinate. The data where the gradient was negative (hand moving backwards) was grouped and sorted in descending order by the x-coordinate. These two sorted groups of points were then joined together to produce a matrix of point coordinates.

A smoothing spline was fitted to the ordered matrix of hand coordinate points using the Matlab function csaps. The smoothing parameter for this function was determined individually for each data set to minimise localised oscillations or kinks in the splines

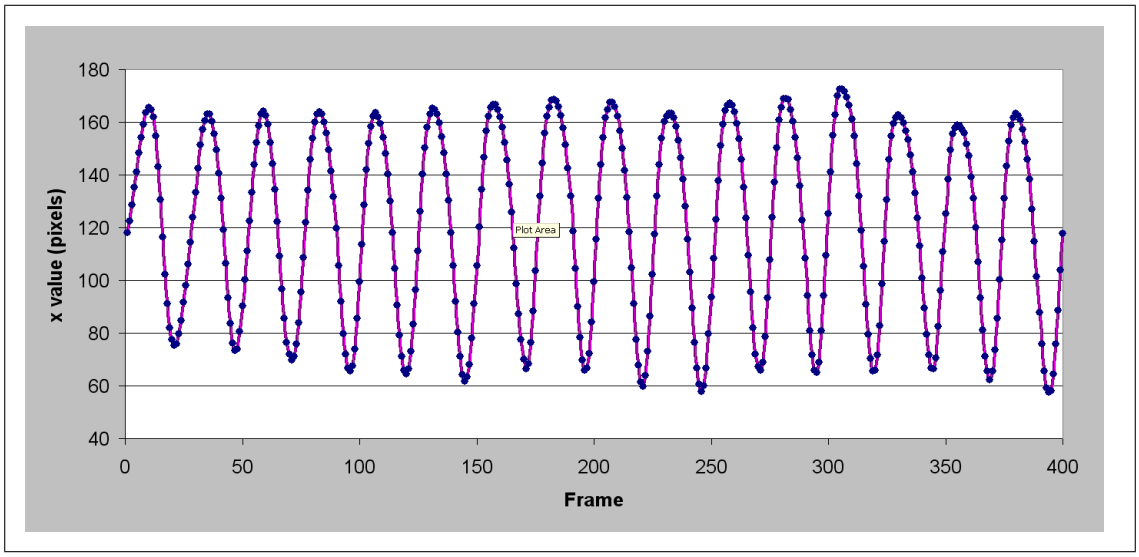

Figure 2.4: Variation of the x coordinate of the hand with time

depending on the shape and spread of each individual's data. The smoothing parameter's value varied between 1 x 10^{-2} and 1 x 10^{-5}.

This smoothing process is demonstrated in Figures (2.5a) to (2.5d). Where the red dots indicate data in the accelerating phase which was ignored in the construction of the spline. The spline was plotted alongside the original data in order to distinguish which curves in the spline were due to data spread and which were characteristics of the hand path. The elbows and shoulders of some subjects were also tracked according to the procedure described above.

2.4 Calculations

2.4.1 Velocity and Acceleration

The encoder was an incremental rotary encoder that had a resolution of 4000 counts per revolution and recorded data at a sample frequency f_s of 1000 Hz. Angular velocity of the roller ω_{roller} was calculated from the encoder data according to Equation 2.4 to (2.6).

$$\omega_{roller} = \frac{\triangle\theta_{roller}}{\triangle t} \tag{2.4}$$

Where $\triangle\theta_{roller}$ is the angular displacement of the roller during the time step $\triangle t$. The angular displacement of the roller can be calculated for each sample period of 0.001s

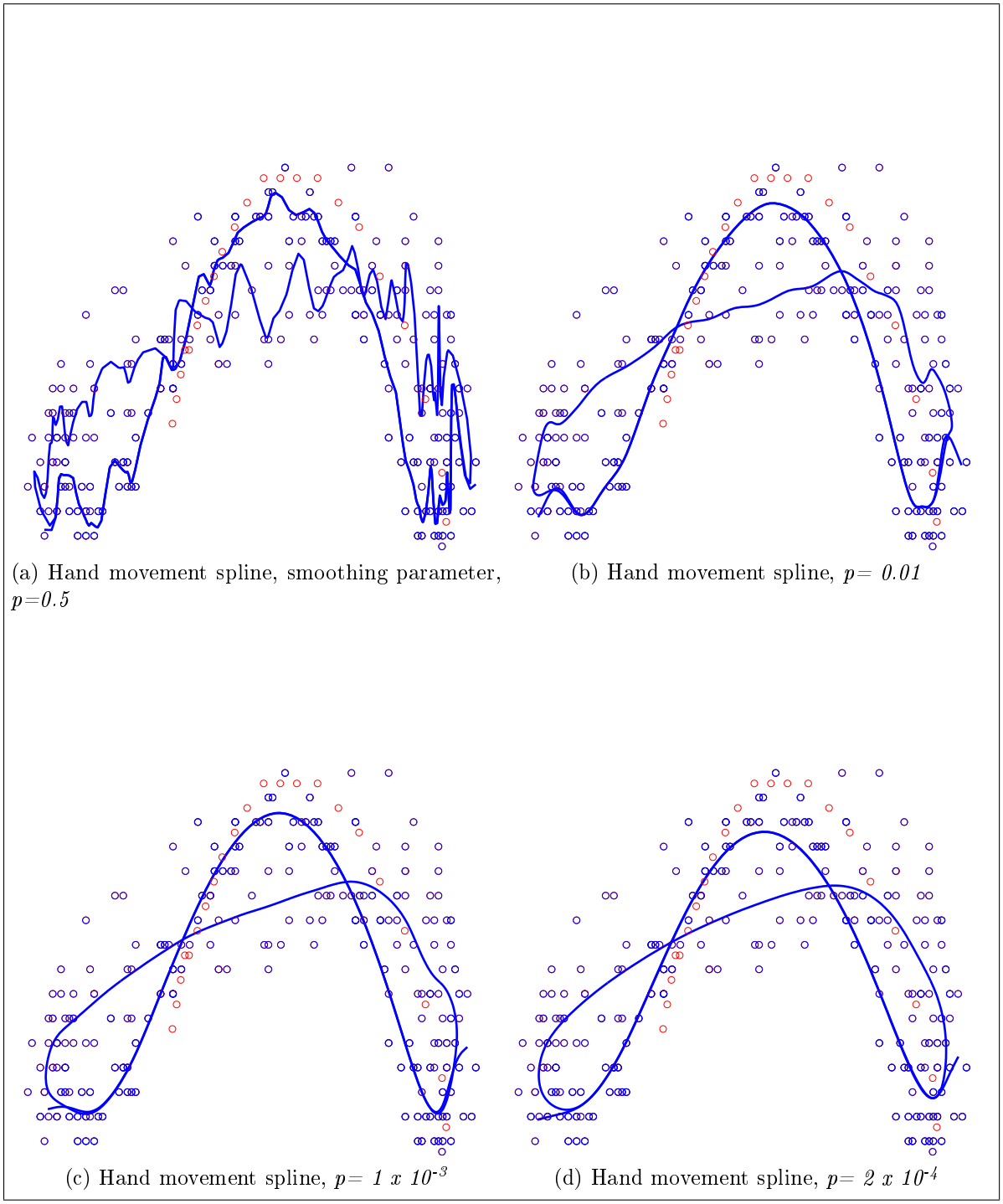

(a) Hand movement spline, smoothing parameter, p=0.5

(b) Hand movement spline, p= 0.01

(c) Hand movement spline, p= 1 x 10^{-3}

(d) Hand movement spline, p= 2 x 10^{-4}

Figure 2.5: Fitting of smoothing spline to tracked hand points

(for a sample rate of 1000 Hz) by multiplying the change in the encoder count by the angular displacement per encoder count, according to Equation 2.5:

$$\triangle\theta_{roller} = (enc_{i+1} - enc_i)\frac{2\pi}{4000} \tag{2.5}$$

Whereenc_{i} is the encoder count at time step i, and enc_{i-1} is the encoder count at the previous time step and $\frac{2\pi}{4000}$is the angular displacement of the roller per encoder count for an encoder having a resolution of 4000 counts per revolution. The angular velocity of the roller can then be expressed:

$$\omega_{roller_i} = 1000(enc_{i+1} - enc_i)\frac{2\pi}{4000} \tag{2.6}$$

Noise was removed from the velocity data by applying a second order low pass Butterworth filter with a normalised cut off frequency between 0.04 and 0.05. Angular acceleration of the roller was calculated from the angular velocity in a similar manner and also passed through a low-pass butterworth filter. The tangential velocity of the wheelchair wheel was then calculated by multiplying the roller angular velocity by the roller radius.

2.4.2 Force, Power and Work Calculations

Rolling Resistance Test

Multiple factors contributed to the resistive forces present in the wheelchair-rig system. Rolling resistance between the tyre and the rollers was a function of the combined mass of the subject and their wheelchair, the position centre of gravity of the subject and their chair, the type of tyres and tubes, and the tyre air pressure. Friction from the bearings in the test rig provided resistance, as well as a small contribution from air resistance. The overall effect of these resistive forces needs to be known to calculate the applied torque.

The combined effect of these forces was approximated using data from the 'coast down' tests. The resistive forces acting on the system were assumed independent of velocity and were calculated from the deceleration measured in the coast down tests. To approximate deceleration, a line was fit to velocity data from the coast down test using linear least squares. These linear models were a good fit to the data, with r-squared values typically >0.995. An example of the least squares fit is shown in figure 2.6. For this subject shown in this figure, coast down tests were performed at two different speeds. In cases where more than one coast down test had been performed, the resistive

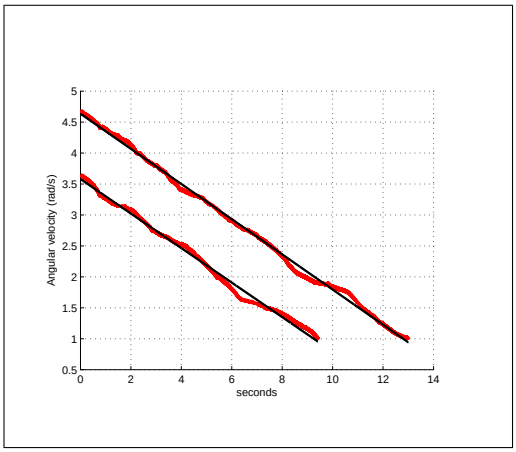

Figure 2.6: Least squares fit to deceleration on coast down tests, used to calculate the coefficient of friction

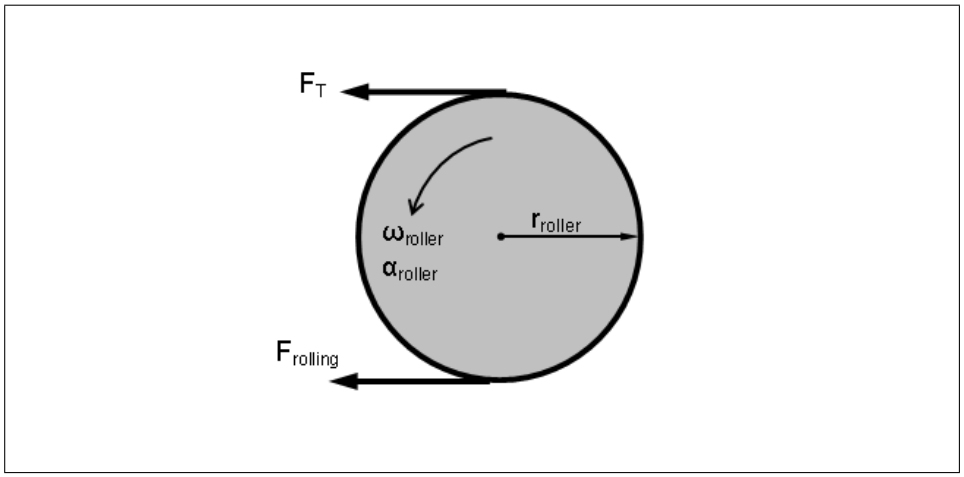

Figure 2.7: Free body diagram showing forces acting on a dynamometer roller

forces calculated from each test were averaged to get a single value for that participant.

Figure(2.7)shows the forces acting on one roller of the dynamometer, where F_T is the tangential force applied to the roller by the wheel. The force applied to the wheelchair wheel by the subject has both a tangential component, and a normal component. It was not possible to calculate the normal component of the applied force from only the encoder data, however assuming no slip between the wheelchair wheel and the roller, the tangential component of the applied force was assumed equal to F_T and calculated according to Equations (2.7) - (2.11) using velocity and acceleration as calculated from the encoder data.

$$T = r_{roller}(F_T - F_{rolling}) \tag{2.7}$$

$$T = I\alpha_{roller} \tag{2.8}$$

Where:

$T =$	The net torque acting on the roller
$I =$	The total inertia of the roller and any attached flywheels
$\alpha_{roller} =$	Roller acceleration
$F_{rolling} =$	Force required to overcome the rolling resistance
$r_{roller} =$	Radius of the dynamometer roller

$F_{rolling}$ can then be calculated by equating Equations (2.7)and (2.8) and setting $F_T = 0$ since there is no applied force during the coast down test:

$$F_T - F_{rolling} = \frac{I\alpha_{roller}}{r_{roller}} \tag{2.9}$$

$$F_{rolling} = \frac{-I\alpha_{coastdown}}{r_{roller}} \tag{2.10}$$

Where α_{roller} = Roller acceleration

The tangential applied force can then be calculated using Equation 2.9:

$$F_T = \frac{I\alpha}{r_{roller}} + F_{rolling} \tag{2.11}$$

Power output P, and work per cycle W, were then calculated from the tangential applied force according to Equations 2.12 to 2.13.

$$W = \int_0^T P dt \tag{2.12}$$

Where:

$$P = I\alpha_{roller}\omega_{roller} + F_{rolling}r_{roller}\omega_{roller} \tag{2.13}$$

Hence, from the encoder outputs, this analysis yields velocity, acceleration, power, work and the tangential component of the applied force.

2.5 Statistical Analysis

A three-way analysis of variance (ANOVA) was performed on the experimental results. The three factors considered were resistance level, injury and stroke number. The statistical analysis was carried out in MATLAB using the function anovan.

2.6 Summary

This chapter presented a test method for measuring wheelchair propulsion characteristics. This method will yield velocity, acceleration, power and work outputs and the tangential component of the applied hand force. Hand motion data will also be collected via the computer vision methods presented. Therefore this method provides the basics for assessing MWC mechanics in a user's own manual wheelchair, in realistic operating conditions, and does so non-invasively.

Chapter 3

Wheelchair Propulsion Study - Results

This chapter presents and discusses the results from the wheelchair propulsion trials described in Chapter 2. Posture and technique observations from the trials are discussed in Section 3.1. After reviewing observed hand paths from existing MWC studies, Section 3.2 then discusses and classifies the hand paths observed in this study and traced using the data processing methods from Chapter 2. Trends in the contact and release angles of the hand paths are explored in Section 3.3.

Section 3.5 summarises the velocity, power, work and force outputs from the trials, and discusses differences between the outputs for subjects with C5-C6 tetraplegia and C7 tetraplegia. Timing characteristics are presented in Section 3.6. For each measured parameter, data from at least the first four push cycles for the maximum velocity trials at both low and high resistances is presented, as this was where the differences between successive strokes and injury levels was most pronounced.

The conclusions from this chapter are later used to aid in developing a hand path comparison model in Chapter 9. Power, velocity and force data from this chapter is used in Chapter 4 to estimate the direction and magnitude of force applied to the wheelchair wheel during propulsion, which was not measured in this study.

3.1 Posture and Technique Observations

3.1.1 Posture

Two distinct posture styles were observed during the propulsion trials. These two postures were termed the 'C' and 'L' postures and were primarily differentiated by the

position of the shoulder. For all subjects in this study with C5-7 tetraplegia, the subject's pelvis was more posteriorly tilted than in a typical able-bodied seated posture. This pelvic tilt is typical for subjects with cervical SCIs (Bolin et al., 2000).

The 'L' posture, shown in Figure 3.1, was characterised by the user sitting back into the chair with their shoulders in line with their spine and behind their pelvis. For the 'C' posture, the subject's spine from their pelvis to shoulders formed a 'C' shape. In this 'C' posture, illustrated in Figure 3.2, the trunk is in contact with the mid-lower chair back but the subject leans forward at their chest. This forward position of the shoulders results in a corresponding forward movement of the subject's centre of mass.

Figure 3.1: Example of a subject sitting with 'L' type posture

For each trial, subjects were classified by the main posture type they adopted for that trial. The results from this classification are given in Tables 3.1 to 3.2. In practice, the difference between the two postures was a continuum and some subjects adopted postures that fell between the two extremes. Where this mix of posture occurred, subjects were classified by the posture closest to that for the steady state phase of the trial. There was also some intra-subject posture variation with resistance and/or acceleration. This variation was also most commonly observed in those subjects whose posture fell between the 'L' and 'C' classifications. Subjects who displayed more than

Figure 3.2: Example of a subject sitting with 'C' type posture

one style tended to move their centre of mass forward for the acceleration phase, by moving their shoulders and head forward, then transition to the more upright state for the stead-state propulsion phase.

Table 3.1: Number of candidates in trials adopting the given positions for steady-state propulsion

SCI Level	**'L' Posture**	**'C' Posture**
C5-C6 (No or pre-TROIDS)	-	2
C5-C6 (post-TROIDS)	4	1
C7	2	4

The leaning back 'L' posture was most common among participants in this study with C5-C6 injuries who had under gone tendon transfer surgery (TROIDS). In an extended study that included data from subjects with SCIs down to the lumbar level, this posture was most common among subjects with SCIs around the fifth and sixth thoracic vertebra (T5 and T6 paraplegia) who could keep their upper body upright and in the plane of the seat back. From observation, subjects adopting a more upright posture also displayed less posterior pelvic tilt. Studies have shown pelvis orientation to influence upper body balance, and upper body posture and balance to influence wheelchair

Table 3.2: Postures adopted by subjects in first three strokes of acceleration phase with double resistance

SCI Level	'L' Posture	'C' Posture
C5-C6 (No or pre-TROIDS)	-	2
C5-C6 (post-TROIDS)	3	2
C7	-	6

propulsion (Bolin et al., 2000; Harms, 1990; Hobson, 1992; Pope et al., 1985).

In each of the two postures described, hand propulsion forces are reacted differently, and due to the changed position of the shoulder, offer the subject different reach envelopes relative to the wheel. In the 'L' posture, the hand force is reacted at the shoulders, against the upper region of the chair back. The force path is from the hand grip, up to the elbows and out through the shoulders. The head is in a neutral position, the line of sight is forward and vision can be over a large range down to looking at the knees without nearing the neck's range of motion limits and straining the muscles. In the 'C' posture, the hand force is reacted lower down the spine, where it contacts with the seat back, the force path is therefore longer than for the 'L' posture. It was hypothesised that due to these differences, a subject's posture would affect their force application patterns and stroke style, this relation is discussed further in Section 3.1.2.

3.1.2 Hand-Wheel contact style

Study participants were categorised according to the method they used to grasp the wheelchair push-rim or wheel. The categories used were the same as in the preliminary study by Yao (2007), shown in Figure 3.3, with the addition of the category 'tyre only' which was a observed for one subject in this study. The results are given in Table 3.3. As for Yao's exploratory study, a wide range of grasp styles were used by subjects within each injury class. Just less than half of the subjects with C5-6 injuries wore gloves while propelling their chairs. Those participants wearing gloves were most likely to use the push rim exclusively during propulsion, but with their hand in the same style as those who used the 'wedge' method, rather than the traditional grasping method.

(a) (b) (c)

Figure 3.3: Different wheel grip techniques (a) wheel rim only (b) tyre and wheel rim (c) 'wedge' method (Yao, 2007)

Table 3.3: Grasp style used in MWC propulsion

SCI Level	**Push Rim Only**	**Tyre Only**	**Tyre and Rim**	**Wedged**
C5-C6 (No or pre-TROIDS)	1	0	0	2
C5-C6 (post-TROIDS)	3	1	0	4
C7	1	0	2	4

The extra friction offered by the glove may have facilitated this propulsion style.

3.2 Hand Paths

3.2.1 Hand Path Classification

Sanderson and Sommer (1985) were the first to classify stroke patterns during wheelchair propulsion. They identified two distinct stroke patterns: 'circular' and 'pumping'. The 'circular' pattern was characterised by the user's wrist following the hand rim, then dropping below the rim for the recovery phase. The pumping style was a shortened stroke in which the subject followed the arc of the push-rim for both the propulsion and recovery phases. These same two stroke patterns were also identified in subsequent studies by Veeger et al. (1989) and Chou et al. (1991). In a larger study with 23 male SCI subjects, including some with cervical injuries, Dallmijer (1994) observed hand movement patterns that fitted neither the 'circular' or 'pumping' characteristics. However, Dallmijer did not classify these other propulsion patterns.

Shimada (1998) observed both the 'circular' style identified by Sanderson and Sommers, and two additional stroke patterns similar to those observed by Dallmijer. Shimada

termed three styles: semi-circular (SC), single looping over propulsion (SLOP), and double looping over propulsion (DLOP). The SC style is that referred to in earlier studies as the 'circular' style, characterised by the subject's hands dropping below the propulsion path during the recovery phase. In SLOP, the hands are lifted over the propulsion path during the recovery phase. In the DLOP pattern the hands are lifted first over the propulsion path, then cross-over and travel under the propulsion path Shimada et al. (1998). Boninger et al. (2002) used Shimada et al.'s classifications, but also observed the 'pumping' motion identified in earlier studies. He re-termed this motion 'arcing' (ARC) defined by the hand following along the push-rim (or the propulsion path) in the recovery phase. These patterns identified by Shimada and Boninger were used in a subsequent study by Richter (2007) and will be used for categorising stroke patterns in this study. Sketches of these four characteristic stroke patterns are given in Figure 3.4.

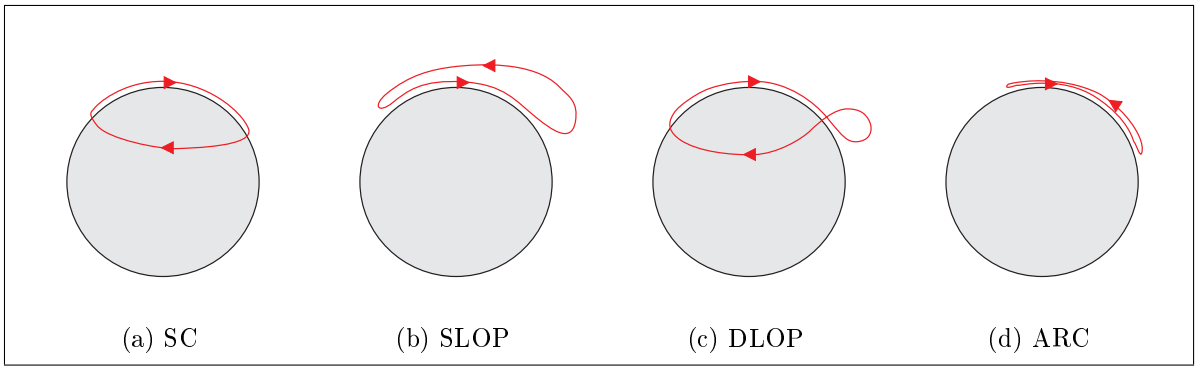

Figure 3.4: Hand path patterns used in Literature (a) Semi-Circular(SC), (b) Single-Looping-Over-Propulsion(SLOP), (c) Double Looping Over Propulsion(DLOP), (d) Arcing(ARC) Shimada98,boninger02

In addition to the four patterns described in the literature, three other propulsion patterns were observed during these experimental trials. First, triple looping over propulsion (TLOP), TLOP was similar to DLOP, but the tracked point moved above the propulsion path a second time before commencing the next stroke. Semi-circular looping over propulsion (SCLOP), was similar to the semi-circular pattern (SC) but, as for TLOP, the hand moves over the propulsion path before commencing the next stroke. Back single looping over propulsion (BSLOP), which was similar to SLOP with the recovery path being above the push path. However, BSLOP was differentiated from SLOP by the distance between the tracked point and the propulsion path being greater at the end of the recovery phase rather than at the start. Sketches of these three additional, new characteristic stroke patterns are given in Figure 3.5.

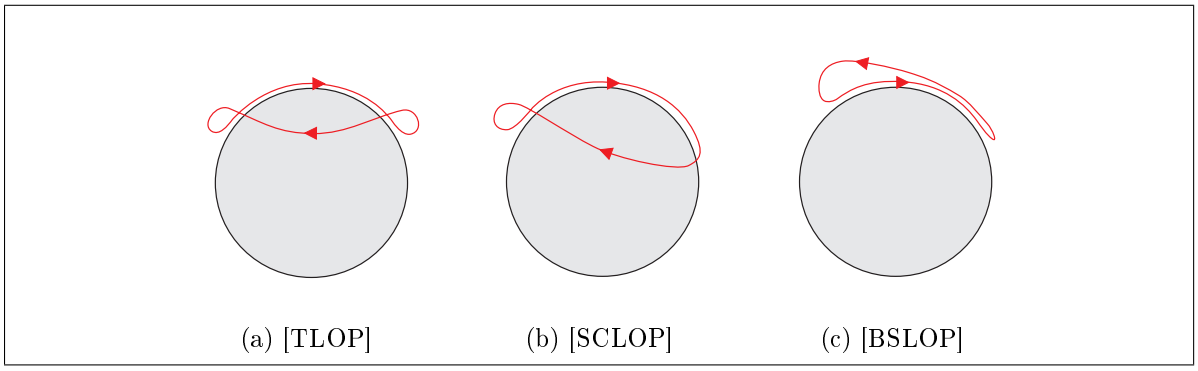

Figure 3.5: Other observed stroke patterns; (a) Triple-Looping-Over-Propulsion(TLOP), (b) Semi-Circular-Looping-Over-Propulsion(SCLOP), (c) Back-Single-Looping-Over-Propulsion(BSLOP)

3.2.2 Hand Paths During the Acceleration Phase

The acceleration phase was defined as the first four propulsion strokes in each trial from rest. Many candidates exhibited different and evolving stroke patterns during these four strokes as they reached their desired speed and stroke style they maintained at constant velocity. Often, only the first one or two strokes were distinctively different from the steady-state characteristics. The difference in hand paths between the accelerating strokes and the steady state paths was more pronounced in maximum velocity trials than for the self-selected normal velocity trials. Hand path selection for the acceleration period in these maximum velocity trials is given in Tables 3.4 to 3.7.

Table 3.4: Stroke pattern types, Push 1 (data includes both normal and double resistance tests)

Injury	BSLOP	SLOP	ARC	SC	SCLOP	TLOP	DLOP
Pre TROIDS C5-6	-	-	1	3	2	-	-
Post TROIDS C5-6	-	-	-	6	3	1	-
C7	-	1	7	1	2	-	1

Table 3.5: Stroke pattern types, Push 2 (data includes both normal and double resistance tests)

Injury	BSLOP	SLOP	ARC	SC	SCLOP	TLOP	DLOP
Pre TROIDS C5-6	-	-	1	3	1	-	-
Post TROIDS C5-6	1	-	1	7	-	1	-
C7	-	4	5	2	2	-	1

Table 3.6: Stroke pattern types, Push 3 (data includes both normal and double resistance tests)

Injury	BSLOP	SLOP	ARC	SC	SCLOP	TLOP	DLOP
Pre TROIDS C5-6	-	-	2	2	2	-	-
Post TROIDS C5-6	-	-	1	7	1	1	-
C7	-	4	3	1	2	-	2

Table 3.7: Stroke pattern types, Push 4 (data includes both normal and double resistance tests)

Injury	BSLOP	SLOP	ARC	SC	SCLOP	TLOP	DLOP
Pre TROIDS C5-6	-	-	1	2	-	1	1
Post TROIDS C5-6	-	-	1	6	-	1	1
C7	1	-	-	6	1	1	1

There were no clear differences between the pre and post TROIDs participants' hand paths. Interestingly, subjects with C5-6 tetraplegia who had undergone the TROIDs procedure displayed the largest range of hand styles across over the acceleration strokes, but also showed the strongest dominance of a single stroke type (SC). There was more variation in hand path styles for all injury levels at normal resistance than at double resistance. The variation in hand cycle paths also increased with progressive push cycles, as the velocity approached the final velocity.

For the first stroke for all resistances, over half of the stroke paths for C5-C6 injured persons was semi-circular (SC) and over half of the stroke paths for C7 candidates were of the arcing (ARC) style. After the first push there was no dominant propulsion pattern for C7 candidates for tests at a normal resistance. For tests at the double resistance, ARC was also the dominant style for C7 candidates for the second push (50%), but this style's dominance reduced to 33% for the third and forth strokes with four other styles each selected in 17% of trials. SC was the dominant hand path at both resistances and for all push strokes during the acceleration phase for subjects with C5-6 tetraplegia. However, the dominance was less at normal resistance and at later push cycles. For example, during the forth push stroke 38% of C5-6 candidates used the SC method at normal resistance, but 80% used it with double resistance. An example of the lengthening of the recovery stroke over the first four pushes is given in

Figure 3.6.

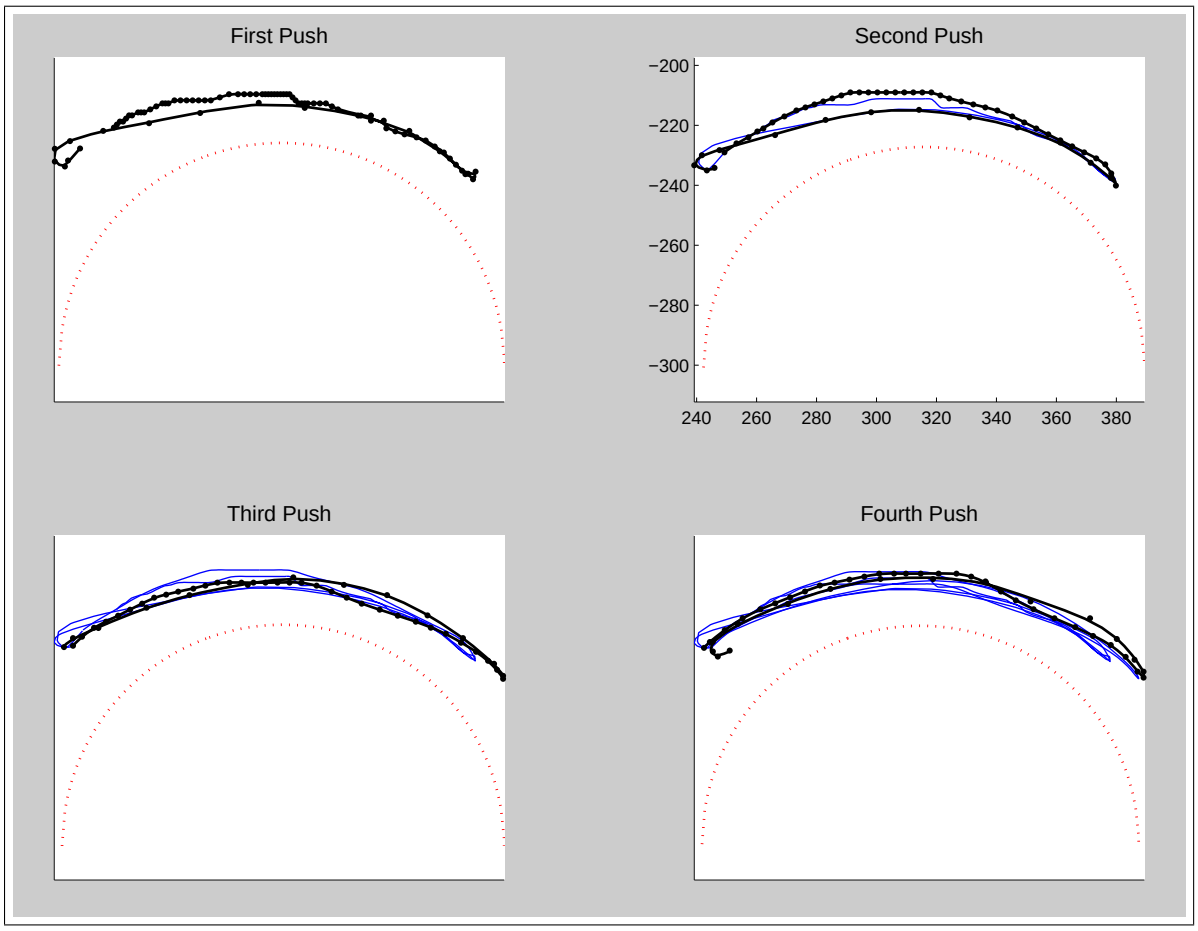

Figure 3.6: Change in the hand stroke path for a subject with C7 tetraplegia over the first four propulsion cycles of a normal resistance trial

The most homogeneity in wheelchair styles was observed during periods of high load, when acceleration, resistance and the subsequent applied force were all high. Subjects with C5-6 tetraplegia adopted the SC pattern and C7 candidates the ARC pattern. The ARC pattern is the pattern with the shortest recovery stroke and the SC pattern is the method with the shortest recovery stroke where the hand is below the push rim. It is plausible that during these times of high load the wheelchair user attempts to minimise the time between consecutive push strokes to minimise any loss of velocity during the recovery phase. It is possible that the path the hand follows changes over long propulsion periods with fatigue, but the periods of propulsion trials in this study were to short to observe any fatigue effects.

Subjects with complete C5-C6 tetraplegia have no triceps use and consequently are unable to easily bring their hand back up over the hand rim, a recovery below the

hand rim enables them to use gravity and their shoulder muscles to return their hand to the beginning of the push stroke. While TROIDs restores some tricep function, from these trials it appears that the functionality gained is not enough to make the ARC style more efficient than the SC stroke. Thus, implying that TROIDs is not useful for mobility.

3.2.3 Constant Velocity Phase

Once a steady-state velocity was reached, the hand path style, shape and size remained consistent for the remainder of the trial for all subjects. Thus, at steady state velocity there was very little intra-individual variation at a given speed and velocity. The consistency of the hand paths is shown by the four examples from subjects in Figure 3.7.

Some subjects' steady-state hand path did change at different speeds or resistances, this variation was largely dependent on the injury level of the subject. Subjects with complete C5-6 tetraplegia pre-TROIDs surgery displayed the most notable variation between speed and resistance levels. All the subjects tested at this level displayed the same type of hand path for all three conditions (normal velocity and resistance, maximum velocity at normal resistance, and maximum velocity at double resistance), but the length of the recovery stroke decreased for each condition. Conversely, none of the subjects with C5-6 tetraplegia who were post-TROIDs displayed any significant variation in their push strokes with these changes in conditions. Figures 3.8 and 3.9 give examples of the variation in the pre-TROIDs subjects and the consistency of the post-TROIDs subjects.

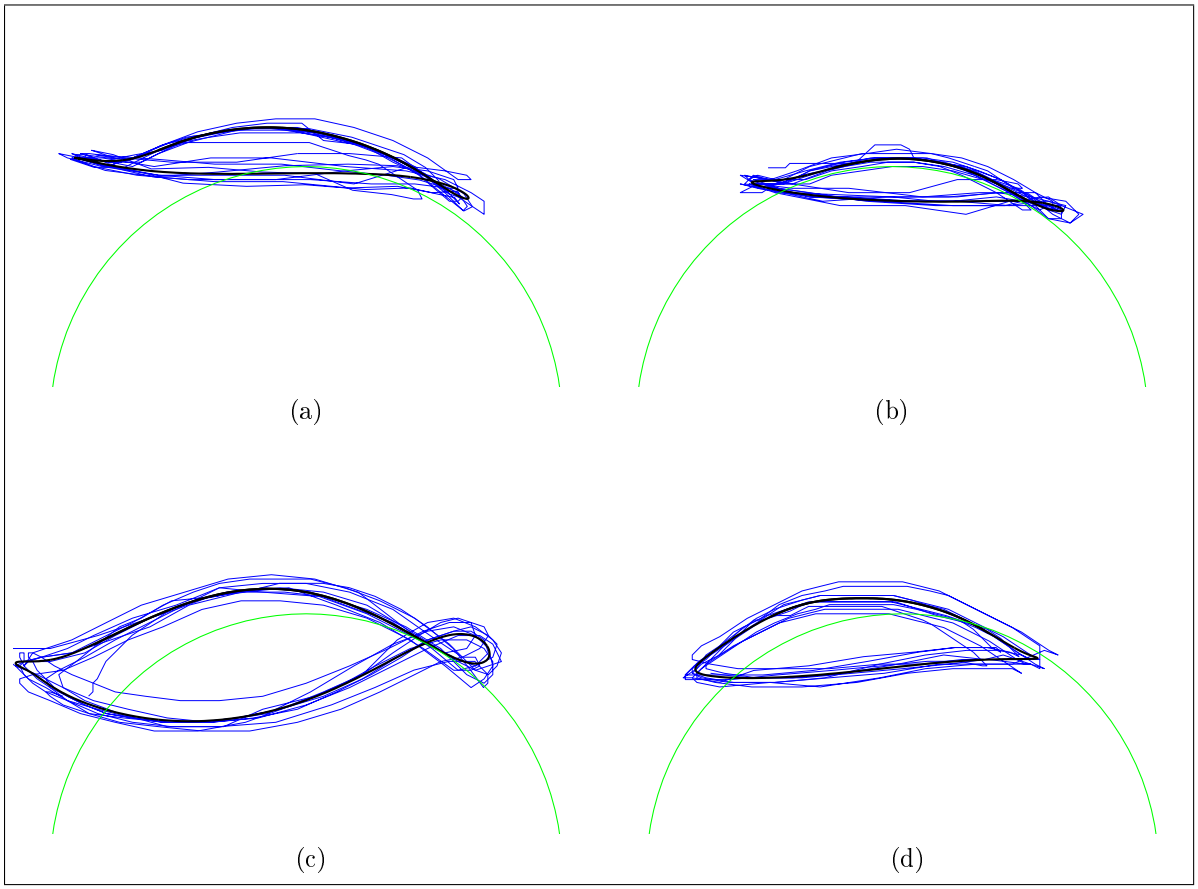

Figure 3.7: Hand paths at constant velocity for four different subjects. The thin blue lines indicate the tracked path from the trials and the bold black lines are the representative curve fitted to the hand path.

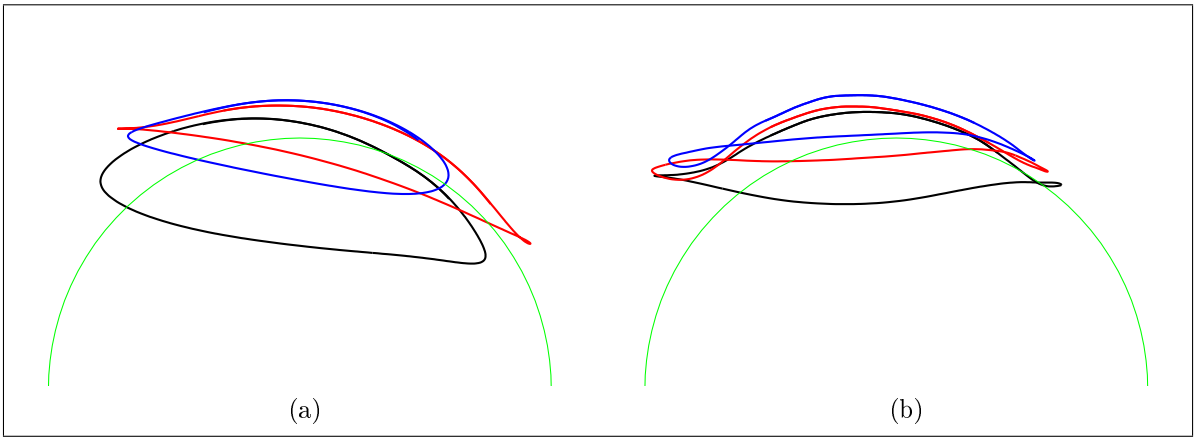

Figure 3.8: Variation in hand path with conditions for two subjects with complete C5-6 tetraplegia who have not undergone the TROIDs procedure.
KEY: Black - normal velocity and resistance, Red - maximum velocity at normal resistance, Blue - maximum velocity at double resistance

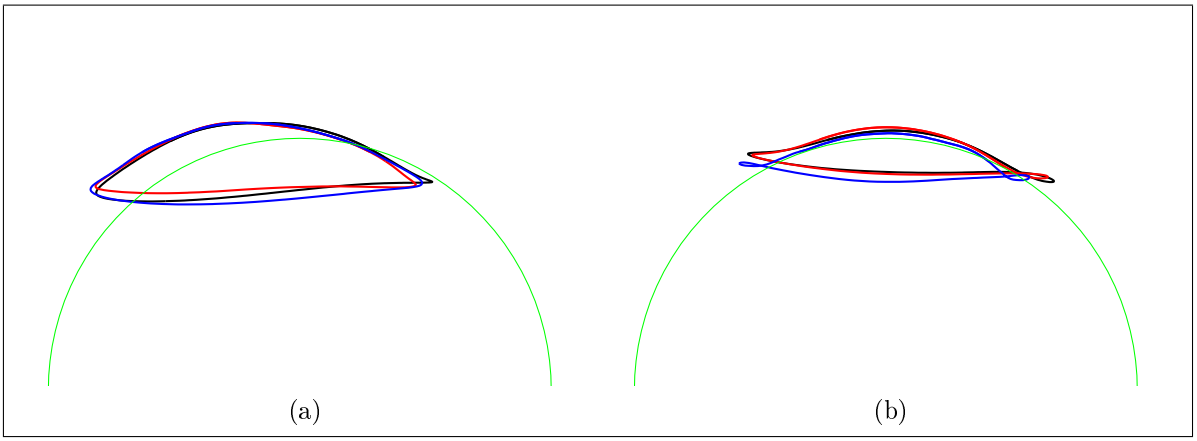

Figure 3.9: Consistency in hand path with different propulsion conditions for two subjects with complete C5-6 tetraplegia who have undergone the TROIDs procedure
KEY: Black - normal velocity and resistance, Red - maximum velocity at normal resistance, Blue - maximum velocity at double resistance

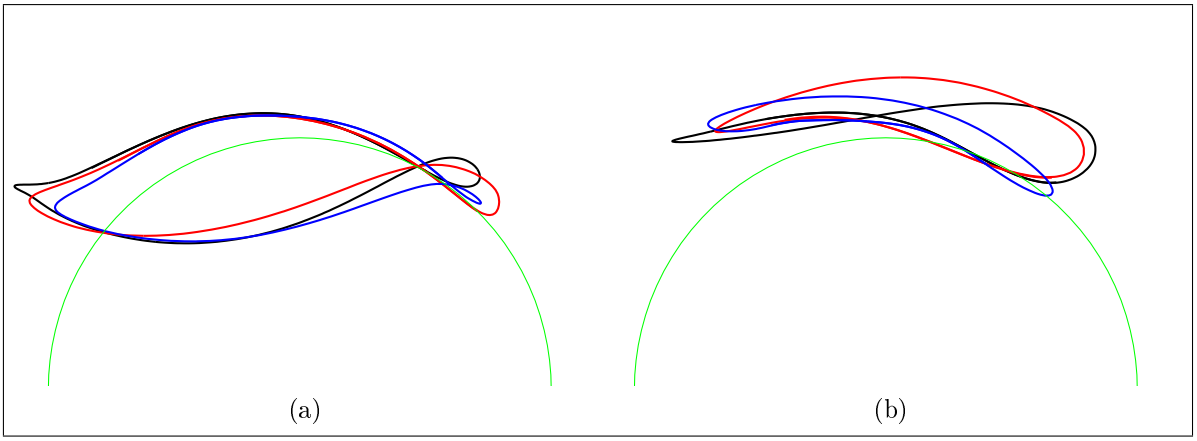

Figure 3.10: Consistency in hand path with different propulsion conditions for two subjects with C7 tetraplegia; (a) this subject displayed the most consistent hand path between trials, while the subject in (b) displayed the most variation in hand paths between conditions
KEY: Black - normal velocity and resistance, Red - maximum velocity at normal resistance, Blue - maximum velocity at double resistance

Some subjects with C7 injuries showed variation in their steady state hand paths over the three conditions, while other participants' hand paths were consistent. Figure 3.10 shows the hand paths for the C7 participants with both the least and the most variation in their hand path over the three conditions. Interestingly, those C7 candidates whose recovery stroke was below the push rim showed consistent hand paths with only subtle changes seen, for example Figure 3.10a, while those with a hand path where the recovery stroke was above the hand rim were more likely to vary their hand path between conditions. The variation in these hand paths was a shortening of the recovery stroke with increasingly demanding conditions. Unlike for the C5-6 pre TROIDs candidates, the length or position of the push stroke didn't vary significantly between conditions for any of the C7 subjects.

3.3 Grab and Release Angles

The mean contact and release angles measured for the first four propulsion cycles under both resistive loads at maximum velocity are given in Tables 3.8 and 3.9. At both resistances, neither contact nor release angles showed any statistically significant difference between C5-6 subjects pre and post TROIDs. However, there was a significant difference ($p<0.05$) in both angles between subjects with C5 or C6 injuries, regardless of surgery status, and C7 candidates. The mean contact angle for the C5-6 subjects was 128°, 8.3° more posterior than the mean for the C7 group. Likewise a similar significant trend was seen in the release angle, with subjects with C5-6 injuries releasing the wheel on average 6.7° earlier than those with C7 injuries. While the push stroke was more posteriorly positioned for the C5-CD6 candidates, there was no significant difference in the total contact arc with variation in injury, resistance or push cycle. A significant difference was found in the release angle with a change in the resistive load. For each injury type, the release point was between 4.5 and 6.2 degrees earlier when the resistive load doubled but no such trend was seen in the grab angle.

3.4 Shoulder and Elbow Paths

Shoulder and elbow markers were tracked for some subjects. Elbow paths, while cyclic, showed few distinctive trends. Shoulder movement patterns were much less cyclic than

Table 3.8: Mean start angles for the first four push cycles at maximum velocity

Injury		**Normal Resistance**	**Double Resistance**	**All trials**
C5-C6 (No or pre-TROIDS)	mean(sd)	129 (5.2)	129 (7.9)	129 (6.6)
	range	*122 - 139*	*115 - 141*	*115 - 141*
C5-C6 (Post TROIDS)	mean(sd)	126 (26.3)	128 (7.7)	127 (8.5)
	range	*103 - 137*	*116 - 140*	*103 - 140*
C5-C6 (All)	mean(sd)	127 (7.9)	128 (7.7)	128 (7.8)
	range	*103 - 139*	*115 - 141*	*103 - 141*
C7	mean(sd)	118* (16.1)	121* (14.0)	119* (15.0)
	range	*82 - 144*	*92 - 142*	*82 - 144*

*Significantly different from mean start angle for C5-6 subjects, $p<0.05$

Table 3.9: Mean release angles for the first four propulsion cycles

Injury		**Normal Resistance**	**Double Resistance**	**All trials**
C5-C6 (No or pre-TROIDS)	mean(sd)	51 (12.0)	57* (7.6)	54 (10.3)
	range	*31 - 61*	*50 - 77*	*31 - 77*
C5-C6 (Post TROIDS)	mean(sd)	53 (9.1)	57* (9.7)	55 (9.6)
	range	*36 - 62*	*41 - 78*	*36 - 78*
C5-C6 (All)	mean(sd)	52 (10.2)	57* (8.9)	55 (9.8)
	range	*31 - 62*	*41 - 78*	*31 - 78*
C7	mean(sd)	45 (4.7)	51* (7.7)	48* (6.9)
	range	*33 - 50*	*39 - 70*	*33 - 70*

*Significantly different from mean release angle for normal resistance, $p<0.05$

the hand or elbow patterns, and normally didn't follow a consistent curve, as illustrated in Figure 3.11. It was concluded that tracking the sagittal position of these points was not going to identify any strong trends and thus was abandoned.

Figure 3.11: Tracked shoulder motion for one subject (with fitted spline)

3.5 Power, Force and Velocity

3.5.1 Velocity

There were clear significant ($p<0.005$) trends in velocity with push stroke, resistance level and injury type. The maximum wheel velocity increased each successive push stroke as the subject accelerated from rest. As expected, velocity was lower for the double resistance trial than for the trial at maximum velocity at normal resistance.

There was no significant difference in velocity characteristics between people with C5-6 injuries pre and post the TROIDs procedure. C7 candidates produced velocities over 50% faster than the C5-6 subjects, regardless of their TROIDS status for the first four push strokes at both resistances. Figure 3.12 illustrates these main trends in maximal velocity for each push cycle.

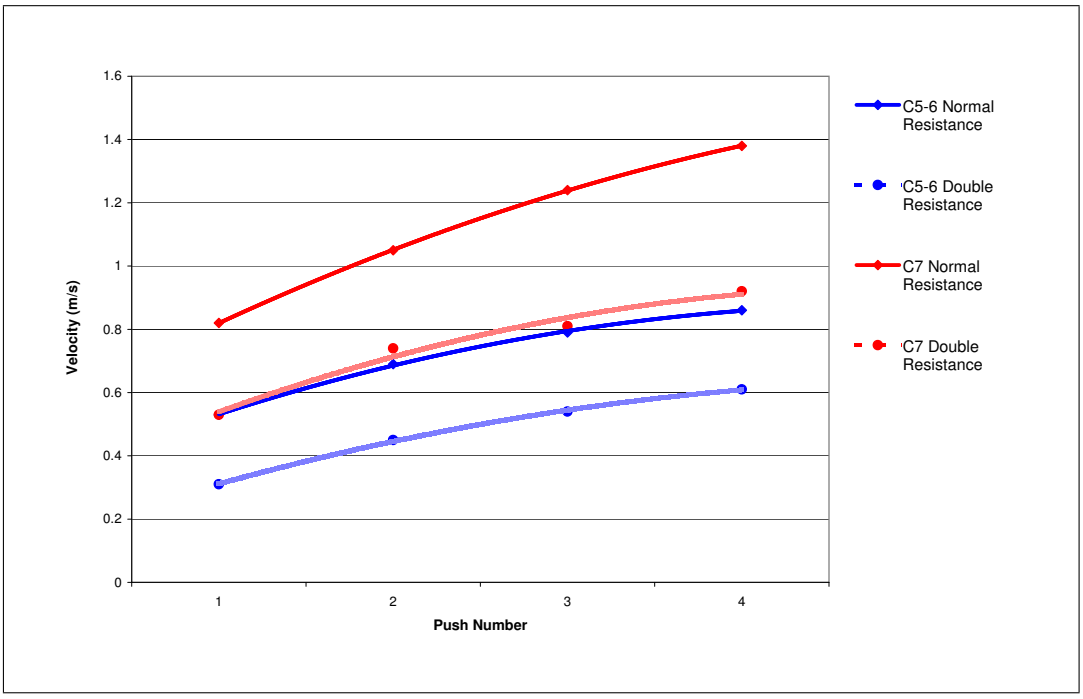

Figure 3.12: Comparison of maximum velocity for the first four push cycles between subjects with C5-6 tetraplegia and those with C7 injuries at both resistances

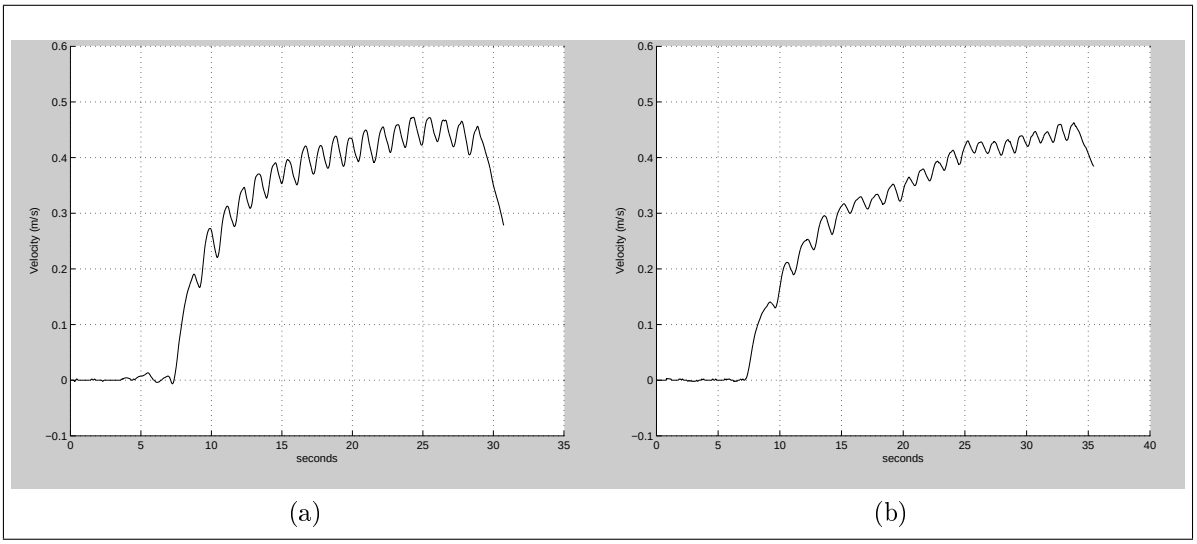

(a) (b)

Figure 3.13: Velocity for a subject with C6 tetraplegia at (a) normal resistance and (b) double resistance

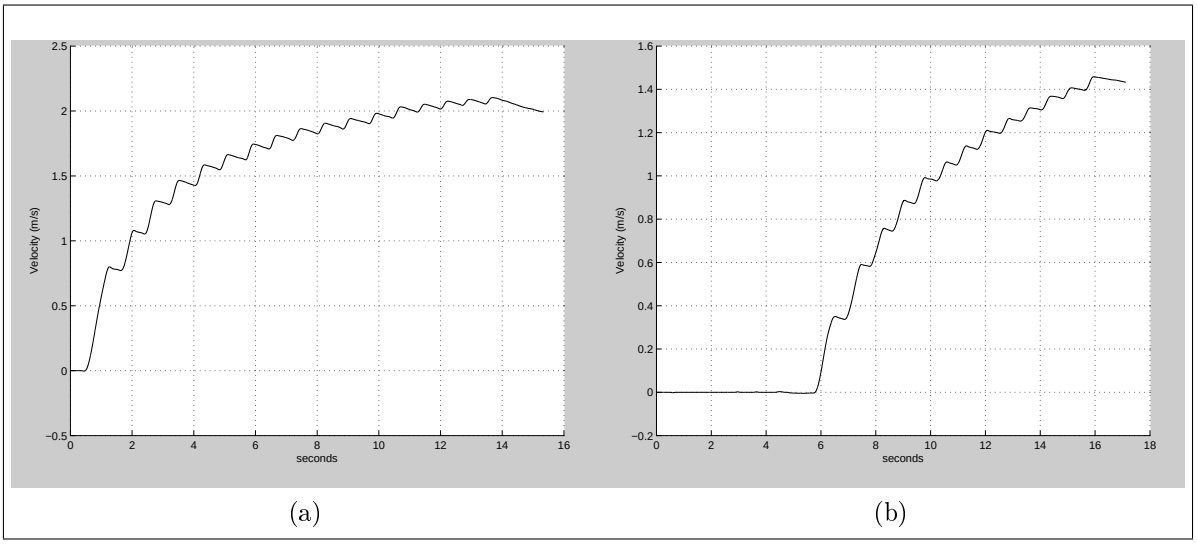

(a) (b)

Figure 3.14: Velocity for a subject with C7 tetraplegia at (a) normal resistance and (b) double resistance

While the most acceleration occurred over the first few push cycles, velocity generally continued to increase for 15-30s depending on the individual. Subjects took longer to reach their desired speed at the higher resistance. Figures 3.13 and 3.14 show examples of velocity profiles and these difference acceleration rates for the trial for a subject with C6 tetraplegia (post TROIDS) and another with C7 tetraplegia. Each peak on the graphs represents the release point of the push cycle; the wheel decelerates as the subject moves their hand to commence the next cycle.

3.5.2 Power

Maximal power output was calculated for each push cycle. Summary data for the first four push cycles is given in Table 3.10. There was no statistically significant difference between maximal power at the different resistances. There was also no significant variation in peak power between successive push cycles.

Subjects with C7 injuries were found to have a considerably higher power output than subjects with C5-C6 injuries under both resistive loading conditions ($p<0.05$). The average for all trials for C7 subjects was $91\,W$, but only $28\,W$, for C5-6 participants. Despite this large difference, there was no difference in peak power before and after the TROIDs procedure.

Table 3.10: Mean maximum power (Watts) for the first four propulsion cycles

Injury		**Normal Resistance**	**Double Resistance**	**All trials**
C5-C6 (No or pre-TROIDS)	mean(sd)	23.8 (13.7)	26.4 (18.6)	25.1 (16.0)
	range	*10.2-49.8*	*2.5-60.0*	*2.5-60.0*
C5-C6 (Post TROIDS)	mean(sd)	37.1 (30.0)	21.0 (16.3)	29.1 (25.2)
	range	*2.6-98.6*	*2.3-58.3*	*2.3-98.6*
C5-C6 (All)	mean(sd)	32.1 (25.7)	23.0 (17.1)	27.6 (22.1)
	range	*2.6-98.6*	*2.3-60.0*	*2.3-98.6*
C7	mean(sd)	91.8* (35.9)	90.4* (89.3)	91.1* (67.4)
	range	*35.9-165.6*	*21.4-359.1*	*21.4-359.1*

*Significantly different from mean power for C5-6 subjects, $p<0.05$

3.5.3 Work

Work done during the push phase of the propulsion cycle, like peak power output and velocity, was greater by subjects with C7 tetraplegia than those with C5 or C6 tetraplegia, regardless of their surgery status ($p<0.05$). This difference was very pronounced, with C7 candidates performing approximately twice as much work per cycle (27 J) than their C5-6 counterparts (12 J). No significant change in work performed was found with variation in resistive load or between successive propulsion cycles, nor was there a difference between those candidates with C5 or C6 tetraplegia who had undergone TROIDS surgery and those who had not. Table 3.11 contains a summary of work performed per propulsion cycle for the trials.

Table 3.11: Mean work (J) performed during the push phase for the first four propulsion cycles

Injury		**Normal Resistance**	**Double Resistance**	**All trials**
C5-C6 (No or pre-TROIDS)	mean(sd)	8.9 (4.0)	13.4 (7.1)	11.1 (6.1)
	range	*3.7-15.4*	*1.7-24.5*	*1.7-24.5*
C5-C6 (Post TROIDS)	mean(sd)	13.2 (11.5)	11.7 (8.5)	12.5 (10.0)
	range	*2.5-49.6*	*3.0-28.6*	*2.5-48.6*
C5-C6 (All)	mean(sd)	11.6 (9.6)	12.4 (7.9)	12.0 (8.7)
	range	*2.5-19.6*	*1.7-28.6*	*1.7-49.6*
C7	mean(sd)	22.2* (11.7)	31.7* (25.6)	26.9* (20.2)
	range	*18.2-63.9*	*12.1-108*	*12.1-108*

*Significantly different from mean work for C5-6 subjects, $p<0.05$

3.5.4 Force

Like for work and power outputs, mean maximum force per stroke was greater for subjects with C7 tetraplegia than those with C5 or C6 tetraplegia ($p<0.05$), and there was no difference among C5-6 subjects with TROIDs surgery status. Peak force was unaffected by the change in resistive load. Compared with the second, third and forth propulsion cycles, mean maximum force was higher for the first push stroke from rest. At $p=0.17$, this difference was not statistically significant at 95% level. However, it is possible that this trend would be stronger with a larger sample size. Table 3.12 gives a summary of the peak tangential forces measured during the first four propulsion cycles at both resistances.

Table 3.12: Mean peak applied tangential force performed (N) for the first four propulsion cycles

Injury		**Normal Resistance**	**Double Resistance**	**All trials**
C5-C6 (No or pre-TROIDS)	mean(sd)	39.8 (15.8)	53.3 (21.2)	46.6 (19.6)
	range	*16.3-65.9*	*25.8-80.1*	*16.3-80.1*
C5-C6 (Post TROIDS)	mean(sd)	52.5 (34.7)	49.0 (18.6)	50.8 (27.5)
	range	*26.5-179.5*	*28.2-85.9*	*26.5-179.5*
C5-C6 (All)	mean(sd)	47.8 (29.4)	50.6 (19.4)	49.2 (24.5)
	range	*16.3-179.5*	*25.8-85.9*	*16.3-179.5*
C7	mean(sd)	96.1* (39.3)	134.5* (110)	115.3* (46.9)
	range	*38.7-163.7*	*53.4-464*	*38.7-464*

*Significantly different from mean work for C5-6 subjects, $p<0.05$

There were also trends in the position where this peak tangential force was applied. Peak force was applied was significantly further back (earlier in the push phase) in the first push stroke than in cycles 2 - 4 ($p<0.05$). There was no significant difference in the position of maximal force application with propulsion cycle after the first push. Nor was there a difference in the location of the peak applied tangential force between resistive loads. Interestingly, this maximal force application point was further back in the push arc for those subjects with C5-6 tetraplegia post TROIDs than both those pre surgery and for the C7 subjects ($p<0.05$). There was no significant difference in force application position between the pre-surgery C5-6 candidates and the C7 candidates. Figures 3.15 to 3.18 give examples of tangential force magnitude for subjects of different injury levels at both resistances.

Subjects with C5-6 tetraplegia commonly exhibited jerky force application at double resistance. However, no subjects with C7 tetraplegia displayed this jerkiness. This may be due to the increased resistance test being closer to the strength limit of the C5-6 subjects and any decrease in cycle time for this group. Triceps are the antagonist pair to the biceps, it may also be that for C7 subjects, who retain some triceps function, the triceps are able to stabilise the biceps motion, contributing to a smoother applied force.

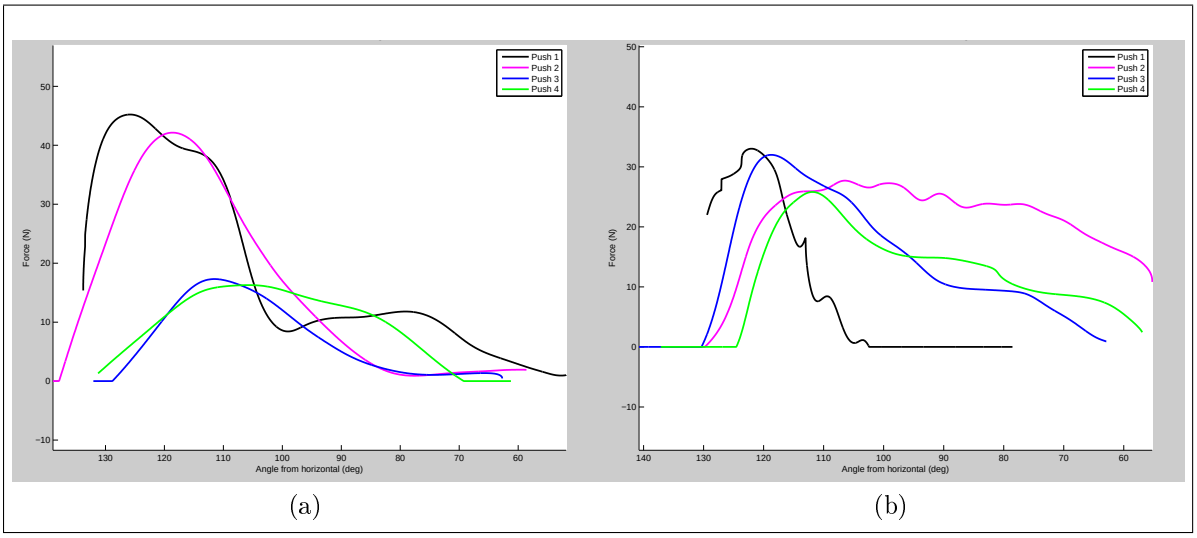

Figure 3.15: Variation in magnitude of applied tangential force for the first four pushes of trials at (a) normal resistance and (b) double resistance for a subject with C6 tetraplegia who has not undergone the TROIDs procedure

A full summary table of results is given in Appendix A.1-A.2

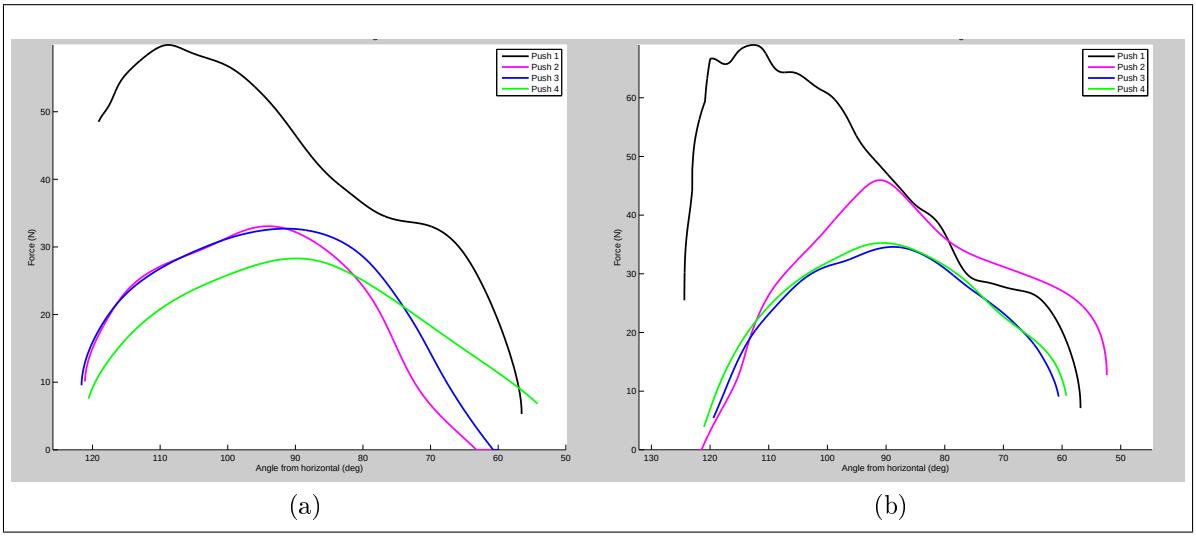

Figure 3.16: Variation in magnitude of applied tangential force for the first four pushes of trials at (a) normal resistance and (b) double resistance for a subject with C5 tetraplegia who has undergone the TROIDs procedure

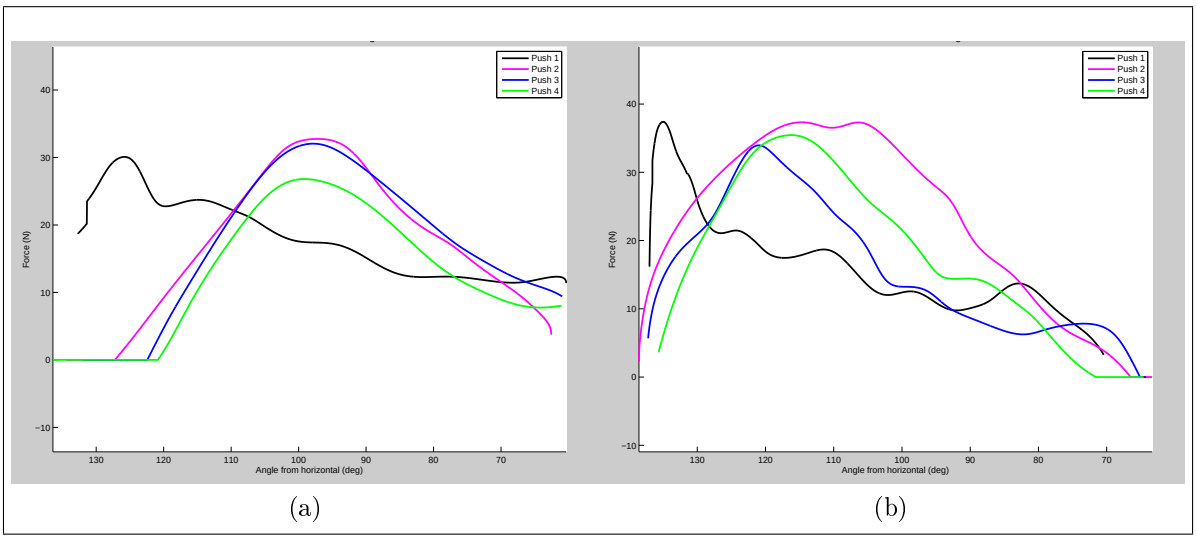

Figure 3.17: Variation in magnitude of applied tangential force for the first four pushes of trials at (a) normal resistance and (b) double resistance for a subject with C6 tetraplegia who has undergone the TROIDs procedure

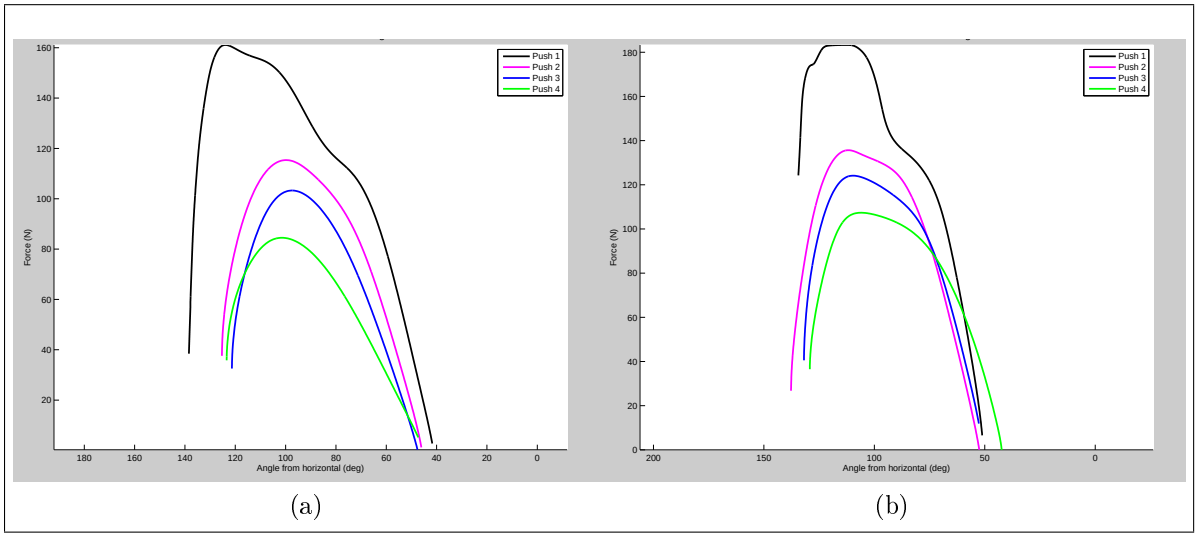

Figure 3.18: Variation in magnitude of applied tangential force for the first four pushes of trials at (a) normal resistance and (b) double resistance for a subject with C7 tetraplegia

3.6 Timing Characteristics

3.6.1 Push Phase Period

The period of the push phase was taken as the time from first applying force to the wheel at the 'grab' point to the release point where the subject commences the recovery stroke. A summary of the push phase periods for the first four pushes is given in Table 3.13. While there was no difference between C5-6 candidates with different TROIDS status, push time for C7 candidates was on average 30-40% shorter ($p<0.05$) than for the C5-6 candidates.

As might be expected, push time was also influenced by resistance ($p<0.05$). For all injury levels the average time at double resistance was 40-50% longer than at normal resistance. The push time for the first push stroke was significantly shorter than for any successive push cycles; on average 50-100% longer than the second push phase and over twice the length of the third and subsequent push phases.

Table 3.13: Mean push-phase period (s) for the first four propulsion cycles

Injury		**Normal Resistance**	**Double Resistance**	**All trials**
C5-C6 (No or pre-TROIDS)	mean(sd)	0.8 (0.38)	1.16$^{\triangle}$ (0.53)	1.00 (0.487)
	range	*0.5-1.65*	*0.64-2.15*	*0.48-2.15*
C5-C6 (Post TROIDS)	mean(sd)	0.72 (0.31)	1.06$^{\triangle}$ (0.46)	0.89 (0.43)
	range	*0.31-1.52*	*0.49-1.95*	*0.31-1.95*
C5-C6 (All)	mean(sd)	0.77 (0.34)	1.09$^{\triangle}$ (0.48)	0.93 (0.45)
	range	*0.31-1.65*	*0.49-2.15*	*0.31-2.15*
C7	mean(sd)	0.49*(0.24)	0.70*$^{\triangle}$ (0.31)	0.60* (0.29)
	range	*0.18-1.04*	*0.26-1.39*	*0.18-1.39*

*Significantly different from mean period for C5-6 subjects, $p<0.05$
$^{\triangle}$ Significantly different from mean period for normal resistance trials, $p<0.05$

3.6.2 Recovery Phase Period

The recovery phase period was taken as the time between consecutive push phases. A summary of the recovery phase periods for the first four pushes is given in Table 3.14. This was the first propulsion characteristic where there was a statistically significant ($p>0.05$) difference between C5-6 candidates before and after TROIDs surgery.

Candidates with C5-C6 tetraplegia who had not undergone tendon surgery showed a longer recovery period between consecutive push-phases than C7 candidates ($p<0.05$). However, the recovery phase periods for candidates with C5-C6 tetraplegia who had undergone surgery were comparable to those of the C7 candidates. Recovery phase time was unaffected by push cycle or resistance.

Table 3.14: Mean recovery-phase period (s) for the first four propulsion cycles

Injury		**Normal Resistance**	**Double Resistance**	**All trials**
C5-C6 (No or pre-TROIDS)	mean(sd)	0.5(0.18)	0.55(0.13)	0.54(0.11)
	range	*0.4-0.71*	*0.34-0.75*	*0.34-0.75*
C5-C6 (Post TROIDS)	mean(sd)	0.38*(0.06)	0.41*(0.06)	0.39*(0.06)
	range	*0.28-0.47*	*0.31-0.51*	*0.28-0.51*
C5-C6 (All)	mean(sd)	0.43(0.11)	0.46(0.11)	0.45(0.11)
	range	*0.28-0.71*	*0.31-0.75*	*0.28-0.75*
C7	mean(sd)	0.40*(0.13)	0.38*(0.11)	0.39*(0.12)
	range	*0.24-0.68*	*0.25-0.57*	*0.24-0.68*

*Significantly different from mean period for C5-6 subjects pre or with no TROIDs, $p<0.05$

3.6.3 Total Cycle Period

Total cycle period was the total time between consecutive push strokes. There was a significant difference ($p<0.05$) in the total cycle period for the first four cycles between all three injury classifications. The total average stroke time across all trials for subjects with C5-C6 tetraplegia post-TROIDs was faster than the average for the pre-TROIDs group, but slower than for the C7 group ($p<0.01$). This difference reflects the results for the push phase periods, in Table 3.15, where post-TROIDs participants behaved like the pre-TROIDs participants and the recovery phase, periods where the post-TROIDs candidates times were comparable to the C7 candidates' times. Average cycle periods are shown with their 95% confidence intervals in Figure 3.19.

Table 3.15: Mean total propulsion cycle period (s) for the first four cycles

Injury		**Normal Resistance**	**Double Resistance**	**All trials**
C5-C6 (No or pre-TROIDS)	mean(sd)	1.29(0.39)	1.70(0.57)	1.49(0.52)
	range	*0.85-2.18*	*0.98-2.62*	*0.85-2.62*
C5-C6 (Post TROIDS)	mean(sd)	1.10(0.33)	1.41(0.39)	1.25(0.39)
	range	*0.65-2.00*	*0.92-2.29*	*0.65-2.29*
C5-C6 (All)	mean(sd)	1.17(0.36)	1.52(0.47)	1.35(0.45)
	range	*0.65-2.18*	*0.92-2.62*	*0.65-2.62*
C7	mean(sd)	0.87(0.25)	1.07(0.34)	0.97(0.32)
	range	*0.42-1.36*	*0.59-1.76*	*0.42-1.76*

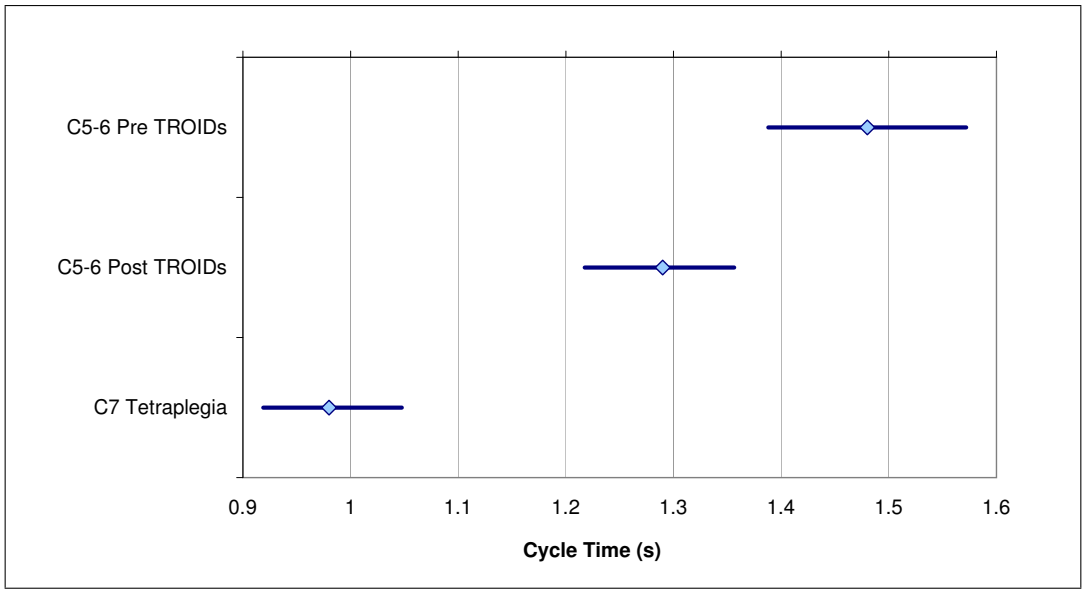

Figure 3.19: Graph showing average push phase duration for the first four push strokes for each injury category, and their associated 95% confidence intervals

3.7 Discussion and Conclusions

3.7.1 Trial Methodology

Data recorded for this study rarely exceeded 30s in length. It was intended that this period would be ample for the subject to accelerate from rest to their final velocity, perform some push cycles at this final velocity. However, trial velocity profiles (e.g. Figures 3.13 and 3.14) show that most subjects took 20-30s for their propulsion velocity to stabilise, and some subjects were still accelerating when their trial was terminated. While this result implies that true steady-state characteristics were not recorded in this study when the velocity didn't stabilise, generally hand path propulsion style, power, force, acceleration and timing characteristics all stabilised and became consistent between strokes once the subject reached 30-40% of their final trial speed. It typically took 4-5 push strokes to reach this speed, but often there were no significant changes in any of these characteristics after only two push cycles. This outcome was also why study of the acceleration phase could be limited to these first four cycles although acceleration continued for cycles past the fourth.

Measuring subjects in their own wheelchairs meant the subjects were more likely to use their actual everyday propulsion techniques. Results from this study show that some characteristics of wheelchair propulsion are posture dependent, likewise Bolin et al. (2000) showed that posture was influenced by wheelchair set up and affected performance. Therefore, other studies that used a generic chair for tests (Dallmeijer and Kappe, 1994; Finley et al., 2004; Kulig et al., 2001; Newsam et al., 1996, 1999; Robertson et al., 1996; Shimada et al., 1998) may have caused the candidates to sit in a way they were not accustomed and consequently adopt a propulsion style that differed from their everyday propulsion style.

Directional applied force was the main component not measured in this study, as instrumented wheels were not used. However, many studies have investigated directional characteristics of applied push rim propulsive forces for a range of SCIs (Ambrosio et al., 2005; Dallmeijer et al., 1998; De Groot et al., 2002; Veeger et al., 1992), and the findings from these studies are discussed in Chapter 4. Observations of different wheel grip methods used by subjects showed that people with C5-7 tetraplegia using the push rim exclusively for propulsion were a minority. Therefore forces measured using instrumented wheels such as the smart wheel may not be reflective of the forces candidates apply during everyday propulsion.

3.7.2 Comparison with Other Studies

Only limited data on wheelchair propulsion characteristics was available in literature suitable for comparison, as few studies that include cervical injured persons in their study also differentiate between subjects with different cervical injuries. Many studies focus only on wheelchair propulsion in persons with paraplegia (Boninger et al., 2002; Koontz et al., 2002). Others state only that the participants were wheelchair users with SCIs, but don't detail the level of their injuries #Robertson96, (Richter et al., 2007; Shimada et al., 1998).

Some studies do compare different level SCIs, but most do this broadly. For example, with and without upper limb impairment (Finley et al., 2004), or cervical (C4-8) compared with high, mid and low thoracic injuries (Dallmeijer and Kappe, 1994). This broad grouping of cervical injuries seems illogical, as there is no impairment of the upper limbs until injuries occur at the cervical level, where as this study has demonstrated, there are significant drops in performance between different level cervical injuries. Indeed, Dallmeijer and Kappe (1994) found no differences in propulsion characteristics between the thoracic and lumbar injury groups, but did find significant differences between these subjects and the cervical injury population.

Though they did not observe it in their study, Dallmeijer and Kappe (1994) theorised that subjects without triceps function would contact the push further back than subjects with active triceps. This would occur so that they could propel the wheel using an upward pulling motion employing their biceps, and the grab angle would move back to accommodate this change in style. This trend was not observed in this study. In fact, there was no significant difference in grab angle between injury groups. While it is true subjects with no triceps would likely produce more force employing a 'pulling' motion, being able to grip the hand rim is a pre-requisite to propelling using this style. However, most subjects with impaired triceps function also have impaired wrist and grip function and are unable to grasp the push rim to pull up.

Hand paths

Dallmeijer and Kappe (1994) has been referenced in some studies (Shimada et al., 1998; Yao, 2007) as observing a difference in hand paths between subjects with cervical and thoracic SCIs. While Dallmeijer and Kappe gave examples of stroke paths from subjects with thoracic lesions that differed from example stroke paths from subjects with cervical injuries, they did not claim these hand paths were typical for those injury categories. Rather Dallmeijer and Kappe (1994) commented that they observed large

inter-individual variation in propulsion technique. Likewise, Vanlandewijck and Daly (2000) and Van der Woude et al. (1988) have been unable to prove different propulsion styles for different injury groups. Thus, results from these studies support the absence of significant trends in hand paths between injury groups and the variability observed in hand paths in this study.

Velocity

The magnitude of velocity, power and timing characteristics is comparable to those measured in other studies. Dallmeijer and Kappe (1994), in a study of 6 candidates with C4-8 injuries, measured an average maximal velocity of 1.68 ms^{-1} for a 30 s sprint test and in their study of candidates propelling at a self selected speed. Newsam et al. (1996) measured velocity for C7 candidates at 1.23 ms^{-1} and C6 candidates at 0.92 ms^{-1}. These values compare well to the 1.51 ms^{-1} average maximum velocity attained for all C5-7 candidates in this study (C5-6 averaged 1.2 ms^{-1} and C7 subjects 1.9 ms^{-1}).

Maximal power was slightly higher in Dallmeijer and Kappe's study (121.8 W) than the average maximal power for the first four push cycles in these trials (91.8 W for C7 and 32.1 W for C5-6). This difference may be partly because Dallmeijer and Kappe (1994) measured each subject's peak power over the whole cycle, which is by definition higher than the average of their peaks. However, it also may be due do the composition of their sample population that encompassed subjects with only minimal arm impairment (C8) to subjects with a very high level of arm impairment (C4), and half of their subjects had only incomplete injuries. Thus, the greater power could have been a skew from subjects with minimal (C8) impairment.

3.7.3 Propulsion Kinetics

Applied tangential force peaked early in the first push stroke for all injury groups regardless of the resistance level when the subject was overcoming the rotational inertia of the system to start propulsion. After this first stroke, the position of peak force varied between subjects. While there was a difference in peak force position between C5-6 candidates pre and post TROIDs, further investigation shows that this difference is more likely to be related to posture, rather than TROIDs surgery status.

Subjects with a more upright or 'L' posture tended to apply their peak force before top-dead-centre (TDC), while subjects whose shoulders were further forward in the 'C' posture applied peak force post TDC. The difference in peak force position between

subjects pre and post TROIDs was due to the differences in postures adopted in these two groups. This posture was unrelated to the TROIDs procedure.

Acceleration characteristics for most subjects showed a small 'wobble' during the recovery phase, rather than remaining constant, as might be expected if there were no external forces acting on the wheel rim. Vanlandewijck et al. (2001) breaks the propulsion cycle into three phases, where the middle phase is acceleration occurring during the first part of the recovery phase. This acceleration is caused by movement of the arms and torso back in preparation for the next push stroke. While this inertial acceleration phase was not recorded in this study due to the chair being stationary, the movement of the centre of mass caused by moving the arms and in some cases the shoulders back, may have influenced the deceleration during the recovery phase accounting for these 'wobbles'.

3.7.4 Increasing Resistance

Aside from the obvious effect of decreasing the velocity attained, increasing resistance also affected the wheel release angle and push phase period, and consequently the total hand contact arc and total cycle time. Those subjects who modified their stroke between resistances tended to bring their recovery path closer to their push path, regardless of if the recovery path was above or below the push rim. Richter et al. (2007) also observed this same change in recovery stroke with an increase in resistance. While moving the recovery stroke closer to the hand rim often shortens the stroke, no significant difference was found in the recovery stroke period between resistances. This outcome suggests modification of the recovery stroke is not primarily to increase cadence, as originally hypothesised, but rather to provide some other benefit of having the hand near the rim for the whole cycle. Richter et al. (2007) suggested keeping the hand near the wheel may be for stability and control reasons, so the subject could quickly regain contact with the wheel in case of significant deceleration or stability issues, particularly when propelling up an incline.

There was no change in wheel grab angle with increased resistance. This result was in line with Vanlandewijck et al.'s observation that users attempt to keep their grab angles consistent with changes in velocity and resistance. Vanlandewijck et al. also suggested subjects tried to maintain the same release angle and push arc with varying velocity and resistance, while others have found the whole push arc shifts forward with an increase in speed (Vanlandewijck et al., 1994; Veeger et al., 1989) and/or resistance (Vanlandewijck et al., 1994; Vanlandewijck and Daly, 2000). Forward shifts are more

common among paraplegic wheelchair users who are able to move their torso forward to attain a stronger downward force. As subjects in this study had either very limited or no torso control, this trend was not observed. The small 4-6° change in release angle and decrease in total push arc may be due to the reduced force capabilities at the end of the stroke. In particular, the increase in resistance may push the required force beyond the subject's capabilities or comfort range.

Some studies have found increasing resistance up to a certain level is accompanied by a corresponding increase in mean power (Lees and Arthur, 1988; Veeger and Van der Helm, 1991). However, no such relation was observed in this study. Peak power was unaffected and there was a small increase in average work per cycle, but this increase was not significant at 95% level. However, it would be expected that at maximum effort, power would be consistent for any resistance within a subject's ability and velocity would change with resistance.

The increased resistance lengthened the push phase period, as velocity decreased, but the contact arc remained consistent or only slightly shortened. This correspondingly increased the total cycle time and decreased cadence. Applied force in the first one or two push strokes for some subjects with C5-6 tetraplegia was jerky. This effect was more common where the push stroke was longer. The jerkiness of the stroke suggests that overcoming the initial resistance for the double resistance trials was something those candidates were unaccustomed to experiencing or was nearing the limits of their capabilities.

3.7.5 Impact of the TROIDs Procedure on MWC Propulsion

The TROIDs procedure anecdotally improves subjects' functional capabilities including their ability to propel a manual wheelchair. Earlier studies have quantified the improvement in shoulder extension strength (Kirsch et al., 1996; Lieber et al., 2003; Woodfield, 1996). However, none specifically examined or quantified the effect of this procedure on wheelchair propulsion characteristics that TROIDs is anecdotally said to improve.

The TROIDs procedure was shown to have no effect on the push phase of the propulsion cycle. In particular, there was no change in power, contact angles or timing characteristics. However, subjects with C5-C6 tetraplegia who had undergone tendon surgery had an average recovery phase period indistinguishable from that of the C7 candidates and longer than for their counterparts without the surgery. This improvement in the

recovery phase period verses those without the surgery was reflected in the average stroke cycles for the two trials at maximum velocity, as this case was where differences between successive strokes and injury levels was most pronounced.

Across all trials for subjects with C5-C6 tetraplegia, post-surgery stroke period was shorter than the average for the pre-surgery group, but slower than for the C7 group. This demonstrated improvement in stroke rate for subjects with C5-C6 tetraplegia post tendon-transfer surgery has clear advantages for wheelchair propulsion. Even if surgery cannot be shown to improve the driving force or maximum power output for a candidate, an improved recovery rate will have the effect of increasing the amount of work a candidate can perform per propulsion cycle.

The TROIDs surgery also allowed subjects to follow a recovery stroke path closer to the push rim at increased velocities and loads, in a similar manner to the subjects in Richter et al.'s study (2007) and some of the C7 candidates in this study. Under gravity loading only, the TROIDs procedure appears to restore functional ability for this motion to that of subjects retaining the use of their triceps. Force requirements on the 'triceps' during the push phase to improve propulsion may be larger than that provided by the TROIDs surgery.

3.8 Summary

This chapter presented the main findings from a wheelchair propulsion study involving 15 subjects with C5-C7 tetraplegia. The study was more comprehensive than other reported studies on MWC propulsion, collecting both wheel kinetic data and kinematic data for the arm through computer vision methods.

As expected, subjects with C7 tetraplegia displayed MWC characteristics significantly different from C5-C6 subjects for almost every metric measured. These differences included higher power output, higher propulsion velocity and an earlier contact angle with the wheel rim. In addition, C7 candidates were more likely to adopt different postures and use different wheel gripping techniques to subjects with C5-C6 tetraplegia.

The group of subjects with C5-6 tetraplegia included 5 subjects who had undergone the TROIDs procedure to restore some elbow extension capability, and 3 who had not. TROIDs has been anecdotally said to improve MWC propulsion. However, no significant differences to support this claim were found for any of the metrics measured for

the push phase of the propulsion cycle.

Differences were observed in the return phase of the propulsion cycle between candidates with and without the surgery. Subjects who had undergone TROIDs recorded return phase periods and hand paths similar to subjects with C7 tetraplegia. This suggests that TROIDs improves functional ability for the return phase, but not the push phase. This may either be a result of the reduced load on the arm for the return phase, or that triceps are employed more in the return phase than in the push phase. This result, and similarly, the negative result for push phase metrics, may be due to the small sample sizes and inter-subject variation. However, they are equally likely to be representative of the populations.

The significant differences found between C5-6 and C7 tetraplegics suggest that data from studies that broadly group different SCIs will be skewed. Thus, data from these studies would not be optimal for designing for a specific SCI population and could result in over or under designing or a device.

Chapter 4

Push Force Application Direction

In the WCP trials in Chapters 2 and 3 hand force application directions were not measured. Forces applied to wheelchair rims have been shown to be non-tangential (de Groot et al., 2005). To model human-wheelchair or mechanism interactions, it is necessary to have a method for predicting the direction of the applied force to produce a known output. This chapter discusses a method for predicting this force application direction for a known driving force, in the case of MWC propulsion, the known tangential force component.

A model developed by Rozendaal et al. (2003) is employed in this chapter, this model and the original parameters are presented in section 4.1. Rozendaal et al.'s model was embedded in a MATLAB algorithm, which is outlined and verified in Section 4.2. This model was originally developed for a person with full upper body functionality and uses constants based on muscle volumes and maximum joint moments. Section 4.3 proposes new constants to modify Rozendaal et al.'s model to be suitable for people with tetraplegia, and investigates the sensitivity of the model to inaccuracies in these constants.

Using this modified model, the magnitude and direction of the applied force during the experimental trials from Chapters 2 and 3 could then be calculated. The model presented in this chapter is later used in the hand force comparison model in Chapter 9.

4.1 Background

Rozendaal et al. (2003) investigated the hypothesis that the direction of the applied propulsion force in manual wheelchair propulsion was a compromise between the me-

chanical task requirements and the driver's biomechanical possibilities. Rozendaal et al. (2003) proposed a biomechanical model for the metabolic 'cost' of applying a force in a given direction, and predicted that forces would be applied to the wheelchair rim at the direction that results in an optimal compromise between the 'cost' C and the mechanical 'effect' E, defined as output power (Equation 4.1). Metabolic cost (Equation (4.2)) was estimated by multiplying the appropriate muscle volume by the joint moments from the applied force, $\underline{F}$, as a fraction of the maximum joint moments. This model approximated manual wheelchair propulsion as a two-dimensional event in the plane of the wheel.

Rozendaal et al. (2003) collected experimental data from nine wheelchair users with paraplegia at different propulsion velocities between 0.83 ms^{-1} and 1.67 ms^{-1} and power outputs of 10-30 W. This experimental data showed the cost-effect model to be in good agreement with measured forces in the middle and final parts of the push phase. Rozendaal et al.'s methods are outlined in Equations (4.1) to (4.5). Constants used in these equations are listed in Table 4.1. Flexion constants were used when the joint moment from $\underline{F}$ was positive and extension constants were used when this moment was negative. A plot of directions of highest effect:cost ratio are given in Figure 4.1 which also shows the experimentally measured results from Rozendaal et al.'s study. A pictorial representation of these results is given in Figure 4.2 as polar plots for each hand position representing the relative magnitude of the cost-effect ratios in different directions.

$$E = r_{ah} \cdot \underline{F}\omega \tag{4.1}$$

$$C = V_s \frac{|r_{sh} \cdot \underline{F} + M_{0,s}|}{M_{max,s}(\phi_s, \omega_s)} + V_e \frac{|r_{eh} \cdot \underline{F} + M_{0,e}|}{M_{max,e}(\phi_e, \omega_e)} + C_0 \tag{4.2}$$

Where r_{sh}, r_{eh}, r_{se}, and r_{ah} are vectors representing the moment arms of the hand force with respect to the shoulder (s), elbow (e), hand (h), and wheel axis (a):

$$r_{sh} = \begin{bmatrix} -(s_y - h_y) \\ (s_x - h_x) \end{bmatrix} \qquad r_{eh} = \begin{bmatrix} -(e_y - h_y) \\ (e_x - h_x) \end{bmatrix}$$

$$r_{se} = \begin{bmatrix} -(s_y - e_y) \\ (s_x - e_x) \end{bmatrix} \qquad r_{ah} = \begin{bmatrix} (a_y - h_y) \\ -(a_x - h_x) \end{bmatrix}$$

And where M_{max} is the joint angle (ϕ) and velocity (ω) dependent maximum joint moment:

$$M_{max}(\phi, \omega) = M_0 \, f_{M\phi}(\phi) \, f_{M\omega}(\omega) \tag{4.3}$$

Where $f_{M\phi}(\phi)$ is a moment-angle factor and $f_{M\omega}(\omega)$ is a moment-angular velocity factor derived by Rozendaal et al. (2003)from curves of maximum power against angular velocity for experienced wheelchair users from Davis and Shephard, 1990:

$$f_{M\omega}(\omega) = \frac{(1 - \frac{\omega}{\omega_{max}})}{(1 - \frac{\omega}{k\omega_{max}})} \tag{4.4}$$

$$f_{M\phi}(\phi) = c_0 + c_1\phi + c_2\phi^2 + c_3\phi^3 \tag{4.5}$$

Where M_0 represents the maximum isometric moment, and V represents the involved muscle volume and $\omega_{max}$is the maximum joint articulation angular velocity.

Table 4.1: Parameter values used in cost-effect calculations(Rozendaal et al., 2003)

	$\mathbf{M_0}$ (Nm)	$\mathbf{c_0}$	$\mathbf{c_1}$ (rad^{-1})	$\mathbf{c_2}$ (rad^{-2})	$\mathbf{c_3}$ (rad^{-3})	ω_{max} $(rads^{-1})$	k	$\boldsymbol{V}$ (l)
Shoulder Extension	79	0.675	0.47	-0.190	0.017	27	0.33	0.36
Shoulder Flexion	52	1.138	-0.2181	0.073	-0.025	30	0.35	0.32
Elbow Extension	43	0.496	0.228	0.215	-0.104	30	0.40	0.17
Elbow Flexion	37	0.706	0.302	0.008	-0.053	30	0.45	0.19

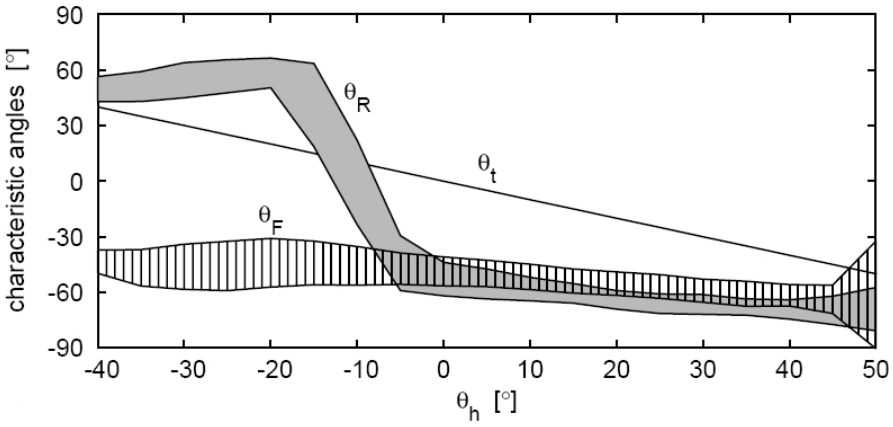

Figure 4.1: Mean direction (± standard deviation) of highest effect:cost (gray band) and mean measured applied force direction (± standard deviation, hashed band) for all subjects, Rozendaal et al. (2003).

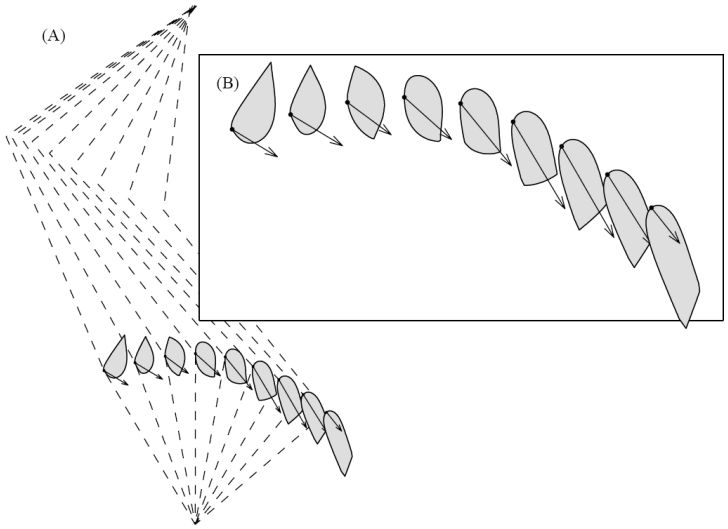

Figure 4.2: Effect-cost contour plots from Rozendaal et al. (2003) for subject moving at 1.39ms^{-1} at 30 W. (A) Broken lines illustrate the arm position and the projection from the hand to the wheel axle, the solid arrow represents the direction and magnitude of the applied force (B) Enlargement of the polar plots.

4.2 Theory and Algorithm Development

Rozendaal et al.'s theory was embedded in a Matlab algorithm to predict the direction and magnitudes of the hand forces for these trials. This section outlines the structure of the code, the verification of the code, and examines the sensitivity of the outputs to changes in the input anthropometrics and kinetics.

4.2.1 Matlab Algorithm

For each hand position during the push cycle, the tangential component of the applied force, F_A, was calculated from the wheel kinetics. This tangential force could have been generated by any applied force with a tangential component equaling the calculated value. These possible sagittal plane (two-dimensional) force vectors that are to produce the required tangential force were calculated in one-degree increments according to Equations (4.6) to (4.8) for angles: $-90 < \theta < 90$.

$$F_A = \frac{F_T}{\cos\theta} \tag{4.6}$$

$$gives \;\; \alpha = \theta + \phi - 90 \tag{4.7}$$

$$\underline{F} = \begin{bmatrix} F_A \cos\alpha \\ F_A \sin\alpha \end{bmatrix} \tag{4.8}$$

The schematic in Figure 4.3 shows the angles and forces used in these calculations. The cost:effect ratio was calculated for each direction using Rozendaal et al.'s equations.

The shoulder-elbow-hand-axle system was modeled as a closed four bar mechanism as shown in Figure 4.4 with the axle-hand link 'driving' the mechanism. Joint angles and velocities were calculated using Equations (4.9) to (4.12) for a four bar mechanism, from Grosjean (1991).

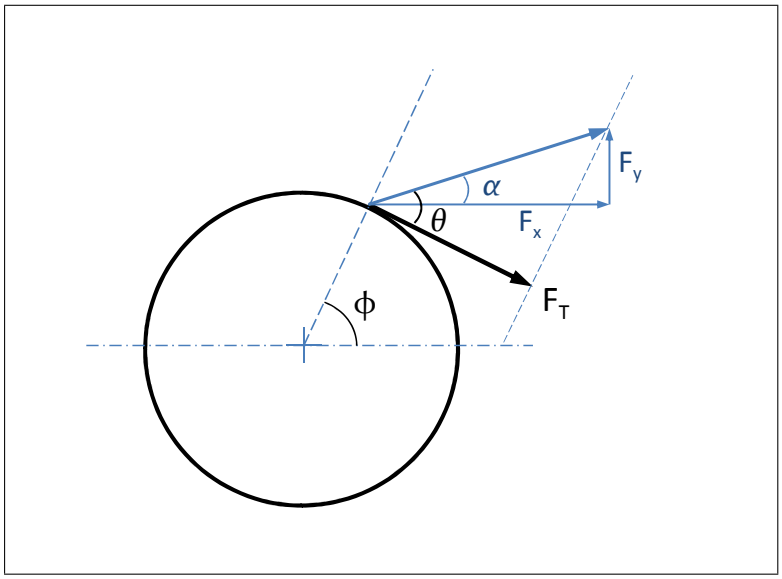

Figure 4.3: Schematic showing angles for applied force calculations

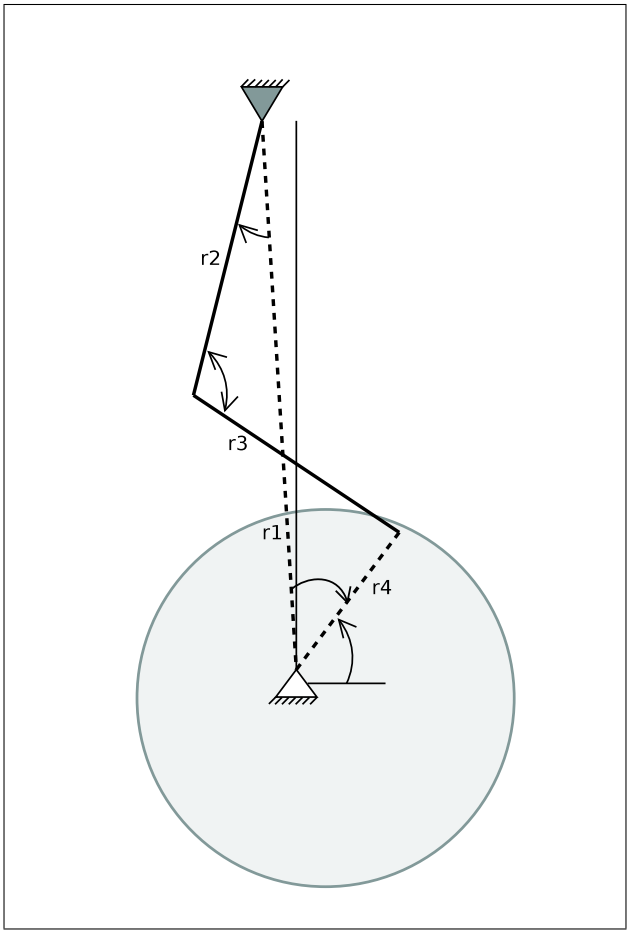

Figure 4.4: Diagram of four bar mechanism used to model arm movement during the wheelchair propulsion push phase

$$\phi = 2\tan^{-1}\left[\frac{A - \sqrt{A^2 + B^2 - C^2}}{B + C}\right] \tag{4.9}$$

where:

$$A = \sin\theta \qquad B = \cos\theta - k_2 \qquad C = k_1\cos\theta - k_3$$

$$k_1 = \frac{r_1}{r_2} \qquad k_2 = \frac{r_1}{r_4} \qquad k_3 = \frac{r_4^2 - r_3^2 + r_2^2 + r_1^2}{2 \cdot r_4 r_2}$$

$$\mu = \cos^{-1}\left[\frac{(r_3^2 + r_2^2) - (r_4^2 + r_1^2) + 2r_4 r_1\cos\theta}{2 \cdot r_3 r_2}\right] \tag{4.10}$$

$$\dot{\psi} = \frac{\sin(\theta - \psi) - k_1\sin\theta}{\sin(\theta - \psi) + k_2\sin\psi}\dot{\theta} \tag{4.11}$$

$$\dot{\mu} = \frac{d\mu}{dt} \tag{4.12}$$

The Matlab algorithm read power and wheel velocity data from an MS Excel spreadsheet and used these values as inputs to the four-bar model. From this input, it was able to calculate cost:effect ratios and predict optimal force application angles according to Equations (4.1) to (4.5).

Anthropometric data was input using the Matlab ginput function with an image of the subject in a stationary position with their hand on the wheel rim prior to trial commencement. Using geometry, the arm dimensions and shoulder position were calculated as a proportion of wheel diameter, and relative to the wheel axle position. To get absolute dimensions these values were scaled using the known wheel diameter. A copy of the Matlab algorithm is included as Appendix B.3.

4.2.2 Verification of Code using Reported Values

A test case with inputs approximating those indicated in Rozendaal et al. (2003) was used to verify the Matlab algorithm. The highest power and velocity situation case

from the study, with power output of 30 W and linear velocity of 1.39 ms^{-1} was used with the stated 0.26 m wheel radius. The shape of the power and velocity input curves were not given in Rozendaal et al. so these were initially modelled as constant. Anthropometric data was estimated using the delft anniman parameters introduced in Chapter 5 for arm length and shoulder height. The shoulder position was assumed to be directly above the wheel.

The inputs for this verification model including the shoulder and angle joint velocities calculated using the four-bar mechanism theory are shown in Figure 4.5. The scale used for push angle varies from that in Rozendaal et al. (2003) to remain consistent with that used in the wheelchair propulsion study in Chapters 2 and 3. Thus, 90° indicates top-dead centre and a push stroke is typically commenced at $\phi > 90$, with the hand typically released at $\phi < 90$. This hand angle reference system varies from Rozendaal et al. (2003), where hand angle is measured clockwise from top-dead-centre.

Polar plots are given in Figure 4.6 for each hand position. The radius of the polar plots indicate the relative cost:effect ratio in that direction. The band of angles with the 90% most optimum cost:effect ratios is given in Figure 4.7 and highlighted in each polar plot.

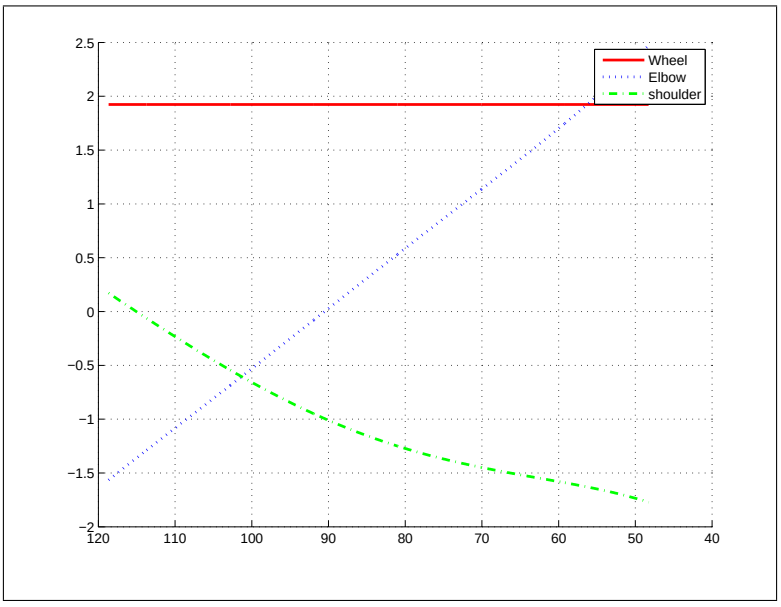

Figure 4.5: Angular velocity inputs for virtual person with flat power and velocity inputs. Elbow and shoulder angular velocities were calculated using the 4-bar mechanism theory outlined above.

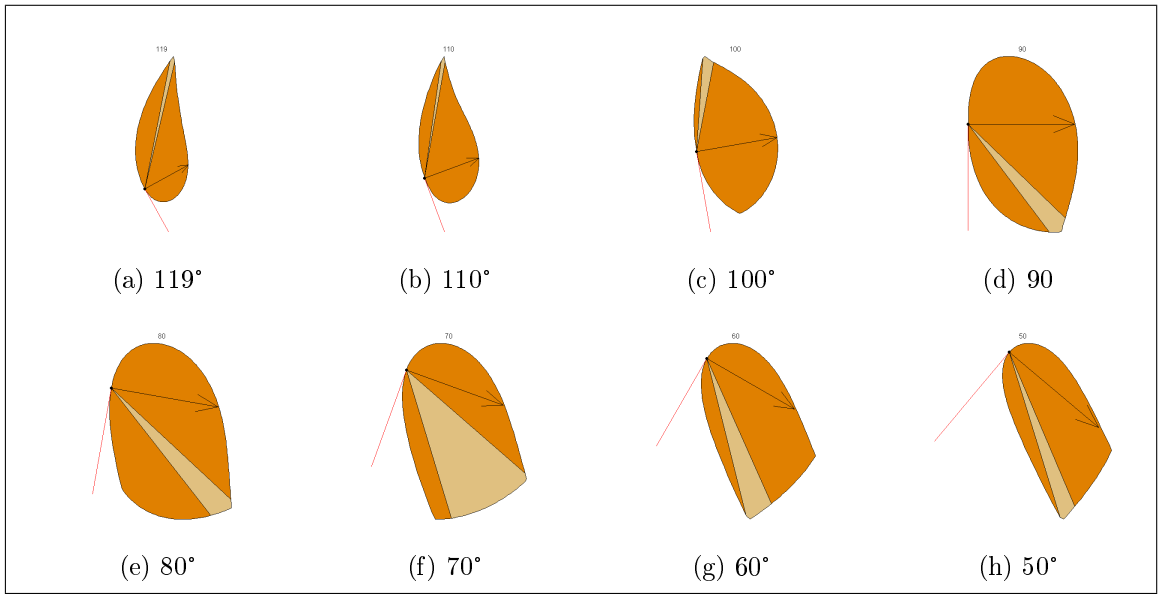

(a) 119° (b) 110° (c) 100° (d) 90

(e) 80° (f) 70° (g) 60° (h) 50°

Figure 4.6: Cost polar plots - Virtual Person with flat velocity and power inputs

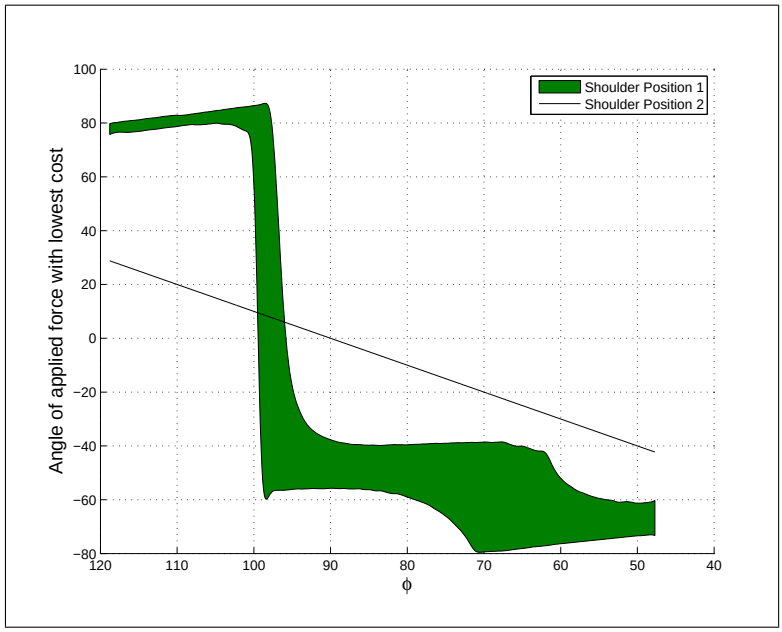

Figure 4.7: Virtual Person with flat velocity and power inputs, shaded band represents directions with an effect:cost over 90% of the maximum

The characteristics of the polar plots are in good agreement with those in Rozendaal et al. (2003), seen in comparison to Figure 4.2. The transition from the optimal applied force being directed upward to downward occurs at the same position as in Rozendaal et al.'s study. However, the transition is steeper and shows a wider region of optimal force at 70°. These differences are likely due to differences in input velocities, power, anthropometrics and due to assuming no movement of the shoulder during propulsion.

4.2.3 Effect of varying input kinetics

A subject with C7 tetraplegia retains at least partial use of both their triceps and biceps, and are thus most like the paraplegic candidates used in Rozendaal et al.'s study. Hence, the velocity and power profiles for the sixth propulsion cycle from a C7 candidate's trial were used as inputs to the Matlab algorithm along with the subject's anthropometric data and wheelchair dimensions. Figure 4.8 shows the wheel angular velocity and the corresponding elbow and shoulder velocity inputs. The characteristic force application angle curves and accompanying polar plots are given in Figures 4.9 and 4.10.

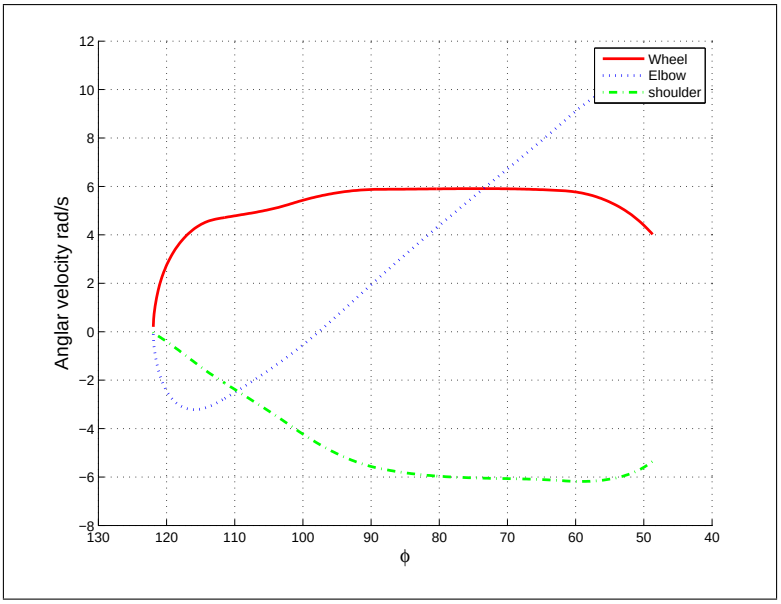

Figure 4.8: Angular velocity inputs for a C7 candidate at normal resistance. Elbow and shoulder angular velocities were calculated using 4-bar mechanism theory outlined above.

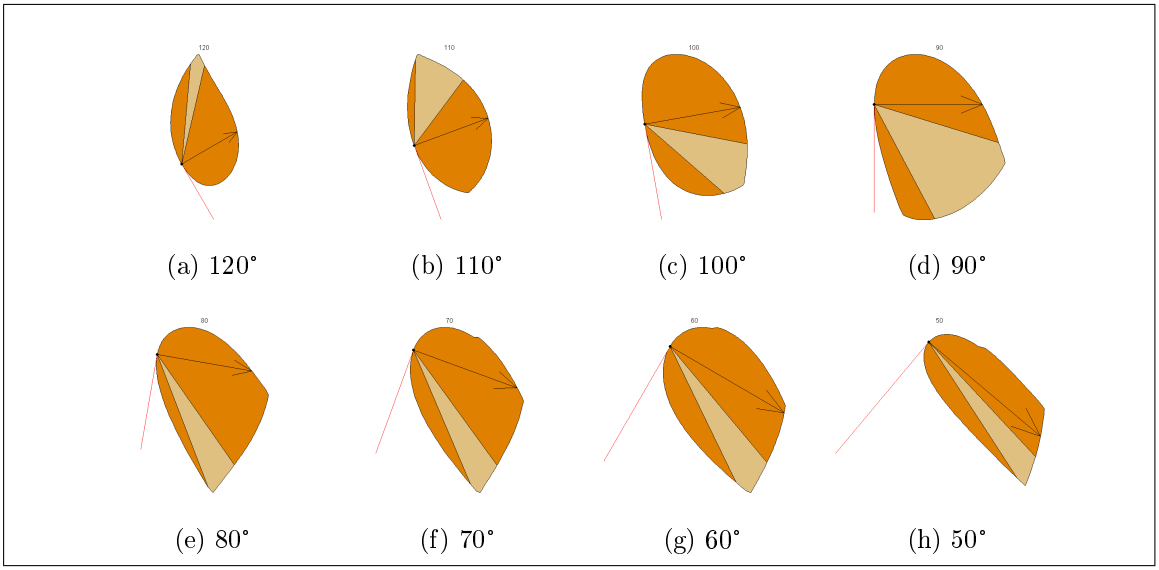

(a) 120˚ (b) 110˚ (c) 100˚ (d) 90˚

(e) 80˚ (f) 70˚ (g) 60˚ (h) 50˚

Figure 4.9: Cost polar plots - C7 candidate, push 6

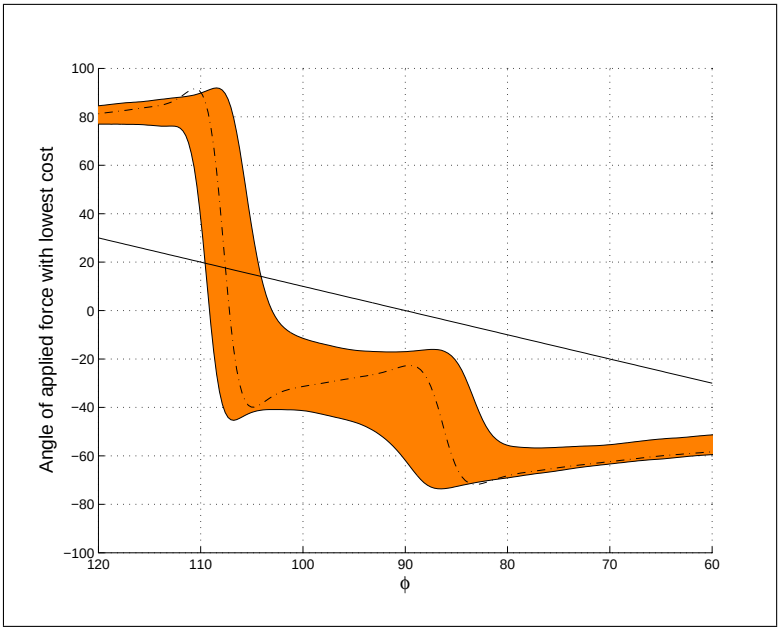

Figure 4.10: C7 Candidate, push 6 (normal resistance). Direction of applied force with highest effect:cost (broken line), shaded band represents directions with an effect:cost over 90% of the maximum

4.2.4 Effect of shoulder position

As the exact location of the subjects' shoulders in Rozendaal et al.'s study was unknown, the sensitivity of the optimum force application angle curve to changes in shoulder position were investigated. The algorithm was run for several shoulder positions, as shown in Figure 4.11. These positions range from 100 mm behind the wheel axis to directly over the wheel axis, and then to 100 mm forward of the wheel axis. They are repeated for two different shoulder heights. The results of these simulations are shown in Figure 4.12.

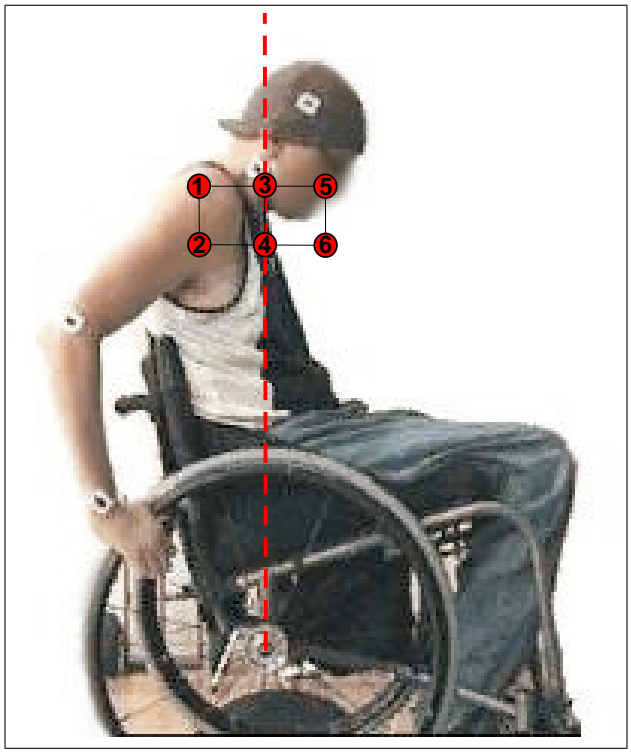

Figure 4.11: Shoulder Position Variations (1) Original shoulder position, 100 mm behind axle; (2) shoulder lowered by 100 mm; (3) and (4) shoulder directly above wheel axle; (5) and (6) Shoulder 100mm forward of wheel axle

Movement of the shoulder forward or downwards resulted in the optimal force direction stepwise characteristic moving forward. The optimal force application direction curve was higher for the lower shoulder position, where the elbow angle is more acute. If the subjects in Rozendaal et al.'s study moved their shoulders or torso forward as the stroke progressed, this difference in curves between shoulder positions may also partly explain the more gradual transition in Rozendaal et al. (2003), which is also evident in Figure 4.12. The curves for the lower positions were also nearer to the tangential

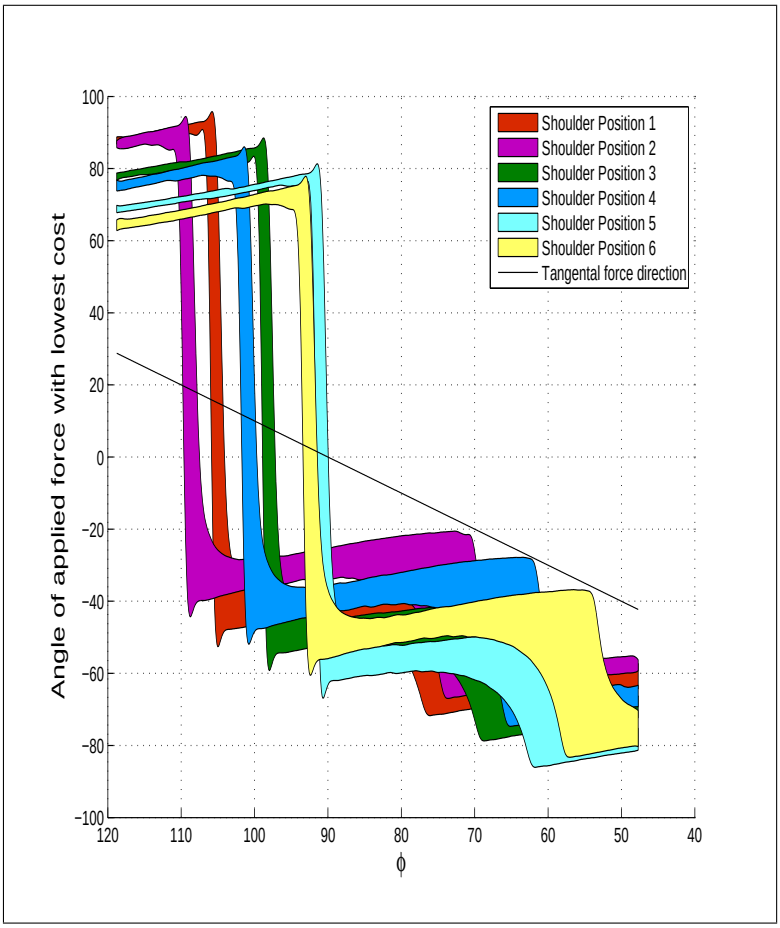

Figure 4.12: Effect of changes in shoulder position relative to the wheel axis on optimum force application angle (band of 98th percentile most optimal force)

direction, suggesting a lower shoulder position resulted in a propulsive stroke where the physiologically optimal direction was nearer the mechanically optimal direction.

4.3 Prediction of Force Application Direction

4.3.1 Modification of Constants for Persons with Tetraplegia

The constants from Rozendaal et al. (2003) in Table 4.1 assume full function in the upper body. This assumption is not valid for subjects with tetraplegia. The differences in capabilities is especially pronounced for those with complete C5 or C6 tetraplegia who have no elbow extension capability against gravity. Therefore, an algorithm using these originally reported constants is unlikely to give an accurate prediction of applied force directions in these populations. Hence, this section proposes new values for these constants for subjects with complete C5-C7 tetraplegia using muscle volume data from studies in the literature.

Rozendaal et al. (2003) used 'involved muscle volumes' for each of elbow and shoulder flexion and extension. These articulation muscle volumes were based on data from Veeger et al. (1991; 1997). These two sources list individual muscle volumes, rather than the total volume for each articulation. However, no description was given by Rozendaal et al. (2003) indicating the method for converting this individual muscle volume information to total articulation muscle volumes.

Hence, two likely approaches were considered. First, one can use the volume of only the primary muscle for each articulation, for example the biceps in elbow flexion. Second, one can sum the volumes of all the muscles involved in the articulation. Neither of these approaches gave muscle volumes similar to those quoted by Rozendaal et al. (2003) for any of the four articulations. The 'active' proportion of each muscle for the articulations was also unknown and other studies in the literature indicated that this value was complex and dependent on joint angles. Therefore, an alternative approach was required.

Total muscle volumes for each articulation were calculated by summing the individual volumes of all the muscles involved in the articulation. This value was calculated for able bodied subjects, then for complete C5, C6 and C7 injured persons using information on typical muscular functionality for each of these injuries, and spinal innervation data for the involved muscles from Kendall et al. (2005).

For muscles whose use was impaired, the active muscle volume was decreased by a factor dependent on the number of the spinal segments from which that muscle's major innervation was spread, and the position of the injury with respect to these innervation

Table 4.2: Joint articulations, associated muscles and their volumes

Articulation	**Involved Muscles** (Kendall et al., 2005)	**Muscle Volume (mL)**
Shoulder Extension	Latissimus Dorsi	217.6 (Veeger et al., 1991)
	Teres Major	85.7(Veeger et al., 1991)
	Pectoralis major lower	100* (Veeger et al., 1991)
	Deltoid - posterior	99** (Veeger et al., 1991)
Shoulder Flexion	Pectoralis major upper	100* (Veeger et al., 1991)
	Deltoid - anterior	99** (Veeger et al., 1991)
	Coracobrachialis	34.4 (Veeger et al., 1991)
	Biceps	114.1 (Veeger et al., 1991)
Elbow Extension	Triceps	379 (Veeger et al., 1997)
	Anconeus	11 (Veeger et al., 1997)
Elbow Flexion	Biceps	114.1 (Veeger et al., 1991)
	Brachialis	122 (Veeger et al., 1997)
	Brachioradialis	66 (Veeger et al., 1997)

* These muscle volumes were estimated from the value in Veeger et al. (1991) for the Deltoideus (297 mL). The Deltoideus contains three main parts; the posterior, lateral and anterior parts

** These muscle volumes were estimated from the value in Veeger et al. (1991) for the Pectorialis Major (199.8 mL).

points. Where a muscle was typically completely paralysed, the active muscle volume was assumed zero. For example, the Latissimus Dorsi used in shoulder extension is primarily innervated from the C6, C7 and C8 spinal segments. These three innervation points were assumed to each control an equal muscle volume. As all of these innervations are below the C5 level, someone with a complete C5 SCI would have no use of the Latissimus Dorsi, and therefore an 'active' muscle volume of 0 mL. A subject with a complete injury at the C6 level would only have use of the parts of the muscle innervated from the C6 segment, assumed to be one-third of the muscle. Likewise, a subject with a C7 injury would have use of the parts of the muscle innervated from the C6 and C7 segments, in this case 66.7% of the Latissimus Dorsi. Only an SCI subject with an injury below C8 would have complete use, and therefore full active muscle volume, of the Latissimus Dorsi.

While this was a simplistic way of estimating muscle volumes for the different SCI groups, there is no consensus in literature as to what parts of each muscle are supplied by each nerve. Similarly, the muscle volumes innervated by these nerve groups are not reported. Note that even if more accurate data were available, it is doubtful whether the improvement in accuracy of the overall model would be greater than the variation in these values between subjects due to inter-individual muscle variation within each

injury classification. Hence, this approach and approximation were assumed sufficient for purposes of this research.

Calculated muscle volumes for the different articulations and injuries are given in Tables 4.3 to 4.6. These values were then used to calculate articulation muscle volumes for each injury group as a proportion of the able-bodied muscle volume. These proportions are given in Table 4.7 and were then used to scale the relevant articulation constants used in Rozendaal et al. (2003) for each injury group. Maximal joint moments were scaled from the original moments in Table 4.1 in proportion to the decrease in active muscle volume for that articulation.

Table 4.3: Muscles used in **shoulder extension** and the degree of muscle use for different injury populations

	Volume	**C5**		**C6**		**C7**	
Muscle	**(mL)**	**Use**	**Volume**	**Use**	**Volume**	**Use**	**Volume**
Latissimus Dorsi	156.0	P	0	I	52.0 (33%)	I	104.0 (67%)
Teres Major	61.4	I	20.5 (33%)	I	40.9 (67%)	N	61.4
Pectoralis major lower	71.7	P	0	I	17.9 (25%)	I	35.9 (50%)
Deltoid (posterior)	71.0	I	35.5 (50%)	N	71.0	N	71.0
Total (mL)	360		56.0		181.9		272.3

P=Paralysed, I=Impaired, N=Normal Use

Table 4.4: Muscles used in **shoulder flexion** and the degree of muscle use for different injury populations

	Volume	**C5**		**C6**		**C7**	
Muscle	**(mL)**	**Use**	**Volume**	**Use**	**Volume**	**Use**	**Volume**
Pectoralis major upper	92.1	I	30.7 (33%)	I	61.4 (67%)	N	92.1
Deltoid (anterior)	91.2	I	45.6 (50%)	N	91.2	N	91.2
Coracobrachialis	31.7	P	0	I	15.8 (50%)	N	31.7
Biceps	105.1	I	52.5 (50%)	N	105.1	N	105.1
Total (mL)	320		128.8		273.5		320

P=Paralysed, I=Impaired, N=Normal Use

Table 4.5: Mussels used in **elbow extension** and the degree of muscle use for different injury populations

	Volume	**C5**		**C6**		**C7**	
Muscle	**(mL)**	**Use**	**Volume**	**Use**	**Volume**	**Use**	**Volume**
Triceps	165.2	P	0	P	0	I	82.6 (50%)
Anconeus	4.8	P	0	P	0	I	2.4 (50%)
Total (mL)	170		0		0		85.0

P=Paralysed, I=Impaired, N=Normal Use

Table 4.6: Mussels used in **elbow flexion** and the degree of muscle use for different injury populations

	Volume	**C5**		**C6**		**C7**	
Muscle	**(mL)**	**Use**	**Volume**	**Use**	**Volume**	**Use**	**Volume**
Biceps	71.8	I	35.9 (50%)	N	71.8	N	71.8
Brachialis	76.7	I	38.35 (50%)	N	76.7	N	76.7
Brachioradialis	41.5	I	20.75 (50%)	N	41.5	N	41.5
Total (mL)	190		95		190		190

P=Paralysed, I=Impaired, N=Normal Use

Table 4.7: Involved muscle volumes for the four articulations as a percent of the able bodied values given in Rozendaal et al. (2003)

	C5	**C6**	**C7**
Shoulder Extension	15.6 %	50.5 %	75.6 %
Shoulder Flexion	40.3 %	85.5 %	100.0 %
Elbow Extension	0 %	0 %	50.0 %
Elbow Flexion	50.0 %	100.0 %	100.0 %

Fukunaga et al. (2001) found a linear relationship between muscle volume and torque for elbow extension and flexion. Muscle volume and cross-sectional area has also been widely shown to be strongly correlated to strength and joint moment (Bruce et al. (1997), Maughan et al. (1983), Young (1985), Ikai and Fukunaga (1968)). Therefore, where total muscle articulation volume had decreased by $n\%$, the maximal moment (M_0) was also decreased by $n\%$. Revised constants for use with the equations from Rozendaal et al. (2003) for the injury groups complete C5, C6 and C7 tetraplegia are given in Tables 4.8 to 4.10.

Table 4.8: Parameter values used in cost-effect calculations: **C5 Tetraplegia**

	$\mathbf{M_0}$ (Nm)	$\mathbf{c_0}$	$\mathbf{c_1}$	$\mathbf{c_2}$	$\mathbf{c_3}$	ω_{max} $(rads^{-1})$	k	$\boldsymbol{V}$ (l)
Shoulder Extension	12.3	0.675	0.47	-0.190	0.017	27	0.33	0.06
Shoulder Flexion	21.0	1.138	-0.2181	0.073	-0.025	30	0.35	0.13
Elbow Extension	0	0.496	0.228	0.215	-0.104	30	0.40	0.00
Elbow Flexion	18.5	0.706	0.302	0.008	-0.053	30	0.45	0.10

Table 4.9: Parameter values used in cost-effect calculations: **C6 Tetraplegia**

	$\mathbf{M_0}$ (Nm)	$\mathbf{c_0}$	$\mathbf{c_1}$	$\mathbf{c_2}$	$\mathbf{c_3}$	ω_{max} $(rads^{-1})$	k	$\boldsymbol{V}$ (l)
Shoulder Extension	39.9	0.675	0.47	-0.190	0.017	27	0.33	0.18
Shoulder Flexion	44.5	1.138	-0.2181	0.073	-0.025	30	0.35	0.27
Elbow Extension	0	0.496	0.228	0.215	-0.104	30	0.40	0.00
Elbow Flexion	37	0.706	0.302	0.008	-0.053	30	0.45	0.19

Table 4.10: Parameter values used in cost-effect calculations: **C7 Tetraplegia**

	$\mathbf{M_0}$ (Nm)	$\mathbf{c_0}$	$\mathbf{c_1}$	$\mathbf{c_2}$	$\mathbf{c_3}$	ω_{max} $(rads^{-1})$	k	$\boldsymbol{V}$ (l)
Shoulder Extension	59.7	0.675	0.47	-0.190	0.017	27	0.33	0.27
Shoulder Flexion	52	1.138	-0.2181	0.073	-0.025	30	0.35	0.32
Elbow Extension	21.5	0.496	0.228	0.215	-0.104	30	0.40	0.09
Elbow Flexion	37	0.706	0.302	0.008	-0.053	30	0.45	0.19

4.3.2 Prediction of Forces from Propulsion Study

Force application directions were predicted for subjects with C5, C6 and C7 tetraplegia. They were calculated using the kinetics measured in the sixth push stroke of the wheelchair propulsion trials at normal resistance and the modified constants from Tables 4.8 to 4.10. The inputs and results for these simulations are given in Figures 4.13 to 4.21.

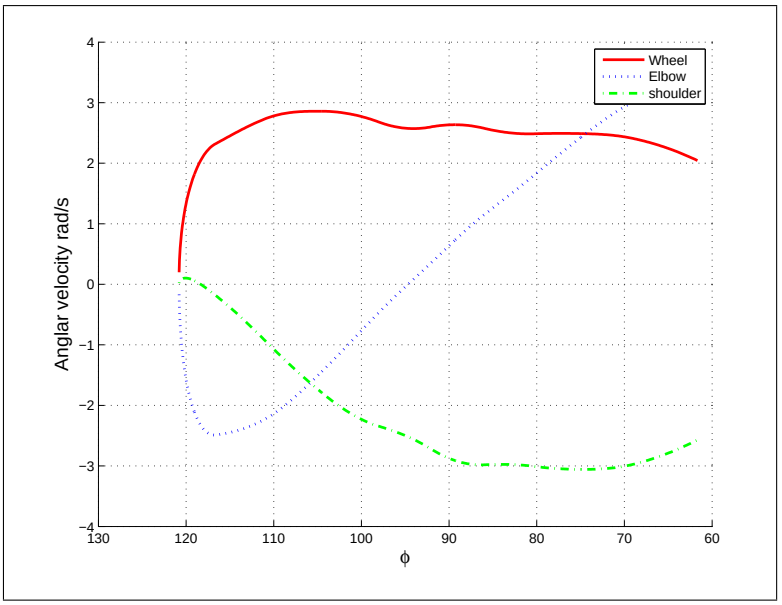

Figure 4.13: Angular velocity inputs for subject with C5 injury at normal resistance. Elbow and shoulder angular velocities were calculated using 4-bar mechanism theory outlined above.

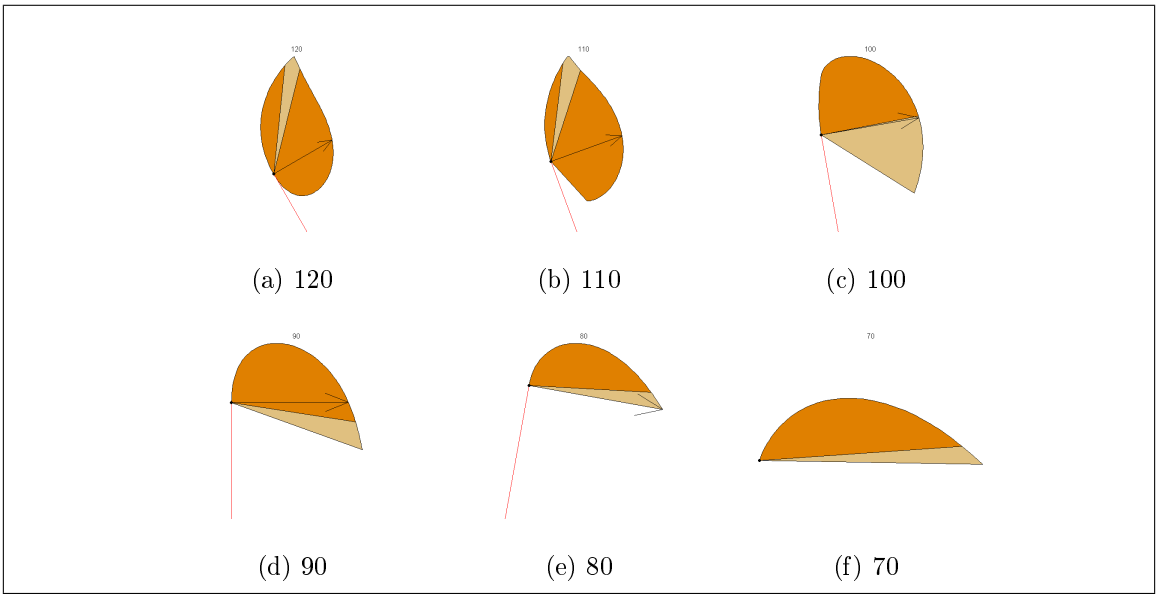

(a) 120 (b) 110 (c) 100

(d) 90 (e) 80 (f) 70

Figure 4.14: Cost polar plots - Subject with C5 tetraplegia, push 6

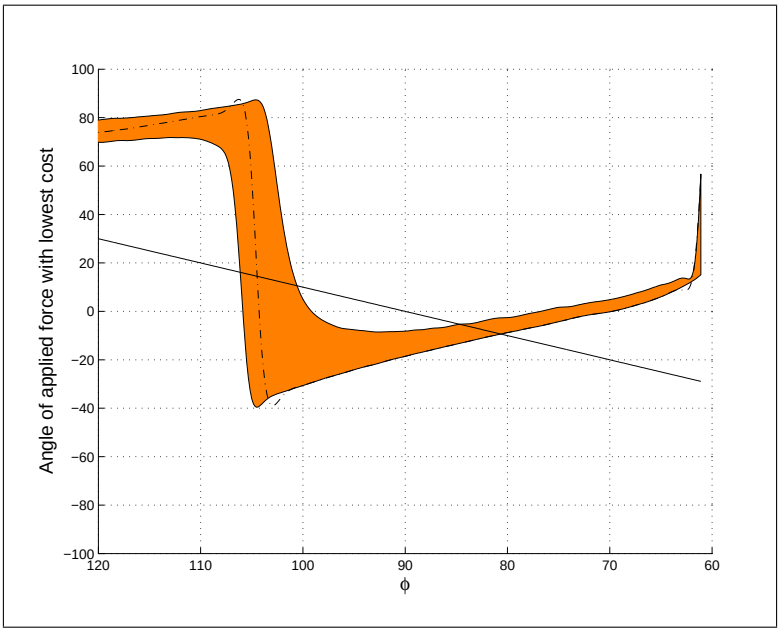

Figure 4.15: Subject with C5 tetraplegia push 6 (normal resistance) - predicted direction of applied force using modified constants. Shaded band represents directions with an effect:cost over 90% of the maximum (broken line)

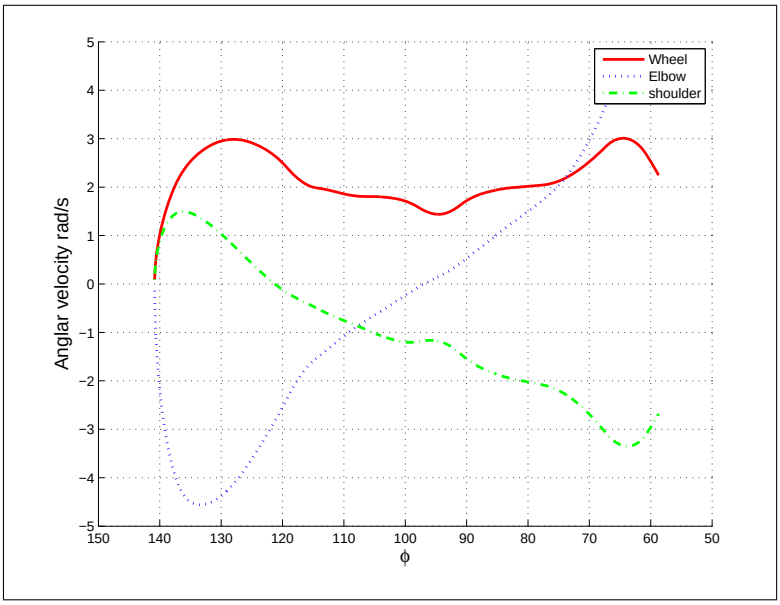

Figure 4.16: Angular velocity inputs for subject with C6 injury at normal resistance. Elbow and shoulder angular velocities were calculated using 4-bar mechanism theory outlined above.

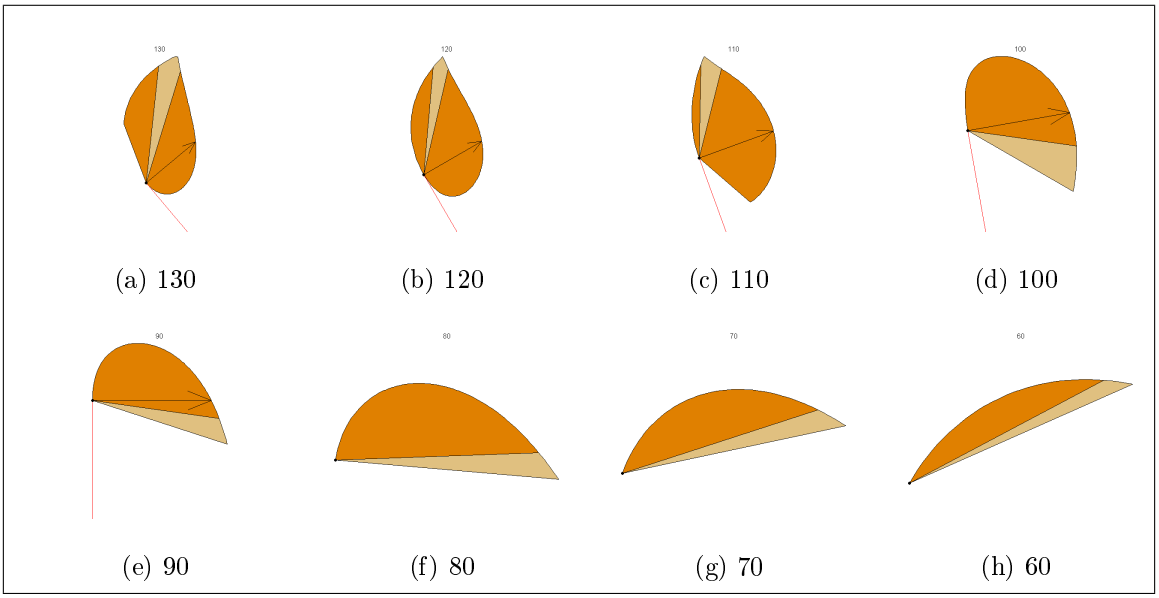

(a) 130 (b) 120 (c) 110 (d) 100

(e) 90 (f) 80 (g) 70 (h) 60

Figure 4.17: Cost polar plots - Subject with C6 tetraplegia, push 6

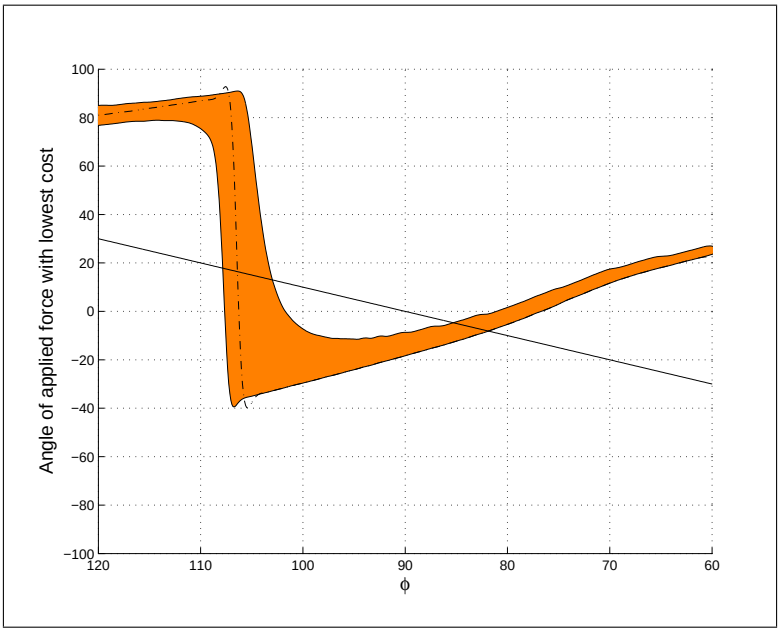

Figure 4.18: Subject with C6 tetraplegia push 6 (normal resistance) - predicted direction of applied force using modified constants. Shaded band represents directions with an effect:cost over 90% of the maximum (broken line)

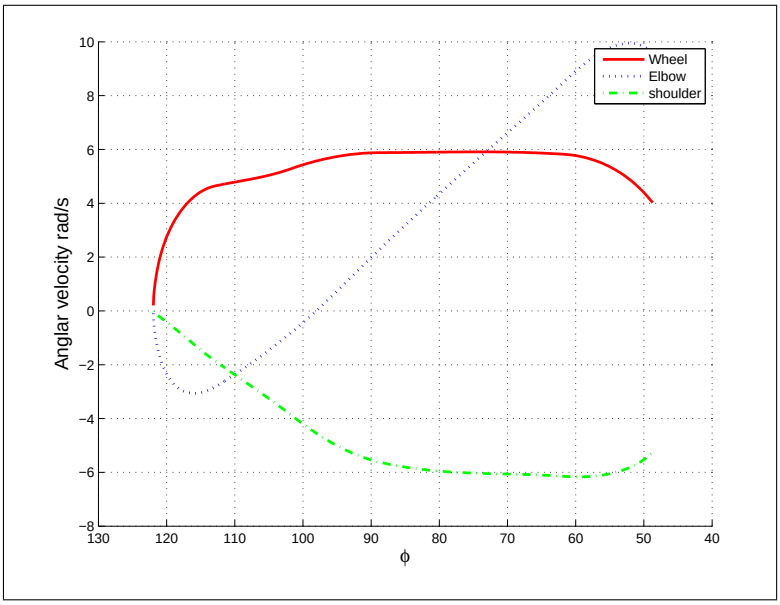

Figure 4.19: Angular velocity inputs for subject with C7 injury at normal resistance. Elbow and shoulder angular velocities were calculated using 4-bar mechanism theory outlined above.

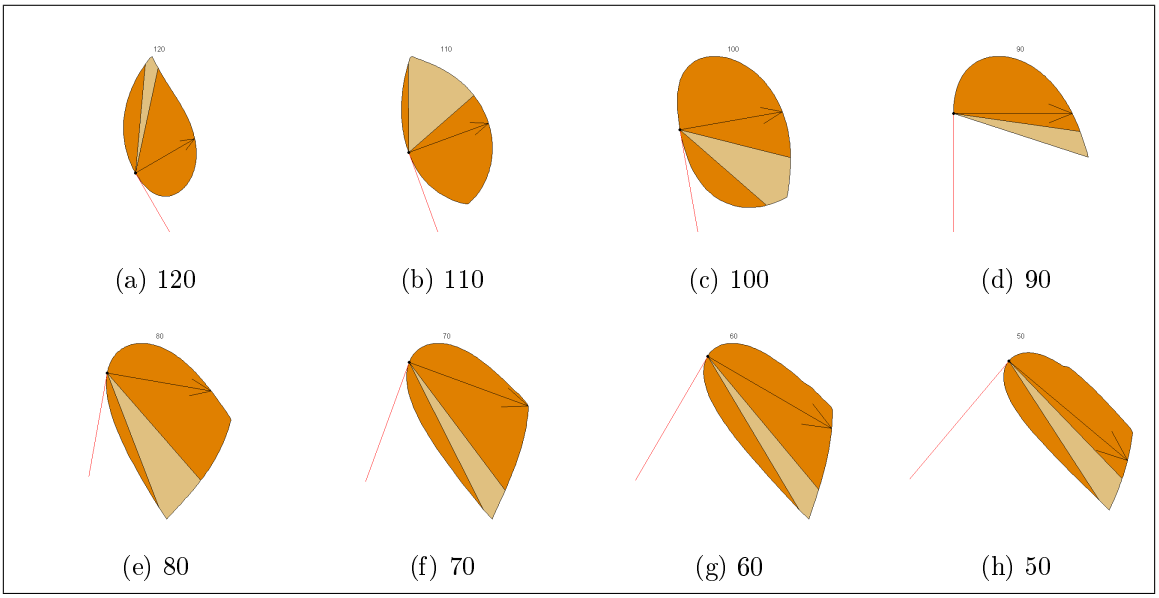

(a) 120 (b) 110 (c) 100 (d) 90

(e) 80 (f) 70 (g) 60 (h) 50

Figure 4.20: Cost polar plots - Subject with C7 tetraplegia, push 6

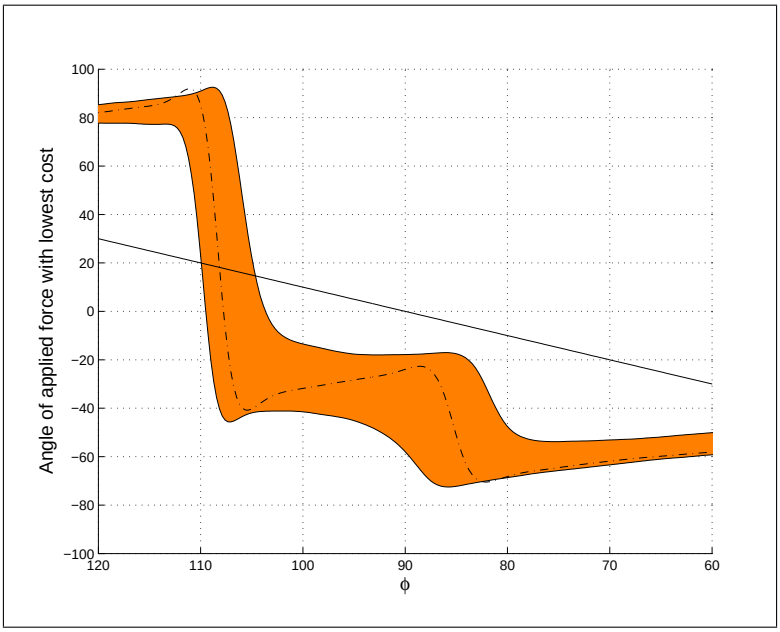

Figure 4.21: Subject with C7 tetraplegia push 6 (normal resistance) - predicted direction of applied force using modified constants. Shaded band represents directions with an effect:cost over 90% of the maximum (broken line)

The predicted direction curve for the C7 candidate in Figure 4.21 was very similar in characteristic to the curve in Figure 4.7 produced using the original constants and the flat input data. It was almost indistinguishable from a simulation using the C7 input data, but the original constants. Hence, the predicted force curve is insensitive to changes in the muscle volume and maximal joint moment constants.

The curves for the C5 and C6 candidates in Figures 4.15 and 4.18 varied significantly from the C7 and able-bodied curves after top-dead-centre. Optimal force direction was higher and the 90% band narrower. This region after top-dead-centre was the part of the stroke where elbow extension provided the optimal applied force for able bodied and C7 subjects. As subjects with complete C5 and C6 tetraplegia have no use of their triceps, this optimal force was restricted to the optimal force from a flexion motion. Consequently, the polar plots were cut off in directions where a elbow flexion force was required. The spike in the curve for the C5 subject in Figure 4.15 was caused by the limit for the hand's reach being met.

There was also very little difference between the curves for the C5 and C6 subjects in Figures 4.15 and 4.18. When input data was the same the two curves were indistinguishable. These results show Rozendaal et al.'s theory to be insensitive to small changes in active muscle volumes. Thus, there would be no benefit in further refining the constants proposed in Section 4.3.1 in Tables 4.8 to 4.10. However, removal of the elbow extension muscle volume successfully limited the force application directions for subjects with C5-7 tetraplegia, as expected.

4.3.3 Impact of other factors on curve shape

Wheel velocity and power together determine the required tangential force component. For the same power output, a larger tangential force component, and correspondingly slower velocity, resulted in a wider band of effective force directions. In contrast, a smaller tangential force and higher velocity resulted in a narrower band of effective force directions. However, when absolute effect:cost ratios are examined, the high velocity, low force case had a much wider band of values over a specified minimum. Figures 4.22 to 4.23 show this effect. This result suggests that at higher velocity and lower force, the force application direction is more likely to coincide with, or be near, the mechanically optimal tangential direction. Hence, a flatter applied force curve is likely to be more physiologically efficient.

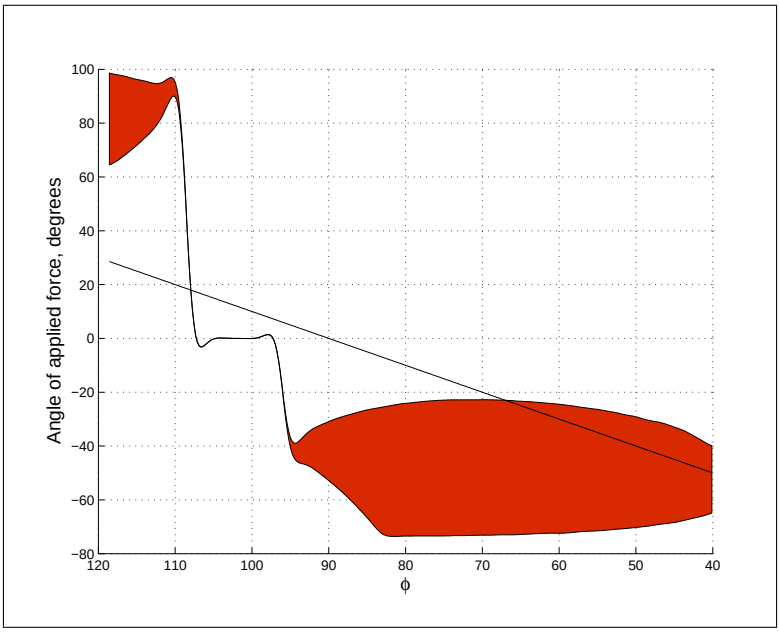

Figure 4.22: Directions with effect:force ratio over 240, 30W constant input, low velocity and high force

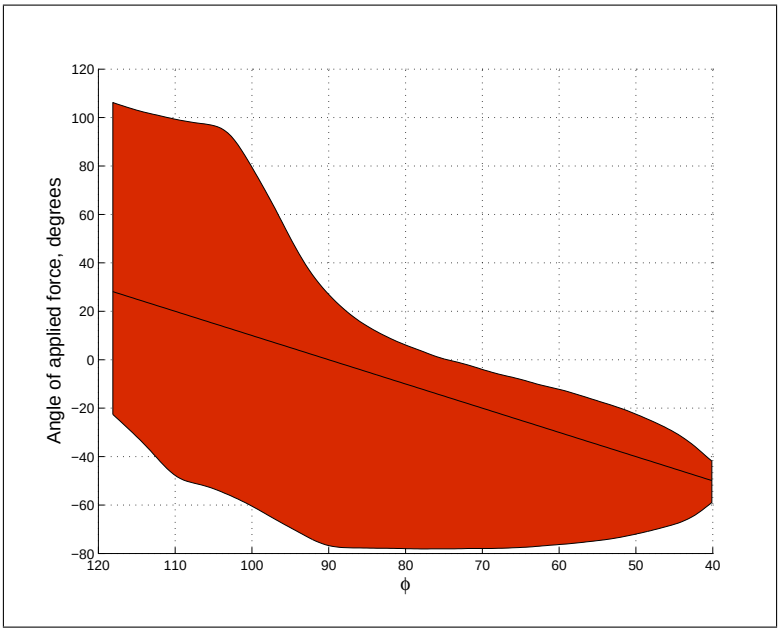

Figure 4.23: Directions with effect:force ratio over 240, 30W constant input, high velocity and low force

4.3.4 Variation between successive push cycles and resistances

The simulations discussed above were for push cycles once the candidate had reached speed and obtained a rhythm. However, there were significant variations in power, velocity and tangential force characteristics within the first four push cycles as the

candidate accelerates from rest. Figures 4.24 to 4.25 show the variation in the theoretical force application direction over these first four cycles. The bands of most effective force application angles were very consistent over the four cycles for both subjects.

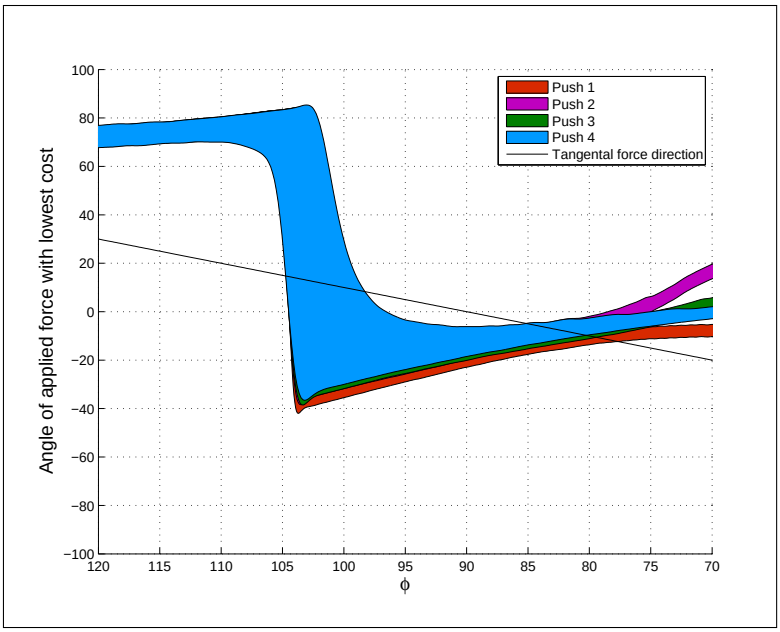

Figure 4.24: C5 Candidate - Variation with progressive push cycle

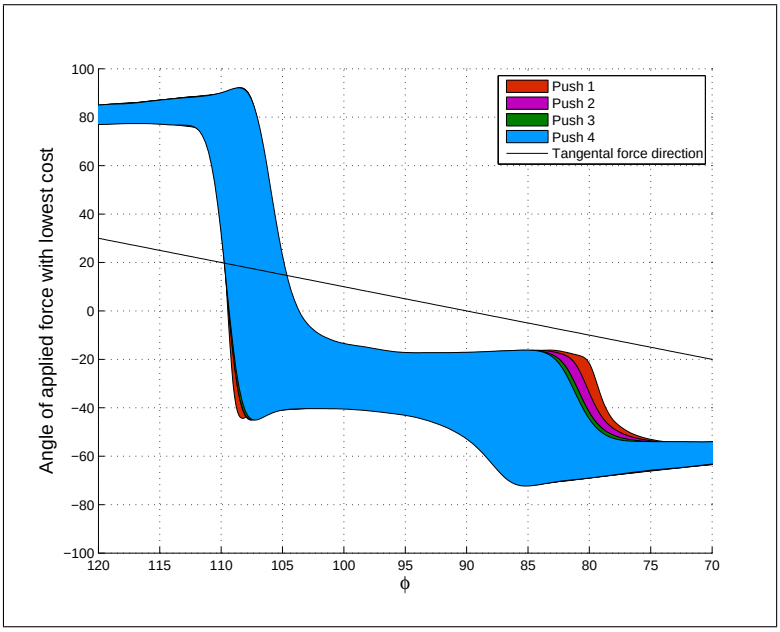

Figure 4.25: C7 Candidate - Variation with progressive push cycle

To view the influence of increased resistance, the simulation was repeated for the trials with a higher inertial load. The comparison of the two resistive cases is shown in

Figure 4.26. The characteristic angle curve was unaffected by changes in load for all subjects tested in this study. Interestingly, this result suggests direction of force application, and thus, the functional effective force (FEF), is independent of load. In everyday wheelchair propulsion, load changes are common due to varying ground surfaces, inclines or a load carried on the chair. This result supports the notion that a wheelchair could be designed to optimise FEF, and that this optimised design would not be constrained to one particular propulsion situation.

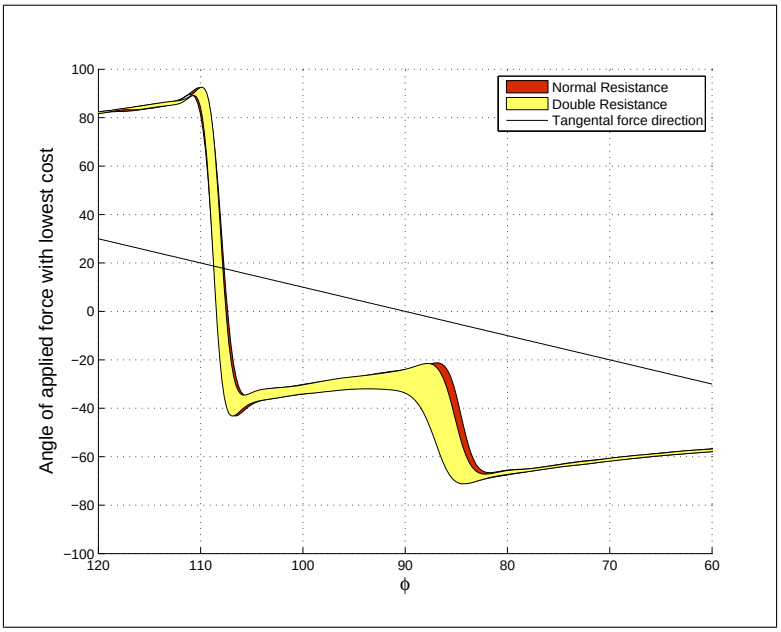

Figure 4.26: C7 candidate - Variation with Resistance

4.4 Discussion and Summary

An algorithm was developed in Matlab to predict the applied force directions based on the theory from Rozendaal et al. (2003), where the optimal direction was that with the lowest physiological cost for the given power output. These optimal force directions were predicted for subjects with C5-7 tetraplegia using wheel kinetics and subject data from the propulsion trials of Chapters 2 and 3, and modified injury-specific muscle velocities and maximal joint moments. There was a significant difference in the trends in optimal force direction between subjects with and without any elbow extension capability.

Rozendaal et al.'s equations were insensitive to small changes in muscle volumes and maximal joint moments, but sensitive to a whole muscle group being 'turned off' as a result of the spinal injury location. Other constants relating to the moment-angle factor

and maximal joint velocities were left unchanged. It may be that these characteristics are also modified by SCIs, and that optimal force direction is more sensitive to changes in these constants. However, there is currently not enough known about the capabilities of people with C5-7 tetraplegia to propose new, more refined values for these constants.

Simulations maintaining power, but modifying wheel velocity and tangential force showed that while the band of most optimal force was narrowed for the high force, low velocity case, the band of values with an absolute effect:cost higher than a nominal value was greater for the low force, high velocity case. This result is useful for consideration in design of any human powered machine.

Rozendaal et al. (2003) also showed that predictions didn't match results before top-dead-center during dynamic tests. Subjects tended to minimise the range of applied force directions over the stroke, going for a dynamically or whole-cycle most optimum force curve, rather than the optimal force at each point. A method for refining the predictions from Rozendaal et al. to give this flatter application angle curve is needed, and would likely require greater knowledge of the specific force capabilities of these populations.

Chapter 5

Human Model

This chapter reviews existing computer-aided models of human anatomy and mechanics and their role in engineering design of therapeutic, assistive and rehabilitative devices. A constraint modeller called SWORDs, and its human manikin along with its constraints and parameters, is introduced in Sections 5.2 and 5.3.

Previously, the SWORDs human manikin has been used in studies for modelling human movement (Mitchell et al., 2007) as purely a geometric model. This geometric model was suitable for predicting or solving posture or reach problems, but lacked the capability for a force to be applied to the manikin or joint kinetics to be modelled. As joint reactions and applied forces are an important consideration in design, the capability for calculating joint reactions SWORDs is developed in Section 5.4. The SWORDs human manikin is later used to compare the effectiveness of different hand paths in Chapter 9.

5.1 Existing Computer-Aided Models

There is currently a range of human modelling software available to designers. Three-dimensional computer-aided human modelling programs have been emerging since the 1960s (Das and Sengupta, 1995) and have been widely utilised for design applications since the early 1990s due to their value in reducing product development time and cost. Human modelling programmes have been most commonly used in the ergonomic evaluation for the design of vehicles, work areas, machine tools, and occupational devices (Kuo and Chu, 2005). Much of the modelling software available has been designed or evolved to suit specific applications, most commonly for military, aerospace or automotive applications. They thus focus on only one aspect of human operator performance, such as biomechanical strength, metabolic rate prediction, reach assessment or timing.

Hence, the designer may need to conduct several analyses using different tools to evaluate and develop different aspects of a complex or multi-functional device or system (Feyen et al., 2000).

A summary of commonly used software packages is given below. The human rendering in these programs ranges from lifelike solid models to simple wire frame images. Most include range-of-motion constraints to prevent the adoption of unnatural postures. Most also have the ability to modify the anthropometrics or stature of the person represented in the model, either by gender, stature or population percentile. Systems such as SAMMIE and COMBIMAN, which have been designed for environment evaluation purposes, focus on reach and fit but not strength. Systems such as 3DSSPP which do consider strength, are often primarily concerned with lifting applications.

3DSSPP (Three-Dimensional Static Strength Program) was developed at the University of Michigan's centre for ergonomics. This model is directed towards evaluating lifting and workplace safety. The program has an AutoCAD interface. Joint angles or hand positions can be input by the user and loads applied to the hands or directly at the joints for the calculation of joint moments. Designers can quantify the biomechanical risk of lifting tasks using calculations based on static strength data, which assumes stationary or very slow motion. If the hand position is specified, the software contains an algorithm to predict posture based on hand position (Feyen et al., 2000).

Sammie was first developed in 1972 at the University of Nottingham (#mAGNEMAT05#). Sammie is a 3D model for determining fit, reach, vision and posture. SAMMIE's primary application is evaluating the layout of equipment and furniture in cockpit and vehicle designs for automotive, industrial, rail and aerospace applications.

COMBIMAN primarily is used to evaluate visual accessibility and reach, collision, and strength analysis for control operation. It utilises CAD drawings and human somatotype type data (Beagley, 1997). It is a tool for workstation development, anthropometric analysis, air force cockpit design, and aviation applications.

JACK is another package, which focuses on vision and reach analyses. It builds humans of different sizes and can position these in a CAD model to evaluate interactions within a virtual environment. The posture of the JACK model can be directly manipulated to the desired posture or a pre-programmed posture selected from a posture

library. JACK is capable of simulating walking, grasping, eye tracking and collision detection. Both force and torque can be calculated for either static or dynamic situations.

AnyBody is a software system for modelling the mechanics of the human body and its interaction with an environment defined by external forces and boundary conditions. The software works within the Windows operating system and contains a complex biomechanical model of the human body with hundreds of muscles and tendons. AnyBody can calculate individual muscle forces, joint forces and moments, metabolism, elastic energy in tendons and antagonistic muscle actions (Technology, 2009). As in JACK, the model's posture (or motion) can be specified by the user or from a library of pre-set postures and motions. Anthropometric data within the model can be scaled to fit a population group or individual. (Technology, 2009)

ERGOMAN was created in 1983, like 3DSSPP and Sammie, primarily for evaluating workspace and layout design. The human model is based on ERGODATA, which includes databases of data on human anthropometry, biostereometry, biomechanics and ergonomics. (Anthropology, 2009)

RAMSIS is a three-dimensional human CAD manikin widely used in industry for the ergonomic design of vehicles and aircraft. The model can be made to simulate people with a variety of body types and dimensions, based on anthropometry databases from all over the world. RAMSIS has evolved to offer more complex functions, such as force-based posture and comfort prediction (van der Meulen and Seidl, 2007).

SAFEWORK is a human model from Genicom that, like the aforementioned packages, creates anthropometrically-correct virtual humans for product design and testing purposes. The software may be used to examine posture, reach, comfort, strength, lifting, collision detection and vision, and can analyse these functions within an imported CAD design. The CAD systems SAFEWORK can import and export solid geometry from a wide range of CAD systems include CATIA, CADDS, Pro/ENGINEER, EUCLID, AutoCAD and SDRC I-DEAS. (Consultants, 1998).

5.2 The Constraint Modeller, SWORDS

SWORDS is constraint modelling software developed at the University of Bath. Constraint modelling is a design method that has been successfully applied to the optimi-

sation of mechanisms and design synthesis most notably for industrial and ergonomic design problems. Collaboration between the University of Bath and the Technical University of Delft has seen human modelling data from Delft imported into the SWORDS constraint modelling environment. The resulting human model within SWORDS is defined by constraints that include connectivity rules at each joint and bounding of segment motion as outlined in this chapter. There is potential for this technology to be developed and applied to the design of devices related to rehabilitation and physical disability.

In most of the modelling systems discussed in Section 5.1, the designer is able to position the human model within a design environment or use pre-programmed postures to investigate an aspect of the human - environment interaction. Such modelling systems are not intelligent design systems. Instead, they may be used to identify errors in design, but offer no means of resolving the error. If a problem is identified, the designer may modify the design in a means of their choosing, and re-check the design to confirm any improvements in an iterative manner. This method is likely to result in sub-optimal design solutions.

Designers often assume that people can adapt easily to a poor or sub-optimum design. However, there is normally a human cost associated with such 'adaptation', which may include musculoskeletal problems. Amongst the elderly and disabled population, such problems may be magnified and a person's ability to 'adapt' to use a design diminished (Porter et al., 2004).

Therefore, the need is for a human model that can, independently seek configurations and postures that meet operational requirements and ergonomic conditions. Such a model should also be able to consider restrictions caused by the geometry of the workspace or the device (Molenbroek and Medland, 2000). This situation is where the constraint modeller is useful.

In the constraint environment, all constraint types, such as strength, range of motion, environmental constraints and rules for a machine or device, can be handled within one unified approach. While some of the discussed modellers, such as SAMMIE and Jack, are capable of manikin animations, these animations need to be defined for each design and subsequently redefined each design modification. In contrast, the SWORDS manikin is able to achieve movement strategies based on movement rules (Williams and Medland, 2001). The program allows users to input variables and specify constraints between these, SWORDS then can modify the variables to search for configurations

that satisfy the given constraints. Constraints may be weighted, to assign them a “priority”, and if constraints are in conflict, SWORDS searches for the solution breaching the fewest lower priority constraints, a "best compromise" solution. This difference makes it a more time efficient method for evaluating and modifying dynamic interactions.

SWORDS uses search and optimisation techniques to find configurations that best satisfy user specified and weighted constraints by modifying user specified variables. These variables may be a combination of human posture components and machine parameters. The constraint modeller contains several solver algorithms. In addition it can ‘talk’ to MATLAB and utilise numerical method and optimisation packages in MATLAB to give the user a large degree of control over the solution method for a given situation. This feature also widens the range of applications to which the constraint modeller can be effectively applied.

5.3 Manikin Model

5.3.1 Model Anthropometrics and Structure

The manikin used in this study was based on an existing model developed within the University of Bath’s constraint environment SWORDS. The upper body is modelled using links as shown in Figure 5.1. The lower body is also modelled using a similar approach, but is not of interest for this study. This model was based on human modelling data from the University of Delft in the Netherlands and has been used in other studies (e.g. Mitchell, 2004). The anthropometric data used for the model is listed in Table 5.1 and was drawn from ADAPS (Technical University of Delft). This data represents a subject 1.74 m tall and 73 kg, but can easily be modified to reflect people of different statures. To change the model to represent a specific individual, either each joint length can be manually changed or the subject’s height can be entered and the link lengths estimated using the relationships in Table 5.2.

The average height of the manikin (1.74 m) is within 3% of the average heights reported in cadvaer studies (Dempster, 1955), which examined 8 subjects with average age 68.5 years and height 1.69 m. Similarly, Clauser et al. (1969) examined 13 subjects with average age 49.3 years and height 1.73 m while Chandler et al. examined 6 subjects aged 45 – 65 years with average height 1.72 m. The average mass of the manikin

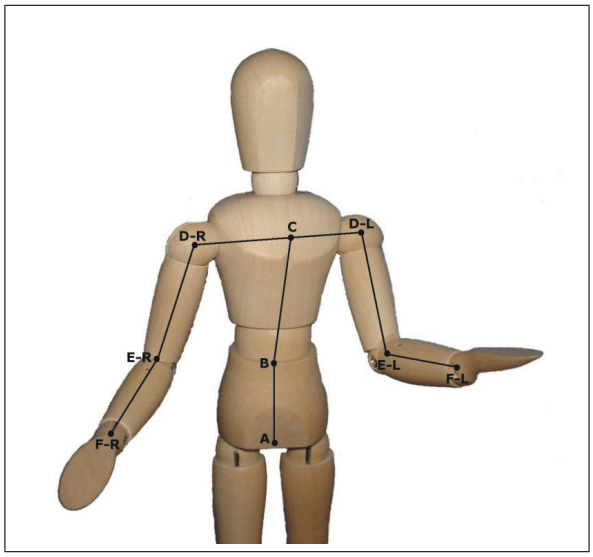

Figure 5.1: Upper Body Model Used in Calculations

(73 kg) is slightly higher than those reported in these same three studies. Dempster (1995) reported 59.8 kg, Clauser et al. (1969) reported 66.5 kg and Chandler et al. reported 65.17 kg. However, the manikin mass is more in line with the more recent larger study on living people by Zatsiorsky and Seluyanov (1979).

This later study by Zatsiorsky and Seluyanov is the largest comprehensive study to date on the inertial properties of living people. Unlike many other studies with an elderly sample population, this study had an average age of 23.8 years and is thus more relevant for this research. Zatsiorsky and Seluyanov (1983) surveyed the anthropometrics of 100 healthy males, who had an average mass or 73 kg, and height 174.1 cm. The inertial parameters of the ADAPS-based manikin also compare well with other values reported, as shown in Figure 5.2.

Table 5.1: Anthropometric Information used in manikin model

Link	Length (mm)	Mass (kg)	Centre of mass position (mm)
AB	47	0	-
BC	325	41 (trunk + head total)	190
CD_R	179	0	-
CD_L	179	0	-
DE_R	289	1.95	131.6
DE_L	289	1.95	131.6
EF_R	262	1.8	196
EF_L	262	1.8	196

Table 5.2: Parameters for estimating anthropometric data for a subject of known height and weight

Link	Length (H=height)	Segment Mass (M=total body mass)
AB	0.270 H	0
BC	0.187 H	0.562 M
CD	0.103 H	0
DE	0.166 H	0.0267 M
EF	0.151 H	0.0247 M

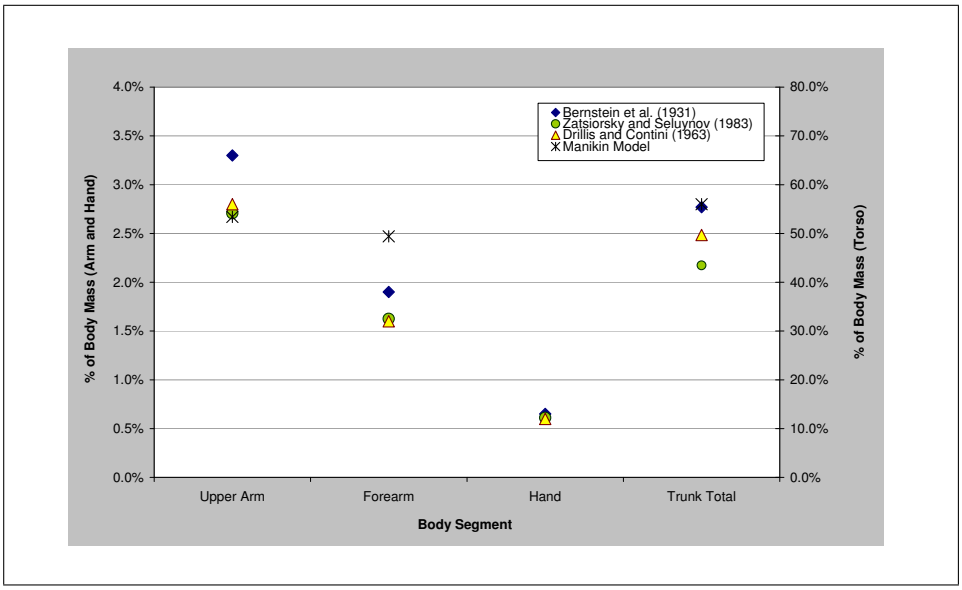

Figure 5.2: Comparison of inertial parameters used in SWORDS manikin model (ADAPS) with 3 other significant studies on body inertial parameters.

5.3.2 Manikin Structure and Coordinate System

The manikin model was constructed within the constraint modeller environment. Each body segment was represented by a "link" within its own model space and associated coordinate system. Each body segment was modelled geometrically by a line the length of that segment, as listed in Table 5.1. Each line was orientated along one of its model space's axes as shown in Figure 5.3. Each model space was defined with respect to its 'parent' model space. For example, the right forearm space, was defined by a fixed offset in the negative-z direction from the right upper arm model space; which in turn was modelled as an x-offset from the right shoulder space. The pelvis was a modelled

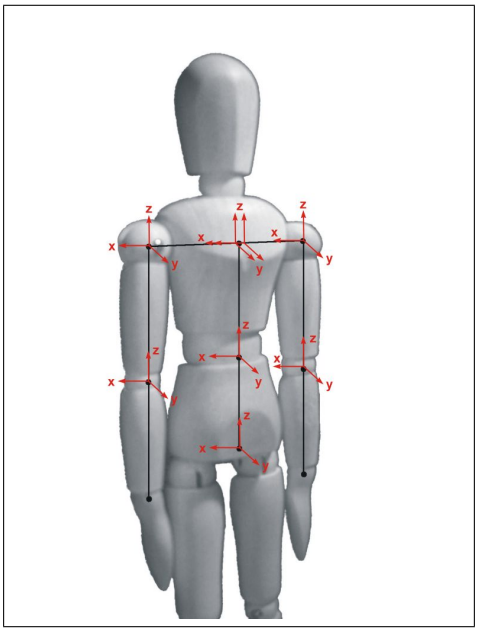

Figure 5.3: Coordinate systems for model spaces in constraint modeller manikin model. Manikin is shown in its 'neutral' position where the model space rotations are all zero.

as a point and was the highest tiered model space in this hierarchy, defined in terms of the constraint modeller's world space.

The linear offsets of the model spaces were fixed. The posture of the human manikin was then manipulated by modifying the relative rotations of each model space. To translate the manikin in space, the linear position of the pelvis with respect to the world space was modified.

5.3.3 Manikin Constraints and Range of Motion Bounds

To limit the manikin to more natural postures, connectivity rules and bounds were applied to the model spaces. Connectivity rules were applied at each joint, and body segment motion was limited by bounding the rotation for each model space according to natural observed limits. These range of motion rotation bounds are given in Table 5.3, and include some axes where no rotation is permitted.

A physical representation of these limits showing permitted joint movement is given in Figure 5.4. The coordinate systems used in the manikin model spaces that these rotation bounds are in respect to are shown in Figure 5.3. The order of rotation is around the link's local x-axis, then its z-axis, and lastly its y-axis.

Table 5.3: Range of motion constraints (able bodied) for manikin model

	x-axis		y-axis		z-axis	
Bounds	Lower	Upper	Lower	Upper	Lower	Upper
Lumbar (AB)	-30	30	Fixed		-15	30
Torso (BC)	-40	0	-90	90	-90	90
R shoulder (CD_R)	Fixed		-30	10	-10	35
R upper arm (DE_R)	-61	188	-130.5	51.5	-97	34
R forearm (EF_R)	0	142	Fixed		-113	77
R hand	Fixed		-102.5	86.5	Fixed	
L shoulder (CD_L)	Fixed		-10	30	-35	10
L upper arm (DE_L)	-61	188	-51.5	130.5	-97	34
L forearm (EF_L)	0	142	Fixed		-77	113
L hand	Fixed		-86.5	102.5		
Neck	0	30	-41	41	Fixed	
Head	-30	61	Fixed		-79	79

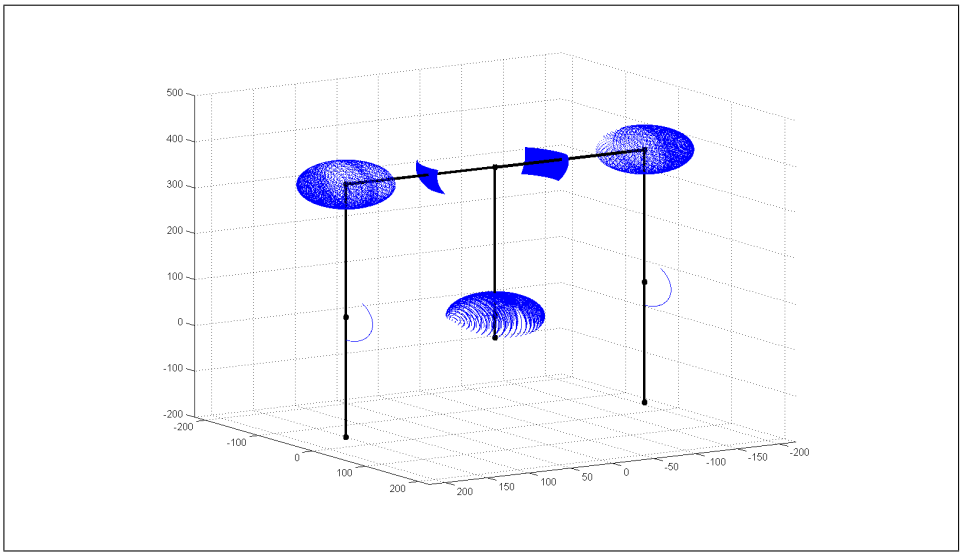

Figure 5.4: Joints range of motion for manikin model, blue regions represent regions of allowable movement

5.4 Development Joint Reaction Capability

At the commencement of this study, the existing manikin within the constraint modeller was a purely geometric model. It was suitable for predicting or solving posture or reach problems, but there was no capability for a force to be applied to the manikin

or joint reactions to be calculated. Joint reactions and applied forces are an important component and consideration in most human-machine interactions. Thus, this capability was developed to expand the applications of the constraint modeller.

5.4.1 Mathematical Model

The upper body is modelled using 8 links, connected and labelled as shown in Figure 5.1. The joint-force reaction capability was initially developed outside of the constraint environment, using MS Excel, VB for Applications, and Matlab due to their familiarity and the ease of trouble shooting calculations and code within their environments. Consequently, the coordinate system used in these joint reaction calculations differed from that employed for the manikin model in the constraint modeller.

In particular, the right-handed Cartesian coordinate system adopted for the joint reaction calculations was more in line with common systems used in biomechanical and anthropometric studies than the manikin's left-handed coordinate system. When the force capability was moved into the constraint modelling environment, transformation matrices were applied to each segment to relate the different coordinate systems.

The coordinate systems used for these joint reaction calculations are shown in Figure 5.5. As with for the constraint modeller's manikin, the point at the bottom of the torso was related to the global coordinate system. In this model, point A, the origin of the torso link, was coincident with the global origin. The coordinate system for each segment had its origin at the parent end of the link. The local coordinate system's axes were denoted p q and r, and were oriented such that the positive q axis was aligned longitudinally with the link.

The reactions in each link are calculated relative to these local coordinate systems. Figure 5.6 shows the sign convention used for reactions relative to the local (pqr) and global (xyz) systems. Force components corresponding to a given link's local coordinate system are referred to as F1, F2 and F3, corresponding to the axial component (acting along axis q), the shear component parallel to the p axis, and the shear component relative to the r axis.

The formulae used to calculate joint reactions are given in Equations (5.1) to (5.6), These equations are listed for the lower torso link, but reactions for other links are calculated similarly, considering force contributions from all that link's child links.

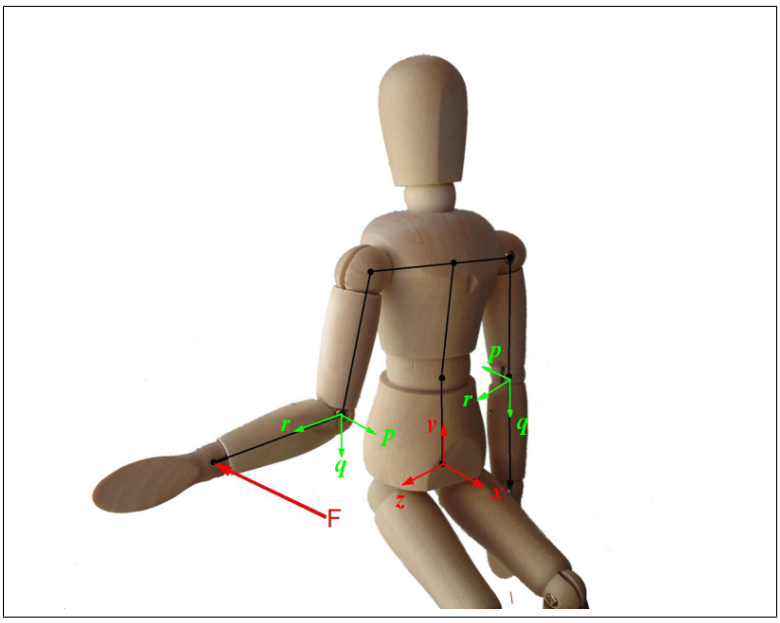

Figure 5.5: Global coordinate system and forearm local coordinate systems for an arbitrary configuration

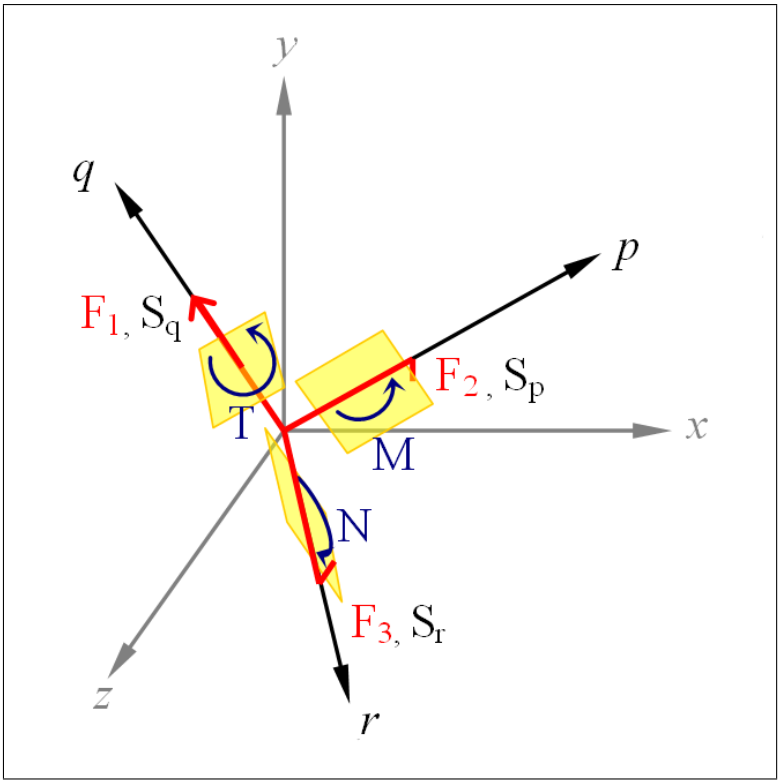

Figure 5.6: Sign convention for reaction forces and moments relative to local coordinate system

For Link AB:

$$Axial\,Force,\ A = -\sum_{i=A}^{E} F1_i \tag{5.1}$$

$$Shear\,Force,\ S_p = -\sum_{i=A}^{E} F2_i \tag{5.2}$$

$$Shear\,Force,\ S_r = -\sum_{i=A}^{E} F3_i \tag{5.3}$$

$$Torque,\ T = \sum_{i=A}^{E} F3_i \cdot p_i - \sum_{i=A}^{E} F2_i \cdot r_i \tag{5.4}$$

$$Moment,\ M = \sum_{i=A}^{E} F2_i \cdot q_i - \sum_{i=A}^{E} F1_i \cdot p_i \tag{5.5}$$

$$Moment,\ N = \sum_{i=A}^{E} F3_i \cdot q_i - \sum_{i=A}^{E} F1_i \cdot r_i \tag{5.6}$$

Where:

$F1 = Axial\,component\,(parallel\,to\,q\,axis)$

$F2 = Shear\,p\,component\,(parallel\,to\,p\,axis)$

$F3 = Shear\,r\,component\,(parallel\,to\,r\,axis)$

$F1_i/F2_i/F3_i$ = Force component at joint i, relative to local coordinate system of link being analysed.

To calculate F1, F2 and F3, the forces applied to each link first were transformed into the link's local coordinate system. In particular, the orientation of a local coordinate system can be described in terms of the angles it forms with the global axes. The angle θ between the y global axis and the link's q axis is found using the link length and endpoint coordinates using Equation 5.7.

$$\theta = \cos^{-1}\left(\frac{AB_y}{AB}\right) \tag{5.7}$$

Where:

AB	is the length of link A-B
AB_y	is the difference in the global y coordinates between the link's two endpoints

An axis of rotation in the transverse plane can then be found (on the plane to find the direction of the link axis and the local coordinate system mapped onto the global system by rotation about this axis.

The angle of the projected link onto the transverse plane, with global axis x is ε. The method for finding a unit vector for the rotation axis depends on the value of ε. As the rotation axis is in the x-z plane, $U_y = 0$

$$Rotation\,Axis\,(Unit\,Vector) = \begin{bmatrix} U_x \\ U_y \\ U_z \end{bmatrix}$$

If $0 < \varepsilon < 90$ or $90 < \varepsilon < 180$:

$$U_x = \sin(\varepsilon) \qquad U_z = \cos(\varepsilon)$$

If $180 < \varepsilon < 270$:

$$U_x = -\cos(\varepsilon) \qquad U_z = -\sin(\varepsilon)$$

If $270 < \varepsilon < 360$:

$$U_x = -\sin(\varepsilon) \qquad U_z = -\cos(\varepsilon)$$

If $\varepsilon = \infty$ or $\varepsilon = 0$ or $\varepsilon = 180$

$$U_x = 0 \qquad U_z = 1$$

If $\varepsilon = 90$ or $\varepsilon = 270$

$$U_x = 1 \qquad U_z = 0$$

The resulting transformation matrix is defined:

$$R = \begin{bmatrix} 1 + (1 - \cos\theta)\left(U_x^2 - 1\right) & (1 - \cos\theta)\, U_x U_y - U_z \sin\theta & (1 - \cos\theta)\, U_x U_z + U_y \sin\theta \\ (1 - \cos\theta)\, U_x U_y + U_z \sin\theta & 1 + (1 - \cos)\left(U_y^2 - 1\right) & (1 - \cos\theta)\, U_y U_z - U_x \sin\theta \\ (1 - \cos\theta)\, U_x U_z - U_y \sin\theta & (1 - \cos\theta)\, U_y U_z + U_x \sin\theta & 1 + (1 - \cos\theta)\left(U_z^2 - 1\right) \end{bmatrix} \tag{5.8}$$

Using this transformation matrix, 3 unit vectors can be found to represent the orientation of the local coordinate system pqr relative to the global system xyz.
$x \rightarrow p$:

$$\begin{Bmatrix} xp_1 \\ xp_2 \\ xp_3 \end{Bmatrix} = \underline{R} \begin{Bmatrix} 1 \\ 0 \\ 0 \end{Bmatrix} \tag{5.9}$$

$y \rightarrow q$:

$$\begin{Bmatrix} yq_1 \\ yq_2 \\ yq_3 \end{Bmatrix} = \underline{R} \begin{Bmatrix} 0 \\ 1 \\ 0 \end{Bmatrix} \tag{5.10}$$

$z \rightarrow r$:

$$\begin{Bmatrix} zr_1 \\ zr_2 \\ zr_3 \end{Bmatrix} = \underline{R} \begin{Bmatrix} 0 \\ 0 \\ 1 \end{Bmatrix} \tag{5.11}$$

Using these unit vectors the angle between the global and local axes can be found:

$$\alpha_{yp} = \frac{xp_2}{\sqrt{xp_1^2 + xp_2^2 + xp_3^2}} \tag{5.12}$$

Where α_{yp} denotes the angle between the local axis p and the global y axis. The values for α_{yq}, α_{yr}, α_{xp}, α_{xq}, α_{xr}, α_{zp}, α_{zq} , α_{zr} can be found in the same way.

These angles are now used to calculate the components of applied and weight forces relative to each link's local coordinate system. For a weight force, F, or a **vertical** applied force, F, the force components relative to a chosen coordinate system are defined:

$$F1 = F \cdot \cos\alpha_{yq} \qquad F2 = F \cdot \cos\alpha_{yp} \qquad F3 = F \cdot \cos\alpha_{yr} \tag{5.13}$$

For a force, F, applied **parallel** to the x axis, the force components relative to a chosen coordinate system are defined:

$$F1 = F \cdot \cos\alpha_{xq} \qquad F2 = F \cdot \cos\alpha_{xp} \qquad F3 = F \cdot \cos\alpha_{xr}$$

For a force, F, applied **parallel** to the z axis, the force components relative to a chosen coordinate system are defined:

$$F1 = F \cdot \cos\alpha_{zq} \qquad F2 = F \cdot \cos\alpha_{zp} \qquad F3 = F \cdot \cos\alpha_{zr} \tag{5.14}$$

5.4.2 Structure of Code

A routine titled reactions.mac was written to calculate the reactions at each joint in the manikin within the SWORDs environment, via the use of several sub-routines. It first called a subroutine named getforces.mac, which reads in applied forces either from a data file or forces could be specified directly in this routine. For each link, a ForcesXX.mac routine was created where XX was the link name. This routine calculated the reactions in that joint due to the applied forces. To do this calculation, applied forces were transformed into the local coordinate system using another subroutine, CoordRotate.mac. These routines are included in Appendix B.1 and B.2.

This approach of having a specific routine for each link was used to improve calculation speeds in cases where only one joint was of interest. For example, when only shoulder reaction forces were of interest, only the subroutine for the shoulder link need be called. Hence, it is a clearer and more efficient abstraction of the problem mathematics into the computational environment.

5.4.3 Mathematical Validation of the Code

The SWORDS code written to calculate the reaction forces was verified using multiple loading configurations. These tests began with simple two-dimensional massless configurations with a single applied load and progressed to more complex three-dimensional configurations incorporating the self-weight of the links. Configurations were checked

where the links were orientated at right angles to each other and at arbitrary angles to ensure the program was robust for any configuration. Checking basic configurations with only a single applied load and progressively verifying more complex configurations and loading cases also made it easier to systematically identify and isolate coding errors.

Excel was used with a Visual Basic for Applications macro to generate a csv file that could be read into the constraint modeller. This input file contained data to set the manikin's configuration with applied force information. The macro was operated from a user-form that the user input the required manikin configuration and the macro output the model space rotations for the SWORDS model.

In all configurations, an arbitrary load of 120 N was applied 90 mm from the first end of the selected link, or 20 mm from the end of the load were being applied to link AB. The position of the applied force was also arbitrary. The only requirement was that it be a value that did not coincide with the centre of mass or the exact midpoint in any of the links. The load and position values were kept consistent in all of the verification configurations for simplicity, as changing these values would provide no further advantage.

Reaction forces and moments were calculated manually for significant points in the model and compared with the outputs from the model. The 'significant' points were the endpoints of links, points where a force was applied, and, for cases where the self-weight was included, the link's centre of mass. Three two-dimensional configurations were analysed with all the links assumed massless and orientated within the coronal plane. Likewise, four three-dimensional configurations with weightless links were simulated.

The configurations were selected to check the program's versatility in correctly predicting the reaction forces for any given configuration. The test cases included configurations containing right angles, planar configurations and more complex three-dimensional cases. For each configuration, a single applied force was applied to each arm link in turn, and for configuration 1, to the torso links AB and BC. Each configuration was simulated first assuming the links were massless, then considering the self weight of each link as a point load applied through its centre of gravity. Both cases were tested to aid in debugging and checking that both the reaction due to applied load and the components due to gravity were both correctly calculated.

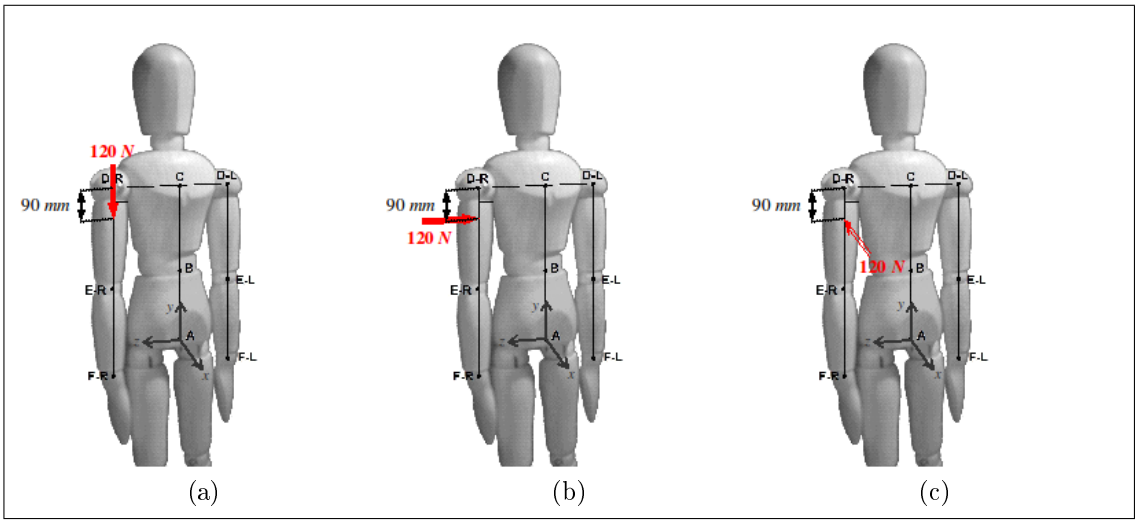

Figure 5.7: Most simple two-dimensional loading configuration tested in code verification (a) Vertical force applied 90mm along Link EF-R (b) Side force (120N from right) applied 90mm along link EF-R (c) Front force (120N from right) applied 90mm along link EF-R

In the test configurations, the vertical, horizontal sagittal, and horizontal coronal applied forces were all tested. To illustrate the loading configurations tested, a simple example is provided in Figure 5.7 showing 3 loading cases for the right upper arm for the first two-dimensional configuration. Each of these loading configurations was simulated for forces applied in each of the three global directions, for each of the left and right forearm and upper arm links. This analysis was done first assuming the links weightless, then incorporating the self weight of the limb. The macro was found to work for each of these test cases.

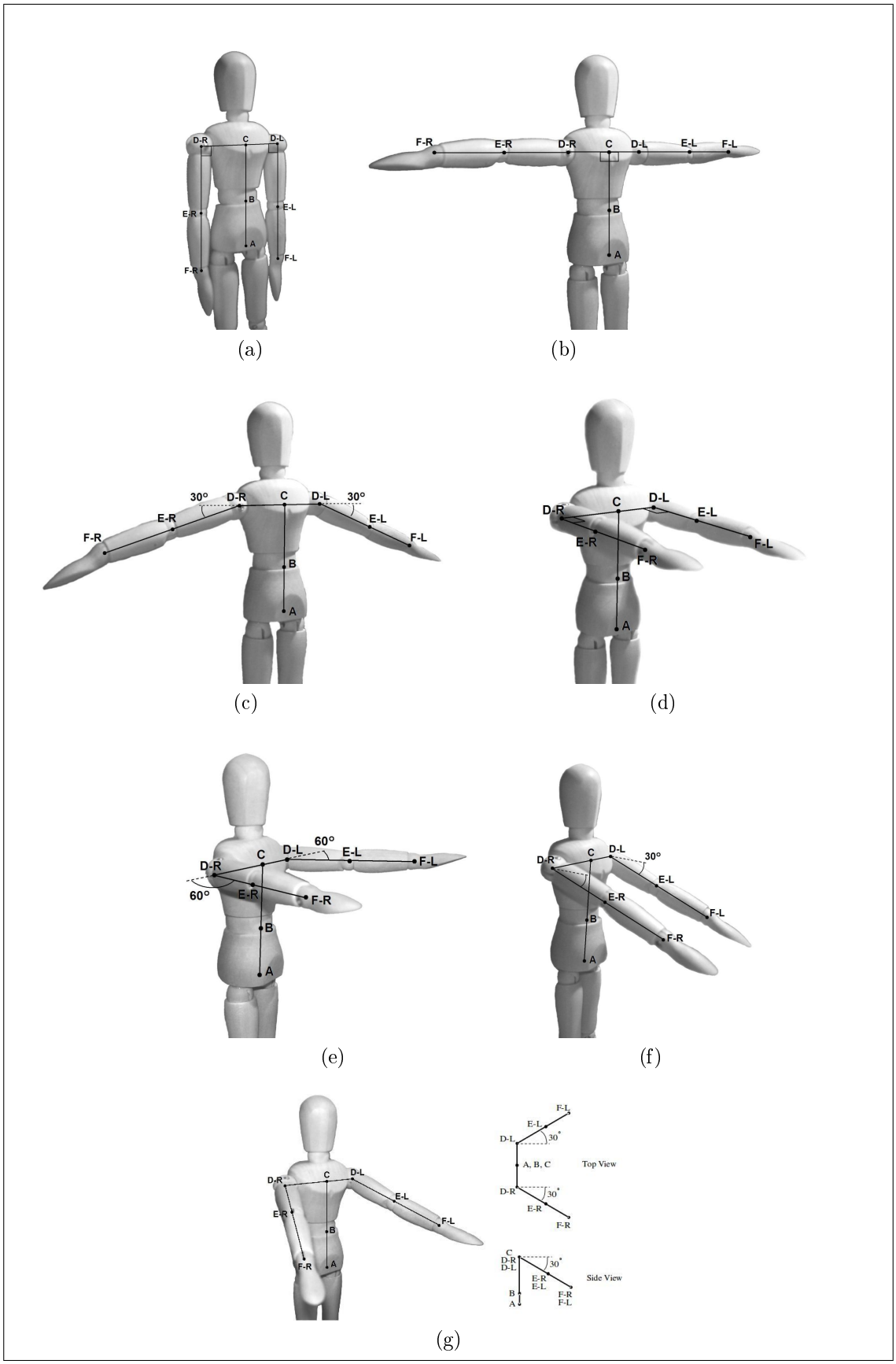

Figure 5.8: Upper body configurations used in verification of force code

5.5 Summary

The capability of the SWORDs manikin has been developed to enable the calculation of joint moments and reactions caused by any force applied to the manikin. As well providing information on these reactions, there is the potential for the allowable reactions at each joint to be bounded to limit applied forces in modelled human-machine interactions to allow design within people's strength limits and to health and safety guidelines.

Due to the simplification of the joint models in the upper body by using pin joints in the manikin, the joint reaction forces were not directly comparable to those reported in the literature, which were normally biomechanical. However, the overall joint moments should be well correlated to these biomechanical forces, and the computational methods to calculate these are computationally fasted than for complex biomechanical models.

Chapter 6

Strength Study: Prior Research

This chapter introduces the strength study that forms the second main study in this thesis. In particular this chapter reviews methodologies and data from strength studies in literature for both able-bodied and SCI-injured populations. It evaluates these different strength measurement methods, and reviews existing strength data for both able-bodied and SCI populations.

Section 6.3 discusses studies into push-pull strengths, Section 6.4 discusses articulation and joint strength based studies and models, then Section 6.5 introduces the concept of postural stability diagrams. Existing strength data for subjects with SCIs is presented in Section 6.6, along with a summary of existing methods for measuring strength in the SCI population in Section 6.7. Finally, fatigue and its influence on strength data is considered in Section 6.7. The review in this chapter provides the context for the strength study methodology presented in Chapter 7.

6.1 Introduction

Understanding the maximum strength limits of the operator is imperative in machine design. This understanding allows the designer best use of these capabilities for design optimisation, and to design within the safety limits of the operator to reduce risk of injury. In particular, cumulative trauma disorders can occur where excessive force is required in a repetitive task. Job demand relative to maximum isometric strength has also been shown to be an indicator for injury. Thus, Das and Forde (1999) recommend task strength requirements should not exceed one-third of an operator's maximum isometric strength.

To design within these recommendations, maximal isometric strengths at the required positions for the target population must be known. Hence, to design a wheelchair or device suitable for use by a person with C5, C6 or C7 tetraplegia, the strength characteristics of these populations must first be understood. Wheelchair propulsion is primarily a sagittal plane interaction and consequently most existing MWC propulsion models and studies are two-dimensional for simplicity. Thus, to model and design in the sagittal plane, it is the strength characteristics in this plane that must be understood.

6.2 Prior Research Overview

Numerous studies have been concerned with maximum voluntary strength for various upper body articulations within the able bodied population, particularly shoulder and elbow articulations (Baines, 1975; Chaffin and Martin, 1999; Kroemer and Marras, 1981; Kuhlman, 1992; Kumar et al., 1998; Schanne, 1972; Stobbe, 1982; Takala and Viikari-Juntura, 1991). The strength values were highly variable between studies due to different sample populations and variation in testing positions and methods used in the studies. However, few studies exist containing similar strength data for subjects with SCIs. Strength studies for this population were usually focused on the strength of a particular articulation or task (Kulig et al., 2001; Woodfield, 1996) or failed to discriminate between different SCI injuries resulting in tetraplegia (Dallmeijer and Kappe, 1994; de Groot et al., 2005, 2007; Finley et al., 2004; Koontz et al., 2002; van Drongelen et al., 2005.

The most common approach to studying upper body strengths is measuring horizontal and vertical push and pull strengths (Das and Forde, 1999; Hoozemans et al., 1998; Kumar, 1995; MacKinnon, 1998; Resnick and Chaffin, 1995), measuring multi-directional strengths (Fothergill et al., 1991; Grieve, 1979; Pheasant and Grieve, 1981) at different points in space, or studying the strength of joint articulations (Amell, 2004; Chaffin and Martin, 1999; Kumar et al., 1998; Kumar, 2004; Kuhlman, 1992; Mayer et al., 1994; Stobbe, 1982; Stoll et al., 2002; Takala and Viikari-Juntura, 1991). Most studies focus on static isometric strength as this metric is the easiest to measure without specialised equipment and has been shown to correlate to dynamic strength and injury risk (Chaffin et al., 1978).

6.3 Push and Pull Data

Pushing and pulling has been estimated to account for almost half of all manual materials handling tasks in industry (Kumar et al., 1995). Consequently, many studies have looked at trends in maximal push and pull strengths. Most of these studies have been for able-bodied persons from a standing position, and for only a few fixed heights (for example, Fothergill et al., 1991; Kumar, 1995; Lee, 1979; Resnick and Chaffin, 1995). In a review of push-pull studies, Hoozemans et al. (1998) found that most studies identified a position of maximal horizontal exertion (from standing) somewhere between one meter high and shoulder height (Ayoub and McDaniel, 1974; Ciriello and Snook, 1983; Kumar, 1995; Kumar et al., 1995; Mital et al., 1993; Snook and Ciriello, 1991; Warwick et al., 1980).

In one such study, Kumar (1995) performed 2-handed tests from a standing position, at 350 mm, 1 m and 1.5 m above the ground and found the mid-level height the strongest position. Ayoub and McDaniel (1974) found the max push force to occur at approximately 70% of a subjects shoulder height; and in a study on single-handed pull strength at four heights from a seated position; Nelson (1998) found the optimal pull position was at waist height. Due to the spatial scarcity of measurements in published studies, this region of highest strength is almost half a metre tall, broadly representing the region from the seat to the shoulder for a seated person. However, there was no information on trends within this region.

Most studies on push and pull strength have been from a standing position. However, significant differences have been identified between forces from standing and seated postures. MacKinnon (1998) found seated pull forces were greater than those produced from a standing position with feet together, but less than those from a 'free-standing' posture with a larger support base at the feet. MacKinnon's average measured seated pull strength values nearest to the shoulder's sagittal plane ranged from 88 N to 138 N, and the difference between these seated forces and standing pull forces in the same position was a function of hand position in the frontal plane. While MacKinnon did not examine the effect of the fore-aft hand position in the sagittal plane on the difference between seated and standing strength, given the known effect of frontal plane position, it is unlikely the seated-standing strength relationship would be independent of sagittal plane position.

While existing push and pull strength studies provide indicative values and broad trends for sagittal plane strength, reported data is sparse. More importantly, data from

standing studies cannot be readily extrapolated and applied to a seated strength model without first understanding how sagittal plane hand position affects the correlation between seated and standing strength. Even the limited reported seated data present (Hoozemans et al., 1998) is too sparse and generalised for developing a model of sagittal plane strength and only exists for able-bodied persons. Hence, for the purposes of this research, there is no readily applicable prior art, although indicative trends are reported and some methods may be adaptable.

6.4 Articulation and Joint Strengths

The most common method used in studying strength characteristics is by measuring joint articulation strengths, such as shoulder or elbow flexion or extension for example. Studies on articulation strengths most commonly measure maximal static isometric strength. Some studies obtain articulation strengths for each joint at only one joint angle (Chaffin and Martin, 1999; Kroemer and Marras, 1981; Stobbe, 1982), while other studies measured joint articulation strength over the joint's range of motion (Amell, 2004; Baines, 1975; Kumar et al., 1998; Stoll et al., 2002). These studies have shown joint articulation strengths to be a function of joint angle, and due to some muscles spanning more than one joint, they are also dependent on the angles at multiple joints (Schanne, 1972). For example, elbow flexion strength is a function of shoulder abduction/adduction angle, as well as the elbow angle (Schanne, 1972). This joint interdependence phenomenon is more pronounced in some articulations than in others, but implies that articulation strengths measured in isolation from other joints cannot reliably be used to predict joint articulation strength for any position.

Schanne (1972) developed a hand force capability model, modelling each major shoulder or elbow articulation strength as a function of multiple joint angles. However, Schanne's model significantly under predicted a person's hand force capabilities (Schanne, 1972). This under prediction of strength was attributed to the assumption made in creating the model, that the strength of one muscle group was independent of the loading on adjacent joints. Conversely, Schanne's results suggested the higher the level of whole body muscular activation, the greater the interactive effect between a particular muscle group about a given articulation and the torque loading adjacent to that joint. The outcome was that various contracting muscle groups acting together would have a combined effect greater than the sum of their individual effects. Schanne's models for shoulder and elbow articulations are given in Equations (6.1) - (6.3).

$$Elbow\ Flexion: \quad T_E = 336.294 + 2.088\alpha_E - 0.015\alpha_E^2 - 3.364\alpha_{VS} + 0.019\alpha_{VS}^2 \tag{6.1}$$

$$Elbow\ Extension: \quad T_E = 264.153 - 0.575\alpha_E - 0.425\alpha_{VS} \tag{6.2}$$

$$Vertical\ Shoulder\ Abduction: \quad T_S = 227.338 + 0.525\alpha_E - 0.372\alpha_{HR} - 0.296\alpha_{VS} \tag{6.3}$$

Where α is the joint angle and the subscripts E, VS and HR refer to elbow angle, vertical shoulder angle, and shoulder horizontal rotation respectively.

6.5 Postural Stability Diagrams

Push-pull data is of limited use for design applications, as it offers no information on strength capabilities at directions other than horizontal or vertical. However, for interactions such as MWC propulsion, the applied force is almost exclusively directed in an angle deviating from the vertical or horizontal. Postural stability diagrams (PSDs) are polar plots where the radius represents the magnitude of the force for the exertion angle, theta. PSDs were first used by Pheasant and Grieve (1981) to illustrate the horizontal and vertical components of static forces in all directions in the sagittal plane.

Pheasant and Grieve (1981) produced PSDs each using 36 measurements taken at 10 degree increments, for six positions in the sagittal plane, 0.25m, 1.0m and 1.75m, 0.0m and 0.5m in front of the subject's toes. These tests were performed from a standing position with feet together, and then with feet staggered. Forces varied substantially and systematically as a function of exertion angle. Fothergill et al. (1991) produced PSDs from measured maximal forces in all directions in the sagittal plane at heights 1.0m and 1.75m from a standing position. Fothergill et al. found the ratio of one handed strength: two-handed strength varied between 0.64 - 1.04. There are no published PSDs for strength in the sagittal plane from a seated position.

Accurately measuring the multi-directional forces required to produce PSDs at different positions requires specialist measurement apparatus and n times more measurements than for a single directional study covering the same area, where n is the number of

directional measurements at each position. Pheasant and Grieve's study on strength in only 6 positions required over 200 strength measurements for each subject in each stance. For a tetraplegic individual, such a large number of measurements could readily induce fatigue and skew results.

This large data requirement may be a reason why studies that have measured multi-directional forces at different positions have only done this at a few positions. In particular, collecting such a large data set for one subject requires multiple test sessions to counter fatigue. Multiple testing sessions also present more of a challenge in ensuring repeatability, and, due to the time commitment, subject recruitment. Additionally, the motivation behind some spatial strength studies is task specific. Hence, the study can be limited to the relevant direction/s or positions for that task.

Pheasant and Grieve (1981) developed limiting equations to define bounds that the PSDs fell within. They also found push down forces were limited by a subject's body weight. However, no method for predicting PSD shapes has been developed. Additionally, these limiting equations by Pheasant and Grieve's are for a standing position and based on feet position. They are thus not appropriate for seated strength positions.

6.6 Strength in Subjects with SCIs

Very little data exists on the upper-body strength of people with spinal cord injuries. This fact may be due to the reduced population of subjects to test when compared with the able-bodied population, and the variation in abilities within this population group due to the complexities of SCIs. Few studies distinguished between people with different levels of tetraplegia, complete and incomplete injuries or investigated strengths for a range of motions. For example, there are a large number of studies examining elbow extension strength before and after deltoids-to-triceps muscle tendon transfer surgery, but not the overall three-dimensional force capability at the hand before and after surgery.

Other studies on people with cervical SCIs have focused on specific biomechanical reactive forces experienced at a joint for a given activity. For example, glenohumeral forces during MWC propulsion (van Drongelen et al., 2005). The motivation behind many of these studies is an understanding of, or reduction in, specific task-related injuries, or

the data is intended for musculoskeletal modelling of a joint.

The most complete study on hand force capabilities in persons with SCIs is that by Das and Forde (1999). Das and Forde measured seated right-handed isometric push-up and push-down arm strength in 24 positions for subjects with C4-T11 SCIs. Test positions were defined by the angles of the candidate's arm and forearm, and were not limited to the sagittal plane. Das and Forde found the push-up strengths of the candidates were only 30% of that of the able bodied forces measured by Hunsicker (1955), and the pull down forces were approximately 50%. However, Das and Forde did not distinguish between candidates with different level SCIs and did not include subjects with higher level tetraplegia.

A table of strengths from the literature for subjects with SCIS is given in Table 6.1. Using the Delft anthropometric data, the spatial positions for Das and Forde's measurements in the sagittal plane were calculated from joint angles with the shoulder located at (0, 1000) mm so comparisons could be made with spatial data from other studies and with data to be gathered in this study. The strengths in the study by Acosta and Kirsch (2000) are smaller than the minimum reported by Das and Forde (1999). This difference is most likely due to subjects with lower SCIs, and therefore only minimal upper body impairment, skewing results in Das and Forde's study.

6.7 Measuring Strength Among the SCI Population

There are several methods currently employed by physiotherapists for evaluating muscular strength in spinal cord injured persons, which are outlined in this section. The most common methods of measuring strength in the clinical environment are subjective, qualitative, methods such as the manual muscle testing (MMT) performed by the physiotherapist without any instrumentation. However, a wide range of instrumentation is available for qualitative muscular strength evaluation, to measure either static or dynamic strength. Hand held dynamometers, which measure static strength, are also widely available. Hand held dynamometers are versatile and can be used on all limbs and for most articulations. Specially designed dynamometers are available to measure the grip and pinch strength in the hand. Larger machines are available to measure dynamic / isokinetic strength of muscles. These machines have higher accuracy, but

Table 6.1: Strengths in the sagittal plane from literature, for subjects with SCIs

Reference	x (mm)	y (mm)	Value	S.Dev	Direction	Subject	n
Acousta 2000*	-	-	43.6 N	(24 N)	Up	C5	1
			20.0 N	(11 N)	Down	C5	1
Das and Forde 1999**	518	812	51.2 N	(21.5 N)	Up	C4-T11	8
	551	1000	56.9 N	(24.3 N)	Up	C4-T11	8
	1390	390	67.8 N	(31.7 N)	Up	C4-T11	8
	262	711	115.3 N	(42.2 N)	Up	C4-T11	8
	503	765	93.3 N	(27.3 N)	Up	C4-T11	8
	518	812	78.1 N	(66.5 N)	Down	C4-T11	8
	551	1000	80.4 N	(67.9 N)	Down	C4-T11	8
	1390	390	115.7 N	(100.0 N)	Down	C4-T11	8
	262	711	93.7 N	(25.3 N)	Down	C4-T11	8
	503	765	139.5 N	(47.0 N)	Down	C4-T11	8

*(an elbow, abduction shoulder)
**Positions in space calculated using delft anthros with shoulder at (0, 1000)

are less versatile. In addition, their higher cost and size prohibits them from being widely used by physiotherapists for rehabilitation in comparison to simpler tests.

Manual Muscle Testing (MMT)

Manual muscle testing is a non-instrumented form of strength testing where a clinician gauges the strength of an articulation by opposing the articulation themselves. As no instrumentation is involved, the outcomes from this kind of testing are subjective with poor reliability and repeatability. Standardised processes for MMT have been developed, such as the Daniels and Worthingham method, where resistance is applied either throughout the full range of motion or only at the range of motion limits. The Kendall method, applies maximum resistance in the middle of the range (O'Sullivan and Schmitz, 1994) and was developed to improve consistency in results. Strength is graded according to four or five main categories plus some graduations according to how 'normal' it is. Despite graduations in the grading scales, this method is typically insensitive to small changes ($<$25%) in strength and scores can differ by as much as 50 – 60% between clinicians (O'Sullivan and Schmitz, 1994). MMT has traditionally been used for determining patterns in muscle weakness and comparative muscle strengths, as well as monitoring the progress of a therapeutic program, but is inaccurate for determining muscle capacity.

Hand Held Dynamometry

Hand held dynamometers provide an objective measure of the strength of arm, shoulder and leg muscles. Strength is measured using either a 'break' test, in which the tester exerts force against the subjects limb until it gives way, or a 'make' test, in which the patient exerts force against a stationary dynamometer. Studies into the accuracy of hand held dynamometers report mixed results on their reliability. Some claim the dynamometers are very reliable Bohannon, 1986; Hayes et al., 2002, with high repeatability, while other studies report large variability in measurements (Lennon and Ashburn, 1993; Riddle et al., 1989). To obtain accurate results, most dynamometers only measure force in one plane and therefore need to be held perpendicular to the limb during testing. Angulation of the device can introduce errors. Difficulties can be encountered stabilising a subject's limb or the device, and, as for manual muscle testing, the tester must be stronger than the subject.

Mechanical and electrical dynamometers are widely available commercially. Mechanical dynamometers normally consist of a spring or hydraulic mechanism with a dial gauge. Electrical dynamometers contain load cells or strain gauges with a digital display. Most hand held dynamometers don't measure inclination so typically the position of the arm additionally needs to be measured using a goniometer, ruler, other system, or, most commonly, by visual estimation; all of which may introduce error from the measurement position estimate.

Dynamic Dynamometry – Isokinetic Testing

In this method of strength testing, isokinetic machines measure the strength of the limb as it moves at a constant speed through its range of motion. The machine changes the resistance throughout the limb's motion to match the user's applied force. The advantage of these machines is that they can measure the maximum muscle strength through the entire range of motion of the joint or machine, endurance and fatigue can also be measured. As there is no acceleration or jerk, this is relatively safe for strength testing. However, the tests don't simulate reality where motions are rarely performed at constant or smooth velocities.

Isokinetic machines are typically large, bulky and costly. The ranges of motion and muscle groups each machine can test are also limited. Hence, this method of testing is uncommon in physiotherapy.

Trunk/Whole Body Dynamometry

Different methods and devices are employed when testing the strength of muscles in the torso than those used for limb muscle groups. Methods include cable tensometers, where a harness is secured around the torso and cable from the harness connected to fixed object such as a wall or floor. Tension in the cable is measured to determine peak torques. Strain gauge dynamometers are also sometimes used to test the isometric strength at multiple positions in the trunk. Isokinetic trunk dynamometers operate in the same manner as for limb-muscle measurements. Isoinertial trunk dynamometers measure torque and velocity of trunk motion.

Various tests exist for measuring static and dynamic lifting strength, which include measurements of trunk strength, upper and/or lower body strength. These tests are typically used during the rehabilitation of spinal injuries, not involving the spinal cord, and in industry for evaluating health and safety factors and acceptable workloads. These are not of much interest for this study as subjects with complete C5-7 tetraplegia have no trunk functionality. However, they may be useful for future studies with a different focus population.

Outcome Measures

Outcome measures or functional performance evaluations are not strictly strength or range of motion tests. These measures are widely used by occupational therapists and tend toward a holistic approach with the aim to measure and monitor the subject's abilities and limitations. Functional assessments involve standardised tests to measure functional performance in self-care, mobility and communication, among others.

A large number of assessment processes and grading methods exist, amongst these are Functional Independence measures (FMI), the Barthel Index, PULSES (Physical/health, Upper limb functions, Lower limb functions and mobility, Sensory, Excretory, Support), the Klein-Bell ADL Scale, the Katz index and the Kenny self-care evaluation (Tan and Lee, 1998). In the context of SCI testing for this study and modelling, these outcome metrics are of limited use due to their qualitative nature.

6.8 Fatigue and Endurance

Endurance is the ability to persist in a physical task, and is typically measured in time to exhaustion or failure. Muscle fatigue is "any reduction in the ability to exert force

in response to voluntary effort" (Edwards 1981, Bigland-Ritchie et al 1995, Chaffin and Martin, 1999). Fatigue is related to the intensity of a task, and the maximum voluntary contraction (MVC) or strength of an individual. The lower the intensity of the task, the longer the individual can persist.

A primary reason claimed for localised muscle fatigue is due to the reduced blood flow within the statically contracted muscle. The degree by which blood flow is reduced depends on exertion level. Studies have shown blood flow is hindered at between 10-50% of maximum exertion, and entirely occluded above 50% (Chaffin and Martin, 1999; MacIntosh and Devrome, 2004; **?**; Blangsted et al., 2005).

The concept of an endurance limit (Rohmert, 1973) or critical power (Bishop et al., 1998) has been suggested in some fatigue models. Such a limit presumes that fatigue is asymptotic with load and a minimum load limit exists below which an individual can perform a task indefinitely without fatigue. Rohmert 1960 placed this limit at 15% of MVC and Bjorksten and Jonsson 1977 at 8%. However, more recent studies suggest that fatigue develops at any contraction level (Bjorksten and Jonsson, 1977; Mathiassen and Ahsberg, 1999; Sato et al., 1984; **?**) and was most likely not detected by these previous studies due to insufficient test durations. Finally, fatigue relative to MVC has been shown to be affected by gender, training and psychological factors (Chaffin and Martin, 1999; MacIntosh and Devrome, 2004), but not by age.

For intermittent tasks, such as the collection of static strength values, fatigue has been shown to be a function of the type of task, the subject's physiology and training, and the exercise-to-rest ratio (Chaffin and Martin, 1999). Time to fatigue is prolonged by even short rest periods (Lee, 1979; **?**), where longer rest periods allow longer endurance times for a given contraction or task. Consequently, most strength studies have attempted to mitigate the effect of fatigue on strength data by specifying minimum rest periods between static strength measurements.

For example Hughes et al. (1999) specified a rest of 5 s - 2 minutes between measurements, Resnick and Chaffin (1995) specified 2 minutes, MacKinnon (1998) 60 s, Das and Forde (1999) 60 s and Kumar (1995) 2 minutes between each set of 3 measurements. Schanne (1972) specified a ratio of rest:work of 24:1, and also found a longer rest was necessary ever 10 measurements to prevent fatigue. Additionally, measurements for studies requiring large numbers of measurements sometimes collect the data in multiple sittings over several days, as in the studies of Schanne (1972) who used

1350 test positions, Fothergill et al. (1991) and Kumar (1995).

Several studies have developed models for the ratio of holding time T_{hold} to rest time T_{rest} as a function of MVT or maximum holding time (MHT) (Bystrom and Fransson-Hall, 1994; Milner, 1985; Price, 1990; Rohmert, 1973; Rose et al., 1992). These models are listed in Equations (6.4) -(6.8). The rest times they predict for different applied forces as a fraction of MVC, for 1 s, are given in Table 6.2.

$$\frac{T_{rest}}{T_{hold}} = 18 \times \left(\frac{\%MVC}{100}\right)^{1.4} \times \left(\frac{\%MVC}{100} - 0.15\right)^{0.5} \times 100 \quad (Rohmert,\ 1973) \tag{6.4}$$

$$\frac{T_{rest}}{T_{hold}} = 0.164 \left[4.61 + \ln\left(\frac{1}{100 - \frac{100}{\%MHT}}\right)\right]^{-1} \times 100 \quad (Milner,\ 1985) \tag{6.5}$$

$$\frac{T_{rest}}{T_{hold}} = 3 \times mMHT^{-1.52} \times 100 \quad (Rose\,et\,al.,\ 1992) \tag{6.6}$$

$$\frac{T_{rest}}{T_{hold}} = \left[\frac{\%MVT}{15} + 1\right] \times 100 \quad (Bystrom\,and\,Fransson-Hall,\ 1995) \tag{6.7}$$

$$\frac{T_{rest}}{T_{hold}} = \frac{18\,(T_{hold})^{1.4}\left(\frac{\%MVC}{100} - 0.15\right)^{0.5}}{MHT} \quad (Price\,1990) \tag{6.8}$$

Table 6.2: Rest times (s) predicted by each of the fatigue models (Equations 6.4 to .6.8) for a force application time of one second

Applied force as a fraction of MVC	**Max holding time (s) Van dieen**	**Price, 1990**	**Milner, 1985**	**Rose et al., 1992**	**Bystrom and Fransson-Hall, 1994**	**Rohmert, 1973**
0.02	612	0.0	0.0	0.0	0.0	0.0
0.1	426	0.0	0.0	0.0	0.0	0.0
0.3	174	2.4	0.0	0.1	100	0.5
0.5	72	8.9	13	0.5	233	2.7
0.7	24	33.4	59	2.4	367	15.6
0.9	12	77.9	124	6.9	500	48.1

Of these different models, Rohmert (1973) is that most commonly used for engineering design purposes. However, it is based on the assumption that no fatigue occurs at less that 15% MVC. Unfortunately, the rest times predicted by these models vary significantly and, to date, no study appears to have evaluated the accuracy of these different models (El ahrache and Imbeau, 2009).

The models by Bystrom and Fransson-Hall (1994) and Rose et al. (1992) are simpler models which don't consider the holding time as a percentage of the maximum. Milner's model was developed for a specific posture at 100% forward reach and where the applied force was zero, and no studies have evaluated the accuracy of this model for applied loads.

Thus, Rohmert (1973) and Price (1990) are the most relevant models for developing a protocol for this study. It should be noted that essentially no research is available verifying Price's model (El ahrache and Imbeau, 2009), however it is more conservative than Rohmert's model.

6.9 Summary of Existing Test Methods

Very little data was available in the literature concerning the upper body strength of people with C5-C7 tetraplegia, and there was no data set for this group comprehensive enough from which to develop a model of strength in the Sagittal plane. Data from the most common measurement methods employed by physiotherapists, such as MMT, is qualitative and provides only a measure of weakness, not of strength. Thus, it is not sufficient for building a strength capability model. Quantitative data gathered by physiotherapists was not comprehensive enough and was for isolated articulations that Schanne (1972) showed was an inadequate predictor of hand force capability.

No studies were found that investigated variations in hand force capability in multiple force application directions over a person's full reach in the sagittal plane from a seated (or standing) position. The most common approach to measuring strength amongst literature was that of measuring the strength of various articulations, although no such studies of strength with joint angle for multiple articulations were identified for subjects with C5-C7 Tetraplegia. However, as this articulation based data has been shown to be inadequate for developing hand force models, experimental data is required to develop an upper body strength model. Finally, Fatigue is an important

consideration in developing a measurement protocol for strength measurements and the model by Rohmert (1973) (Equation 6.4) would be the most appropriate model for designing a protocol with an appropriate rest time between strength measurements.

All of these outcomes from this prior art will be used in the development of a test rig and methodology for this research and population, as covered in Chapter 7.

Chapter 7

Strength Study: Methodology

In Chapter 6 it was shown that there have been no comprehensive studies to date into the upper-body strength of people with tetraplegia, and reported strength data for this population is sparse. This chapter develops an experimental methodology for collecting that data so that a suitable strength model can be developed.

The considerations in developing a strength model are outlined in Section 7.1. Section 7.2 evaluates possible approaches for measuring strength, and describes a preliminary exploratory study that was used to evaluate the approaches. A test protocol and test rig was developed using insight from Sections 7.1 and 7.2, and was used to collect strength measurements. The protocol, the rig, and experimental trials are presented and discussed in the remainder of the chapter. Results from these trials are later presented in chapter 8.

7.1 Considerations

Inter-subject Variation

Even if the sample population is limited to subjects with complete C5-C7 injuries, there will still be significant variation in abilities between people with the same level injury in the same way there is variation in strength ability among the able-bodied population. Subject age, time since injury, rehabilitation and activity levels or sports participation will all contribute to variation in strength capabilities between subjects. Additionally, reports in the literature show no consensus on the segmental innervations of muscles due to neurological variability between individuals, and some studies suggest variations in innervation between individuals. Consequently, two people with 'identical' injuries

may have different muscular functionality.

Unconventional Movements

People with tetraplegia often use "tricks", such as locking joints, to perform tasks in a unconventional manner and better utilise their reduced muscle capabilities. In addition to these "tricks", some deliberate motions performed by a person with tetraplegia are accompanied by antagonistic actions where antagonist muscles for that motion have been paralysed and are thus unable to balance the actions of the other muscles. For example, in some people with tetraplegia contraction of the biceps causes elbow forearm supination, as well as elbow flexion.

These unconventional and antagonist movements cause further complications in predicting strength capabilities in the sagittal plane from isolated articulation strength data, beyond those complications and limitations already identified in Schanne's study (1972). These movements would be a function of several joint angles. Thus, the complexities of these tricks and antagonist actions would need to be understood and incorporated into any model based on articulation strength data to prevent underprediction of strength. Conversely, if spatial hand force data were gathered, it could be expected that the trial subject would adopt their most effective force application posture for each sample, including some of these unconventional methods. Thus, the data would already contain the complex interactions and effects of these "tricks" and antagonist movements. Finally, it is likely that identified the interactive effect of multiple joints identified in Schanne's study (1972) differs in the SCI population from that for the able bodied population.

Balance

A person's ability to balance when seated depends on their torso and upper extremity strength. An individual's ability to balance affects their reaching, object movement and force application abilities. People with C5-C7 tetraplegia have paralysed torso muscles and in many cases rely on external forces to stabilise themselves. Thus, it is likely the characteristics of one-sided strength will be significantly different from those for symmetric measurements, where the torque about the torso produced by the load at one side is reacted by the load at the other hand or point of grip. One-sided strength characteristics will be strongly dependent on any external constraints or any

other asymmetric forces at the other hand. As wheelchair propulsion is primarily a symmetric motion, two handed symmetric force information needs to be gathered in this research to produce a reliable model.

Static or Dynamic Measurements

Isometric static strength is the easiest type of strength to measure and consequently is the most common type of strength reported in literature. While the data is intended for use with a a model of dynamic interactions, static strength data has been shown to correlate to dynamic strength (Chaffin et al., 1978) and thus is suitable for this purpose. Hence, it provides a simple and effective means of measurement that with added tools can also provide insight into dynamic motions, as well.

7.2 Methodology

Two options were identified for measuring strength, spatial-based measurements or non-isolated articulation measurements. Non-isolated articulations would allow adjacent joints to be loaded during testing, as they would be during tasks. Thus, they would be a more accurate predictor of strength than isolated articulation data.

As the capability for calculating reactive forces and moments at each joint has been built into the constraint modeller as described in chapter 5, the simplest means of constraining the manikin would be to bound these reactive forces or joint torques. These bounds could either use single, angle independent upper and lower bound for each reaction force and moment, or be a function of one or more joint angles. A model with single torque or force bounds at each joint would be computationally fastest. However, articulation strength has consistently been shown to be a function of joint angle (Baines, 1975; Chaffin and Erig, 1991; Chaffin and Martin, 1999; Kumar, 2004; Schanne, 1972). Therefore, joint articulation models from the literature were investigated to estimate the error introduced by modelling articulation strength as joint independent or as a function of only one joint angle.

Schanne's model for elbow flexion (1972) is shown in Figure 7.1. If measurements were only taken throughout the elbow's range of motion, then the resulting model is that shown in Figure 7.2 and the error is shown in Figure 7.3. This simplification results in a maximum error of almost 40% when the vertical shoulder angle is 90^{o}. It was

hypothesised that for C5-6 injuries this error would be smaller as the triceps span both the shoulder and elbow and are paralysed in this population. However, those with C7 injuries retain some triceps function and thus the error level for that population is likely to still be too high to justify these simplifications. Hence, if the manikin was to be constrained using joint moments, articulation strength would need to be gathered for different elbow and shoulder joint angle combinations.

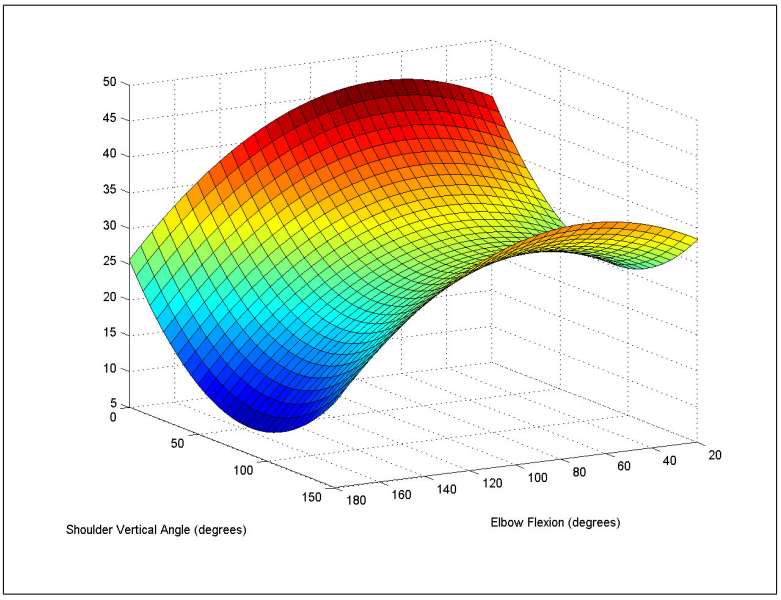

Figure 7.1: Predicted elbow flexion strength as a function of elbow and shoulder angles Schanne (1972)

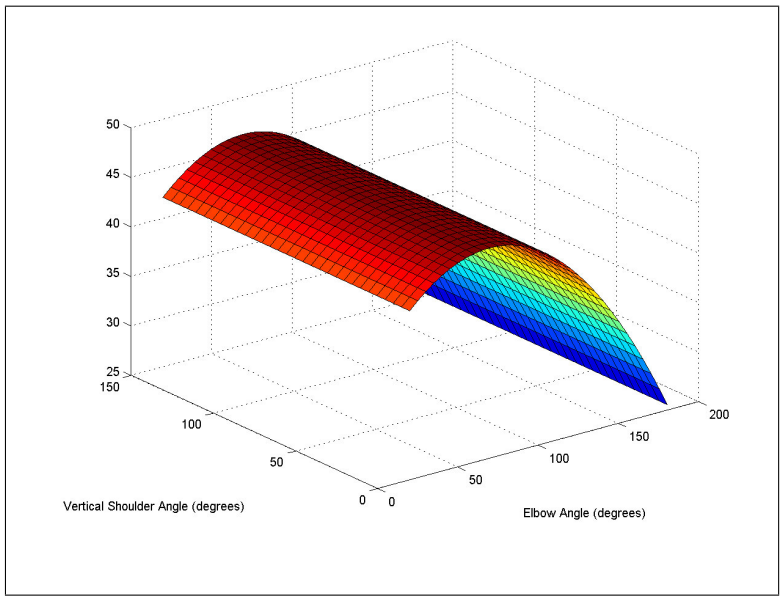

Figure 7.2: Predicted elbow flexion strength if strength were assumed to be only a function of elbow angle

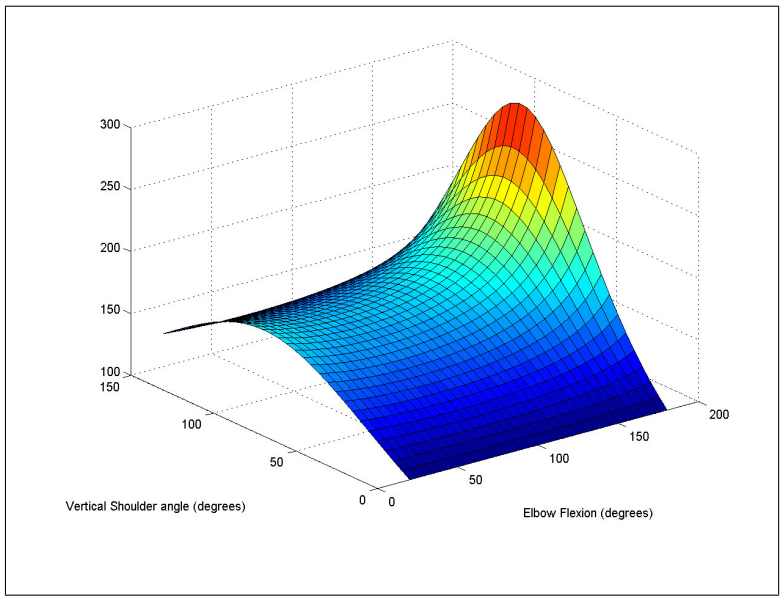

Figure 7.3: Error, based on Schanne (1972), introduced by assuming elbow flexion independent of shoulder angle

7.2.1 Exploratory Strength Study

To evaluate the viability of using a hand-held dynamometer for gathering strength measurements, a series of preliminary tests were carried out on able bodied persons. The static strength of ten articulations were measured, as outlined in Table 7.1. Seven able-bodied males of average age 22 and height 1.77 m were tested using a hand held dynomometer supplied by Independent Research Limited (IRL). Each articulation was measured three times and the best of the three measurements recorded. The participants, who each gave their informed consent to participate, were instructed to apply maximum force to the dynamometer force plate. The participants were seated for all measurements and all of the measurements were unsupported with no parts of the body restrained. The order of strength measurements was random and varied between participants. After all articulation strengths had been measured for a participant, 'spot' checks were performed by re-measuring the strength of the first two articulations to check for fatigue. The results of these trials are shown in Figure 7.4.

Table 7.1: Definitions of Articulations for Able Bodied Strength Measurements

Articulation	**Description** (exrx.net 2009)	**Measurement method**
Shoulder Abduction	Lateral movement away from the mid line of the body; moving the upper arm up to the side away from the body.	Elbow bent 90^{o}, upper arm by side. Dynomometer placed at elbow to measure lateral force
Shoulder Flexion	Bending the joint resulting in a decrease of angle; moving the upper arm upward to the front.	Arm straight by side, dynomometer placed at inside of elbow to measure frontal force.
Shoulder Extension	Straightening the joint resulting in an increase of angle; moving the upper arm down to the rear.	Starting with elbows above the head, dynomometer placed on bony landmark at elbow. Force measured from rotating arm downwards towards front.

Articulation	**Description** (exrx.net 2009)	**Measurement method**
Shoulder Adduction	Medial movement toward the mid line of the body; moving the upper arm down to the side toward the body.	Starting with elbow above the head, upper arm rotated so forearm is bent medially. Dynomometer placed on elbow, force measured from rotating arm downwards laterally towards side.
Horizontal Flexion	Medial movement toward the mid line of the body in a horizontal plane; moving the upper arm toward and across the chest with the elbows facing out to the sides.	Arms out to side so elbow is at the same height as the shoulder. Elbow bent so forearm is upwards. Dynomometer on front of elbow to measure frontal force.
Shoulder External Rotation	Rotary movement around the longitudinal axis of the upper arm away from the center of the body; turning the upper arm outward	Elbow bent 90^{o}, upper arm by side. Dynomometer placed laterally on wrist, lateral force measured from rotation about the upper arm.
Shoulder Internal Rotation	Rotary movement around the longitudinal axis of the bone toward the center of the body; turning the upper arm inward.	From the same position as for shoulder external rotation, but dynomometer placed medially on wrist and medial force measured from rotation about the upper arm
Elbow Flexion	Bending the joint resulting in a decrease of angle; bringing forearm toward upper arm.	Bicep curl, elbow bent 90^{o}, upper arm by side. Dynomometer placed on the inside of the wrist wrist

Articulation	**Description** (exrx.net 2009)	**Measurement method**
Wrist Extension	Straightening the joint resulting in an increase of angle; moving the back of the hand toward the back of the forearm.	Palm facing down, dynomometer placed against back of hand to measure upwards force
Wrist Flexion	Bending the joint resulting in a decrease of angle; moving the palm of the hand toward the front of the forearm.	Palm facing up, dynomometer placed against palm to measure downwards force.

Subject 7 was a serious kayaker, and consequently recorded higher values for most articulations compared with the other participants. No other subjects actively participated in sports heavily reliant on upper body strength. Amongst the able-bodied participants elbow flexion was the strongest articulation measured using the hand-held dynamometer. This result was contrary to reports in the literature, where shoulder articulations were generally reported to be stronger.

Static isometric elbow flexion values in the literature at 90 degrees flexion ranged from 77 Nm (Stobbe, 1982) to 141 Nm (Kroemer and Marras, 1981). These values are much higher than the approximately 65 Nm average moment measured in these trials. It is unlikely the populations in these other studies were significantly stronger than the populations used in these trials, but that differences in these values were due to different measurement protocols and techniques.

Shoulder articulation values were significantly lower than those in reported in the literature. The shoulder abduction values in literature. ranged from 47 Nm (Mayer et al., 1994) to 195 Nm (Essendrop et al., 2001), and adduction from 67 Nm (Stobbe, 1982) to 177 Nm (Veeger et al., 2002). Median shoulder flexion from the preliminary trials was 54 Nm, less that half of the 122 Nm reported by Baines (1975) and 110 Nm by Stoll et al. (2002). Where multiple values were presented in the literature for articulation strengths, values for the dominant hand, the right hand and/or the 50th percentile were used for comparison.

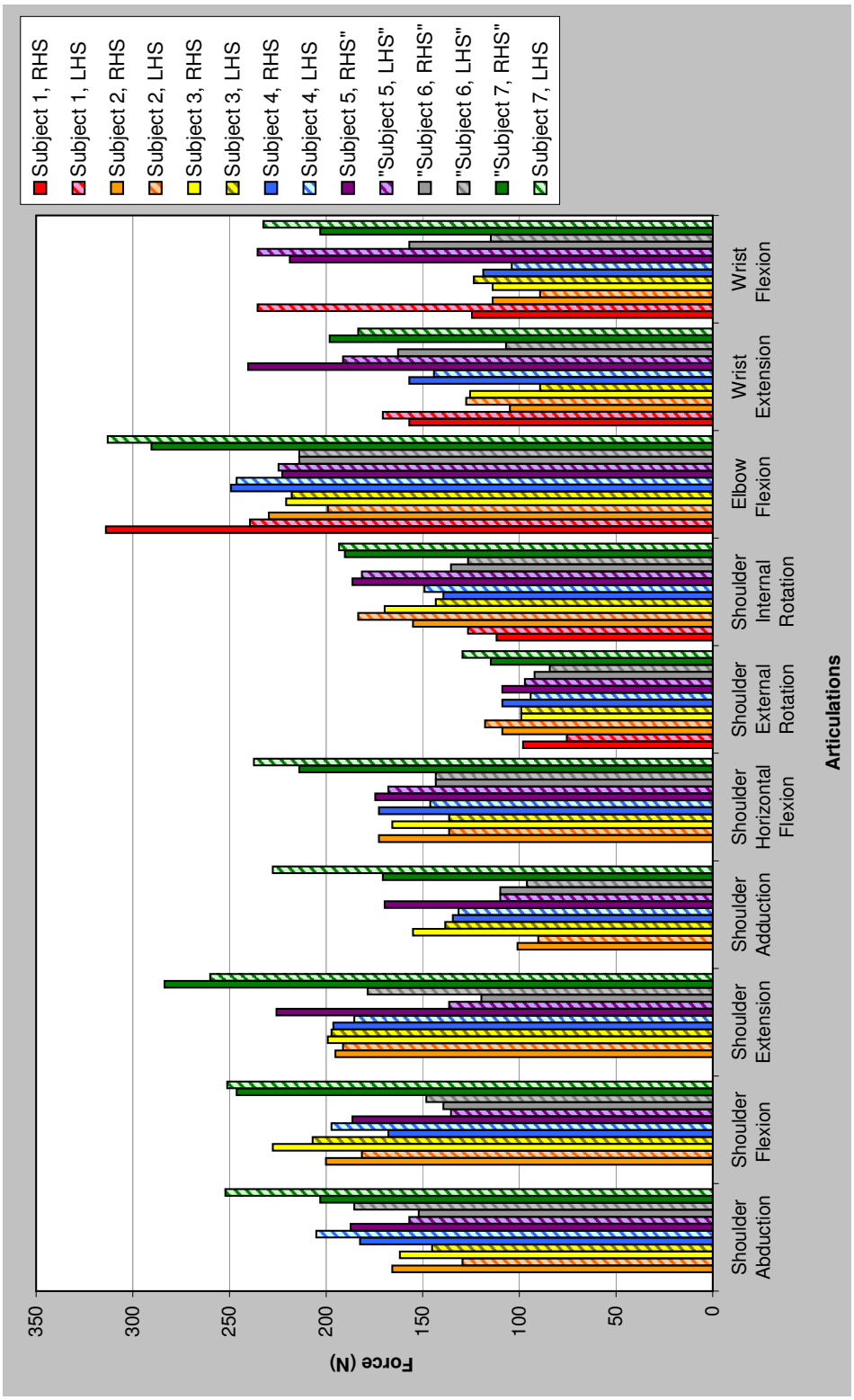

Figure 7.4: Results from Able-Bodied Joint Articulation Measurements

During data collection, problems were encountered accurately controlling the posture and angle of the participant's limbs as no measurement devices were used to position the subject's arms for measurement. As the participant began loading the dynamometer, it was often displaced slightly before the tester reacted to counteract the applied force. Consequently, even if the arm was accurately positioned initially, the angle at which the force was applied was dependent on the reaction speed of the tester holding the dynamometer.

The most significant limitation using the hand-held dynamometer was reliance on the tester's own strength. Accurate values were only possible where the tester was able to hold the dynamometer stationary against the applied force. This issue was a lesser problem for the smaller muscle groups, such as for wrist flexion and extension. However, it was a problem for some shoulder articulations and may explain the discrepancy between the measured data and literature values.

Scapular articulations were unable to be measured using the hand-held dynamometer, as the forces were too large to be reacted. Because the tester had to brace the dynamometer at the force application point to keep it steady and react the applied force, the position of the measurements affected the accuracy of measurement. Often the force application point was in a position where the tester's most comfortable or strongest brace position placed the dynamometer at an angle to the applied force and consequently only measured the force component perpendicular to the dynamometer.

For the purpose of this exploratory study, subjects were instructed to only apply force using the joint in question to enable literature comparisons. However, each articulation was not isolated and thus the influence of other muscle groups, for example leaning into a measurement with the torso, were impossible to control. Some participants had better technique for isolating the articulation than others, so caution must be taken when comparing measurements between participants.

Fatigue was not reported to be a problem in elbow or shoulder articulations by any of the participants, and the 'spot' check measurements didn't show any significant fatigue effects. Some subjects did report fatigue, discomfort or pain in wrist measurements, suggesting hand-held dynamometry may not be suitable for measuring wrist strength. Additionally, discomfort was reported for some articulation measurements where the dynamometer was unable to be placed on a bony landmark, such as when measuring shoulder horizontal flexion. Where a participant considers a force application to be uncomfortable or painful, they are less likely to apply a maximum load and therefore

the recorded values are likely to be lower than the true maximum.

In summary, strength articulation values measured in this preliminary study of 7 able-bodied males were significantly lower those reported in literature, particularly for shoulder articulations. This discrepancy in values was most likely caused by measurement inaccuracies caused by the positioning of the dynamometer and reliance on the tester's strength. This would be a lesser problem amongst the disabled population for articulations where strength was reduced, but would still be an issue for measurements in awkward positions or for an articulation where the subject had normal or only slightly reduced capabilities. Discomfort was a problem for the measurement of some articulations and likely resulted in sub-maximal strength values being recorded.

This exploratory study showed that using a hand-held dynamometer for measuring the static strength of unsupported joint articulations yielded inaccurate or highly variable strength measurements and presented difficulties in accurately positioning the limb. These inaccuracies would be compounded when measuring two-handed strength and two testers would be required. Thus, this method was deemed inappropriate for this overall research study.

7.2.2 Chosen Measurement Method

It was decided to measure hand force at various positions in space in a similar manner to the push and pull strength studies discussed in Chapter 6, because this overall force capability at the hand is of most interest for design applications. The inaccuracies from the hand held dynamometer in the exploratory study were primarily caused by the positioning and support of the dynamometer. A dynamometer or load-cell supported by a rig could eliminate these measurer-induced errors and ensure accurate positioning of the limbs.

In such an approach with a fixed test rig, for each force application position the subject would likely choose the posture and arm position for maximum strength for the given direction and position. This method would thus also measure the combined effect of all joint strengths as well as any 'tricks' or the effect of any antagonist movements that wouldn't be accounted for in a joint-based model. A simple rig would be required for accurately positioning a dynamometer or load cell for measurements. To constrain the manikin using spatial data would mean joint reactions wouldn't need to be calculated

for the applied force, although this capability would still be retained.

7.2.3 Data Requirements

For modelling MWC propulsion, sagittal plane strength data was required over a sufficiently fine grid. In addition to the forward, back, up and down forces at each grid point, measurements at intermediate directions were required. Two intermediate directions (30^{o} increments) was considered minimum to produce a representative polar plot of strength, three intermediate directions (22.5^{o} increments) would allow trends to be more readily identified. However, it may be impractical, both due to the number of measurements required and the practicalities of building a rig to accommodate that many positions. As wheelchair propulsion is two-handed symmetrical motion and one-handed strengths have been reported to differ from two-handed strengths (Fothergill et al., 1991; Kumar et al., 1995) due in part to the asymmetric load on the torso and the different one-handed and two-handed postures adopted for force application at the same position; two-handed strength should be measured.

7.3 Rig Design

The rig designed for data collection consisted of three main parts; the positioning rig, and two load cell brackets attached to the rig. The positioning rig consisted of two parallel RHS lengths mounted to a plywood base. The distance between these two sections was adjustable to allow for wheelchairs of varying widths. An upright piece of RHS was attached perpendicular to each of these base lengths. The position of these upright sections along the base section was adjustable to modify the fore-aft position of the load cell. The load cell brackets were attached to the upright section and the height of these brackets was adjustable. The rig is shown in Figure 7.6, the bar across the top was to limit movement of the upright sections and keep them parallel when a force was applied.

A LPX 50 kg compression load cell was mounted to each load cell bracket. The brackets are shown in Figure 7.5 with the load cells attached. Force is applied by the hand to an aluminium dome hinged above the load cell. Twelve equally spaced holes on the bracket enable the load cell to be angled at 0°, 30°, 60°, 90°, 120°, 150°, 180°, 210°, 240°, 270°, 300° and 330° using a locating pin. The load cell is rotated about the top of the dome, so the force application position in space is the same at all angles. The

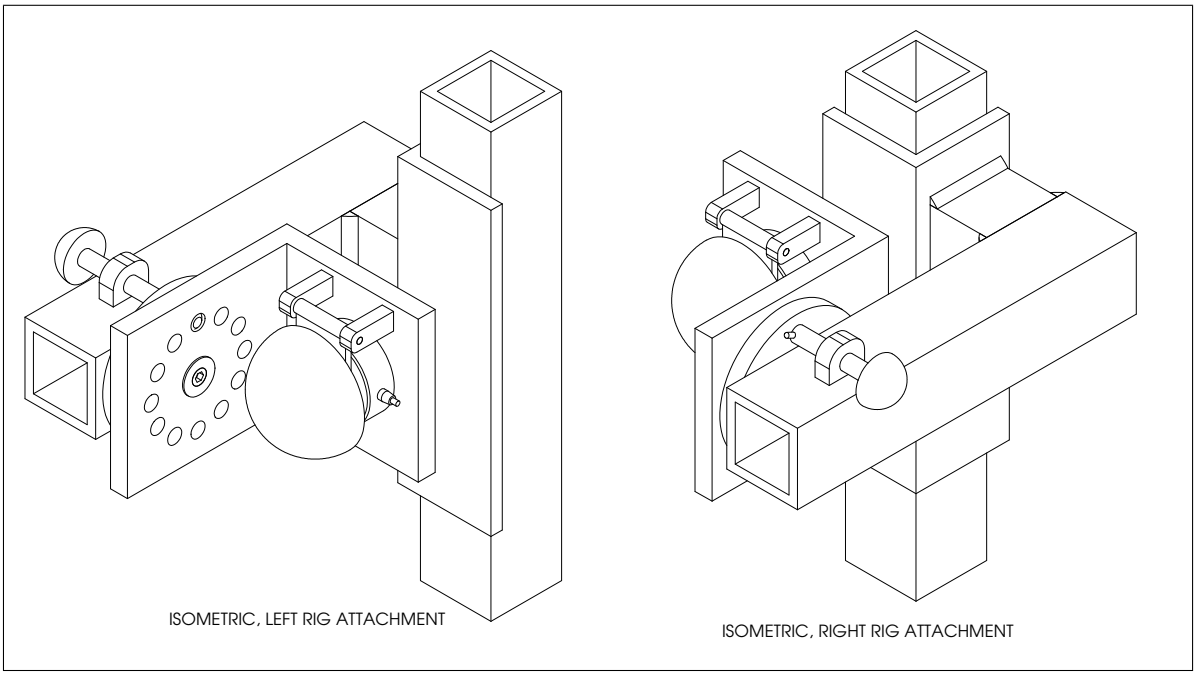

Figure 7.5: Load cell attachment brackets

load cell cables were connected to a carrier port and to a laptop through a USB port.

Data was sampled at 100 Hz. Voltage difference was scaled by an excitation voltage to compensate for any changes in excitation voltage (typically 2-5 V). This voltage was then converted to Newtons using a scale factor of 250,000 and calibrated using known masses.

7.4 Test Protocol

Anthropometric information was gathered for each subject. The upper arm was measured between the bony landmarks the acromion at the shoulder and olecranon at the elbow, and the forearm was measured from the olecranon to the ulnar styloid process at the wrist. Each subject's height and weight was recorded, and the position of their shoulder relative to the wheel axle was measured when they were seated in a neutral position. Before testing, each subject was advised of the testing procedure, and gave their full informed consent to participate.

Each participant was measured seated in their own wheelchair, the chair was positioned on the rig so the wheel axle was aligned with the horizontal measurement origin. The wheelchair was secured in place using four tie-downs. The position of the back apex

of the seat was measured and recorded. The two load cells were positioned as close to the chair wheels as possible; where it was practical the hand rims were removed from the wheelchair.

A grid of 100 mm increments was marked on the horizontal and upright sections, the horizontal origin was the wheel axle and the vertical origin was the base of the rig. Push forces were measured at each grid position within a subject's reach. The subject was allowed to apply force in the manner that they found was most natural or strongest. No attempt was made to keep the shoulder position fixed. The subject was permitted sub-maximal trials before the trial formally commenced and as they wished as the testing progressed to get used to the rig and the setup.

A random horizontal starting position forward of the wheel axle was selected, and the load cell was mounted in the highest vertical position. The subject was instructed to push the dome on the load cell as hard as they could. They were permitted three successive pushes and the highest force measured for each hand over these three pushes was recorded. These three pushes took approximately 3-5 seconds in total, including micro-breaks between the efforts. Where multi-directional strength was being measured, the orientation of the load cell was rotated 30° clockwise starting from the vertical 'up' measurement position. A total of twelve measurements were recorded for each vertical position for the load cell. The testing was continued in this manner and horizontal test positions were alternated between positions forward and behind the chair axle to change the muscle groups being employed in testing. The load sells were zeroed at each measurement position. Where a test position was outside a subject's reach, a value of zero was recorded.

The subjects were given approximately one minute rest between each vertical movement of the load cell, a longer rest was allowed between each horizontal position. Much of this rest time was absorbed by the time taken to record data and reposition the load cell bracket. Longer rests were given if the participant felt they were necessary to mitigate fatigue. If the subject reported feeling fatigued and this fatigue didn't improve with longer rest breaks, the trial was terminated.

Test sessions were limited to 60 to 90 minutes and most sets of push strength data were collected over two sessions with a break of at least two hours between sessions. Where multi-directional measurements were collected, only one horizontal position was measured per test session, and no more than two were measured in a day. To check for the effect of fatigue and repeatability, at least three measurements were re-measured

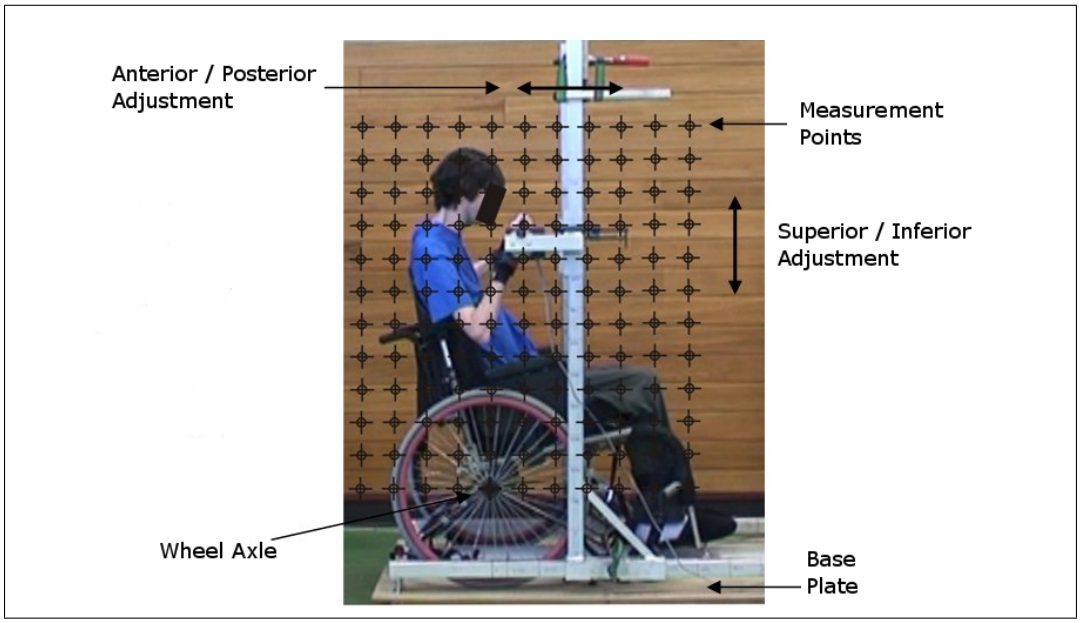

Figure 7.6: Photo showing test positions

Table 7.3: Grid positions for strength test measurements

	Direction Distance from the centre of the wheel (mm)										
Anterior/Posterior	-400	-300	-200	-100	0	100	200	300	400	500	600
Superior/inferior	0	100	200	300	400	500	600	700	800	900	1000

at the end of each measurement session. Figure 7.6 shows the test positions (Table 7.3) relative to the wheelchair.

Able-bodied subjects were instructed not to use their feet to aid react the applied forces and were encouraged to let their feet hang beyond the foot rest so this was not a temptation. Excluding the feet, means the data is applicable to subjects with a lower SCI and full use of their torsos, and in a wider range of seated situations for the able-bodied population.

7.5 Data Processing

Data was recorded in an Excel spreadsheet for both the right and left hands separately, and the combined two-handed strength. Distances were normalised with respect to a person's arm length, and from the base of the chair. Push forces were normalised with respect to the maximum force recorded during the trial.

7.6 Subjects

Tetraplegic subjects selected for testing were males aged 16-60 with a complete C5-C7 SCI and at least twelve months post surgery. A series of tests were also carried out on able-bodied subjects both for proof of concept and protocol refinement. They were also performed to gather a control data set that was missing in the literature. Due to time constraints, limited access to subjects with tetraplegia, and the time commitment required by subjects for such comprehensive data collection, only push strength was measured for subjects with tetraplegia. A full comprehensive multi-directional data set was gathered for an able-bodied subject to develop the modelling concepts.

7.7 Discussion

In addition to the measurement apparatus and protocol, maximum voluntary contractions could be influenced psychological factors, such as competition, verbal encouragement (McNair et al., 1996) or intrinsic motivation. External factors were, as much as possible, kept consistent between trials. Intrinsic motivation varied between individuals. However, it was assumed that motivation was unaffected by test position and thus did not influence the trends in the force data. Re-measuring some test positions periodically allowed detection of any psychological fatigue, as well as physical fatigue. Limiting the length of test sessions also minimised the likelihood of psychological fatigue. For the multi-directional strength measurements, to avoid significant temperature variations between sessions, all test sessions were conducted in an air conditioned room.

Strength data was normalised for each individual to allow easier comparison of hand force trends between data sets of people of differing statures and strengths. It is the relative data that is of most use in design refinement and allows comparison between different motions.

At some positions and angles the size of the dome on the load cell rig and the hinge attachment allowed higher forces to be recorded by the subject by directing the force at a direction deviating from that being measured and sometimes perpendicular to the direction being measured. This outcome tended to occur in more awkward positions. The subjects were instructed to only apply force to the top of the dome and in the direction being measured. This force application technique was closely monitored and any suspicious measurements re-tested. For future strength measurements, a flat force plate would solve this problem. For each push attempt, the maximum force was

recorded for each hand separately and these summed to give the two-handed force. Consequently, the recorded two-handed forces were higher than the actual two handed strength applied when the maximum force for each hand was not applied simultaneously.

7.8 Summary

This section developed a method for measuring multi-directional hand forces in the sagittal plane by way of construction. An exploratory study deemed using a hand-held dynamometer inappropriate for this overall research study, due to inaccuracies and variability of the strength data measured using this method.

A rig and test protocol has been designed and built to measure strength in 12 direction at 132 positions in the sagittal plane. The measurement planes were in line with wheelchair hand rims to ensure data could be used in modelling MWC propulsion.

With such a large number of test positions, fatigue was proposed as the most likely influence to skew results. Guidelines were included in the protocol that included minimum test session lengths, and rests between measurements, to mitigate fatigue. Additionally, a process of re-measuring test points throughout the test sessions was suggested to provide a means of monitoring fatigue levels and ensuring repeatability.

Chapter 8

Strength Study: Results and Modelling

This chapter presents the results, conclusions and models developed in the strength study described in Chapters 7 and 8. Results for two handed sagittal push strengths for able bodied subjects are presented in section 8.1, and modeled using a fourth order polynomial. Results for two handed sagittal push strengths for tetraplegic subjects are then presented in section 8.2, for which no model was developed owing to significant variations in observed trends.

Section 8.3 presents multidirectional strength data collected for an able bodied subject, comprising 1,584 measurements, and develops a model for this data using a series of 12 fourth order polynomials. This strength model is later used in Chapter 9 for comparing the effectiveness of different hand force paths.

8.1 Able Bodied Push Strength

8.1.1 Subjects

The test population consisted of 8 subjects aged 21 - 60 (median age 23.5); 7 male and 1 female. Only data from the male subjects were used in the development of the model, but the data from the female subject has been included in this section for interest.

8.1.2 Results

A clear pattern was shown in the push strength characteristics in the sagittal plane. All subjects recorded their maximum push strength in a position forward and below the shoulders. The value and position of these maximum forces is given in Table 8.1. Contour plots showing the relative forces for each subject are shown in Figures 8.1 to 8.2. These plots were produced by fitting a cubic interpolating spline between all data points. The view is from the subject's right, the position of the chair is indicated on each plot. Finally, areas of highest push force strength are indicated in red, and the lowest strength regions in blue.

Most subjects displayed one focused region of maximum push strength, and strength decreased gradually in all directions away from this region. Subjects 6 and 7 (Figures 8.2b and 8.2c) showed a larger, elongated regions of maximal strength compared with other subjects. While this result may reflect the subjects' strength characteristics, it may also have been caused by different force application techniques by these subjects or variation in effort between test positions.

The average maximum push force had a mean of 1217 N and range of 879 N - 1417 N (for male data) representing a 62% difference in strength between the strongest and weakest candidates. However, once data was normalised both these candidates displayed similar trends in their push force as seen in Figures 8.1a and 8.2a. This normalisation allows easier comparison of strength regions and characteristics across subjects.

Table 8.1: Magnitude and location of maximum push force in able-bodied trials

Subject	**Maximum Push Force (N)**	**Location of maximum force, horizontal distance from seat back (fraction of arm length)**	**Location of maximum force - height above seat (fraction of arm length)**
1	879	0.206	0.523
2	1295	0.203	0.359
3	1275	0.559	0.559
4	1168	0.359	0.359
5	1417	0.365	0.524
6	1360	0.508	0.354
7	1128	0.371	0.371
8*	797	0.579	0.579
Average	1217	0.367	0.436
Std Dev	180	0.135	0.094

* Candidate 8 was female; as all other subjects were male her result was not included in the average statistics, but was included in this list for interest

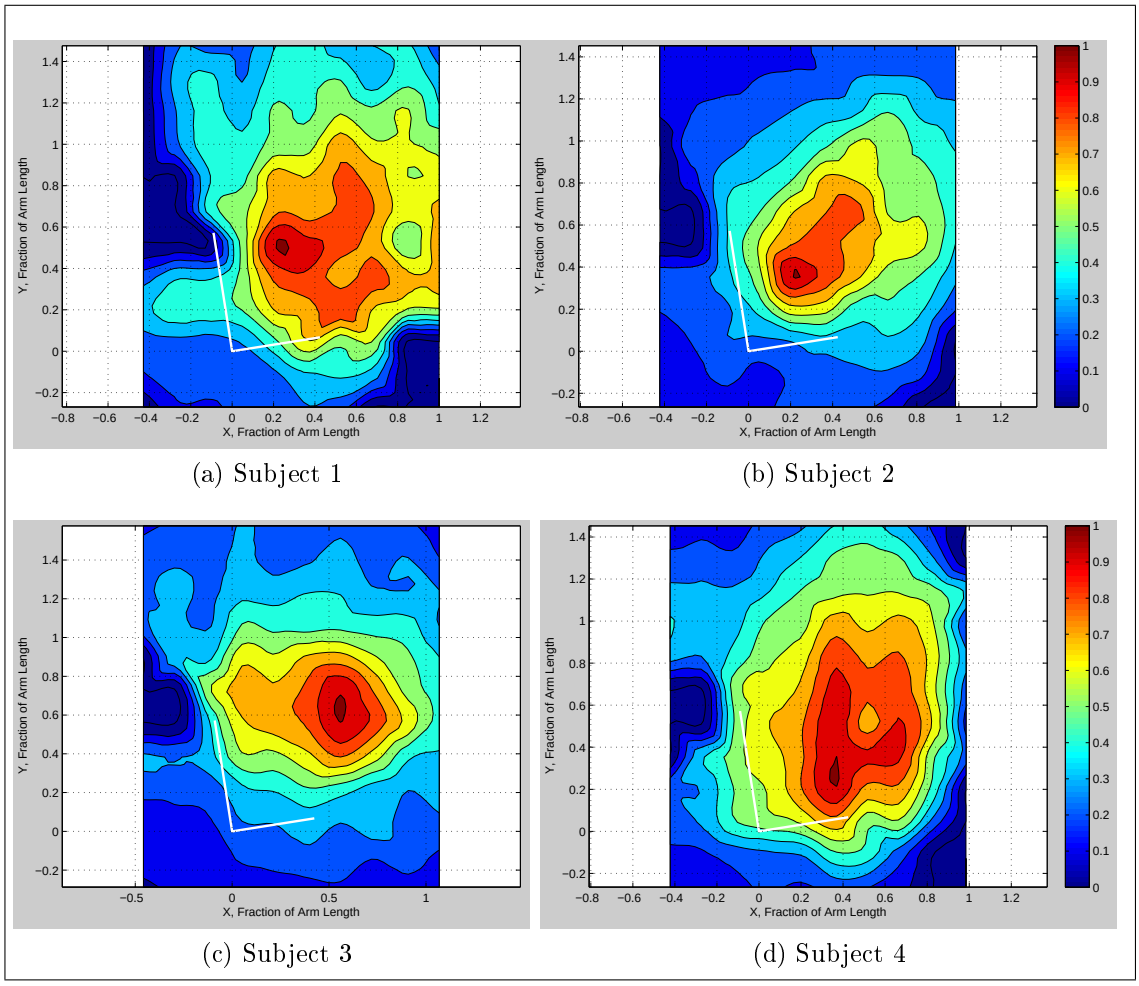

(a) Subject 1 (b) Subject 2

(c) Subject 3 (d) Subject 4

Figure 8.1: Contour plots showing push force in the sagittal plane as a fraction of each subject's maximum recorded force; subjects 1 - 4

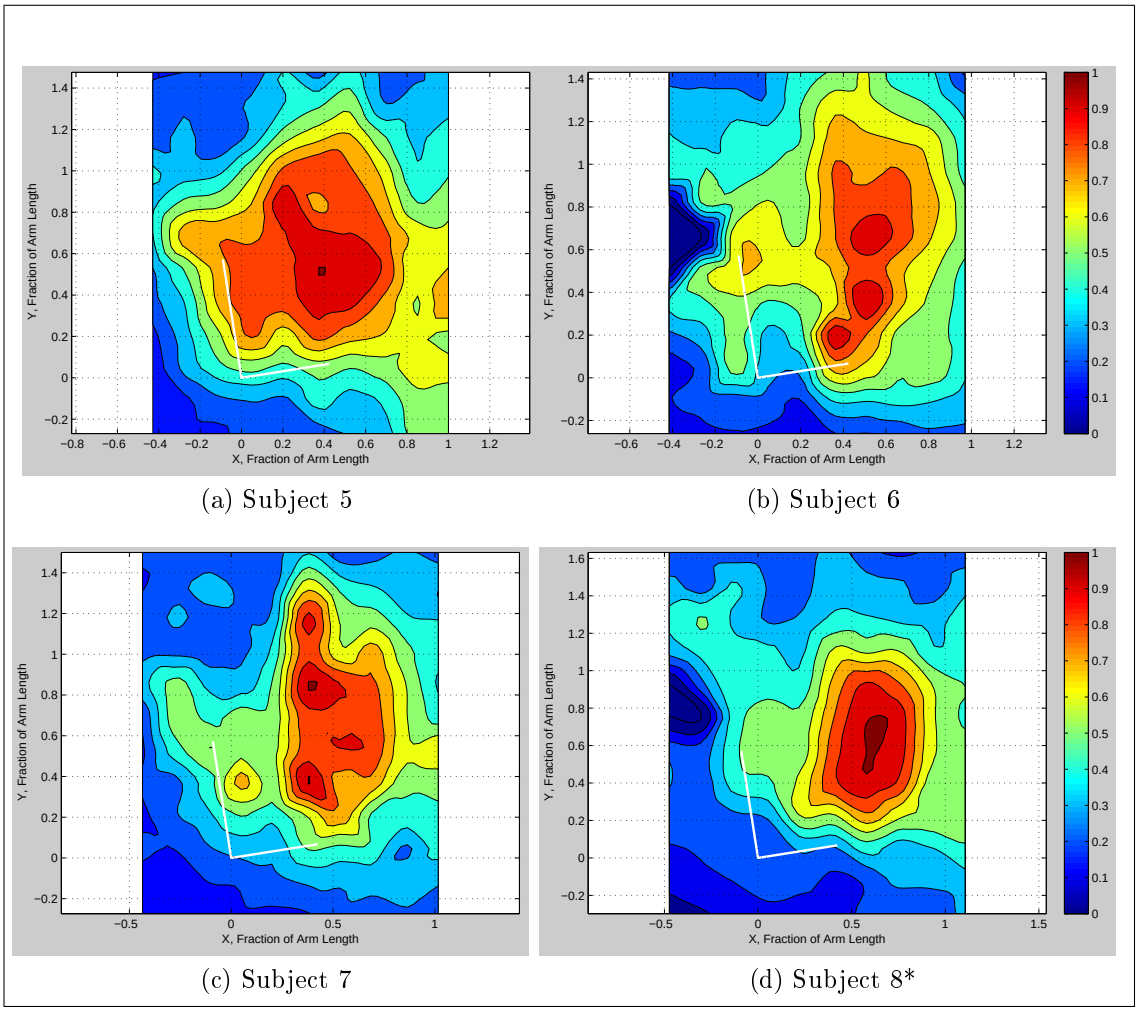

(a) Subject 5 (b) Subject 6

(c) Subject 7 (d) Subject 8*

Figure 8.2: Contour plots showing push force in the sagittal plane as a fraction of each subject's maximum recorded force; subjects 5 - 8

8.1.3 Model

A fourth order polynomial was fitted to the able bodied push strength data. Higher order polynomials yielded closer fits to the experimental data. However, increasing the order of the model above fourth order increased the number of coefficients for the model to over 20 for only a very slight improvement in the goodness of fit.

A second order model had an R-squared of 0.68, and a third order model a value of 0.73. While the third order model captured the trends in the data adequately, the improved fit with the fourth order model justified the increase in model complexity. The final model is given in Equation 8.1 and had an adjusted R-squared value of 0.80. The push forces predicted by this model are shown in Figure 8.3 as a contour plot.

$$F_{90}(x,y) = 0.2943 + 0.4806\,x + 0.7202\,y - 0.0219\,x^2 + 0.88\,x\,y + 0.09209\,y^2 - 0.8201\,x^3 - 0.813\,x^2y - 0.5093\,x\,y^2 - 1.106\,y^3 + 0.4153\,x^4 - 0.3581\,x^3y + 0.8604\,x^2y^2 - 0.109\,xy^3 + 0.462\,y^4 \quad (8.1)$$

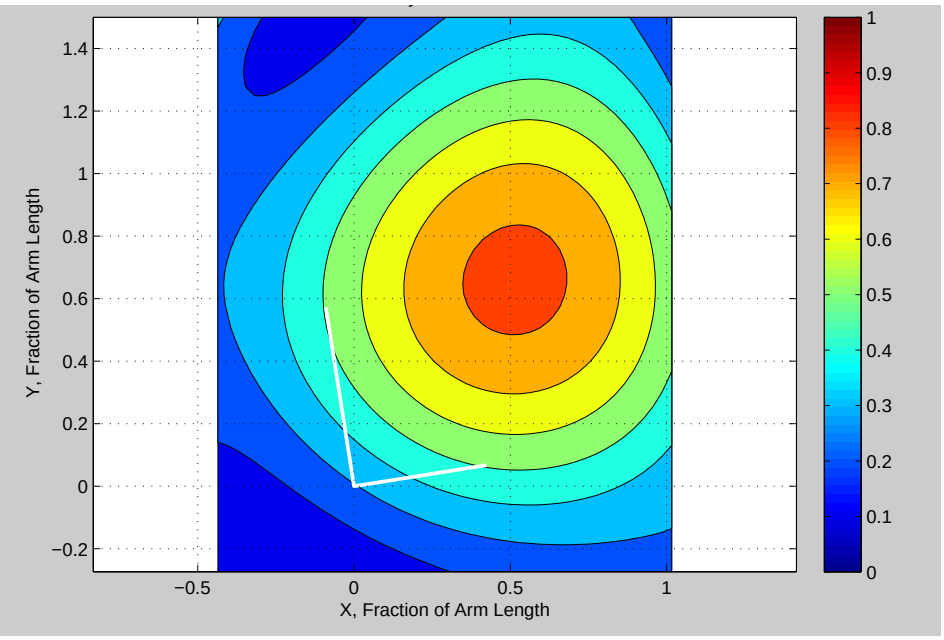

Figure 8.3: Contour plot of fourth order model (Equation (8.1)) for able-bodied push strength in the sagittal plane

8.2 Tetraplegic Push Strength

8.2.1 Subjects

Sagittal push strength for four male subjects with C5-C7 tetraplegia were tested. Each subject had a different injury as indicated in Table 8.2.

8.2.2 Results

Significant differences in sagittal horizontal push strength patterns were observed between all tetraplegic subjects and from the able-bodied trends. The value and position

of these maximum forces is given in Table 8.2 and contour plots showing the relative forces for each subject are shown in Figure 8.4. These plots were produced in the same manner as those for the able-bodied subjects in Figures 8.1-8.2.

The three subjects with SCIs at C6 or higher displayed a significantly smaller range of motion than the able bodied subjects, while subject 2 who had a C7 SCI was able to reach all the points in the test region. Interestingly, all the four subjects tested displayed a local maxima in push force near the top of the seat. The average maximum push force had a mean of 302 N, a quarter of that for the able-bodied subjects. Strength maxima ranged from 104 N to 607 N. The strongest candidate thus had almost six times the maximum push force of the weakest candidate.

The considerable differences between subjects' push force characteristics in Figure 8.4 are likely to be due to the injury differences between these four candidates. Due to the small sample size, these plots and differences between injury classifications cannot be assumed to be representative of the population. It is apparent that subjects with C5-6 injuries have considerably reduced reach in the sagittal plane and push strengths significantly less than for the able-bodied population. These initial findings suggest positions of maximum strength also differ from the able bodied population and may vary between injury groups. More measurements need to be carried out to confirm these hypotheses.

Due to the variation in strength characteristics between the four subjects, no model was fitted to this data. It is likely that once more data has been collected a model will need to be fitted for each injury group separately.

Table 8.2: Magnitude and location of maximum push force in able-bodied trials

Subject	**Injury Level**	**Maximum Push Force (N)**	**Location of maximum force, horizontal distance from seat back (fraction of arm length)**	**Location of maximum force - height above seat (fraction of arm length)**
1	C6 post TROIDS	218	0.37	0.37
2	C7	607	0.30	0.17
3	C5/6 No TROIDS	278	0.98	0.51
4	C5/6 No TROIDS	104	-0.10	0.64
	Average	302	0.467	0.423
	Std Dev	216	0.469	0.201

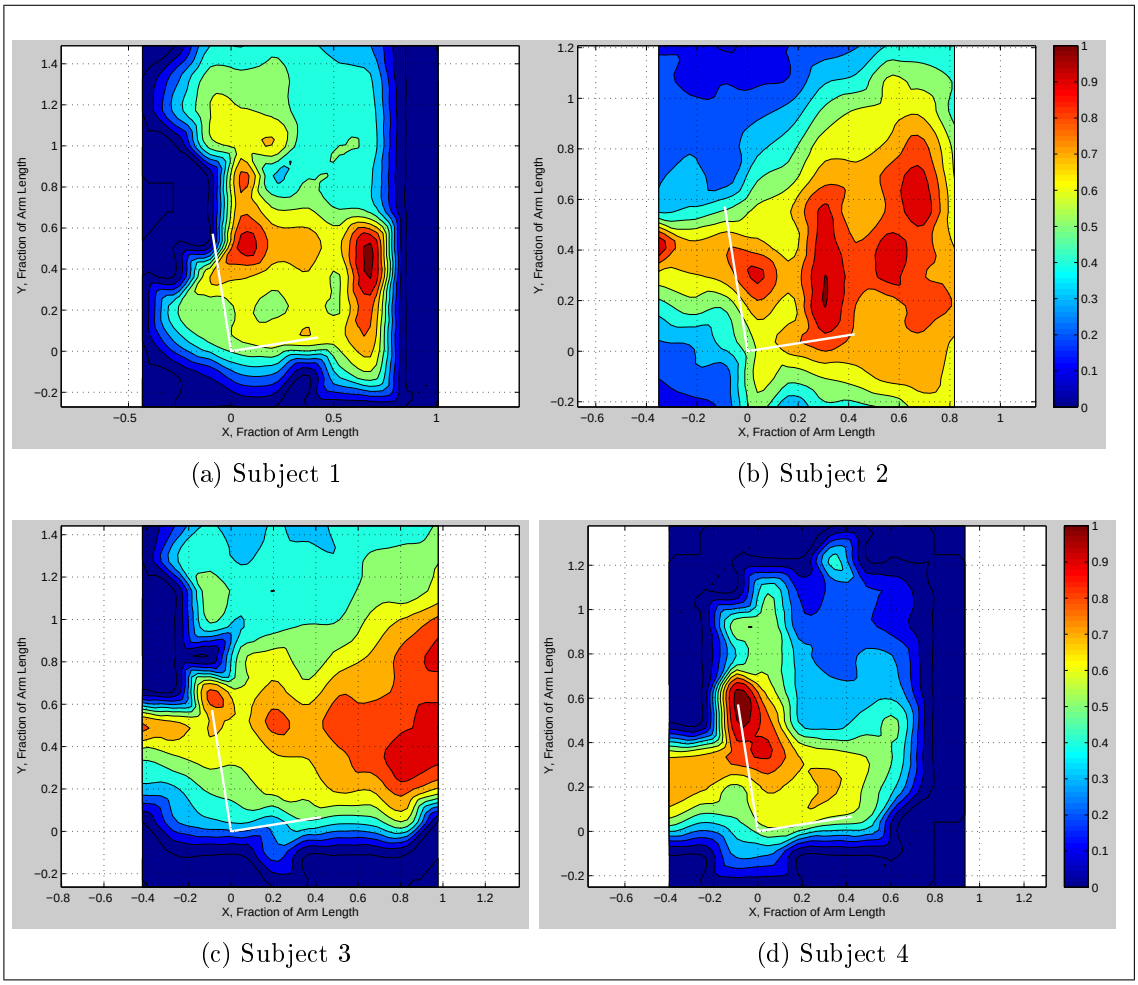

(a) Subject 1

(b) Subject 2

(c) Subject 3

(d) Subject 4

Figure 8.4: Contour plots showing push force in the sagittal plane as a fraction of each subject's maximum recorded force for candidates with tetraplegia

8.3 Able Bodied Multi-directional Strength

8.3.1 Data

A complete set of multi-directional two-handed strength for the sagittal plane was collected for one able bodied subject (aged 25) according to the methodology detailed in Chapter 7. Strength was measured for 1,584 direction and position combinations covering 12 different heights, 11 horizontal positions, and in 12 directions at each of these positions. The 12 directions are shown in Figure 8.5. Force values were normalised to the maximum across for the 1584 measurements. The measured forces are represented as polar plots in Figure 8.6. The origin of each polar plot, indicated by the dots, shows the position in the sagittal plane, while the radius of the plots represents the magnitude of force measured in each direction. Each polar plot was constructed by fitting a cubic interpolating spline to the 12 measured data points.

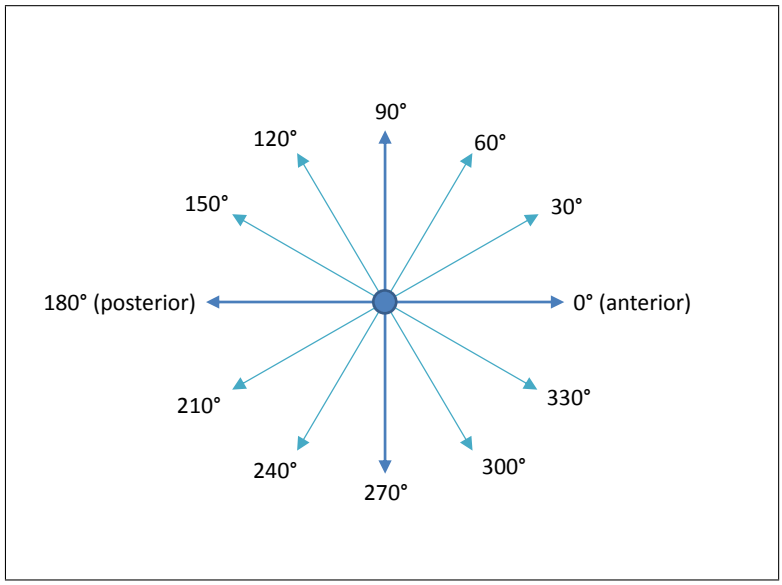

Figure 8.5: Diagram showing force directions (ϕ) in the sagittal plane. The view in this figure is from subject's right

Force tended to be strongest in the directions radiating from the top of the seat. Small strength values were recorded at points behind the seat where reach was awkward. No significant differences were noticed between data sets from different test sessions. Points that were re-measured during each testing session to check for fatigue and monitor repeatability indicated an uncertainty of $\pm 10\%$ for maximum voluntary forces for this individual.

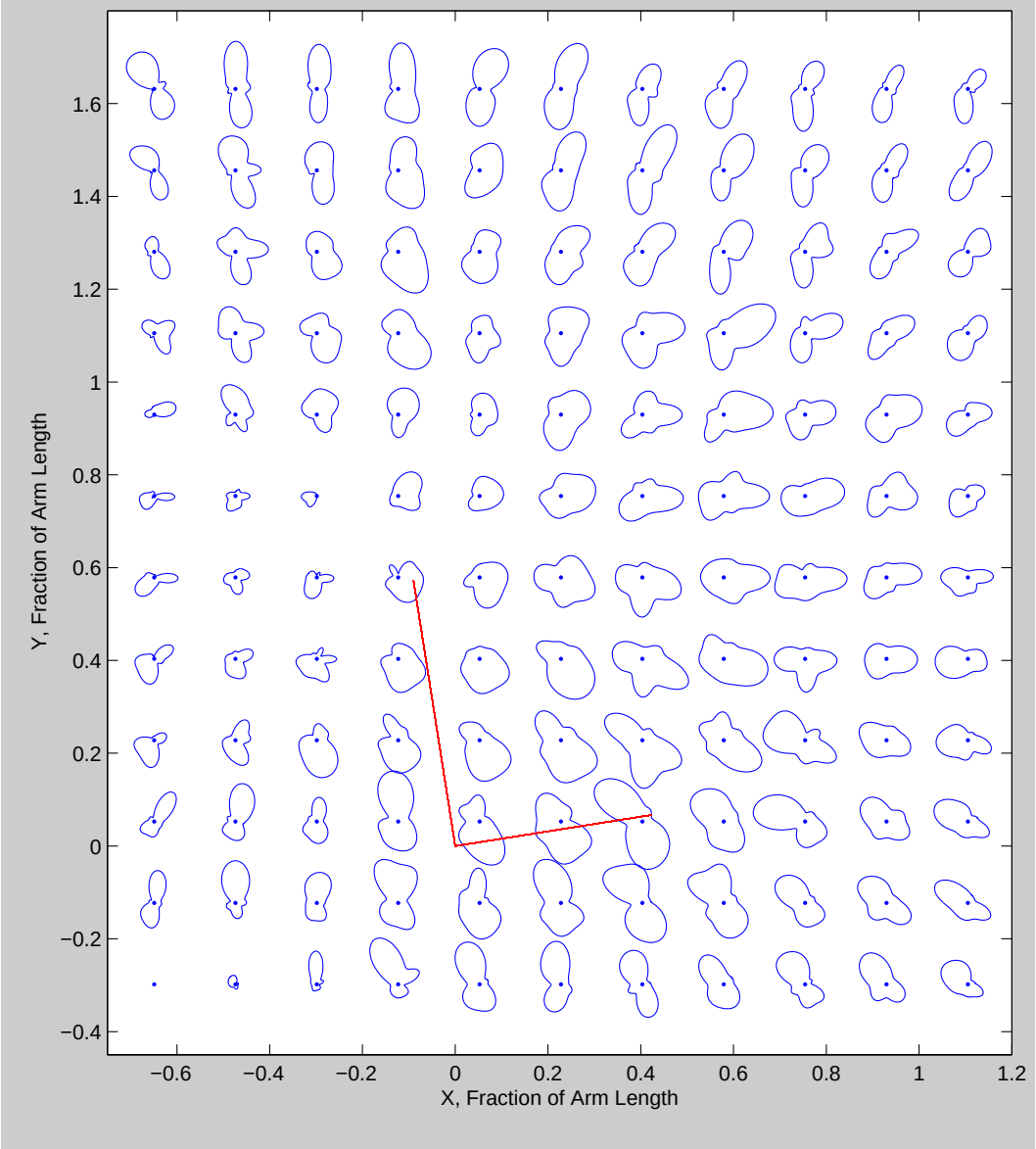

Figure 8.6: Polar plots of measured multi-directional forces for an able-bodied subject

8.3.2 Model

The experimental data was modelled by fitting a fourth order polynomial to the sagittal plane data set for each of the 12 directions. The general form of the model is given in Equation (8.2). Figure 8.5 shows the measurement angles and the coefficients for directional models for each of these angles are given in Table 8.3. The average adjusted R-squared values for these models was 0.7325, standard deviation of 0.055 and range 0.640 (90^{o}) to 0.749 (150^{o}). Contour plots of the forces predicted by the models are

given in Figures 8.7 to 8.10.

$$F_\phi(x,y) = c_{00} + c_{10}\,x + c_{01}\,y + c_{20}\,x^2 + c_{11}\,x\,y + c_{02}\,y^2 + c_{30}\,x^3 + c_{21}\,x^2y + c_{12}\,x\,y^2 + c_{03}\,y^3 + c_{40}\,x^4 + c_{31}\,x^3y + c_{22}\,x^2y^2 + c_{13}\,xy^3 + c_{04}\,y^4 \quad (8.2)$$

Table 8.3: Constants for multi-directional force model (Equation 8.2)

ϕ	**0°**	**30°**	**60°**	**90°**	**120°**	**150°**	**180°**	**210°**	**240°**	**270°**	**300°**	**330°**
c_{00}	0.186	0.232	0.368	0.536	0.566	0.421	0.297	0.367	0.464	0.6505	0.627	0.46
c_{10}	0.228	0.0585	-0.0935	-0.036	0.4137	0.675	0.257	0.2448	0.269	0.4326	0.4204	0.6088
c_{01}	0.515	0.201	0.0389	-0.537	-0.552	-0.0756	0.242	0.148	0.103	0.1885	0.1825	0.4764
c_{20}	0.204	0.0273	-0.1171	-0.405	-0.549	-0.0976	0.0965	-0.245	-0.406	-0.6014	-0.5845	-0.4074
c_{11}	0.289	0.160	0.0190	-0.136	-0.267	-0.163	-0.0006	-0.192	-0.407	-0.3119	-0.2759	0.1599
c_{02}	0.244	-0.196	-0.925	-0.3013	-0.386	-0.887	-0.692	-0.559	-0.879	-1.88	-1.719	-1.15
c_{30}	-0.168	-0.0856	0.0733	0.438	0.0281	-0.507	-0.0740	-0.407	-0.527	-0.631	-0.2222	-0.6085
c_{21}	-0.351	-0.0814	-0.0725	0.385	0.456	-0.0441	0.0419	0.340	0.378	0.06623	-0.1328	-0.6679
c_{12}	-0.120	0.408	1.40	0.395	-0.247	-0.672	-0.302	0.492	0.926	0.6234	-0.0116	-0.538
c_{03}	-0.701	0.382	0.531	0.957	1.01	1.12	0.476	0.370	0.922	2.128	2.035	0.956
c_{40}	-0.176	-0.0409	-0.0220	-0.248	0.0265	0.169	-0.0538	0.397	0.512	0.52	0.197	0.4353
c_{31}	0.0266	-0.109	0.0324	0.00408	-0.0714	0.148	0.0337	-0.0496	0.0538	0.07046	0.254	0.2111
c_{22}	0.188	0.00810	-0.134	-0.176	0.0173	0.150	-0.0510	-0.233	-0.317	0.02482	0.1752	0.44
c_{13}	-0.0714	-0.249	-0.251	-0.285	0.0812	0.283	0.138	-0.203	-0.359	-0.3034	-0.0843	0.1269
c_{04}	0.227	-0.186	-0.482	-0.337	-0.394	-0.377	-0.111	-0.066	-0.258	-0.6342	-0.6614	-0.2827

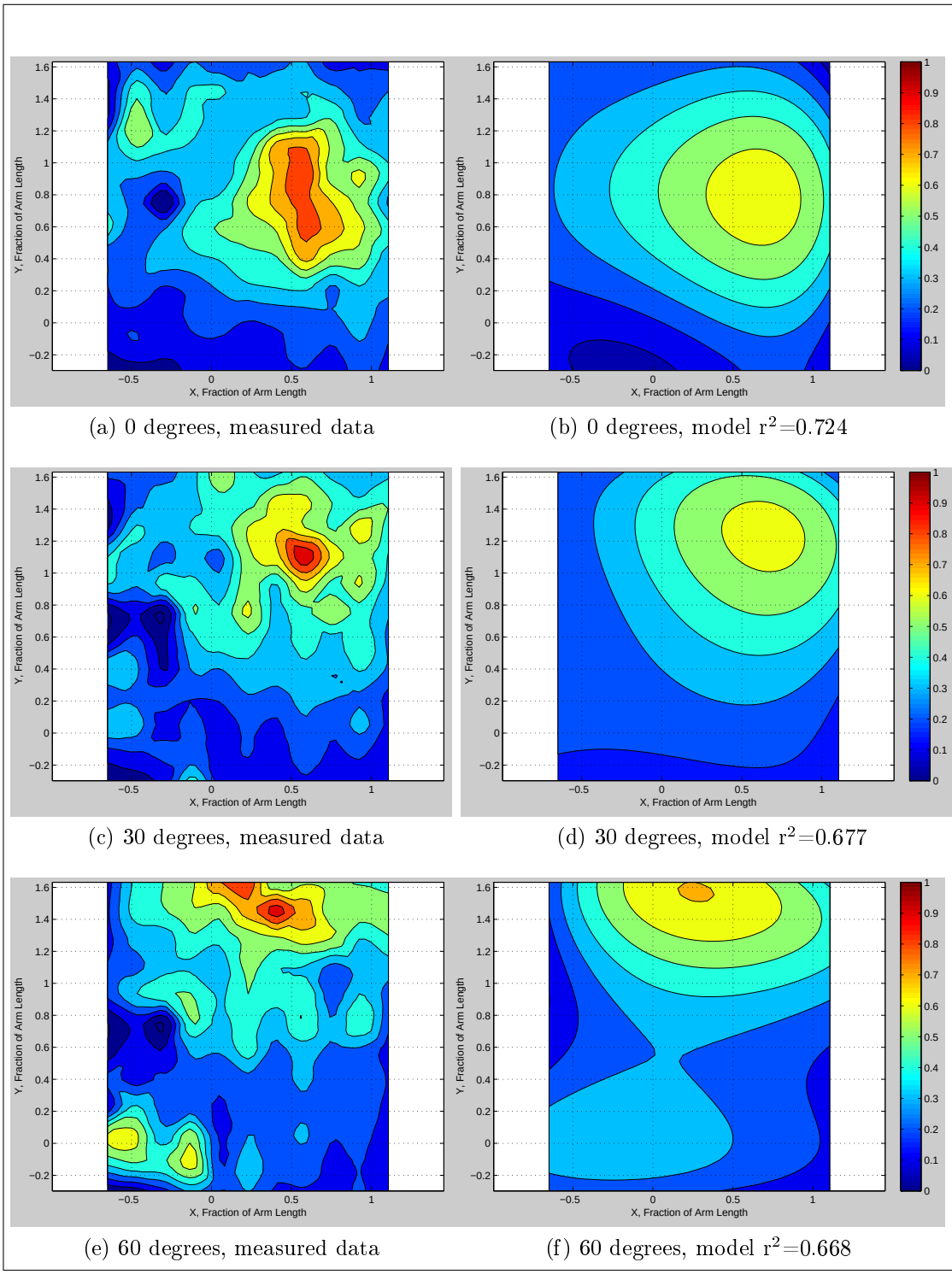

(a) 0 degrees, measured data

(b) 0 degrees, model r^2=0.724

(c) 30 degrees, measured data

(d) 30 degrees, model r^2=0.677

(e) 60 degrees, measured data

(f) 60 degrees, model r^2=0.668

Figure 8.7: Contour plots for measured and modelled sagittal plane forces directed at 0°, 30° and 60°

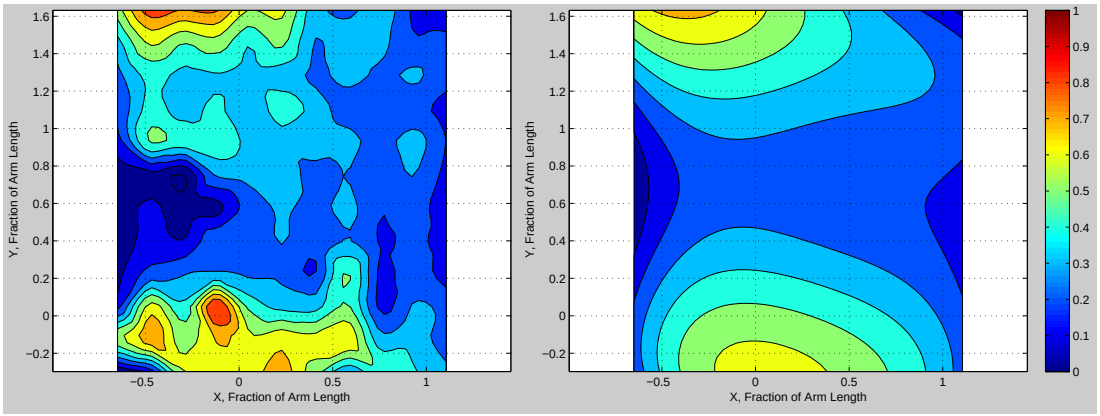

(a) 90 degrees, measured data

(b) 90 degrees, model r^2=0.640

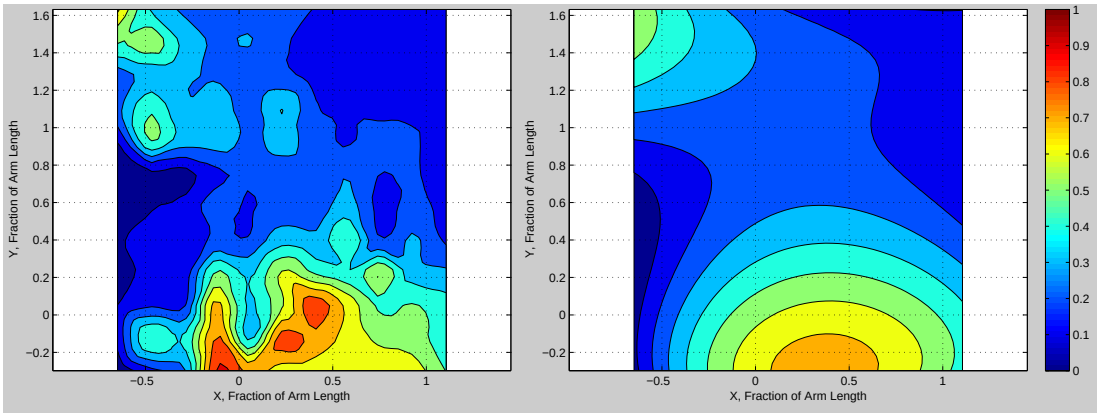

(c) 120 degrees, measured data

(d) 120 degrees, model r^2=0.774

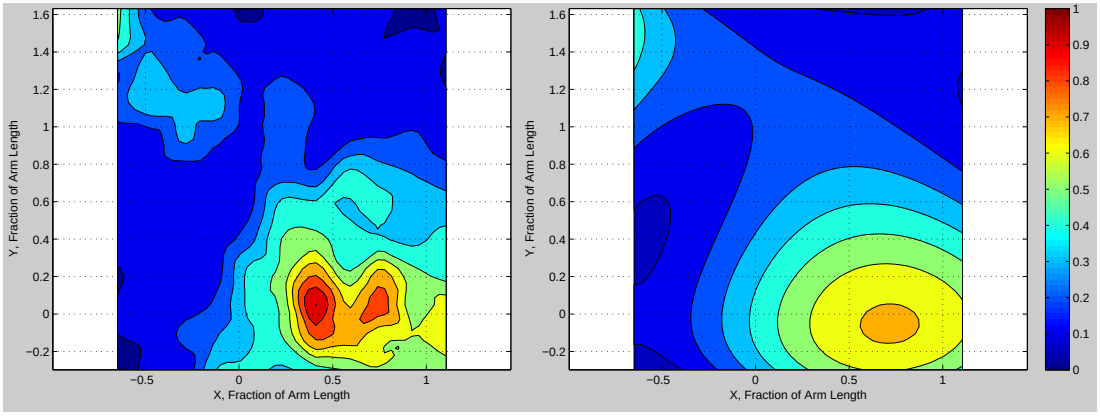

(e) 150 degrees, measured data

(f) 150 degrees, model r^2=0.849

Figure 8.8: Contour plots for measured and modelled sagittal plane forces directed at 90°, 120° and 150°

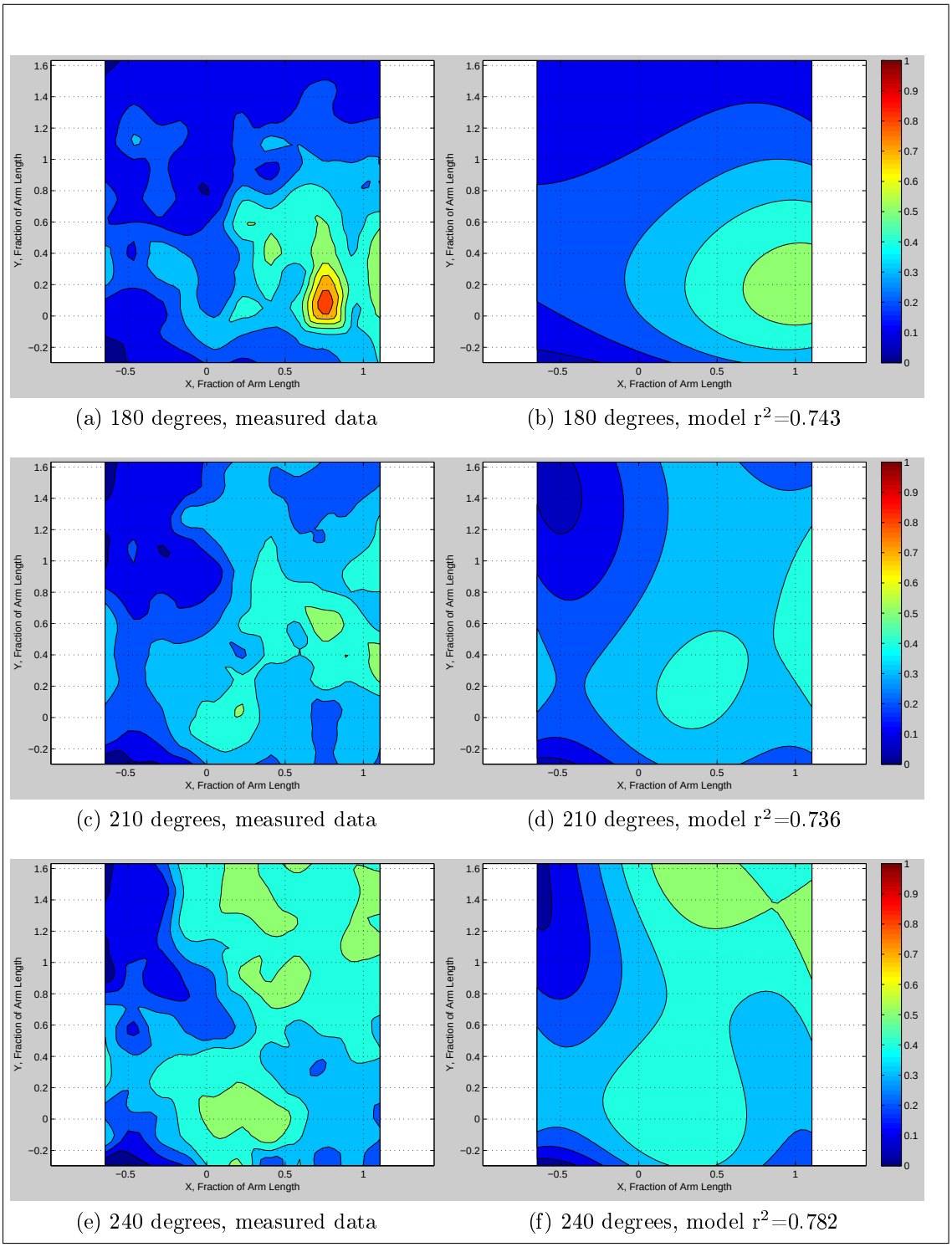

(a) 180 degrees, measured data

(b) 180 degrees, model r^2=0.743

(c) 210 degrees, measured data

(d) 210 degrees, model r^2=0.736

(e) 240 degrees, measured data

(f) 240 degrees, model r^2=0.782

Figure 8.9: Contour plots for measured and modelled sagittal plane forces directed at 180°, 210° and 240°

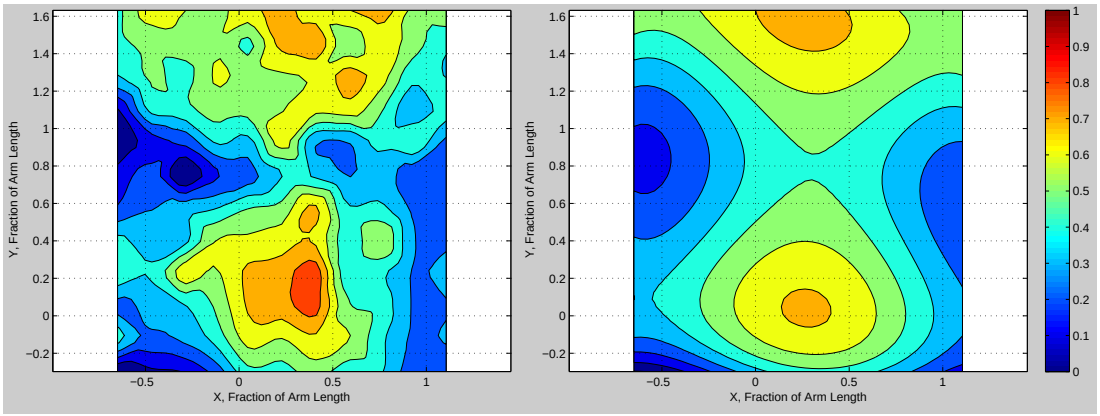

(a) 270 degrees, measured data (b) 270 degrees, model r^2=0.732

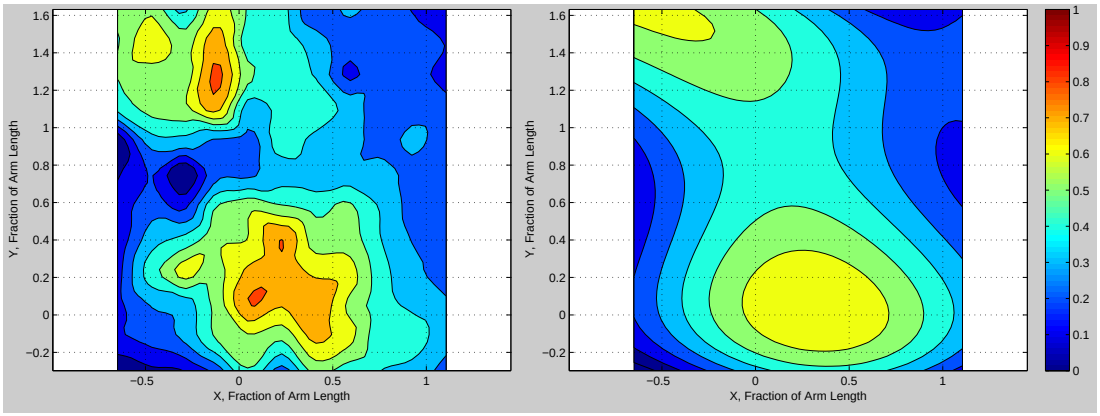

(c) 300 degrees, measured data (d) 300 degrees, model r^2=0.724

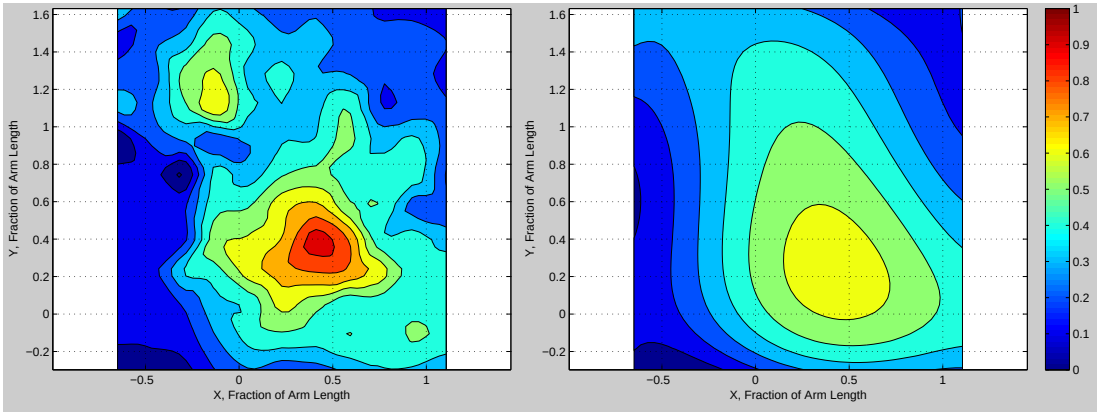

(e) 330 degrees, measured data (f) 330 degrees, model r^2=0.733

Figure 8.10: Contour plots for measured and modelled sagittal plane forces directed at 270°, 300° and 330°

The models capture the positions of maximum force well. However, the peak forces predicted by the model are lower than the measured forces. The models never predict a force greater than 80% of the maximum recorded in the trials, resulting in models that are flatter than the measured data. Push strength data for able-bodied subjects in Section 8.1 show that some subjects as seen in Figure 8.2a, displayed a sharp peak in maximum strength in one small region, and that the location of this maximum varied between individuals. A flatter model is thus more appropriate for use in design. While a flatter model captures the regions of highest strength it also does not weight a design towards these maximums that would, in practice, be sensitive to individual variables and posture.

Three-dimensional models could have been fitted to the data by horizontal position or height (positional), or angle (directional). Both positional and directional models were developed and evaluated. Polynomial models fitted to horizontal or vertical positions all had poor goodness of fit. Where R-squared values ranged from 0.30 to 0.62. Data grouped by position tended to show three or more local maxima that polynomial models were unable to capture. Figure 8.11 gives a comparison of predicted force values for all points and directions at $x = -0.47$. The directional model of Equation (8.2) is compared with a horizontal position based polynomial model (R-squared of 0.48) and measured data. In this case, for all x and y positions the directional model gave better predictions than the positional models.

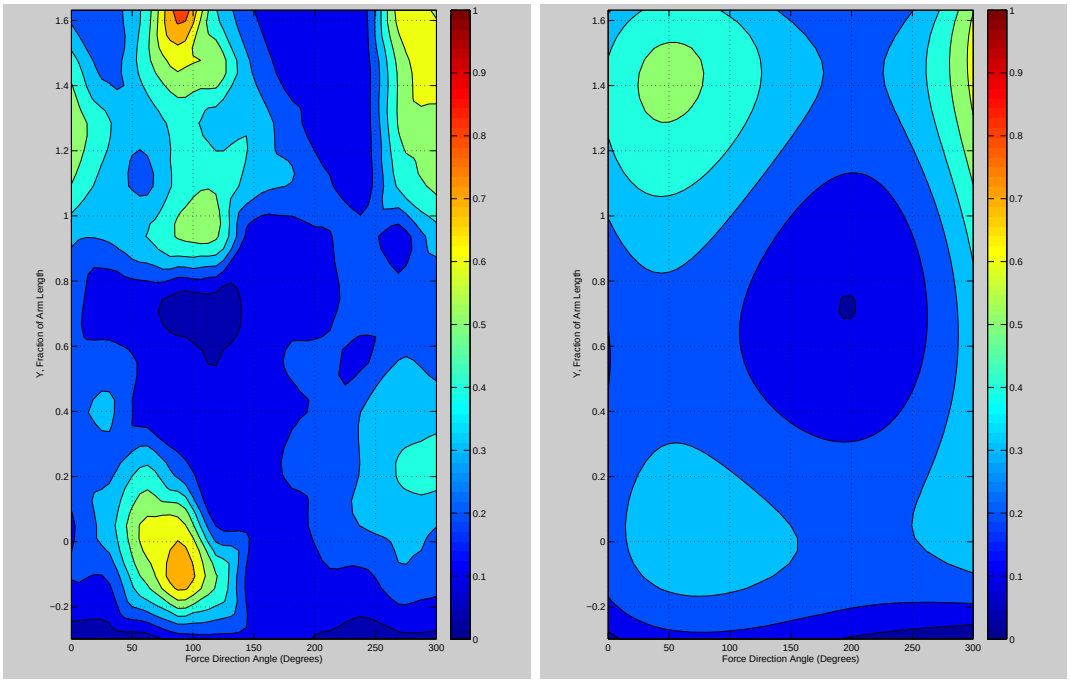

(a) x=-0.47, measured data

(b) Forth-order polynomial fit

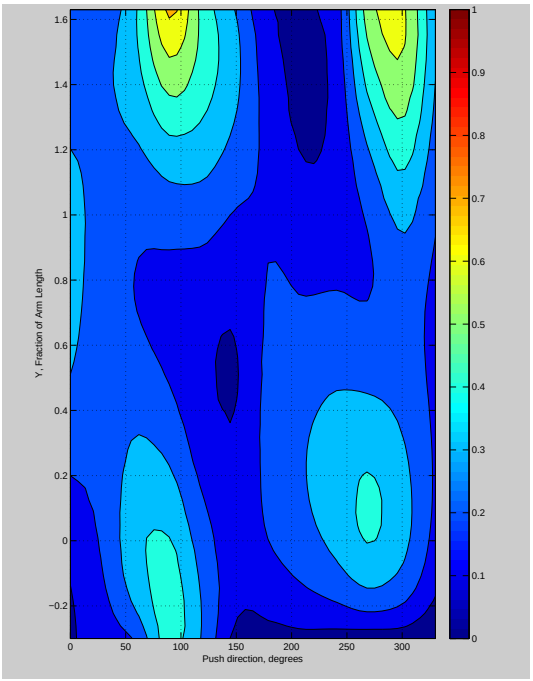

(c) Interpolated from direction-based models

Figure 8.11: Comparison of predicted force values for points at $x = -0.47$ for a direction-based model and a horizontal position based model

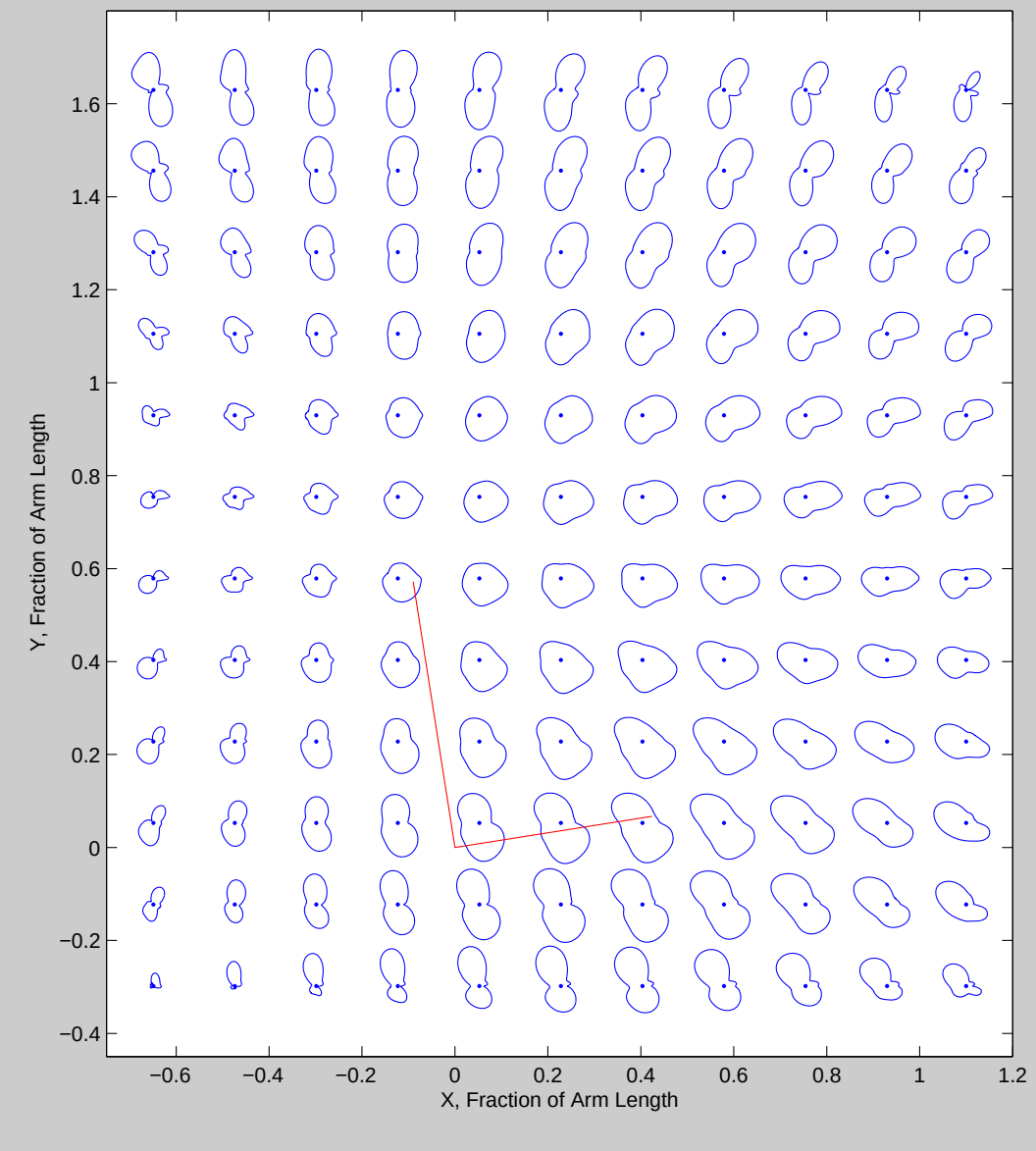

Figure 8.12: Polar plots of measured multi-directional forces for an able-bodied subject

A series of polar plots were produced for the multi-directional strength model (Equation 8.2) in a similar manner to those in Figure 8.6. Thirty-six push forces were calculated for each position in 10 degree increments. For values at intermediate angles not listed in Table 8.3, for which there was no model, a cubic spline interpolation was performed between the two adjacent angles. The resulting polar plot is shown in Figure 8.12. While the plot shows that the strength model doesn't capture every detail from the measured datum, it does show that it captures the overall trends and characteristics well.

8.3.3 Summary

Sagittal plane push strength tests were conducted for 8 able bodied and 4 tetraplegic subjects. Able bodied subjects commonly showed one focused region of maximum push strength. A fourth order polynomial was successfully used (R-squared 0.8) to model the sagittal normalised push strength for the able-bodied population. There was significant variation in sagittal plane push strength characteristics amongst tetraplegic subjects, thus no generalised model could be fitted.

A series of multi-directional strength tests were performed on an able-bodied subject. Results from these tests showed the position of maximal strength capability in the sagittal plane varied with force application direction. The directions of maximum strength tended to be those radiating from the top of the chair seat back, possibly as this was where the loads could be reacted.

A series of fourth order polynomials were fitted to this sagittal plane hand strength data for twelve different directions. These models captured the overall trends and characteristics of the data well. These models are currently based only on a data set for one individual. However, similarities in sagittal plane push-strength characteristics for able bodied subjects, suggest this model could be indicative of population wide trends.

Chapter 9

Comparison of Hand Force Paths

This chapter uses the results and the force prediction method from the manual wheelchair propulsion study in Chapters 1 to 4, together with the sagittal plane strength model from the strength study in Chapters 6 to 8 and the SWORDS human maikin described in Chapter 5, to develop a method for comparing the effectiveness of different hand force paths.

Section 9.1 proposes a methodology for comparing hand paths; the remainder of this chapter applies this method to compare the effectiveness of a traditional wheelchair propulsion hand path, with a similarly shaped path positioned higher and more forward of the wheelchair. Section 9.3 discusses the limitations and the potential of this method as a tool to optimise the design of any human powered device to best make use of the user's capabilities.

9.1 Method

The flowchart in Figure 9.1 shows the method employed for comparing different hand force paths. The power output for these two paths should be the same, and the desired velocity specified. From the power and velocity information, the required driving force vectors can be calculated at various points along the paths.

The human manikin in the SWORDs constraint modelling environment discussed in Chapter 5, was used to predict the posture of the human for placing its hands at each of these points in turn. Symmetry of the right and left sides was forced. This model thus rendered the joint positions and angles.

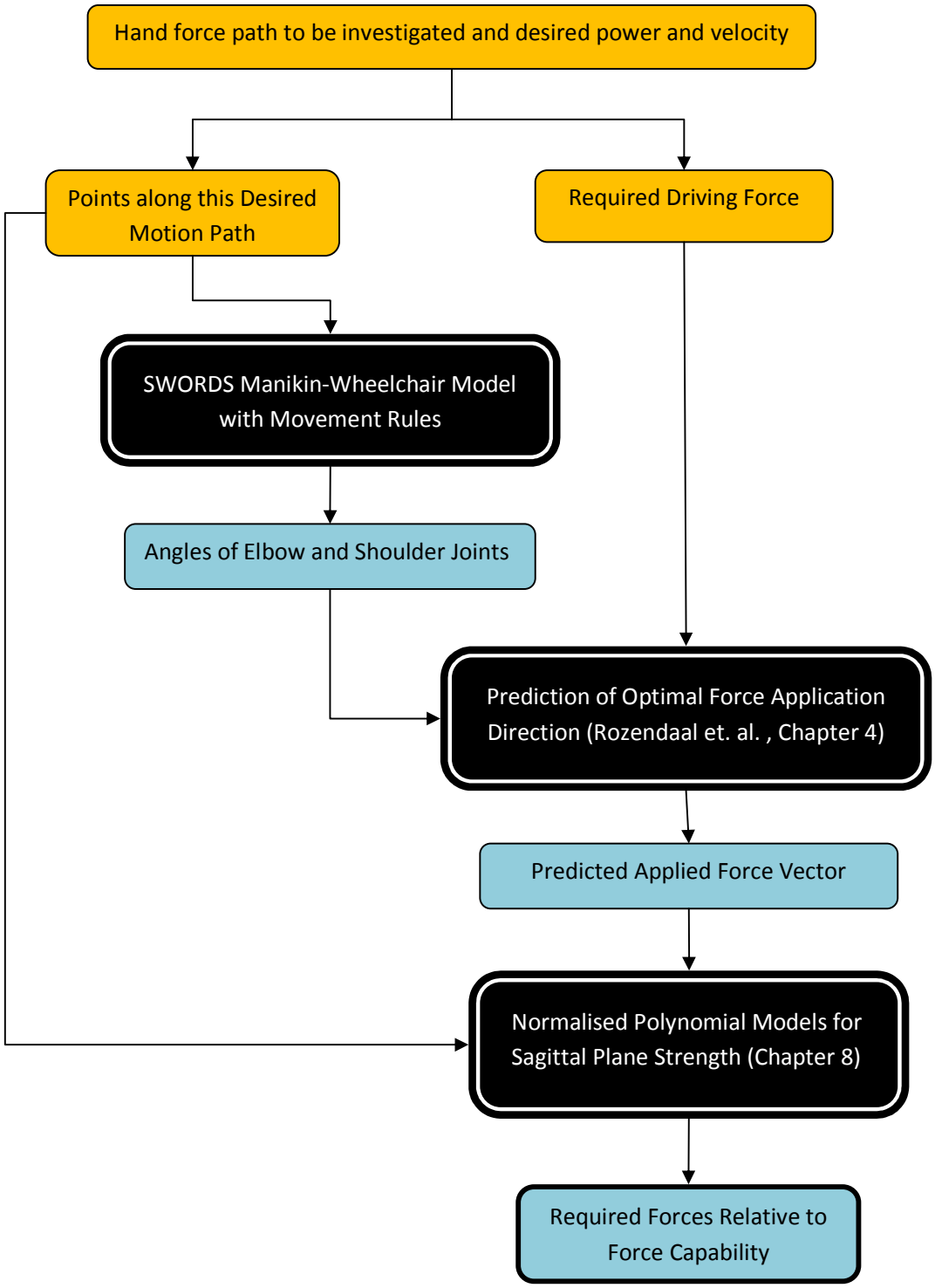

Figure 9.1: Flowchart showing method for comparing hand force paths

The method of Rozendaal et al. (2003) was then employed to predict the force application direction at each of these hand positions. Joint velocities were estimated from the change in the joint angles between hand positions and the output velocity of the wheels. The force application direction was calculated to be the most optimal direction according to Rozendaal et al.'s theory.

Once force application directions were known, the models developed in Chapter 8 were used to calculate strength in these positions and directions as a fraction of maximal strength. These fractions were used along with applied force magnitudes to compare the likely efficiency of the hand paths. The overall result is a tool that can analyse hand path trajectories for efficiency relative to, or including, the force capability of the specific individual.

9.2 Comparison of Two Hand Paths

Two hand paths were compared using the Method outlined in Section 9.1. These two hand paths are shown in Figure 9.2. The first hand path followed a traditional wheelchair rim profile. The second push arc was the same cord length and diameter as the first, but was near chest height and in front of the subject. These two push arcs are shown in Figure 9.2. The second push path was selected due to its position near where the crank for a hand cycle may be located, and due to the different trends in hand force capability measured in the multi-directional strength tests for this region.

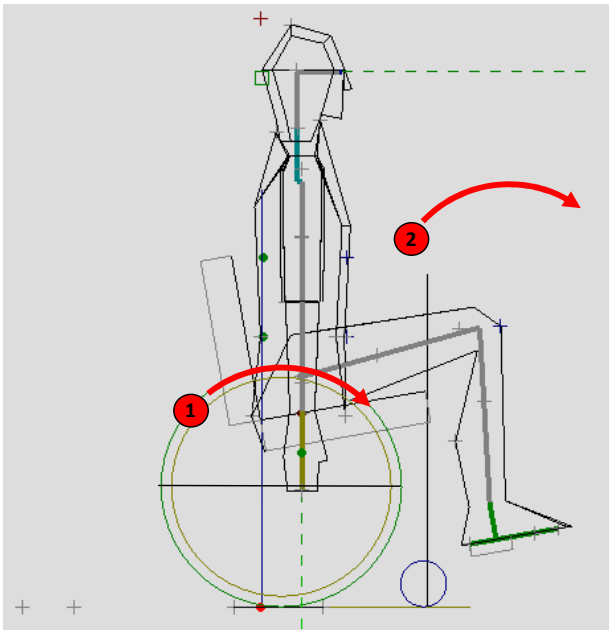

Figure 9.2: The two different hand paths compared

9.2.1 SWORDs Joint Angles

A kinetic simulation of these two motions was performed in SWORDS, with the hand paths represented by 15 points at 5 degree increments. The manikin was seated and a connection rule was applied between the manikin's hand and each path point. This rule was applied to the right hand side only and then a symmetry rule was applied.

Powell's method was employed to solve for a posture satisfying the constraints, for each of the path points in turn. The positions and angles of the elbow and shoulder joints were output.

Figures 9.3-9.5 show screen-shots from the constraint modeller for the first contact angle for each of the hand paths. As shown in Figure 9.3, the posture for the wheel rim case contained significant forward lean. This lean may have been due to the SWORDs manikin sitting further forward in the wheelchair than is typical, and the resulting grab points were further anterior from the shoulder than in practice. However, a second simulation was performed for this hand path, in which the torso was fixed to rectify this problem.

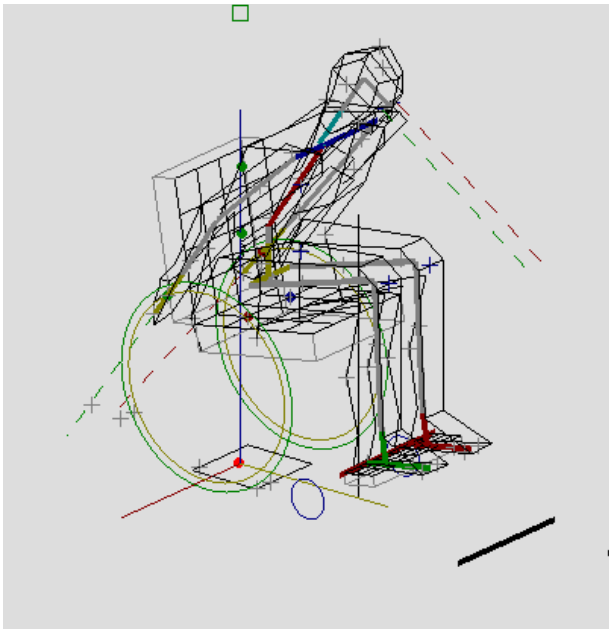

Figure 9.3: Screen shot showing the SWORDs Manikin at the beginning of the traditional MWC push stroke with torso movement permitted

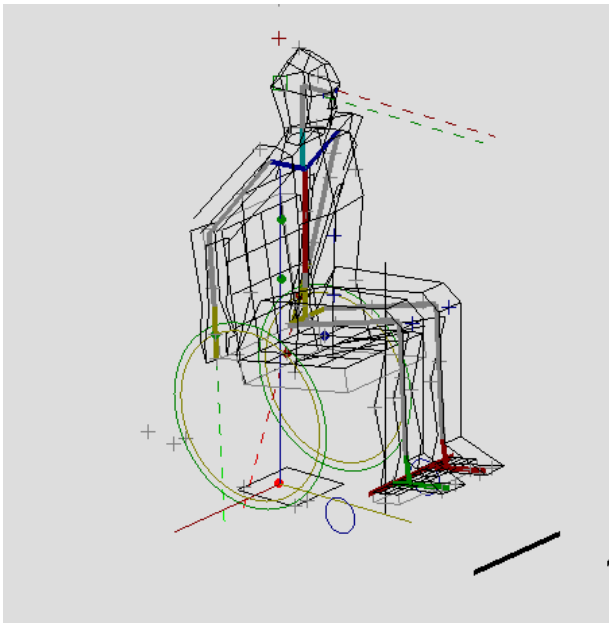

Figure 9.4: Screen shot showing the SWORDs Manikin at the beginning of the traditional MWC push stroke with no torso movement permitted

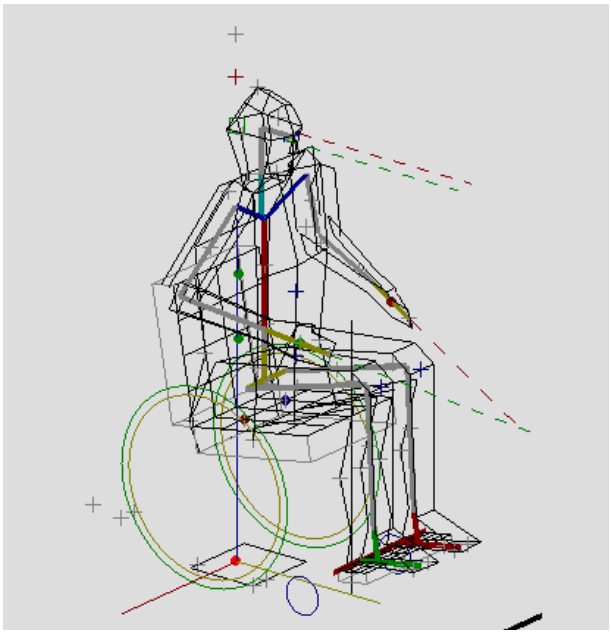

Figure 9.5: Screen shot showing the SWORDs Manikin at the beginning of the posterior push path above their seat

9.2.2 Predicted Applied Force Direction

Figures 9.6 and 9.7 show the predicted force application directions for both of the hand paths. The 'optimal' direction for force to be applied for both of these paths was 30-60 degrees below horizontal. While this force application direction has been shown to be adopted for wheelchair propulsion (Rozendaal et al., 2003), it is a surprising result for the higher hand path. Considering the difference in elbow and shoulder angles and the results from Chapter 8 that showed directions radiating from the shoulders to be of highest strength, one would have expected optimal applied force to be directed higher.

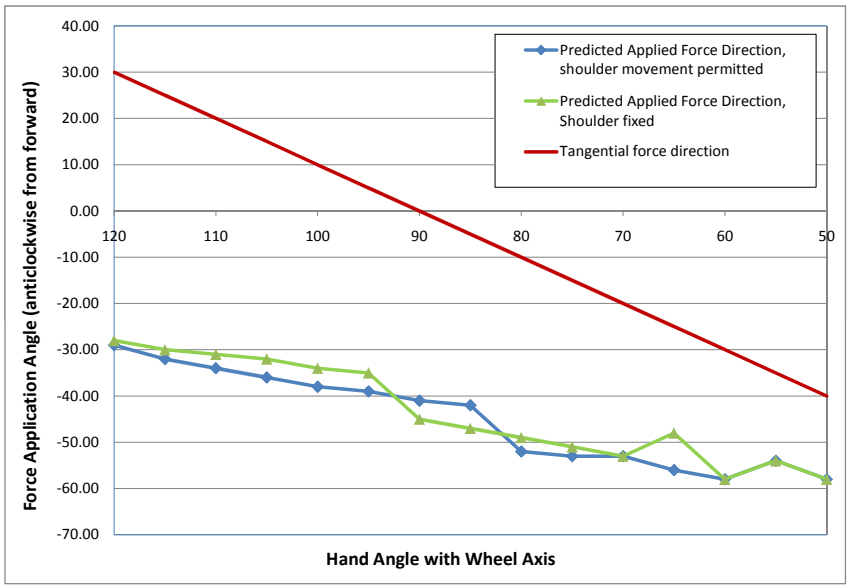

Figure 9.6: Predicted and driving force directions for hand path at traditional wheelchair rim position

Figure 9.7: Predicted and driving force directions for the second hand path

It is important to note that Rozendaal et al.'s theory was developed for wheelchair propulsion. Thus, it has not been tested for configurations that deviate substantially from the traditional wheelchair setup as this second path may. Further investigation may be necessary to measure the applied force for a path such as path two in Figure 9.2, to determine if it is valid to apply Rozendaal et al.'s theory at different hand positions.

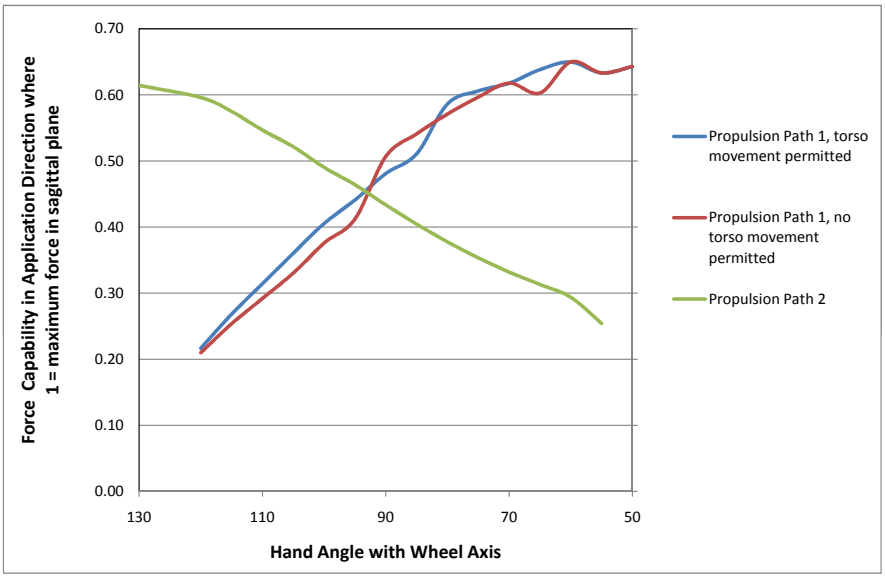

Figure 9.8: Force capabilities in the force application directions, as a fraction of maximal sagittal plane strength

9.2.3 Comparison of Hand Paths

Hand position data was normalised with respect to the manikin's arm lengths, and relative to the lower end of the Manikin's lumbar segment. The series of fourth-order polynomials discussed in Chapter 8 were then used to predict the hand force capabilities for each applied force as a fraction of the maximal sagittal plane strength. Figure 9.8 shows these predicted hand force capabilities. This figure shows that the predicted hand kinetics for the second hand path is in a stronger direction during the start of the stroke. Conversely, for the first hand path, the later part of the stroke is associated with stronger force directions.

Therefore, the average strengths for these two paths are very similar. However, the magnitude of the applied forces must also be considered. A smaller force to strength ratio would represent working at a lower percentage of their maximal capacity. Figure 9.9 shows these force to strength ratios for the two hand paths.

For a constant power and velocity output, the effort for the first push path was steadier throughout the stroke and lower on average than for the second hand path. There was no meaningful difference between the two models with different motion rules for the torso. The ratio in the first part of the second hand path was higher than for the second part. This difference is due to the predicted force being in a weak direction for that point, casting further doubt on the viability of applying Rozendaal et al.'s theory

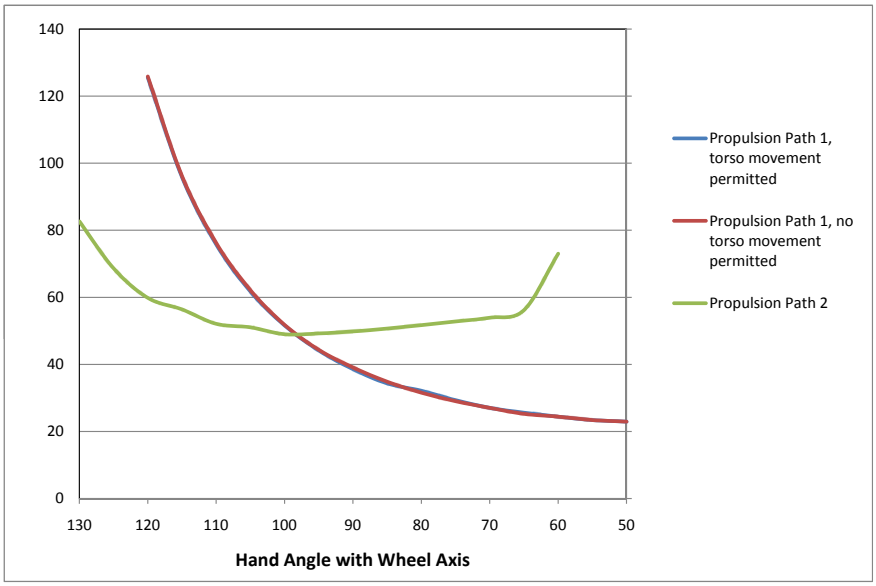

Figure 9.9: Applied force divided by the normalised strength for that direction. Smaller values indicate lower effort.

to positions that significantly differ from a typical MWC setup.

9.3 Discussion and Summary

This chapter proposed a method for predicting and comparing hand force paths and predicting their relative effectiveness. SWORDs was used to predict the posture that the subject would adopt to follow these paths. The solver used in this SWORDs simulation favours moving the most extreme links, such as the hands and forearms, over parent links, such as the shoulder and torso. This sensitivity method is conducive to more natural and realistic motion prediction.

It has been widely shown that forces during MWC propulsion are not applied in the tangential direction (Dallmeijer et al., 1998; De Groot et al., 2002; Desroches et al., 2005; Koontz et al., 2005). Thus, it was necessary to predict the direction of these applied forces. This prediction was done using the theory and methods of Rozendaal et al. (2003), as discussed in Chapter 4. However, Rozendaal et al.'s theory has only been used for predictions for typical MWC propulsion set ups, and its validity has not been reportedly tested beyond this range.

Force application directions predicted using Rozendaal et al. (2003) for a hand path beginning near the subject's chest, were not in the expected upwards or frontal directions. They were also in a direction significantly different from the direction of highest measured force from the multi-directional strength trials in Chapter 8. These two results indicate that prediction using Rozendaal et al. (2003) may be inappropriate for this direction.

Further research needs to be carried out to determine the suitability of this force prediction method. If Rozendaal et al.'s theory is inappropriate, a new method will need to be developed. It is likely there is a relationship between the multi-directional strength measured and modelled in Chapter 8, the required driving force component, and the direction of the applied force. It was often observed in the strength trials, that the strongest force component a subject could generate in a given direction was produced by a force directed at an angle. It is possible this angle indicates the 'optimal' force direction. However, this hypothesis needs to be investigated further, and in both analytical and clinical trials. Finally, if concerns with the supplied force predictions was be resolved, this procedure has the potential to be a powerful tool for assisting in the design of wheelchairs or human powered devices for any population.

Chapter 10

Conclusions and Future Work

This chapter summarises the main contributions made by this thesis and draws conclusions from this research. This chapter also recommends future work based on the foundation of this work, which would contribute to a better understanding of wheelchair propulsion in persons with tetraplegia and provide designers with useful tools for modelling human-machine interactions.

10.1 Summary of contributions

The work in this thesis contributes to the understanding of wheelchair propulsion and strength characteristics in persons with C5-C7 tetraplegia. In particular this thesis makes three main contributions:

- It provides manual wheelchair propulsion kinematic and kinetic data for people with complete C5-C6 tetraplegia that is considerably more comprehensive than that in any existing studies, and identifies characteristic differences in manual wheelchair propulsion between C5-C6 candidates with no triceps function and C7 candidates with triceps function.

- It presents a novel method for measuring seated sagittal plane strength, horizontal push strength data at 132 points for eight able-bodied subjects, four tetraplegic subjects, and strength data at 132 points for 12 directions for an able bodied candidate. Based on this data it also provides a model of the hand force capability of a seated person in any direction in the sagittal plane.

- It proposes a novel method for predicting and comparing the relative efficiencies of different hand force paths at a different powers and velocities. This method

has the potential to be adopted as a design tool to help optimise the design of assistive, mobility and other human powered devices.

10.2 Conclusions

10.2.1 MWC Propulsion study

The study on kinetic and kinematic MWC propulsion characteristics of 15 subjects with C5-C7 tetraplegia was more comprehensive than other reported studies on MWC propulsion. Additionally, this study distinguished between subjects with C5-6 and C7 injuries, and those C5-6 subjects who had or had not undergone the TROIDs procedure. TROIDs is anecdotally said to improve MWC propulsion. However, there is no other reported study, other than that by Yao (2007), on which this study builds, that attempts to quantify the effect of this TROIDs procedure on MWC propulsion. Hence, this work addresses a significant gap in knowledge.

Subjects with C7 tetraplegia, who retain some triceps function, are found to be capable of higher MWC propulsion velocities and powers than C5-6 subjects. These C7 subjects also coped with an increase in wheel resistance better than their C5-6 counterparts, displaying better consistency in hand paths between resistances and smoother power and velocity profiles. In addition, C7 candidates were more likely to adopt different postures and use different wheel gripping techniques to subjects with C5-C6 tetraplegia. Thus, it is imperative when considering the design of wheelchairs, that these two populations are considered and designed for individually which is not currently the case.

Despite anecdotal evidence to the contrary, no significant differences in push phase metrics were found to support the claim that TROIDs improves MWC propulsion. This is not to say that there is no benefit to the TROIDs procedure, it is claimed to provide improved functionality for other day to day tasks. However, it remains that it provides no significant benefit for mobility, which is an important clinical consideration in evaluating the need for surgery.

It was expected that hand stroke paths for subjects with and without elbow extension would be a characteristically different. However, while significant inter-individual differences were observed, no difference was found in hand paths between any of the

injury groups. Hence, this result reiterated the potential of injury - and patient - specific designs or adoptive designs to maximise mobility.

The small samples sizes for these populations must be considered when interpreting these findings. While the statistical analyses took these sample sizes into account, significant inter-subject variation was present in the measured data. Therefore larger data sets are necessary to confirm and reinforce the significance of these findings.

10.2.2 Static Strength Study

The concepts of measuring in-plane hand force capabilities, or measuring these for different directions, are not new. However, there are no reported studies that measure these forces for more than a few points in the sagittal plane. It follows then that there are no reported studies that achieve this for a seated position, nor for subjects with SCIs. Hence, in designing wheelchairs for specific patients or injury types, there is no means of obtaining the data necessary for optimised design

This thesis presented a novel method for measuring and modelling seated sagittal plane strength characteristics for any SCI or able-bodied population. Unlike commonly reported joint articulation strength data, data collected using this method was inclusive of the combined and interactive effect of multiple joint and muscular interactions. These interactions are complex, not well understood, and expected to differ between able-bodied subjects and those with different SCIs. Data inclusive of these effects is therefore more representative of actual functional ability, and thus more useful for design purposes.

Comprehensive seated, sagittal, horizontal push strength data was collected at 132 points for 8 able-bodied subjects. This in itself was a notable contribution, as no other data on push strength capability over the whole sagittal plane is reported in the literature from a seated position. This lack of data was surprising considering the, industrial and design applications for such data.

The able-bodied push strength data sets commonly contained one region of maximum push strength located between the chair and shoulders, forward of the subject. A generalised fourth order polynomial model for able-bodied sagittal push strength was fitted to normalised data. This model successfully captured the push force characteristics and provides a useful tool for designers of interactions dependent on push force

strength, and does so in a patient-specific and easily obtained fashion.

The same seated, sagittal, horizontal push strength measurements were performed with four subjects with tetraplegia. There was significant variation in these push strength characteristics among the tetraplegic subjects. The push force characteristics also varied from the able-bodied population. These results imply that any interaction optimised for able-bodied push strength would not be optimal for tetraplegic subjects. Due to the variation in the data sets, no generalised model was fitted, which further indicates the patient-specific aspects required to optimise design and mobility.

A single comprehensive data set containing 1584 measurements, at 132 points for 12 directions, was collected from an able-bodied individual. Measured force characteristics and positions of maximal strength varied systematically with different force angles. Hand force was strongest in directions radiating from the top of the seat back, potentially due to this being a key point where the hand forces were reacted. A series of fourth-order polynomials were successfully fitted to this data, thus providing a model for predicting hand force strength for any direction and position in the sagittal plane.

10.2.3 Propulsion modelling

A method for predicting the relative effectiveness of different hand force paths was developed, with a view to the design and improvement of manual wheelchairs. This prediction method involved modelling the proposed motion using a geometric human model in the constraint modeller SWORDS. As it has been widely shown that forces during MWC propulsion are not applied in the tangential direction (Dallmeijer et al., 1998; De Groot et al., 2002; Desroches et al., 2005; Koontz et al., 2005), applied force directions were predicted using Rozendaal et al.'s equations (2003).

As Rozendaal et al.'s theory was designed for paraplegic subjects, who have full upper body strength. New, more refined constants for muscle volumes and maximal joint moments, were proposed for subjects with C5, C6 and C7 tetraplegia. Rozendaal et al.'s theory was insensitive to small changes in these muscle volumes and maximal joint moments, but very sensitive to a whole muscle group being 'turned off' as occurs with C5-C6 fractures. As would be expected, these changes resulted in different predicted force application directions for subjects with and without elbow extension.

Force application directions were predicted using Rozendaal et al. (2003) for two different hand paths. The first following the wheel rim on a traditional wheelchair, and

a second hand path beginning near the subject's chest. The predicted directions for the second path were different to the expected upwards or frontal directions, which were also strongest directions at those points from the multi-directional strength data. These two results indicate that prediction using Rozendaal et al. (2003) may be inappropriate for hand paths that vary significantly from the traditional wheelchair push path for which the theory was developed.

From the predicted force application directions and the fourth-order models for sagittal plane strength, a measure of effectiveness was proposed by means of the applied force:strength ratio for each point on the path. A smaller force to strength ratio would represent working at a lower percentage of their maximal capacity. This procedure has the potential to be a powerful tool for assisting in the design of wheelchairs or human powered devices for any population. However, unfortunately, concerns about the applicability of Rozendaal et al.'s theory to non-traditional hand force paths, prevent this method of hand force path comparison being used to draw any reliable conclusions or make any recommendations regarding optimal force paths for MWC propulsion.

More importantly, the limitations exposed here do provide, with the results of this thesis, a significant and effective platform to reformulate and translate these methods to the SCI patient groups

10.3 Suggested Future Work

10.3.1 Data Collection

Small sample sizes were a limiting factor of this study. These small sample sizes were a symptom of the limited subject population, and the difficulty of accessing suitable candidates. This issue was particularly acute for subjects with C5-6 tetraplegia who had not undergone the TROIDs procedure. The collection of further MWC propulsion data from C5-7 candidates would strengthen the study and conclusions.

Comprehensive strength measurements were collected for only one able bodied subject. Now that this thesis has shown this measurement method to be viable and useful for modelling, the opportunity exists to collect this comprehensive data for more able-bodied subjects. This data would subsequently allow the development of a more robust model for sagittal plane strength. Such a model for the able-bodied population would

have far reaching benefits as and aid for ergonomic, safe and optimal design of man-machine interactions. The same methods might also be used for injury - or patient - specific MWC solutions.

Further data needs to be collected regarding the strength of subjects with tetraplegia. Collection of further sagittal push strength would be a worthy starting point. If trends were identified in this push strength for different injury groups, then further collection of multi-directional strength data would be warranted.

10.3.2 Modelling

Further research needs to be carried out to determine the suitability of this force prediction method employed for hand paths significantly different from traditional MWC propulsion paths. The current theory may need to be refined or a new method developed. It would be interesting to examine the relationship between measured applied force direction and measured PSD data for the same subject. It is possible that applied force direction could be predicted using information provided in the strength model.

The current method for predicting applied hand forces assumes power, velocity and the driving force all remain constant throughout the stroke. As shown in the MWC propulsion trials, this constant assumption is not the case in reality. The output power and velocity is likely to be a function dependent on a wide range of variables such as strength capability, joint angle, momentum, and gravity. The sensitivity of the method to changes in power and velocity should be determined, and, if necessary, a method for predicting this power profile developed. Such a method would likely be iterative.

The current method for comparing hand paths requires running a series of programs in both Matlab and SWORDS, with output values from the programs stored in a spreadsheet. If the whole procedure were embedded in SWORDS, which has the ability to dialogue with Matlab, it could be easily automated to compare a range of path motions, and eventually used for optimisation.

List of Publications Resulting from Work in this Thesis

Hollingsworth, L., Gooch, S. D., Woodfield, T., Rothwell, A. G. and Yao F. (2009), The Effect of Triceps Function on Wheelchair Propulsion for People with Tetraplegia, Fourth Asian Pacific Conference on Biomechanics, April 14-17 2009, University of Canterbury.

Hollingsworth, L., Medland, A.J., Gooch, S.D., Rothwell, A. G., Lintott A. and Woodfield T., (2007), Using Constraint Modelling to Predict the Upper Body Strength Capabilities of People with Tetraplegia, International Meeting on Upper Limb in Tetraplegia Conference, September 17-20, Shriners Hospitals for Children, Philadelphia, Pennsylvania.

Gooch, S. D., Woodfield, T., Hollingsworth, L., Rothwell, A. G., Medland, A. J. and Yao F. (2008), On the Design of Manual Wheelchairs for People with Spinal Cord Injuries, Proceedings of the 10th International Design Conference, Design 2008, pp 387-394, May 19 – 22 2008, Dubrovnik, Croatia.

References

A. M. Acosta and R. F. Kirsch. Estimating shoulder maximum muscle forces in individuals with c5-c6tetraplegia. *Engineering in Medicine and Biology Society, 2000. Proceedings of the 22nd Annual International Conference of the IEEE*, 1, 2000.

F. Ambrosio, M. L. Boninger, A. L. Souza, S. G. Fitzgerald, A. M. Koontz, and R. A. Cooper. Biomechanics and strength of manual wheelchair users. *The Journal of Spinal Cord Medicine*, 28(5):407, 2005.

T Amell. *Shoulder, Elbow and Forearm Strength.* Muscle strength, Chapter 12. CRC, 2004.

Laboratory of Applied Anthropology. www.biomedicale.univ-paris5.fr. 2009.

MM Ayoub and JW McDaniel. Effects of operator stance on pushing and pulling tasks. *IIE Transactions*, 6(3):185–195, 1974.

Thomas M. Baines. Interactive biomechanical computerized model for predicting human static strengths in the sagittal plane. Technical report, University of Michigan, 2006 1975.

M. Batavia, A. I. Batavia, and R. Friedman. Changing chairs: anticipating problems in prescribing wheelchairs. *Disability and Rehabilitation*, 23(12):539–548, 2001.

N Beagley. Human body modeling as a human factors engineering tool, 5-9 December 1997 1997.

D Bishop, DG Jenkins, and A Howard. The critical power function is dependent on the duration of the predictive exercise tests chosen. *International journal of sports medicine*, 19(2):125–129, 1998.

M Bjorksten and B Jonsson. Endurance limit of force in long-term intermittent static contractions. *Scandinavian journal of work, environment and health*, 3(1):23, 1977.

AK Blangsted, G SjÃžgaard, P Madeleine, HB Olsen, and K SÃžgaard. Voluntary low-force contraction elicits prolonged low-frequency fatigue and changes in surface electromyography and mechanomyography. *Journal of Electromyography and Kinesiology*, 15(2):138–148, 2005.

R. W. Bohannon. Test-retest reliability of hand-held dynamometry during a single session of strength assessment. *Physical Therapy*, 66(2):206, 1986.

I Bolin, P Bodin, and M Kreuter. Sitting position-posture and performance in c5-c6 tetraplegia. *Spinal cord: the official journal of the International Medical Society of Paraplegia*, 38(7):425, 2000.

Michael L. Boninger, Aaron L. Souza, Rory A. Cooper, Shirley G. Fitzgerald, Alicia M. Koontz, and Brian T. Fay. Propulsion patterns and pushrim biomechanics in manual wheelchair propulsion. *Archives of Physical Medicine and Rehabilitation*, 83(5):718–723, 2002.

C. E. Brubaker. Wheelchair prescription: an analysis of factors that affect mobility and performance. *J Rehabil Res Dev*, 23(4):19–26, 1986.

S. A. Bruce, S. K. Phillips, and R. C. Woledge. Interpreting the relation between force and cross-sectional area in human muscle. *Medicine and Science in Sports and Exercise*, 29(5):677, 1997.

S Bystrom and C Fransson-Hall. Acceptability of intermittent handgrip contractions based on physiological response. *Human Factors: The Journal of the Human Factors and Ergonomics Society*, 36(1):158–171, 1994.

Anderson G.B.J. Chaffin, D.B. and B.J. Martin. *Occupational Biomechanics*. John Wiley and Sons, Inc., New York, third edition edition, 1999.

D. B. Chaffin and M. Erig. Three-dimensional biomechanical static strength prediction model sensitivity to postural and anthropometric inaccuracies. *IIE Transactions*, 23 (3):215–227, 1991.

DB Chaffin, GD Herrin, and WM Keyserling. An updated position. *Journal of Occupational and Environmental Medicine*, 20(6):403, 1978.

VM Ciriello and SH Snook. A study of size, distance, height, and frequency effects on manual handling tasks. *Human Factors: The Journal of the Human Factors and Ergonomics Society*, 25(5):473–483, 1983.

Genicom Consultants. www.safework.com. *accessed August 2009*, 1998.

A. J. Dallmeijer, L. H. V. van der Woude, H. E. J. Veeger, and A. P. Hollander. Effectiveness of force application in manual wheelchair propulsion in persons with spinal cord injuries. *American Journal of Physical Medicine and Rehabilitation*, 77 (3):213, 1998.

Annet J. Dallmeijer and Yvonne J. Kappe. Anaerobic power output and propulsion technique in spinal cord injured subjects during wheelchair ergonometry. *Journal of Rehabilitation Research and Development*, 31(2):120, 1994.

B. Das and M. Forde. Isometric push-up and pull-down strengths of paraplegics in the workspace: 1. strength measurement profiles. *Journal of Occupational Rehabilitation*, 9(4):277–289, 1999.

B Das and AK Sengupta. Computer-aided human modelling programs for workstation design. *Ergonomics*, 38(9):1958–1972, 1995.

S. De Groot, H. E. J. Veeger, A. P. Hollander, and L. H. V. Van Der Woude. Consequence of feedback-based learning of an effective hand rim wheelchair force production on mechanical efficiency. *Clinical Biomechanics*, 17(3):219–226, 2002.

S. de Groot, A. J. Dallmeijer, O. J. Kilkens, F. W. van Asbeck, A. V. Nene, E. L. Angenot, M. W. Post, and L. H. van der Woude. Course of gross mechanical efficiency in handrim wheelchair propulsion during rehabilitation of people with spinal cord injury: a prospective cohort study. *Archives of physical medicine and rehabilitation*, 86(7):1452–1460, 2005.

S. de Groot, A. J. Dallmeijer, F. W. van Asbeck, M. W. Post, J. B. Bussmann, and L. van der Woude. Mechanical efficiency and wheelchair performance during and after spinal cord injury rehabilitation. *International journal of sports medicine*, 28 (10):880, 2007.

G. Desroches, R. Aissaoui, D. Bourbonnais, and C. Y. Perron. The effect of force direction at the pushrim on joint moments in the upper extremities during manual wheelchair propulsion. pages 338–340, 2005. Proc. 10th Ann. Conf. Int. Functional Electr. Stimulation Soc.(IFESS.

A. Di Marco, M. Russell, and M. Masters. Standards for wheelchair prescription. *Australian Occupational Therapy Journal*, 50(1):30, 2003.

K El ahrache and D Imbeau. Comparison of rest allowance models for static muscular work. *International Journal of Industrial Ergonomics*, 39(1):73–80, 2009.

M Essendrop, B Schibye, and K Hansen. Reliability of isometric muscle strength tests for the trunk, hands and shoulders. *International Journal of Industrial Ergonomics*, 28(6):379–387, 2001.

Robert Feyen, Yili Liu, Don Chaffin, Glenn Jimmerson, and Brad Joseph. Computer-aided ergonomics: A case study of incorporating ergonomics analyses into workplace design. *Applied Ergonomics*, 31(3):291–300, 2000.

M. A. Finley, E. K. Rasch, R. E. Keyser, and M. M. Rodgers. The biomechanics of wheelchair propulsion in individuals with and without upper-limb impairment. *Journal of Rehabilitation Research and Development*, 41(3B):385–394, 2004.

D. M. Fothergill, D. W. Grieve, and S. T. Pheasant. Human strength capabilities during one-handed maximum voluntary exertions in the fore and aft plane. *Ergonomics*, 34 (5):563–573, 1991.

T Fukunaga, M Miyatani, M Tachi, M Kouzaki, Y Kawakami, and H Kanehisa. Muscle volume is a major determinant of joint torque in humans. *Acta Physiologica Scandinavica*, 172(4):249–255, 2001.

D. W. Grieve. The postural stability diagram (psd): personal constraints on the static exertion of force. *Ergonomics*, 22(10):1155, 1979.

J. Grosjean. *Kinematics and dynamics of mechanisms*. McGraw-Hill, 1991.

M. Harms. Effect of wheelchair design on posture and comfort of users. *Physiotherapy*, 76(5):266–271, 1990.

Kimberley Hayes, Judie R. Walton, Zoltan L. Szomor, and George A. C. Murrell. Reliability of 3 methods for assessing shoulder strength. *Journal of Shoulder and Elbow Surgery*, 11(1):33–39, 2002.

D. A. Hobson. Comparative effects of posture on pressure and shear at the body-seat interface. *Journal of Rehabilitation Research and Development*, 29:21–21, 1992.

M. J. M. Hoozemans, A. J. Van Der Beek, M. H. W. Fringsdresen, F. J. H. Van Dijk, and Luchv Van Der Woude. Pushing and pulling in relation to musculoskeletal disorders: a review of risk factors. *Ergonomics*, 41(6):757–781, 1998.

R. E. Hughes, M. E. Johnson, S. W. O'Driscoll, and K. N. An. Age-related changes in normal isometric shoulder strength. *The American Journal of Sports Medicine*, 27 (5):651, 1999.

P. A. Hunsicker. Arm strength at selected degrees of elbow flexion. *Wright Air Development Center Report*, pages 54–548, 1955.

M Ikai and T Fukunaga. Calculation of muscle strength per unit cross-sectional area of human muscle by means of ultrasonic measurement. *European Journal of Applied Physiology*, 26(1):26–32, 1968.

Florence Peterson Kendall, Elizabeth Kendall McCreary, Patricia Geise Provance, Mary McIntyre Rodgers, and William Anthony Romani. *Muscles : testing and function with posture and pain*. Lippincott Williams and Wilkins, 2005.

R. F. Kirsch, A. M. Acosta, E. J. Perreault, and M. W. Keith. Measurement of isometric elbow and shoulder moments: position-dependent strength of posterior deltoid-to-triceps muscle tendon transfer in tetraplegia. *Rehabilitation Engineering, IEEE Transactions on [see also IEEE Trans. on Neural Systems and Rehabilitation]*, 4(4):403–409, 1996. 1063-6528.

AM Koontz, RA Cooper, ML Boninger, AL Souza, and BT Fay. Shoulder kinematics and kinetics during two speeds of wheelchair propulsion. *Journal of Rehabilitation Research and Development*, 39(6):635–650, 2002.

AM Koontz, RA Cooper, ML Boninger, Y Yang, BG Impink, and LHV van der Woude. A kinetic analysis of manual wheelchair propulsion during start-up on select indoor and outdoor surfaces. *Journal of Rehabilitation Research and Development*, 42(4): 447, 2005.

B. R. Kotajarvi, M. B. Sabick, K. N. An, K. D. Zhao, K. R. Kaufman, and J. R. Basford. The effect of seat position on wheelchair propulsion biomechanics. *Journal of rehabilitation research and development*, 41(3B):403–414, 2004.

KHE Kroemer and WS Marras. Evaluation of maximal and submaximal static muscle exertions. *Human Factors: The Journal of the Human Factors and Ergonomics Society*, 23(6):643–653, 1981.

J. R. Kuhlman. Isokinetic and isometric measurement of strength of external rotation and abduction of the shoulder, 1992.

K. Kulig, C. J. Newsam, S. J. Mulroy, S. Rao, J. A. K. Gronley, E. L. Bontrager, and J. Perry. The effect of level of spinal cord injury on shoulder joint kinetics during manual wheelchair propulsion. *Clinical Biomechanics*, 16(9):744–751, 2001.

S Kumar. *Muscle strength*. CRC, 2004.

S Kumar, Y Narayan, and C Bacchus. Symmetric and asymmetric two-handed pull-push strength of young adults. *Human factors*, 37(4), 1995.

S Kumar, S Rodgher, and Y Narayan. Measurements of shoulder adduction strength in different postures. *International Journal of Industrial Ergonomics*, 22(3):195–206, 1998.

Shrawan Kumar. Upper body push-pull strength of normal young adults in sagittal plane at three heights. *International Journal of Industrial Ergonomics*, 15(6):427–436, 1995.

CF Kuo and CH Chu. An online ergonomic evaluator for 3d product design. *Computers in industry*, 56(5):479–492, 2005.

MW Lee. A stochastic model of muscle fatigue in frequent strenuous work cycles. *Unpublished Doctoral Dissertation, The University of Michigan, University Microfilms, Inc., Ann Arbor, Michigan, and London*, 1979.

A. Lees and S. Arthur. An investigation into anaerobic performance of wheelchair athletes. *Ergonomics*, 31(11):1529–1537, 1988.

S. M. Lennon and A. Ashburn. Use of myometry in the assessment of neuropathic weakness: testing for reliability in clinical practice. *Clinical Rehabilitation*, 7(2):125, 1993.

R. L. Lieber, J. FridÃ©n, T. Hobbs, and A. G. Rothwell. Analysis of posterior deltoid function one year after surgical restoration of elbow extension. *Journal of Hand Surgery*, 28(2):288–293, 2003.

B.R. MacIntosh and A.N. Devrome. *The Ability to Persist in a Physical Task.* Chapter 5 in Muscle strength. CRC, 2004.

S. N. MacKinnon. Isometric pull forces in the sagittal plane. *Applied Ergonomics*, 29 (5):319–324, 1998.

S E Mathiassen and E Ahsberg. Prediction of shoulder flexion endurance from personal factors. *International Journal of Industrial Ergonomics*, 24(3):315–330, 1999.

RJ Maughan, JS Watson, and J Weir. Strength and cross-sectional area of human skeletal muscle. *The Journal of Physiology*, 338(1):37, 1983.

F Mayer, T Horstmann, K Rocker, HC Heitkamp, and HH Dickhuth. Normal values of isokinetic maximum strength, the strength/velocity curve, and the angle at peak torque of all degrees of freedom in the shoulder. *International journal of sports medicine*, 15(1):19–25, 1994.

P. J. McNair, J. Depledge, M. Brettkelly, and S. N. Stanley. Verbal encouragement: effects on maximum effort voluntary muscle: action. *British Medical Journal*, 30(3): 243, 1996.

N P Milner. *Modelling fatigue and recovery in static postural exercise, PhD Thesis.* PhD thesis, 1985.

A Mital, A.S. Nicholson, and Ayoub M.M. A guide to manual materials handling, 1993.

Ross H Mitchell. *Understanding sit-to-stand throught experimentation and modelling.* PhD thesis, 2004.

Ross H. Mitchell, Anthony J. Medland, and Aki I. T. Salo. A design methodology to create constraint-based human movement patterns for ergonomic analysis. *Journal of Engineering Design*, 18(4):293 – 310, 2007.

Johan F. M. Molenbroek and Anthony J Medland. The application of constraint processes for the manipulation of human models to address ergonomic design problems. *TMCE 2000 - Tools and Methods for Competitive Engineering*, Delft, April, 2000, 2000. in: , Horvath, I., Medland, A. J. and Vergeest, J. S. M., ed., „ 827-835 (ISBN:).

C. J. Newsam, S. J. Mulroy, J. K. Gronley, E. L. Bontrager, and J. Perry. Temporal-spatial characteristics of wheelchair propulsion: Effects of level of spinal cord injury, terrain, and propulsion rate. *American journal of physical medicine and rehabilitation*, 75(4):292–299, 1996.

C. J. Newsam, S. S. Rao, S. J. Mulroy, J. A. K. Gronley, E. L. Bontrager, and J. Perry. Three dimensional upper extremity motion during manual wheelchair propulsion in men with different levels of spinal cord injury. *Gait and Posture*, 10(3):223–232, 1999.

SB O'Sullivan and TJ Schmitz. Physical rehabilitation: assessment and treatment, 1994.

ST Pheasant and DW Grieve. Principal features of maximal exertion in the sagittal plane. *Ergonomics*, 24:327–38, 1981.

M. H. Pope, T. Bevins, D. G. Wilder, and J. W. Frymoyer. The relationship between anthropometric, postural, muscular, and mobility characteristics of males ages 18-55. *Spine*, 10(7):644, 1985.

J. Mark Porter, Keith Case, Russell Marshall, Diane Gyi, and Ruth Sims Nee Oliver. 'beyond jack and jill': Designing for individuals using hadrian. *International Journal of Industrial Ergonomics*, 33(3):249–264, 2004.

AD Price. Calculating relaxation allowances for construction operatives-part 2: local muscle fatigue. *Applied ergonomics*, 21(4):318, 1990.

M. Raison, C. Gaudez, S. Le Bozec, and P. Y. Willems. Determination of joint efforts in the human body during maximum ramp pushing efforts. *Journal of Biomechanics*, In Press, Corrected Proof.

M. L. Resnick and D. B. Chaffin. An ergonomic evaluation of handle height and load in maximal and submaximal cart pushing. *Applied Ergonomics*, 26(3):173–178, 1995.

W. M. Richter. The effect of seat position on manual wheelchair propulsion biomechanics: a quasi-static model-based approach. *Medical Engineering and Physics*, 23 (10):707–712, 2001.

W. M. Richter, R. Rodriguez, K. R. Woods, and P. W. Axelson. Stroke pattern and handrim biomechanics for level and uphill wheelchair propulsion at self-selected speeds. *Archives of physical medicine and rehabilitation*, 88(1):81–87, 2007.

D. L. Riddle, S. D. Finucane, J. M. Rothstein, and M. L. Walker. Intrasession and intersession reliability of hand-held dynamometer measurements taken on brain-damaged patients. *Physical Therapy*, 69(3):182, 1989.

RN Robertson, ML Boninger, RA Cooper, and SD Shimada. Pushrim forces and joint kinetics during wheelchair propulsion. *Archives of physical medicine and rehabilitation*, 77(9):856–864, 1996.

W Rohmert. Ermittlung von erholungspausen fÃŒr statische arbeit des menschen. *European Journal of Applied Physiology and Occupational Physiology*, 18(2):123–164, 1960.

W Rohmert. Problems in determining rest allowances part 1: use of modern methods to evaluate stress and strain in static muscular work. *Applied ergonomics*, 4(2):91, 1973.

L Rose, M Ericson, B Glimskar, B Nordgren, and R Ortengren. Ergo-index: Development of a model to determine pause needs after fatigue and pain reactions during work. *Computer Applications in Ergonomics, Occupational Safety and Health*, pages 461–468, 1992.

L. A. Rozendaal, H. E. Veeger, and L. H. van der Woude. The push force pattern in manual wheelchair propulsion as a balance between cost and effect. *Journal of biomechanics*, 36(2):239, 2003.

M. B. Sabick, B. R. Kotajarvi, and K. N. An. A new method to quantify demand on the upper extremity during manual wheelchair propulsion. *Archives of physical medicine and rehabilitation*, 85(7):1151–1159, 2004.

D. J. Sanderson and H. J. Sommer 3rd. Kinematic features of wheelchair propulsion. *J Biomech*, 18(6):423–9, 1985.

H Sato, J Ohashi, K Iwanaga, R Yoshitake, and K Shimada. Endurance time and fatigue in static contractions. *Journal of human ergology*, 13(2):147–154, 1984.

F. J. Schanne. *A Three-dimensional Hand Force Capability Model for a Seated Person.* University of Michigan, 1972.

S. D. Shimada, R. N. Robertson, M. L. Bonninger, and R. A. Cooper. Kinematic characterization of wheelchair propulsion. *J Rehabil Res Dev*, 35(2):210–8, 1998.

SH Snook and VM Ciriello. The design of manual handling tasks: revised tables of maximum acceptable weights and forces. *Ergonomics*, 34(9):1197, 1991.

TJ Stobbe. *The development of a practical strength testing program for industry.* PhD thesis, 1982.

T Stoll, E Huber, and B Seifert. *Isometric muscle strength measurement.* George Thieme Verlag, 2002.

EP Takala and E Viikari-Juntura. Loading of shoulder muscles in a simulated work cycle: Comparison between sedentary workers with and without neck-shoulder symptoms. *Clinical Biomechanics*, 6:145–152, 1991.

JC Tan and MHM Lee. *Practical manual of physical medicine and rehabilitation: diagnostics, therapeutics and basic problems.* Mosby Inc, first edition edition, 1998.

AnyBody Technology. www.anybodytech.com. (October), 2009.

P van der Meulen and A Seidl. Ramsis-the leading cad tool for ergonomic analysis of vehicles. *LECTURE NOTES IN COMPUTER SCIENCE*, 4561:1008, 2007.

L. H. V. Van der Woude, H. E. J. Veeger, R. H. Rozendal, G. J. van Ingen Schenau, F. Rooth, and P. Nierop. Wheelchair racing: effects of rim diameter and speed on physiology and technique. *Medicine and Science in Sports and Exercise*, 20(5):492, 1988.

S. van Drongelen, L. H. van der Woude, T. W. Janssen, E. L. Angenot, E. K. Chadwick, and D. J. H. Veeger. Glenohumeral contact forces and muscle forces evaluated in wheelchair-related activities of daily living in able-bodied subjects versus subjects with paraplegia and tetraplegia. *Archives of physical medicine and rehabilitation*, 86 (7):1434–1440, 2005.

Y Vanlandewijck, D Theisen, and D Daly. Wheelchair propulsion biomechanics. *Sports Med*, 31(5):339–367, 2001.

Y. C. Vanlandewijck and D. J. Daly. Wheelchair propulsion kinematics: movement pattern adaptations to speed changes in elite wheelchair rugby players. In *Proceedings of the Fifth Paralympic Congress*, pages 11–13, Sydney, 2000. Proceedings of the Fifth Paralympic Congress.

Y. C. Vanlandewijck, A. J. Spaepen, and R. J. Lysens. Wheelchair propulsion efficiency: movement pattern adaptations to speed changes. *Medicine and Science in Sports and Exercise*, 26(11):1373, 1994.

H. E. Veeger, L. H. van der Woude, and R. H. Rozendal. Wheelchair propulsion technique at different speeds. *Scandinavian journal of rehabilitation medicine*, 21 (4):197, 1989.

H. E. J. Veeger and F. C. T. Van der Helm. Biomechanics of manual wheelchair propulsion. *Ergonomics of manual wheelchair propulsion: state of art, Milan, Italy: Edizioni pro Juventute*, pages 201–13, 1991.

H. E. J. Veeger, L. H. V. Van der Woude, and R. H. Rozendal. Effect of handrim velocity on mechanical efficiency in wheelchair propulsion. *Medicine and Science in Sports and Exercise*, 24(1):100, 1992.

H. E. J. Veeger, L. A. Rozendaal, and F. C. T. Van der Helm. Load on the shoulder in low intensity wheelchair propulsion. *Clinical Biomechanics*, 17(3):211–218, 2002.

HE Veeger, FC Van der Helm, LH Van der Woude, GM Pronk, and RH Rozendal. Inertia and muscle contraction parameters for musculoskeletal modelling of the shoulder mechanism. *Journal of biomechanics*, 24(7):615, 1991.

HEJ Veeger, B Yu, KN An, and RH Rozendal. Parameters for modeling the upper extremity. *Journal of biomechanics*, 30(6):647–652, 1997.

D Warwick, G Novak, A Schultz, and M Berkson. Maximum voluntary strengths of male adults in some lifting, pushing and pulling activities. *Ergonomics*, 23(1):49, 1980.

MA Williams and AJ Medland. The creation of techniques for the design of machines compatible with human posture. *Design Methods for Performance and Sustainability*, page 347, 2001.

T Woodfield. *The Design and Development of Diagnostic Equipment to Measure Elbow and Wrist Extension Strength*. Project report, 1996.

F. Yao. Measurement and modeling of wheelchair propulsion ability for people with spinal cord injury: Master's thesis. Technical report, University of Canterbury, 2007.

A. Young. Strength training and cross-sectional area of muscles. *British Journal of Sports Medicine*, 19(1):48, 1985.

V Zatsiorsky and V Seluyanov. The mass and inertia characteristics of the main segments of the human body. *Biomechanics VIII-B*, pages 1152–1159, 1983.

Appendix A

Summary of MWC Propulsion Results

A.1 Summary of Results From MWC Propulsion at Normal Resistance

		Normal Resistance																																
		Push 1									Push 2									Push 3									Push 4							5
Subject	Injury	grab angle	release angle	push phase period (s)	return phase period (s)	Cycletime (s)	Velocity (m/s)	Force Max (N)	Max Power (W)	Work (J)	grab angle	release angle	push phase period (s)	return phase period (s)	Cycletime (s)	Velocity (m/s)	Force (N)	Max Power (W)	Work (J)	grab angle	release angle	push phase period (s)	return phase period (s)	Cycletime (s)	Velocity (m/s)	Force (N)	Max Power (W)	Work (J)	grab angle	release angle	push phase period (s)	return phase period (s)	Cycletime (s)	Velocity (m/s)	Force (N)	Max Power (W)	Work (J)	grab angle
1	C6 (Pre TROIDS)	123	42	1.4	0.4	1.8	0.4	31	10.2	6.9	122	31	0.7	0.4	1.1	0.5	34	16	7.4	122	35	0.6	0.3	0.9	0.6	31	18	6.7	123	33	0.5	0.4	0.9	0.7	30	21	5.8	127
2	C6 (Pre TROIDS)	134	52	1.6	0.5	2.2	0.5	45	12.4	8.9	139	59	0.9	0.6	1.6	0.7	42	23	8.6	132	61	0.8	0.6	1.4	0.7	17	12	3.7	131	61	0.7	0.6	1.2	0.8	16	12	4.9	133
3	C6 (Pre TROIDS)	130	56	1.2	0.4	1.6	0.5	66	29.2	15	130	60	0.7	0.5	1.2	0.7	54	35	14	123	60	0.5	0.4	0.8	0.9	60	50	15	131	61	0.5	0.4	0.9	0.9	50	47	8.4	128
4	C6 (Post TROIDS)	130	39	1.5	0.5	2	0.7	69	40	29	133	36	0.7	0.5	1.2	1	66	58	22	135	42	0.6	0.4	1.1	1.2	60	64	21	136	42	0.6	0.3	0.9	1.3	55	67	18	135
5	C6 (Post TROIDS)	137	47	1	0.3	1.3	0.9	180	98.6	50	129	45	0.5	0.3	0.9	1.1	72	71	22	112	49	0.3	0.3	0.6	1.2	79	87	18	112	40	0.3	0.3	0.7	1.2	62	74	10	103
6	C6 (Post TROIDS)	118	61	1	0.4	1.4	0.6	40	16.2	9	122	61	0.6	0.4	1	0.7	37	23	7.5	125	62	0.5	0.4	0.9	0.9	29	22	6.4	124	59	0.4	0.4	0.8	0.9	26	23	5.9	126
7	C5 (Post TROIDS)	119	56	1.1	0.3	1.4	0.5	60	17	14	122	60	0.6	0.3	0.9	0.6	33	17	6.5	122	60	0.6	0.3	0.9	0.6	33	19	7.5	121	54	0.4	0.4	0.9	0.7	28	19	6.1	118
8	C6 (Post TROIDS)	133	59	1.2	0.4	1.6	0.2	30	2.65	2.5	135	62	0.8	0.4	1.2	0.3	33	7.1	3.3	134	61	0.8	0.4	1.2	0.3	32	8.4	3.3	136	60	0.8	0.3	1.1	0.3	27	8.2	3.1	136
9	C7 ASIA D	123	44	0.8	0.4	1.2	0.8	61	35.9	15	124	49	0.5	0.4	0.8	0.9	49	42	9.1	126	47	0.4	0.4	0.8	1.1	47	49	9.9	126	49	0.4	0.4	0.8	1.2	39	45	8.2	125
10	C7 ASIA C	117	48	0.6	0.4	1.1	0.8	164	90.9	34	112	48	0.5	0.4	0.9	0.9	155	119	27	110	38	0.4	0.4	0.8	1	137	126	23	105	34	0.3	0.3	0.6	1	70	69	11	117
11	C7 ASIA C	119	49	0.9	0.3	1.2	0.8	96	52.8	23	123	48	0.5	0.3	0.8	1.1	80	77	19	121	49	0.3	0.5	0.8	1.3	79	94	20	120	50	0.3	0.5	0.8	1.5	65	89	16	116
12	C7 ASIA A	140	42	1	0.3	1.4	1	161	108	64	128	46	0.4	0.3	0.7	1.3	115	131	39	124	48	0.3	0.3	0.6	1.5	103	140	31	124	47	0.3	0.3	0.6	1.6	85	128	27	119
13	C7 ASIA A	98.2	33	0.8	0.3	1.1	0.6	113	55.9	26	88	40	0.3	0.3	0.6	0.9	131	104	21	90	46	0.2	0.3	0.5	1.1	159	166	22	90	45	0.2	0.2	0.4	1.3	119	147	15	82
14	C7 ASIA B	116	48	1	0.5	1.5	0.9	90	73.3	22	144	47	0.5	0.7	1.2	1.2	65	77	16	139	42	0.4	0.6	1	1.5	65	94	19	144	43	0.5	0.7	1.1	1.7	55	90	17	138
15		119	40								128	36								126	38								125	39								124

A.2 Summary of Results From MWC Propulsion at Normal Resistance

		Double Resistance																																
		Push 1									Push 2									Push 3									Push 4							5
Subject	Injury	grab angle	release angle	push phase period (s)	return phase period (s)	Cycletime (s)	Velocity (m/s)	Force (N)	Max Power (W)	Work (J)	grab angle	release angle	push phase period (s)	return phase period (s)	Cycletime (s)	Velocity (m/s)	Force (N)	Max Power (W)	Work (J)	grab angle	release angle	push phase period (s)	return phase period (s)	Cycletime (s)	Velocity (m/s)	Force (N)	Max Power (W)	Work (J)	grab angle	release angle	push phase period (s)	return phase period (s)	Cycletime (s)	Velocity (m/s)	Force (N)	Max Power (W)	Work (J)	grab angle
1	C6 (Pre TROIDS)	116	66	1	0.5	1.5	0.4	80	27.1	18	121	57	0.9	0.5	1.3	0.6	78	44	25	115	53	0.7	0.4	1	0.7	79	54	22	122	53	0.6	0.3	1	0.9	75	60	22	127
2	C6 (Pre TROIDS)	133	77	2.1	0.5	2.7	0.1	33	2.54	1.7	136	53	1.7	0.6	2.2	0.3	28	5.8	6.8	141	61	1.4	0.5	2	0.4	32	9.8	6.9	137	57	1.2	0.5	1.7	0.5	26	10	6.2	137
3	C6 (Pre TROIDS)	135	53	2	0.6	2.6	0.4	61	19.5	15	125	50	0.9	0.5	1.5	0.5	54	25	14	127	52	0.8	0.5	1.3	0.6	54	32	13	131	53	0.7	0.5	1.2	0.7	41	27	11	129
4	C6 (Post TROIDS)	125	43	1.8	0.4	2.2	0.5	86	29.3	28	129	43	1	0.3	1.3	0.7	76	46	29	125	41	0.7	0.4	1.1	0.8	75	57	24	128	43	0.7	0.4	1.1	0.9	68	58	23	130
5	C6 (Post TROIDS)	140	50	1.8	0.5	2.3	0.4	71	21.1	18	136	58	0.7	0.4	1.1	0.6	59	28	13	134	54	0.6	0.4	1.1	0.6	51	30	13	131	56	0.5	0.4	0.9	0.7	36	25	9.3	133
6	C6 (Post TROIDS)	116	78	1.4	0.4	1.8	0.2	28	4.98	3.4	116	60	1	0.5	1.5	0.3	39	12	6.7	117	67	0.7	0.5	1.2	0.4	31	12	4.7	120	62	0.7	0.4	1.1	0.5	32	15	5.1	126
7	C5 (Post TROIDS)	126	55	1.9	0.5	2.4	0.3	69	12.5	15	122	52	1	0.4	1.4	0.4	46	15	9.4	120	61	0.8	0.4	1.2	0.4	35	14	7.9	121	59	0.7	0.4	1.1	0.5	35	16	8.1	123
8	C6 (Post TROIDS)	137	70	1.9	0.4	2.3	0.1	37	2.29	3	139	62	1.1	0.4	1.5	0.2	37	6.7	4.1	137	64	1.2	0.4	1.6	0.3	34	7.3	4.4	136	65	1	0.4	1.4	0.3	35	9.2	4.8	137
9	C7 ASIA D	117	58	1.2	0.3	1.5	0.4	77	21.4	15	120	56	0.7	0.3	1.1	0.5	56	26	11	123	49	0.7	0.4	1.1	0.7	54	32	13	127	53	0.6	0.4	1.1	0.8	53	37	14	114
10	C7 ASIA C	121	41	1	0.5	1.5	0.8	464	290	88	122	57	0.5	0.5	1.1	1.1	383	359	108	104	70	0.3	0.3	0.6	0.8	0	0	0	117	45	0.5	0.3	0.8	0.9	347	266	66	116
11	C7 ASIA C	112	65	0.7	0.4	1	0.4	145	29.5	12	117	55	0.6	0.3	0.9	0.6	120	60	23	121	47	0.5	0.3	0.9	0.8	95	67	24	121	49	0.5	0.3	0.8	0.9	95	79	23	120
12	C7 ASIA A	134	51	1.2	0.3	1.5	0.7	183	85	63	138	52	0.6	0.3	0.9	0.9	136	106	46	132	53	0.4	0.3	0.7	1.1	124	119	40	130	42	0.4	0.3	0.7	1.2	107	117	32	125
13	C7 ASIA A	109	39	1.4	0.3	1.7	0.4	128	33.9	29	92	45	0.5	0.3	0.8	0.6	117	62	22	99	45	0.4	0.3	0.8	0.7	107	72	20	95	39	0.4	0.3	0.8	0.8	111	87	24	95
14	C7 ASIA B	132	54	1.4	0.6	2	0.5	94	38.9	20	139	50	0.9	0.6	1.5	0.7	75	46	21	140	54	0.7	0.6	1.2	0.8	79	61	22	141	47	0.6	0.6	1.2	1	77	72	24	142
15																																						132

Appendix B

Code

B.1 SWORDS Code for Calculating Reactions in the Upper Arm

```
function forcesDE_L
{Link="DE_L";
 CoordRotate();
 ii = 1000 * DE_L;
$coordinates at start of link (point1)
P1x=PointMx[Indx4, 0];
P1y=PointMx[Indx4, 1];
P1z=PointMx[Indx4, 2];

$forces relative to segment DE_Left

$Contribution From Vertical Component
direction = "vertical";
RelCompF = FvdL;
RelComponents();
FdL1vec[0] = relF[0];
FdL2vec[0] = relF[1];
FdL3vec[0] = relF[2];
RelCompF = FveL;
RelComponents();
FeL1vec[0] = relF[0];
FeL2vec[0] = relF[1];
FeL3vec[0] = relF[2];

$Contribution From Horiz side Component
direction = "side";
RelCompF = FsdL;
RelComponents();
FdL1vec[1] = relF[0];
FdL2vec[1] = relF[1];
FdL3vec[1] = relF[2];
RelCompF = FseL;
RelComponents();
FeL1vec[1] = relF[0];
FeL2vec[1] = relF[1];
FeL3vec[1] = relF[2];
```

```
FeL1vec[2] = relF[0];
FeL2vec[2] = relF[1];
FeL3vec[2] = relF[2];

$Contribution From mass Component
direction = "vertical";
RelCompF = FmdL;
RelComponents();
FMdL1 = relF[0];
FMdL2 = relF[1];
FMdL3 = relF[2];
RelCompF = FmeL;
RelComponents();
FMeL1 = relF[0];
FMeL2 = relF[1];
FMeL3 = relF[2];

$Forces in each member relative to DE_L (123)
FdL1 = FdL1vec[0] + FdL1vec[1] + FdL1vec[2];
FdL2 = FdL2vec[0] + FdL2vec[1] + FdL2vec[2];
FdL3 = FdL3vec[0] + FdL3vec[1] + FdL3vec[2];

FeL1 = FeL1vec[0] + FeL1vec[1] + FeL1vec[2];
FeL2 = FeL2vec[0] + FeL2vec[1] + FeL2vec[2];
FeL3 = FeL3vec[0] + FeL3vec[1] + FeL3vec[2];


$Forces in each member relative to DE_L (123)
$Link EF Left
PPi=7;
getPP();
FMMult();
eL_rel = AR;
eL_p = eL_rel[0];
eL_q = eL_rel[1];
eL_r = eL_rel[2];
PP[0, 0] = comPmatrix[4, 0] - P1x;
PP[1, 0] = comPmatrix[4, 1] - P1y;
PP[2, 0] = comPmatrix[4, 2] - P1z;
FMMult();
eeL_rel = AR;
eeL_p = eeL_rel[0];
eeL_q = eeL_rel[1];
eeL_r = eeL_rel[2];

loop(i, 0, ii)
{   x = i / 1000;

    M = -FeL1 * eL_p - FMeL1 * eeL_p + FeL2 * (eL_q- x) + FMeL2 * (eeL_q- x);

    N = -FeL1 * eL_r - FMeL1 * eeL_r + FeL3 * (eL_q- x) + FMeL3 * (eeL_q- x);

    T = FeL3 * eL_p + FMeL3 * eeL_p - FeL2 * eL_r - FMeL2 * eeL_r;

    Axial = -(FeL1 + FMeL1);
    Sp = -(FeL2 + FMeL2);
    Sr = -(FeL3 + FMeL3);
```

```
    jj = jj + 1;

    $IF need to incorp influence force DL
    if(x <= Pvector[6])
    {  M = M + FdL2 * (Pvector[6] - x);
       N = N + FdL3 * (Pvector[6] - x);
       T = T;
       Axial = Axial - FdL1;
       Sp = Sp - FdL2;
       Sr = Sr - FdL3;
    }

    $IF need to incorp influence  mass
    if(x <= comPvec[6])
    {  M = M + FMdL2 * (comPvec[6] - x);
       N = N + FMdL3 * (comPvec[6] - x);
       T = T;
       Axial = Axial - FMdL1;
       Sp = Sp - FMdL2;
       Sr = Sr - FMdL3;
    }

    outpvector[jj, 0] = jj - 6;
    outpvector[jj, 1] = Axial;
    outpvector[jj, 2] = Sp;
    outpvector[jj, 3] = Sr;
    outpvector[jj, 4] = M;
    outpvector[jj, 5] = N;
    outpvector[jj, 6] = T;

    $write summary file
    if((i==0)||(i==ii)||(x == Pvector[6])||(x == comPvec[6]))
    {fwriteln(2, "DEL", jj - 6, Axial, Sp, Sr, M, N, T);
    }
}
}
```

```
Ang_zr = acos(vecZU[2] / sqrt(vecZU[0] ^ 2 + vecZU[1] ^ 2 + vecZU[2] ^ 2));

vecAngRot[0] = Ang_yp;
vecAngRot[1] = Ang_yq;
vecAngRot[2] = Ang_yr;
vecAngRot[3] = Ang_xp;
vecAngRot[4] = Ang_xq;
vecAngRot[5] = Ang_xr;
vecAngRot[6] = Ang_zp;
vecAngRot[7] = Ang_zq;
vecAngRot[8] = Ang_zr;

$Construct transformation matrix to transform position applied force into local axis
RPtmatrix[0, 0] = 1 + (1 - cos(-AngR)) * (RUx ^ 2 - 1);
RPtmatrix[1, 0] = (1 - cos(-AngR)) * RUx * RUy + RUz * sin(-AngR);
RPtmatrix[2, 0] = (1 - cos(-AngR)) * RUx * RUz - RUy * sin(-AngR);
RPtmatrix[0, 1] = (1 - cos(-AngR)) * RUx * RUy - RUz * sin(-AngR);
RPtmatrix[1, 1] = 1 + (1 - cos(-AngR)) * (RUy ^ 2 - 1);
RPtmatrix[2, 1] = (1 - cos(-AngR)) * RUy * RUz + RUx * sin(-AngR);
RPtmatrix[0, 2] = (1 - cos(-AngR)) * RUx * RUz + RUy * sin(-AngR);
RPtmatrix[1, 2] = (1 - cos(-AngR)) * RUy * RUz - RUx * sin(-AngR);
RPtmatrix[2, 2] = 1 + (1 - cos(-AngR)) * (RUz ^ 2 - 1);

}
```

B.2 SWORDS Coordinate Transform Function

```
$Rotation Transformation matrix
dec real Rmatrix[3, 3];
dec real Xplace[3], Yplace[3], Zplace[3];
dec real vecXU[3], vecYU[3], vecZU[3];

dec real Ang_yp, Ang_yq, Ang_yr;
dec real Ang_xp, Ang_xq, Ang_xr;
dec real Ang_zp, Ang_zq, Ang_zr;

dec real vecAngRot[9];
dec int Indx1, Indx2, Indx3, Indx4;


function CoordRotate
{
$Index to pull angles from proj/ang/L vectors

if(Link == "AB")
{Indx1 = 0;
 Indx2 = 16;
 Indx3 = 1;
}
if(Link == "BC")
{Indx1 = 1;
 Indx2 = 17;
 Indx3 = 2;
}
if(Link == "CD_R")
{Indx1 = 2;
 Indx2 = 18;
 Indx3 = 3;
}
if(Link == "DE_R")
{Indx1 = 3;
 Indx2 = 19;
 Indx3 = 4;
}
if(Link == "EF_R")
{Indx1 = 4;
 Indx2 = 20;
 Indx3 = 5;
}
if(Link == "CD_L")
{Indx1 = 5;
 Indx2 = 21;
 Indx3 = 6;
```

```
}
if(Link == "DE_L")
{Indx1 = 6;
 Indx2 = 22;
 Indx3 = 7;
}
if(Link == "EF_L")
{Indx1 = 7;
 Indx2 = 23;
 Indx3 = 8;
}

$Calculate Unit Vectors for Axis to rotate coordinate system about
RUy = 0;

if(((AngVector[Indx2] < 90) && (AngVector[Indx2] > 0)) || ((AngVector[Indx2] < 180) && (
AngVector[Indx2] > 90)))
{   RUx = sin(AngVector[Indx2]);
    RUz = cos(AngVector[Indx2]);
}
Else
{ if((AngVector[Indx2] < 270) && (AngVector[Indx2] > 180))
  {   RUx = -cos(AngVector[Indx2]);
      RUz = -sin(AngVector[Indx2]);
  }
  Else
  { if((AngVector[Indx2] < 360) && (AngVector[Indx2] > 270))
    {   RUx = -sin(AngVector[Indx2]);
        RUz = -cos(AngVector[Indx2]);
    }
    Else
    { if((AngVector[Indx2] == 99999) || (AngVector[Indx2] == 0) || (AngVector[Indx2] == 18
      {   RUx = 0;
          RUz = 1;
      }
      Else
      { if((AngVector[Indx2] == 90) || (AngVector[Indx2] == 270))
        {   RUx = 1;
            RUz = 0;
    }
      }
    }
  }
}


$Get angle of rotation
if(Link == "CD_L")
{   Indx4 = 2;
}
else
{   Indx4 = Indx3 - 1;
}

$fix it bit for my wierd problem
if(abs(Lvector[Indx1] - abs(PointMx[Indx3, 1] - PointMx[Indx4, 1]))<0.00001)
   {if(PointMx[Indx3, 1] > PointMx[Indx4, 1])
```

```
     {AngR=acos(1);
     }
     else
     {AngR=acos(-1);
     }
    }
else
    {AngR = acos((PointMx[Indx3, 1] - PointMx[Indx4, 1]) / Lvector[Indx1]);
     if(PointMx[Indx3, 2]<PointMx[Indx4, 2])
     {AngR=360-AngR;
     }
     if((RUz==1) && (PointMx[Indx3, 0]>PointMx[Indx4, 0]))
     {AngR=360-AngR;
     }
    }

$Construct transformation matrix to rotate coordinate system
Rmatrix[0, 0] = 1 + (1 - cos(AngR)) * (RUx ^ 2 - 1);
Rmatrix[1, 0] = (1 - cos(AngR)) * RUx * RUy + RUz * sin(AngR);
Rmatrix[2, 0] = (1 - cos(AngR)) * RUx * RUz - RUy * sin(AngR);
Rmatrix[0, 1] = (1 - cos(AngR)) * RUx * RUy - RUz * sin(AngR);
Rmatrix[1, 1] = 1 + (1 - cos(AngR)) * (RUy ^ 2 - 1);
Rmatrix[2, 1] = (1 - cos(AngR)) * RUy * RUz + RUx * sin(AngR);
Rmatrix[0, 2] = (1 - cos(AngR)) * RUx * RUz + RUy * sin(AngR);
Rmatrix[1, 2] = (1 - cos(AngR)) * RUy * RUz - RUx * sin(AngR);
Rmatrix[2, 2] = 1 + (1 - cos(AngR)) * (RUz ^ 2 - 1);

Xplace[0] = 1;
Xplace[1] = 0;
Xplace[2] = 0;
Yplace[0] = 0;
Yplace[1] = 1;
Yplace[2] = 0;
Zplace[0] = 0;
Zplace[1] = 0;
Zplace[2] = 1;

$Rotate Coordinate system
vecXU = Rmatrix*Xplace;    $x --> x'
vecYU = Rmatrix*Yplace;    $y --> y'
vecZU = Rmatrix*Zplace;    $z --> z'
$outputs base 1

$Calculate Angles of local coords with global y

Ang_yp = acos(vecXU[1] / sqrt(vecXU[0] ^ 2 + vecXU[1] ^ 2 + vecXU[2] ^ 2));
Ang_yq = AngR;
Ang_yr = acos(vecZU[1] / sqrt(vecZU[0] ^ 2 + vecZU[1] ^ 2 + vecZU[2] ^ 2));

$Calculate Angles of local coords with global X
Ang_xp = acos(vecXU[0] / sqrt(vecXU[0] ^ 2 + vecXU[1] ^ 2 + vecXU[2] ^ 2));
Ang_xq = acos(vecYU[0] / sqrt(vecYU[0] ^ 2 + vecYU[1] ^ 2 + vecYU[2] ^ 2));
Ang_xr = acos(vecZU[0] / sqrt(vecZU[0] ^ 2 + vecZU[1] ^ 2 + vecZU[2] ^ 2));

$Calculate Angles of local coords with global
Ang_zp = acos(vecXU[2] / sqrt(vecXU[0] ^ 2 + vecXU[1] ^ 2 + vecXU[2] ^ 2));
Ang_zq = acos(vecYU[2] / sqrt(vecYU[0] ^ 2 + vecYU[1] ^ 2 + vecYU[2] ^ 2));
```

```
$ ****************************************CoordRotate.mac
$ *                                                      *
$ * Calculates rotation axis and angle of rotation       *
$ * Constructs transfofrmation matrix to transform coord *
$ * system and positions to local system                 *
$ *                                                      *
$ ***************************Laura Hollingsworth 28/06/07

$Unitvector components for axis of rotation
dec real RUy, RUx, RUz, AngR;

$Rotation Transformation matrix
dec real Rmatrix[3, 3];
dec real Xplace[3], Yplace[3], Zplace[3];
dec real vecXU[3], vecYU[3], vecZU[3];

dec real Ang_yp, Ang_yq, Ang_yr;
dec real Ang_xp, Ang_xq, Ang_xr;
dec real Ang_zp, Ang_zq, Ang_zr;

dec real vecAngRot[9];
dec int Indx1, Indx2, Indx3, Indx4;


function CoordRotate
{
$Index to pull angles from proj/ang/L vectors

if(Link == "AB")
{Indx1 = 0;
 Indx2 = 16;
 Indx3 = 1;
}
if(Link == "BC")
{Indx1 = 1;
 Indx2 = 17;
 Indx3 = 2;
}
if(Link == "CD_R")
{Indx1 = 2;
 Indx2 = 18;
 Indx3 = 3;
}
if(Link == "DE_R")
{Indx1 = 3;
 Indx2 = 19;
 Indx3 = 4;
}
if(Link == "EF_R")
{Indx1 = 4;
 Indx2 = 20;
 Indx3 = 5;
}
if(Link == "CD_L")
{Indx1 = 5;
 Indx2 = 21;
 Indx3 = 6;
```

B.3 Code to Calculate Applied Force Direction

```
%% Constants from literature
C0 = 0.005;
%shoulder extension constants
SE_M0 = 79;          SE_c0 = 0.675;       SE_c1 = 0.471;
SE_c2 = -0.195;      SE_c3 = 0.017;       SE_wmax = 27;
SE_k = 0.33;         SE_V = 0.36;
%shoulder flexion constants
SF_M0 = 52;          SF_c0 = 1.138;       SF_c1 = -0.218;
SF_c2 = 0.073;       SF_c3 = -0.025;      SF_wmax = 30;
SF_k = 0.35;         SF_V = 0.32;
%elbow extension constants
EE_M0 = 43;          EE_c0 = 0.496;       EE_c1 = 0.228;
EE_c2 = 0.215;       EE_c3 = -0.104;      EE_wmax = 30;
EE_k = 0.40;         EE_V = 0.17;
%elbow flexion constants
EF_M0 = 37;          EF_c0 = 0.706;       EF_c1 = 0.302;
EF_c2 = 0.008;       EF_c3 = -0.053;      EF_wmax = 30;
EF_k = 0.45;         EF_V = 0.19;

%% Subject data
WrkBk = 'Q:\PhD Work\Rozendaals theory stuff\Subject Data For Matlab.xls';
WrkBk2 = 'Q:\PhD Work\Rozendaals theory stuff\Hand Paths by Participant 1xR.xls';
WkSht =  'Steve H 1R';
WkSht2 =  'Steve H';
% WkSht = 'Grant 1R';
% WkSht2 = 'Grant';
% WkSht = 'Richard 1R';
% WkSht2 = 'Richard';
data = xlsread(WrkBk, WkSht, 'A2:F1000');
r_wheel = xlsread(WrkBk2, WkSht2, 'F44');    %wheel radius
ax = xlsread(WrkBk2, WkSht2, 'F42');         %wheel axle position
ay = -xlsread(WrkBk2, WkSht2, 'F43');         %wheel axle position

button =  questdlg('Click the subject''s shoulder, elbow then hand','Point Selection', 'OI
'OAK', 'OK');
% im1=imread('GrantMVR_N1.jpg');
%  im1=imread('RichardMVRN172.jpg');
 im1=imread('SteveHMVR_N135.jpg');
figure(1); imagesc(im1);
hold on
plot(ax,ay,'o','MarkerEdgeColor','r','MarkerFaceColor','w')
plot(ax,(ay-r_wheel),'o','MarkerEdgeColor','k','MarkerFaceColor','r')
plot((ax-r_wheel),ay,'o','MarkerEdgeColor','k','MarkerFaceColor','r')
plot((ax+r_wheel),ay,'o','MarkerEdgeColor','k','MarkerFaceColor','r')
[sx,sy] = ginput(1); %shoulder xy position
[epx, epy] = ginput(1);
[hpx, hpy] = ginput(1);
clear im1;  close(1)

l_ua = sqrt((sy-epy)^2+(sx-epx)^2);
l_fa = sqrt((epy-hpy)^2+(epx-hpx)^2);
```

```
ang_s_old=0;    omega_old=0;    ang_e_old=0;

%pixels per mm
ppmm = 1000*r_wheel/300;
r_wheel = 0.33;      ax = ax/ppmm;    ay = -ay/ppmm;
sx = sx/ppmm;       sy = -sy/ppmm;
l_ua = l_ua/ppmm;   l_fa = l_fa/ppmm;

points(:,1) = [130; 120; 110; 100; 90; 80; 70; 60; 50];
points(:,2) = ones(length(points),1);

%% loopy bit
    %distance between shoulder and rim
    r1=sqrt((sy-ay)^2+(sx-ax)^2);
    beta=atand((ax-sx)/(sy-ay));
    E = 20;  %Power Watts, Rozendaal
    %omega = 1.39/r_wheel;  %1.39m/s constant - rozendaal
    %phi = round(data(1,2));

    %starting position
    phi = data(1,2);     %'grab' angle
    sigma = 90 - phi + beta;
    %elbow angle
    ang_e_old = acosd(((l_fa^2+l_ua^2)-(r_wheel^2+r1^2)+2*r_wheel*r1*cosd(sigma)) ...
                    /(2*l_fa*l_ua));
    range=89;

for i=2:length(data)
    % for each position of phi, hand position changes, read in data
    %phi = phi-1;
    phi = data(i,2);     %'grab' angle
    omega = data(i,3);   %angular velocity wheel
    E = data(i,4);       %power
    Ft = data(i,5);      %Tangental Force
    hx = ax + r_wheel*cosd(phi);          %hand position
    hy = ay + r_wheel*sind(phi);          % - assuming in contact with rim

    %constants - 4 bar mech calcs
    K1 = r1/l_ua;      K2 = r1/r_wheel;
    K3 = (r_wheel^2-l_fa^2+l_ua^2+r1^2)/(2*r_wheel*l_ua);
    sigma = 90 - phi + beta;
    A = sind(sigma);    B = cosd(sigma)-K2;   C = K1*cosd(sigma)-K3;
    %shoulder angle  (between r1 and upper arm)
    ang_s = 2*atand((A-sqrt(A^2+B^2-C^2))/(B+C));
    %elbow angle
    ang_e = acosd(((l_fa^2+l_ua^2)-(r_wheel^2+r1^2)+2*r_wheel*r1*cosd(sigma)) ...
                    /(2*l_fa*l_ua));
    %elbow position
    ex = sx - l_ua*sind(ang_s-beta);
    ey = sy - l_ua*cosd(ang_s-beta);
    %elbow angular velocity
    omegaE = deg2rad(ang_e-ang_e_old)/0.001;          %change in elbow ang per .001s
    %shoulder angular velocity
    omegaS = omega*(sind(sigma-ang_s)-K1*sind(sigma)) ...
                    /(sind(sigma-ang_s)+K2*sind(ang_s));
    VMx(i,:)=[phi omega omegaE omegaS];
```

```
    %vectors
    r_sh = [ -(sy-hy); (sx-hx)];
    r_eh = [ -(ey-hy); (ex-hx)];
    r_ah = [ (ay-hy); -(ax-hx)];
    r_se = [ -(sy-ey); (sx-ex)];
%   to work out if flexion or extension
    fe_sh = [ -(hy-sy); (hx-sx)];
    fe_eh = [ -(hy-ey); (hx-ex)];
%   fe_sh = [ -(sy-hy); (sx-hx)];
%   fe_eh = [ -(ey-hy); (ex-hx)];

    j=1; CostV=[]; Rvec=[];
    for theta = -range:1:range

        alpha = (theta + phi)-90;
        Fh = Ft/cosd(theta);
    %Fh= 1.1*Ft;
        Fx = Fh*sind(theta + phi);
        Fy = -Fh*cosd(theta + phi);
        F = [Fx; Fy];

        if theta == 56
                debug=1;
        end

        if  dot(fe_sh,F) < 0; % shoulder Extension
            M0S = SE_M0;     c0S = SE_c0;
            c1S = SE_c1;     c2S = SE_c2;
            c3S = SE_c3;     wmaxS = SE_wmax;
            kS = SE_k;       VS = SE_V;
        end
        if dot(fe_sh,F) >= 0  %if shoulder Flexion
            M0S = SF_M0;     c0S = SF_c0;
            c1S = SF_c1;     c2S = SF_c2;
            c3S = SF_c3;     wmaxS = SF_wmax;
            kS = SF_k;       VS = SF_V;
        end

        if dot(fe_eh,F) >= 1  %if elbow Flexion
            M0E = EF_M0;     c0E = EF_c0;
            c1E = EF_c1;     c2E = EF_c2;
            c3E = EF_c3;     wmaxE = EF_wmax;
            kE = EF_k;       VE = EF_V;
        end
        if  dot(fe_eh,F) <0;   %if elbow Extension
            M0E = EE_M0;     c0E = EE_c0;
            c1E = EE_c1;     c2E = EE_c2;
            c3E = EE_c3;     wmaxE = EE_wmax;
            kE = EE_k;       VE = EE_V;
        end

        %radians
        angrad_s = -deg2rad(ang_s);
        angrad_s = abs(angrad_s);
        angrad_e = deg2rad(ang_e);
        fm_angS = c0S + c1S*angrad_s + c2S*angrad_s^2 + c3S*angrad_s^3;
        fm_angE = c0E + c1E*angrad_e + c2E*angrad_e^2 + c3E*angrad_e^3;
```

```
        fm_omegaS = (1 - abs(omegaS)/wmaxS)/(1 + abs(omegaS)/(kS*wmaxS));
        fm_omegaE = (1 - abs(omegaE)/wmaxE)/(1 + abs(omegaE)/(kS*wmaxE));
        MmaxS = M0S*fm_angS*fm_omegaS;
        MmaxE = M0E*fm_angE*fm_omegaE;

        C = VS*(abs(dot(r_sh,F))/MmaxS) + VE*(abs(dot(r_eh,F))/MmaxE);
%   end

    if C<0;         C=0;      end
    C=C+C0;

        CVariables1(i,j)=dot(fe_sh,F);
        CVariables3(i,j)=dot(fe_eh,F);
        MmaxSMx(i,j)=MmaxS;
        MmaxEMx(i,j)=MmaxE;
%     RMx(i,j) = E/C;

        CostV(j) = C;          j=j+1;
        Rvec(j) = E/C;

        if E/C == max(Rvec) && C>0;
            MaxMx(i,:) = [phi theta alpha E C E/C M0E M0S ];
            for t=1:length(points)
                if abs(phi-points(t,1))< abs(MaxMx(points(t,2), 1)-points(t,1))
                    points(t,2)=i;
                end
            end
        end
    end
    RMx(i,:)= Rvec;
    CMx(i,:)= CostV;
    ANG1(i)=ang_s;
    ANG2(i)=ang_e;
    ang_s_old = ang_s;       omega_old = omega;
    ang_e_old = ang_e;
    CostMx(i,:) = CostV;
end

%% Polar Plots

limit = ceil(max(max(1./CMx(1:(i-5),:))));

for m=1:length(points)
    ploti=points(m,2);
    RR=deg2rad([-range:range]-90+MaxMx(ploti,1));
    figure
    r_max  = 10;
    [X1,Y1] = pol2cart(RR,1./CMx(ploti,1:end));
    [X2,Y2] = pol2cart([0 deg2rad(-90+MaxMx(ploti,1))], [0, 1./CMx(ploti,90)]);
    plot([0 X1],[0 Y1])
    fill([0 X1], [0 Y1], [1 0.5 0])
    hold on
    %plot 80% range
    theta80=[]; C80=[];
    theta80(1)=0;    C80(1)=0;    q=2;
    limit = 1/min(CMx(ploti,:));
    for p=1:(2*range-1);
```

```
        if(1/CMx(ploti,p))>(0.90*limit)
            theta80(q) = RR(p);
            C80(q) = 1/CMx(ploti,p);
            q=q+1;
        end
    end
    theta80(q)=0;   C80(q)=0;
    [X3,Y3] = pol2cart(theta80,C80);
    fill(X3, Y3, [1 0.75 0.5])
    compass(X2, Y2, 'k')
      [V,Z] = pol2cart([0 deg2rad(-180+MaxMx(ploti,1))], [0, 1./CMx(ploti,90)]);
      plot(V,Z, 'r')
    plot(0, 0, 'o', 'MarkerEdgeColor', 'k', 'MarkerFaceColor','k', 'MarkerSize',4)
    title(num2str(round(MaxMx(ploti,1))))
    %axis([-5 limit -limit 10])
    grid off;   axis off,
axis equal; h=gcf;
    name=['Cost_', WkSht, '_', num2str(round(MaxMx(ploti,1))), 'deg'];
    saveas(h, name,'bmp')
end

%% Angle plots

for ii=2:length(MaxMx)
   RRdeg =[-range:range]-90+MaxMx(ii,1);
   %plot 80% range
    theta80=[]; C80=[]; q=0;
    limit = 1/min(CMx(ii,:));
    for p=1:(2*range-1);
        if(1/CMx(ii,p))>(0.90*limit)
            q=q+1;
            theta80(q) = RRdeg(p);
        end
    end
    Tang(ii-1)= -90+MaxMx(ii,1);
    Lower80(ii-1) = theta80(1);
    Upper80(ii-1) = theta80(q);
end

figure
hold on
set(gca,'XDir','reverse')
[b,a] = butter(2,12/100);
filt{i}.y1 = filtfilt(b,a,Lower80);
filt{i}.y2 = filtfilt(b,a,Upper80);
FillX = [MaxMx((2:end),1); flipud(MaxMx((2:end),1))];
FillY = [filt{i}.y1 fliplr(filt{i}.y2)];
fill(FillX, FillY, [1 0.5 0])
plot(MaxMx((2:end),1), Tang, 'k');
xlabel('\phi','FontSize',14)
ylabel('Angle of applied force with lowest cost','FontSize',14)
ylim([-100 100]);
xlim([60 120]);
[c,d] = butter(2,10/100);
filt{i}.y3 = filtfilt(c,d,MaxMx((2:end),2)+MaxMx((2:end),1)-90);
plot(MaxMx((2:end),1), filt{i}.y3,'k-.');
% plot(MaxMx((2:end),1), MaxMx((2:end),2)+MaxMx((2:end),1)-90,':');
```

```
%Save
h=gcf; grid on;
name=['Angles_', WkSht];
saveas(h, name,'pdf')

%% Velocity plots

figure
hold on
set(gca,'XDir','reverse')
plot(VMx((3:end-5),1), VMx((3:end-5),2),'r', VMx((3:end-5),1), VMx((3:end-5),3),'b:', ...
    VMx((3:end-5),1), VMx((3:end-5),4),'g-.', 'LineWidth', 2 )
xlabel('\phi','FontSize',14)
ylabel('Anglar velocity rad/s','FontSize',14)
legend('Wheel','Elbow','shoulder');
name2=['Velocities_', WkSht];
h=gcf;  grid on;
saveas(h, name2,'pdf')
```